SEQUENCE STRATIGRAPHIC CONTROLS OF HYDROCARBON RESERVOIR ARCHITECTURE - CASE STUDY OF LATE PERMIAN (GUADALUPIAN) QUEEN FORMATION, MEANS FIELD, ANDREWS COUNTY, TEXAS

A Dissertation

by

CHANGSU RYU

Submitted to the Office of Graduate Studies of
Texas A&M University
in partial fulfillment of the requirements for the degree of

DOCTOR OF PHILOSOPHY

August 2002

Major Subject: Geology

SEQUENCE STRATIGRAPHIC CONTROLS OF HYDROCARBON RESERVOIR ARCHITECTURE - CASE STUDY OF LATE PERMIAN (GUADALUPIAN) QUEEN FORMATION, MEANS FIELD, ANDREWS COUNTY, TEXAS

A Dissertation

by

CHANGSU RYU

Submitted to Texas A&M University
in partial fulfillment of the requirements
for the degree of

DOCTOR OF PHILOSOPHY

Approved as to style and content by:

Robert K. Popp (Chair of Committee)	Thomas T. Tieh (Member)
Steven L. Dorobek (Member)	Brian J. Willis (Member)
Thomas A. Blasingame (Member)	Andrew Hajash, Jr. (Head of Department)

August 2002

Major Subject: Geology

ABSTRACT

Sequence Stratigraphic Controls of Hydrocarbon Reservoir Architecture -
Case Study of Late Permian (Guadalupian) Queen Formation,
Means Field, Andrews County, Texas. (August 2002)
Changsu Ryu, B.S., Korea University;
M.S., Korea University
Chair of Advisory Committee: Dr. Robert K. Popp

The late Permian Queen Formation (115 m thick) is a succession of mixed clastics, carbonates and evaporites deposited in the northeastern margin of Central Basin Platform of the Permian Basin, west Texas, USA. Depositional facies, stacking patterns of cyclic facies associations and statistical correlation of rock property variations define geologic controls on reservoir rock properties. Textural, compositional, petrophysical and diagenetic variations within lithofacies exhibit systematic changes with stratigraphic position, which can be related to base level changes that were controlled by high-frequency, low-amplitude, sea level fluctuations during a greenhouse period.

Ten lithofacies record variations in clastic input, shallow marine carbonate production, and evaporate precipitation in sabhkas and salinas. Four different types of lithofacies associations define: (1) transgressive deltaic deposits; (2) upward-shallowing evaporite and carbonate tidal-flat deposits; (3) transgressive beach ridge and sand flat deposits; and (4) upward-shallowing evaporite salina-sabhka deposits. Stacking patterns of lithofacies associations define sixteen depositional cycles that can be grouped into eight cycle sets. Cycle sets in turn are grouped to define two high-frequency sequences. Sequence 1 progresses from fluvial to carbonate tidal flat cycles. Sequence 2 consists of salina-dominated upward-shoaling cycles. Lateral continuity of cycles indicates restricted sedimentation on low-accommodation inner platform areas updip of prograding highstand platform-margin carbonate buildups, and a long-term trend of accommodation decrease. The Queen Formation contains two reservoir types; (1) siliciclastic reservoirs capped by evaporites and (2) layer-cake carbonate reservoirs. Of the four reservoir zones identified, R11 in lowstand fluvial-deltaic deposits has relatively little cement and the best reservoir characters.

ACKNOWLEDGEMENTS

This study would not be possible without the academic and financial support of the Department of Geology and Geophysics. This research was supported by financial grants and data from the Exxon Houston Production Company and Mr. Douglas Kenaley. I appreciate Dr. T.A. Blasingame and Mr. Paul White in the Department of Petroleum Engineering at Texas A&M for providing their Department resources, technical support, and encouragement. I would like to thank Dr. S.L. Dorobek, Dr. T.Tieh, Dr. R.R.Berg, Dr. P.D. Rabinowitz, Dr. Jim Mazzullo, and Dr. Willis in the Department of Geology and Geophysics at Texas A&M very much for their continuous constructive criticism and encouragement during this study. Additional thanks go to Wenwu He, Richard Lang, Jared Haight, Veit Matt, and Korean graduate students in the Department of Geology, and Mr. Duk-Hwan Ryu in the Department of Statistics for their endless concern.

Very special thanks go to Soyeon, Kevin, Jasmine, and my parents for their endless and unconditional sacrifice and support. I am also very thankful to the Lord God for carrying me to the end of this journey.

TABLE OF CONTENTS

LIST OF FIGURES

FIGURE Page

FIGURE Page

LIST OF TABLES

INTRODUCTION

The Permian Basin is one of the most important hydrocarbon producing region in North America. Sequence stratigraphic studies of thick carbonate successions in the Permian Basin showed that reservoir occurrence and internal properties could be better predicted where the stratigraphic section was understood in terms of a hierarchy of cycles related to multiple scales of sea level variation. Sequence stratigraphic variations in the evaporites successions on the carbonate platform have been treated as components of carbonate sequence stratigraphic models. Platform evaporite deposition is primarily controlled by brine level and salinity fluctuations rather than directly by changes in relative sea level (Figure 1). Methods of stratigraphic analysis developed for carbonate systems are not useful for the subdivision of platform evaporite successions because: (1) evaporites lack of biostratigraphic control due to few halotolerant organisms; (2) evaporites have very rapid sedimentation rates and complex stratigraphic relationships with the surrounding non-evaporite beds; and (3) evaporites commonly undergo intense early diagenetic modification and are prone to wholesale alteration after deposition (Kendall, 1992; Kendall and Harwood, 1996).

These factors make it more difficult to construct a sequence stratigraphic framework for evaporite deposits (Ball et al., 1971; Meissner, 1974; Bebout et al., 1987; Borer and Harris, 1989; Malicse and Mazzullo, 1990; Kerans and Nance, 1991; Mazzullo et al., 1991; Tucker and Chalcraft, 1991; Andreason, 1992; Kerans et al., 1993; Mazzullo et al., 1996)**.**

There have been few sequence stratigraphic studies for evaporite-dominated deposits formed in arid carbonate platform interiors. Such deposits are formed in the Queen Formation in Means Field and containing complex hydrocarbon reservoir and nonreservoir horizons. This sequence stratigraphic study on hydrocarbon reservoir quality in Queen Formation can be documented more detailed reservoir-nonreservoir sedimentary records and relevant reservoir controls in arid to semiarid carbonate platform interior.

This thesis follows the style and format of the American Association of Petroleum Geologists Bulletin.

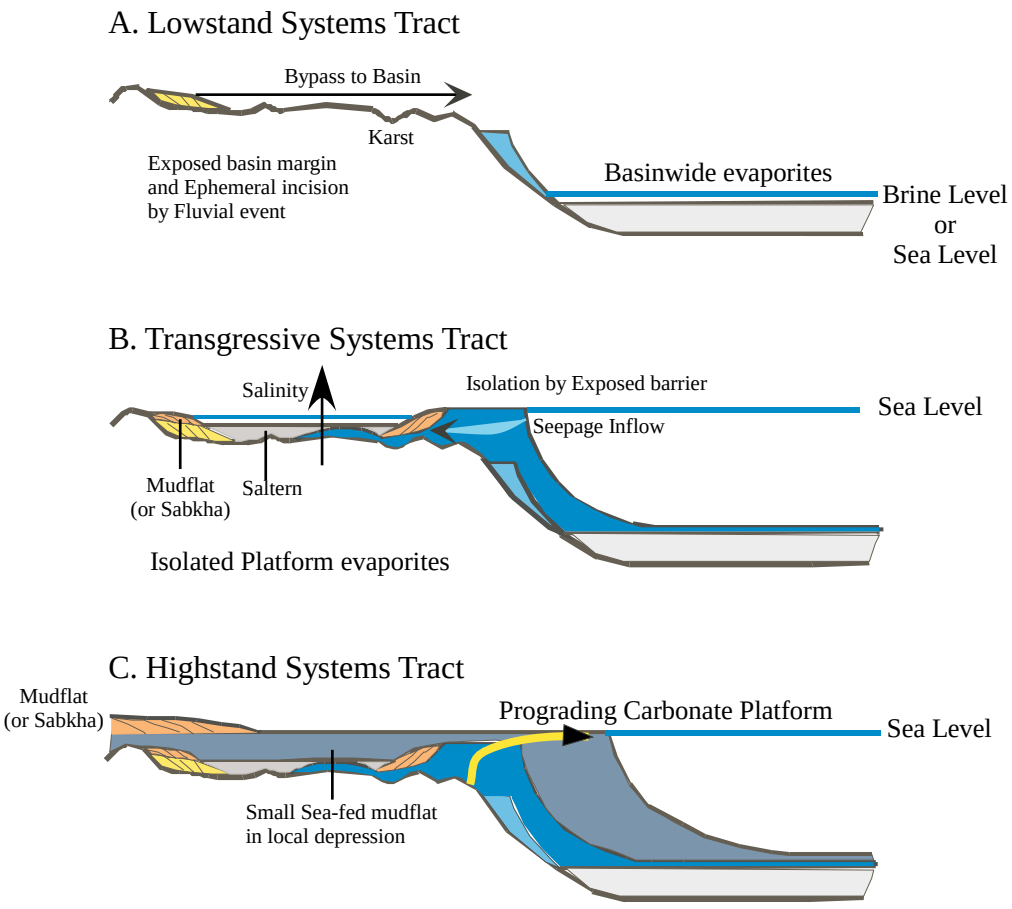

Figure 1. Sequence stratigraphic models for arid carbonate platform systems (After, Warren, 1999).

The Queen Formation is a minor producing interval in the Permian Basin, which has been under production since the 1930s. The Queen Formation is generally subdivided using old stratigraphic and sedimentological concepts (Tait et al., 1962; Ball et al., 1971; Meissner, 1974). The best Queen reservoir horizons were interpreted to be deposits of eolian environments (Nance, 1988; Major and Ye, 1992; Eide and Mazzullo, 1993).

This study examines the current viewpoints of the Queen multiple scale stratigraphic units and the lithofacies spatial distribution in evaporite dominant platform interiors, estimates quantitatively and visualize spatially the relationship between stratigraphic and other geological controls and static Queen reservoir properties by statistical analysis in order to provide a basis for further integrated reservoir descriptions of similar geologic setting, and addresses refined geological reservoir models using modern sequence stratigraphic concepts and integrated database.

REGIONAL GEOLOGIC HISTORY

The Permian basin of west Texas and southeastern New Mexico encompasses about 115,000 mi^2 (300,000 km^2). It is located in the foreland of the Marathon-Ouachita orogenic belt. The Sub-basins and uplifts include the Delaware Basin, the Central Basin Platform, the Ozona Arch, and the Midland Basin. Surrounding basin and uplift are Northwestern, Northern, Eastern Shelves, the Diablo Platform, the Val Verde Basin, Marfa Basin and the Marathon-Ouachita orogenic belt and the Devils River Uplift (Figure 2) (Ward et al., 1986; Yang and Dorobek, 1995).

The Delaware Basin was separated from the Midland Basin to the east by the Central Basin Platform. The Central Basin Platform was bounded to the west by the Diablo Platform, to the north by the Northern and Northwestern Shelf areas, and to the south by the Marathon orogenic belt. The Central Basin Platform between the Delaware Basin and the Midland Basin is composed of several fault-bounded structural zones arranged in a left-stepping, en echelon pattern. The origin of the Central Basin Platform is problematic. Different tectonic models have been proposed to explain its origin, varying from extensional, compressional and strike-slip settings. The Midland Basin bounded on its western side by the Central Basin Platform, and on the east by a complex series of north-south trending Fort Chadbourne Fault Zones, and to the south by Ozona Arch.

At the beginning of Phanerozoic, the entire Permian Basin area was located on the

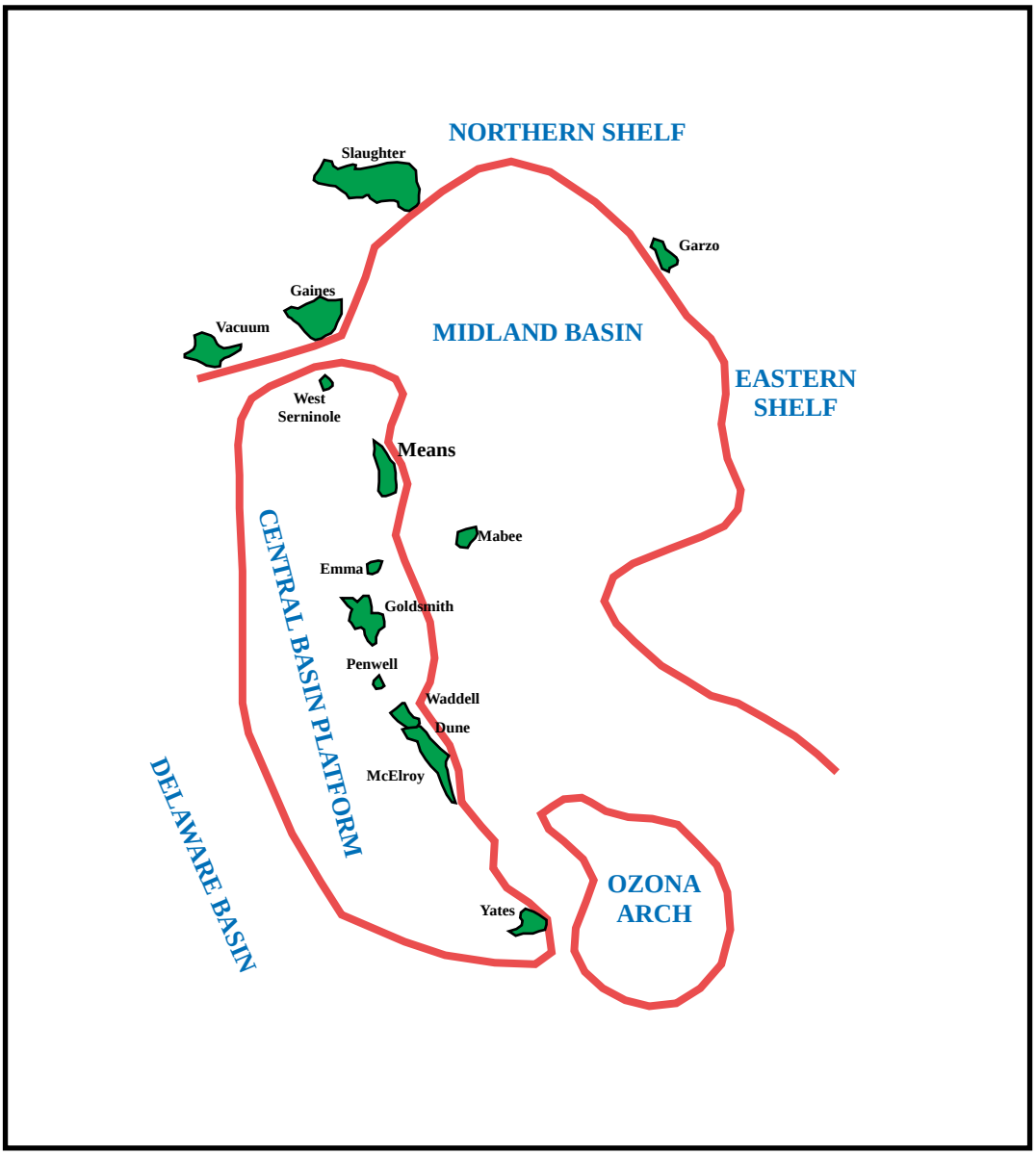

Figure 2. Tectonic elements and major San Andres/Grayburg producing fields in Texas.

southwestern portion of the craton. It gradually subsided during the formation of the shallow Tobosa Basin (Galley, 1958); an intracratonic, asymmetrical structural depression in the Precambrian basement at the southern margin of the North American plate. The Tobosa Basin was evidently a broad shallow, gently dipping structural feature filled with shelf carbonates and fine clastics (Hills, 1984). Tectonism remained relatively mild and uplifts were broad and gentle by the middle Mississippian.

During the Late Devonian Period, the North American craton was covered by shallow sea with sluggish circulation and slow sedimentation. The thick Woodford black shale, a major source rock in this region was deposited during this time. Deposition of the Woodford Shale continued into early Mississippian time.

At early Mississippian time, southward subduction of the northwest part of the South American continent proceeded initial stages of the Appalachian-Ouchita-Marathin orogeny (Hills, 1984). Differential asymmetrical subsidence due to vertical tectonic reactivation along lines of Proterozoic weakness during the Middle Mississippian Period led to the formation of the incipient Central Basin Platform. Asymmetrical subsidence of the Delaware Basin and differential sedimentation patterns continued in three major tectonic elements: the Delaware Basin; the Central Basin Platform; and the Midland Basin. Compression from the southwest caused the Central Basin Platform to uplift along reactivated steeply dipping reverse faults. Uplift of the Central Basin Platform shed fine clastic sediment that accumulated above early and middle Mississippian carbonates and black shales.

In the Early Pennsylvanian Period, the Delaware Basin was filled with deltaic sediment from uplifted area in central New Mexico to the northwest. Middle and Late Pennsylvanian, tectonic activity increased throughout the region and uplift of the Central Basin Platform peaked. Pennsylvanian faulting and differential subsidence was greater on the western part of the Central Basin Platform. The Delaware Basin formed, and became much deeper than the Midland Basin to the east (Bebout et al., 1987; Yang and Dorobek, 1995). Incipient carbonate platforms began to grow along the basin margin at the end of the Pennsylvanian Period.

Carbonate platforms developed around the edges of the Delaware Basin, the Central Basin Platform, and Midland basins during the Wolfcampian (Early Permian) as tectonism and associated widespread siliciclastic sedimentation of the Pennsylvanian Period died out. By the early Leonardian Period, initial carbonate ramps were already developing barriers along their seaward edge. Carbonate barrier at the platform edge evolved into distinct rimmed carbonate

margins (Ward et al., 1986). As high-energy grainstone bars and reefs developed along platform margins, platform interiors were restricted in circulation with open-marine water. This lead to low-energy carbonate and evaporite deposition in the Leonardian and Guadalupian (Late Permian) Stage. From the late Wolfcampian through the Guadalupian, the Midland and Delaware Basins were areas of siliciclastic sedimentation, whereas the platform and shelves filled with carbonates. A major change of basin configuration occurred during the Guadalupian Period. The rate of deposition of carbonate decreased on the Eastern Shelf, the Midland Basin, and the Central Basin Platform greatly reduced and this region became the site of cyclic sedimentation of sandstone, anhydrite, and halite. Since Late Permian time, the Central Basin Platform region has been stable tectonically. The Late Permian structural configuration of the Central Basin Platform region was similar to the present configuration.

Based on the absence of Jurassic or basal Cretaceous rocks in this region, intense subaerial erosion occurred. As a final episode of tectonic activity, Laramide orogeny during the Late Cretaceous strongly deformed rocks to the west, and tilted the basin farther to the east along the Precambrian zone of weakness (Hills, 1984). The Permian Basin has experienced relatively stable tectonic conditions since this last tectonic episode.

LATE PERMIAN STRATIGRAPHY

During the late Permian (Guadalupian), the Queen Formation was deposited across back-reef shelves in a semiarid tropical climate near the equator. The Queen Formation consists of complexly interbedded siliciclastic, evaporite, and carbonate successions of inner platform facies. The isolated carbonate platform of the Central Basin Platform was influenced by prevailing northeast trade winds (Walker et al., 1995a). The northeast winds may have influence environments on the Central Basin Platform (Walker et al., 1995a).

The Artesia Group consists of five Formations; the Grayburg, Queen, Seven Rivers, Yates, and Tansill from base to top (Tait et al., 1962). The Artesia Group consists of a broad band of shelf carbonates separating the narrow shelf-margin carbonates and sandstones from broader shelf-interior evaporite and sandstone facies. The Artesia Group is unconformably underlain by the Guadalupian San Andres Formation, and is unconformably overlain by the Ochoan Salado-Rustler Formation and the Triassic Dockum Group (Tait et al., 1962). The Artesia Group is the shelf equivalent of the shelf-marginal Goat Seep-Capitan reefs and the basinal deposits of the Delaware Mountain Group (Galloway et al., 1983 and Ross and Ross,

1987) (Figure 3). The Upper Queen, Shattuck sandstone Member is located stratigraphically adjacent to lower part of Capitan reefs (Tait et al., 1962; Meissner, 1974; Ward et al., 1986; Borer and Harris, 1991; Kerans et al., 1993; Walker et al., 1995a). The Grayburg and Queen Formations in Artesia Group are the major hydrocarbon reservoirs of many fields in the Central Basin Platform and the Northwest Shelf during the late Permian Period. The Queen Formation in Means Field is one of the major producing intervals in this area, which is located along a major productive trend on the eastern edge of the Central Basin Platform.

Previous stratigraphic studies suggested that the Guadalupian Artesia Group comprises a series of high-frequency sequences based on detailed studies of strata exposed in the Guadalupe Mountains: Grayburg and related Cherry Canyon units (G13, G14); Queen, Goat Seep and Cherry Canyon units (G15-G18); Seven Rivers/Bell Canyon sequence (G19-G21); Yates and Bell Canyon Formation (G22-G26); Tansill/Bell Canyon sequence (G27, G28) (Kerans and Nance, 1991; Kerans et al., 1993).

The Artesia Group contains four distinct lithofacies associations; (1) evaporite-dominated inner platform, (2) carbonate-dominated platform and platform margin, (3) carbonate-dominated slope, and (4) sandstone-dominated basin facies. The evaporite-dominated inner platform facies can be subdivided into evaporite/carbonate-dominated and siliciclastic-dominated lithofacies. The Tansill, Sever Rivers and Grayburg Formations are evaporite/carbonate-dominated deposits, whereas the Yates and Queen Formations are siliciclastic-dominated deposits. Previous studies have suggested that highstand carbonates and lowstand clastics were deposited with the fluctuation of low amplitude sea levels (Meissner, 1974; Sarg, 1981; Garber et al., 1989). The carbonate ramp Goat seep and Capitan reef evolved into a rimmed shelf during the Guadalupian time (Garber et al., 1989). A detailed outcrop study in the Guadalupe Mountains area suggests two major growth periods for the Capitan reef: progradation during Seven Rivers time and aggradation during Yates and Tansill time (Sarg, 1981; Garber et al., 1989; Sarg, 1989). These maximum progradation and aggradation of carbonate margins may be associated with changes in salinity and accommodation space on the back-reef (Garber et al., 1989; Sarg, 1989) (Figure 4).

The Queen Guadalupian Sandstone was named by Crandall (1929) for exposures near the Queen Post Office (T-24-S, R-22-E, Section 30) in the Guadalupe Mountains, Eddy County, New Mexico. Crandall did not designate a type section. The name Queen Formation is used in the subsurface for sandstones between the Seven Rivers Formation and the Grayburg Formation.

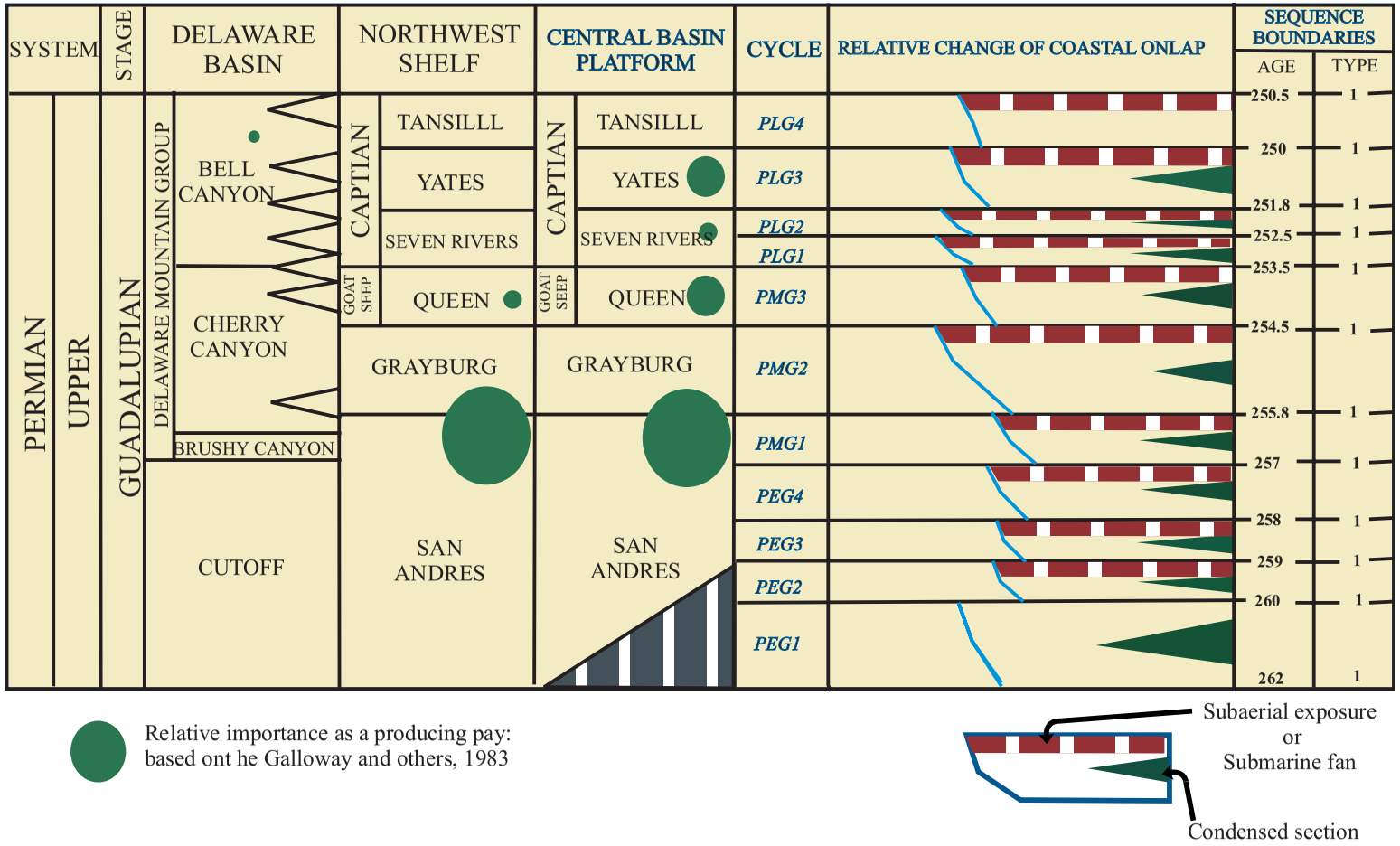

Figure 3. Chronostratigraphic chart of Guadalupian units of the Permian Basin (After, Galloway and others, 1983 and Ross and Ross, 1987)

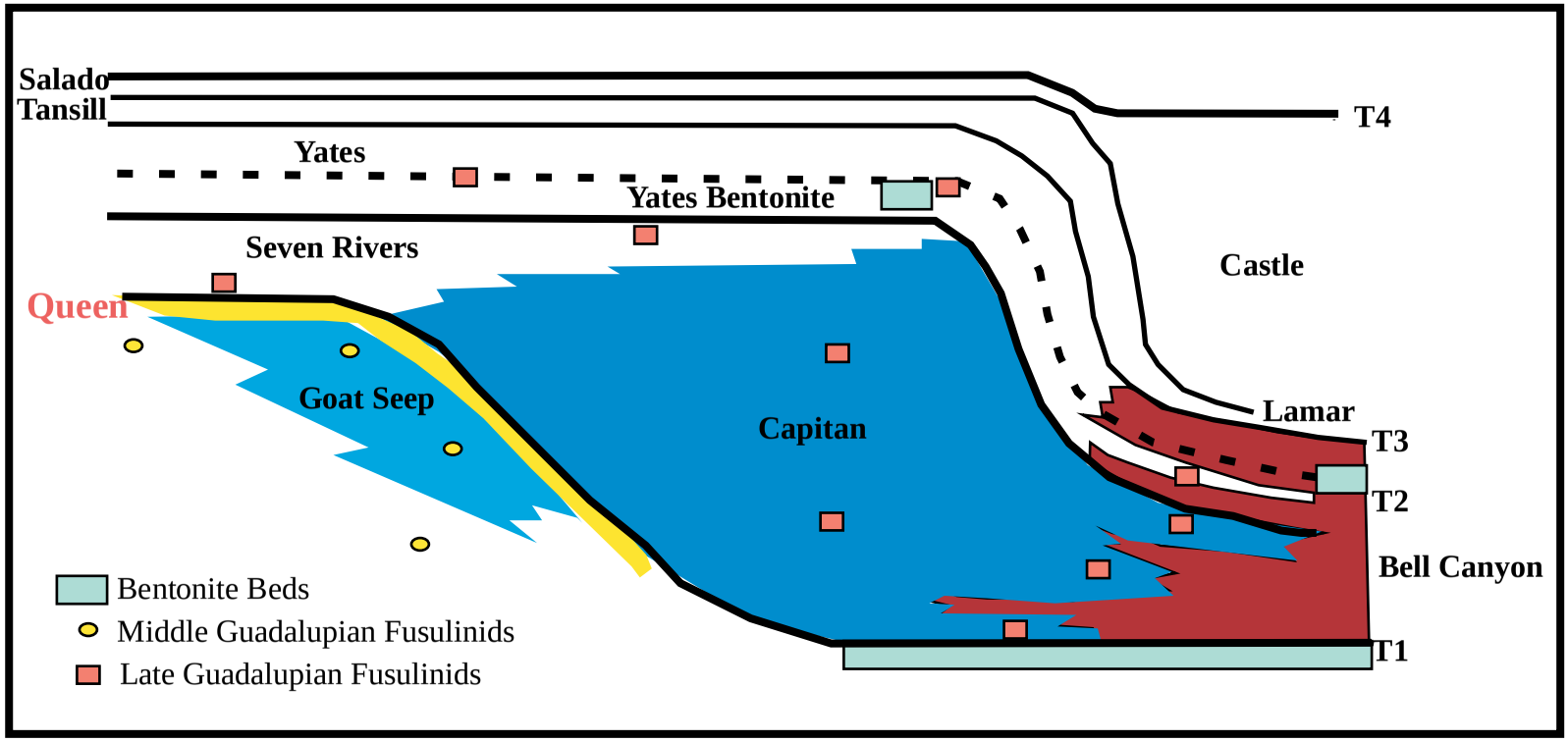

Figure 4. Cross section showing shelf-to-basin correlations of Late Permian strata. Time line are based on stratigraphic relations, correlation of bentonite beds and fusulinid biostratigraphy (After, Garber, 1989).

A type section for the Queen Formation proposed by Moran (1954) is located on the west wall of Dark Canyon in the SW/4 of Section 36, T-24-S, R-22-E of the Guadalupe Mountains. The Shattuck sandstone Member of Queen Formation consists of 99 feet (30 meters) of brown, red-brown and dark brown, cross-bedded and ripple-laminated, coarse-siltstone to very-fine-grained sandstone. Underlying the Shattuck Sandstone Member is 281 feet (85 meters) of fine crystalline dolomite. The basal clastic deposit (Penrose or McElroy Member) is 41 feet (13 meters) of distinctive, brown to red brown, cross-bedded, calcite cemented sandstones (Tait et al., 1962).

In Means Field, the Queen Formation is overlain unconformably by Grayburg carbonates, and is underlain unconformably by Seven Rivers carbonates and evaporites. The Queen Formation is part of the Artesia Group. Deposition of the Queen Formation occurred between 254.5 and 253.5 Ma (Upper Guadalupian) during a period of relatively stable tectonic activity and a greenhouse climate. Following extensive erosion at the Grayburg shelf edge, early Queen strata are evaporites and clastics deposited in the platform interior and relatively high-energy carbonates deposited along the platform margins (Fekete et al., 1986; Franseen et al., 1989). Late Queen deposits are the Shattuck Sandstone Member. The T1 biozone (characterized by *Parafufulina, Eopolydiexodina*, and *Leellafragilis*) is found in the upper Shattuck Sandstone Member in limestone and siliciclastic beds of the upper part of the Cherry Canyon Formation. The Shattuck Sandstone Member can be traced to the edge of the Goat Seep reef, down the foreslope of the reef, and into the Upper Guadalupian Basin (Garber et al., 1989) (Figure 4). Previous sequence stratigraphic studies of the Grayburg and Sever Rivers Formations suggested that the Queen Formation boundaries are regional sequence boundaries (Sarg, 1981; Fekete et al., 1986; Sarg and Lehmann, 1986; Franseen et al., 1989; Tucker and Chalcraft, 1991). Fekete (1986) and Franseen (1989) suggested that the base of the Queen Formation is major erosion surface in the Guadalupe Mountains area. Queen Formation is also floored by a high relief erosion surface into the Grayburg shelf, and that the upper Queen Formation progrades basinward over the Goat Seep Formation in the Bush Mountain area. In the southern end of the Central Basin Platform, Tucker and Chalcraft (1991) suggested that most of the siliciclastic deposits within the Queen Formation were related to increased detrital input during sea level lowstands, while carbonate deposition in this formation occurred during sea level highstands.

The Queen Formation in this study area consists of cyclic interbedded evaporites, carbonates, and siliciclastic lithofacies of fluvial delta and estuary, carbonate tidal flat, evaporite

coastal sabhka, and subaqueous salina environments formed in the arid climatic setting on a carbonate platform interior. High-frequency and low-amplitude eustatic sea level changes during this greenhouse period and associated brine level changes produced layer-cake evaporite-carbonate-siliciclastic cycles.

Depositional environments of the Queen Formation have been previously interpreted by Mazzullo and his students, and a few other workers (Ball et al., 1971; Mazzullo et al., 1984; Holley, 1988; Holley and Mazzullo, 1988; Nance, 1988; Mazzullo et al., 1989; Craig, 1990; Malicse and Mazzullo, 1990; Mazzullo et al., 1991; Tucker and Chalcraft, 1991; Major and Ye, 1992; Mazzullo et al., 1992; Eide and Mazzullo, 1993; Malicse and Mazzullo, 1996; Aller, 1999). They suggested arid to semiarid continental, coastal, and shallow marine depositional environments, including eolian, continental and coastal sabhka, fluvial- dominated deltaic, estuarine evaporites and clastic-dominated shelves. They indicated that eolian and fluvial sandstone facies of the upper Queen Shattuck sandstone Member are the best producing reservoir horizons in the Central Basin Platform and the Northwest shelf of the Permian Basin.

Evaporite-siliciclastic-carbonate Queen sedimentary successions have been related to lowstand bypass of clastic fluvial and eolian sediments and highstand carbonate deposition. Past studies concentrated mainly on sedimentological and petrological changes using few cores and well log data to determine lithofacies and diagenetic events in a lithostratigraphic framework. They overlooked dynamic sedimentation patterns between siliciclastic and evaporite deposition under the influence of fluctuating brine level and the climatic change. These lithostratigraphic studies had limitations for defining an accurate genetic reservoir framework.

Past sedimentological studies of the Queen Formation interpreted regional facies distributions in the Permian Basin (Mazzullo et al., 1984; Holley, 1988; Holley and Mazzullo, 1988; Malicse and Mazzullo, 1990; Mazzullo et al., 1991; Mazzullo et al., 1992; Eide and Mazzullo, 1993; Aller, 1999). Sedimentary environments represented by deposits in the Queen Formation can be summarized as follows: (1) Shattuck Member deposits in the Caprock and Central Cobrin Queen Fields of the Northwest shelf Fluvial, have been interpreted to be deposits of eolian and clastic-dominated sabhka environments (Malicse and Mazzullo, 1990; Mazzullo et al., 1991); (2) Deposits in the Magutex North, Mcfarland North, and Mcfarland Fields of the northeastern CBP have been interpreted to be deposits of fluvial, estuarine, and sabhka environments (Holley, 1988; Holley and Mazzullo, 1988); (3) Deposits in the upper Queen Formation of the Concho Bluff and Concho Bluff North Fields on the eastern side of the CBP

have been interpreted to represent fluvial and sabhka environments (Mazzullo et al., 1992); (4) Deposits in the Millard Field of the southeastern margin of the CBP have been interpreted to be eolian, sabhka mudflat, and shallow subtidal deposits (Mazzullo et al., 1984); (5) Deposits in the Ward-Estes Field of the western margin of the CBP have been interpreted to be deposits of the river-mouth bars with evidence of subaerial exposure, subtidal to intertidal lagoonal, and coastal sabhka facies (Eide and Mazzullo, 1993); and (6) Deposits in the Moose and Virey Queen Fields on the western side of the Midland Basin have been interpreted to be deposits of fluvial sand flat and fluvial-dominated sabhka, hypersaline lagoon, salina, and salt pan environment (Aller, 1999). Most reservoir sand bodies were reported to be secondary porosity, related to the dissolution of anhydrite and dolomite cements, and to partial dissolution of labile feldspar grains (Mazzullo et al., 1984; Holley, 1988; Holley and Mazzullo, 1988; Malicse and Mazzullo, 1990; Mazzullo et al., 1991; Mazzullo et al., 1992). Vertical and lateral lithofacies transitions between continental-dominated, coastal-dominated, and evaporite-dominated lithofacies occur in the different areas of the Northwestern Shelf, these studies of eastern and western parts of the CBP and Midland Basin can be used to understand a large-scale stratigraphic framework.

RESERVOIR STUDY

As the possibility of finding new large reserves in the Permian Basin diminishes, and as most hydrocarbon reservoirs in this region approach maturity, the efficient management and forecasting of remaining hydrocarbon reserves in producing fields requires more quantitative geological reservoir studies to reduce production cost. Recent advances in multidisciplinary hydrocarbon reservoir studies in industry reflect the economic importance of this type of study. Integrating diverse sources of information on reservoir heterogeneity into a predictable sequence stratigraphic reservoir framework is an important first step to improving petroleum reservoir management.

The goal of reservoir characterization is to develop a comprehensive picture of the three-dimensional distribution and continuity of rocks types, pores, and fluids. These variables control reservoir flow pathways and internal barriers (Sneider, 1990). Reservoir characterization requires qualitative and quantitative models of geological, geophysical, and petrophysical properties observed in core, well logs, and seismic data to define reservoir heterogeneities from local to basin scales. The construction of quantitative reservoir models requires: (1) prediction of accurate reservoir geometry; (2) estimation and prediction of petrophysical properties in wells;

and (3) interpolation of this variability regionally between wells (Griffiths, 1990; Moss, 1990; Pereira et al., 1990; Jian et al., 1994; Tinker, 1996). Reservoir description is a crucial building process for the basic skeleton of reservoir simulations that can predict remaining reserves and field economics.

Basic static descriptors of reservoirs are lithology, thickness and continuity of stratal units, depositional environments, depth, porosity, permeability, transmissibility, and fracture (Ebanks, 1987b). Reservoir quality is controlled by vertical and lateral of rock property distribution patterns (e.g., pore space and pore throat geometry). These properties reflect depositional textures, facies and rock types, and subsequent diagenesis. Deposits formed in different depositional environments can contain reservoir bodies with characteristic size, shape, and internal rock properties. Subsequent diagenetic modification of reservoir quality can follow flow paths left by the depositional fabrics and stratigraphic layers (Houseknecht, 1984; Scherer, 1987; Bloch, 1991; Boggs, 1992; Bloch and McGowen, 1994)

Previous studies addressing relationships between porosity, textural and compositional properties of sandstone suggested the following relationships (Rittenhouse, 1971; Beard and Weyl, 1973; Pettijohn et al., 1973; Lake, 1995; Evans et al., 1997; Primmer et al., 1997) (Figure 5): (1) porosity increases with increased sorting; (2) porosity increases as grain size increases; (3) porosity and permeability decrease when the amount of matrix and cement increase; (4) permeability of unconsolidated sand decreases as grain size and sorting decrease; (5) permeability is dependent on the variations in pore/pore throat geometry; and (6) the surface area of pores control permeability, and is also dependent on grain size, pore size, and pore throat (tortuosity). The size and amount of the intra-particle porosity are also major factors controlling permeability in carbonates (Lucia, 1983). These microscopic scale compositional and textural properties are easily obtained by sedimentological and petrological analysis. A sequence stratigraphic framework is constructed to interpolate local properties to reservoir and regional scales.

Compartments of reservoirs within non-reservoir units in specific depositional systems can be characterized by the specific vertical and lateral lithofacies successions. Variations can be interpreted in terms of fluctuations in accommodation through time, and by changes in relative sea level (base level) and other important geological forcing factors (tectonics, eustasy, and climate). During the 1970s and 1980s, the advent of seismic stratigraphy and subsequent concepts of sequence stratigraphy based on well logs, cores and outcrops improved our

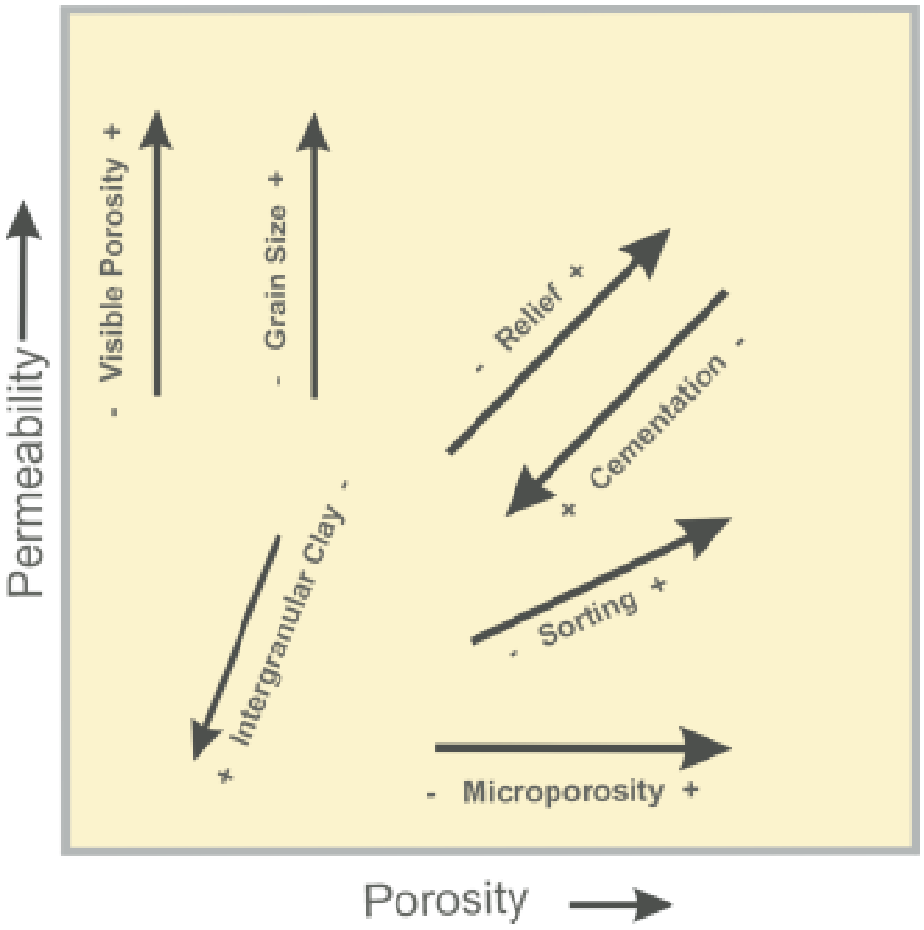

Figure 5. Effects of various geological controls on porosity and permeability (After, Ethier and King, 1991).

understanding of the effects of relative sea level on depositional cyclicity, facies geometry, and stacking patterns (Vail et al., 1977; Posamentier et al., 1988; Posamentier and Vail, 1988; Jervey, 1988; Van Wagoner et al., 1988; Galloway, 1989; Miall, 1989; Van Wagoner et al., 1990; Mitchum and Wagoner, 1991; Posamentier and James, 1993). Development of a high-frequency stratigraphic framework has increased the resolution of prediction of the spatial distribution of source, reservoir, and seal units. Conceptual geological models of facies associations within a high-frequency stratigraphic framework provide a foundation for construction of models of reservoir architecture and heterogeneity between wells. Forcing genetic mechanisms have been shown to affect the distribution of sedimentary bodies of various scales in specific depositional environments defined by chronological boundaries of a hierarchy of depositional strata. Few sequence studies have addressed platform and basinwide evaporites (Tucker and Chalcraft, 1991; Goodall et al., 1992; Strohmenger et al., 1996; Warren, 1999).

Deposits of genetic depositional systems that comprise reservoirs are characterized by the specific lithofacies distributions, which change with variation of accommodation space, brine level and degree of the isolation of the basin (Warren, 1999). The reservoir scale of sedimentary deposit is controlled by less than the 3rd order sea level cycles. 3rd, 4th, and 5th order relative sea level changes may be dependent on eustatic changes driven by Milankovitch's three principal orbital rhythms (eccentricity, obliquity, and precession) and by subsidence rate.

Milankovitch's cycle are thought to produce different relative sea level changes during icehouse and greenhouse climate periods. These differences may control the spatial distribution of evaporite lithofacies. Late Permian Queen evaporite-carbonate-clastic lithofacies successions formed during greenhouse periods. During greenhouse periods, low-amplitude sea level fluctuations (tens of meters for 2nd and 3rd order changes and meter-scales of the 4th and 5th order changes), contrast with high-amplitude sea-level changes during icehouse times (e.g., greater than 100 meters during the 4th and 5th order forcing processes) (Warren, 1999). Thus, the late Permian Queen Formation is expected to contain thicker and more layer-cake-like lithofacies successions.

Rates and magnitudes of eustatic changes control not only accommodation variations and the dispersal pattern for coastal and marine sediment, but also the ultimate base level (or graded profile) for fluvial systems and sediment entry points to deltaic regions. The graded profile of a river also controls the accommodation space for the alluvial environment (Quirk, 1998) and this is dependent on relief and climate in the hinterland (Boggs, 1992). Therefore, the

distribution of fluvial- and tidal-dominated sandstone in deltaic deposits of the Queen Formation can be interpreted to show an interaction between changes in the graded profiles and fluctuation of relative sea level.

This study used high-resolution sequence stratigraphy techniques and concepts to estimate vertical and lateral cyclic sedimentary transitions in order to define a genetic predictive stratigraphic framework, (Van Wagoner et al., 1988; Van Wagoner et al., 1990; Mitchum and Wagoner, 1991; Kerans and Tinker, 1997). Many previous stochastic reservoir descriptions and characterization studies start with a poorly defined classification of reservoir rocks from a geologic viewpoint (Hurst and Archer, 1986; Moss, 1990; Pereira et al., 1990; Jian et al., 1994; Dubrule, 1998). Mathematical simulations of reservoirs, using non-genetic reservoir frameworks, produce complicated models that may not predict reservoir variability accurately.

In order to accurately estimate and delineate relationships between primary and secondary geological genetic controls on a stratigraphic framework and construct realistic reservoir models, petrophysical reservoir properties must be distributed spatially within the petroleum reservoir framework. New advances in sequence stratigraphy with the development of computer technology make it possible to integrate reservoir information from various sources, and to construct an integrated relational database. Such an integrated database can elucidate spatial relationships between genetic geological processes and reservoir properties within stratigraphic framework (ESRI, 1992; Kerans, 1994; SAS-Institute, 1995; Tinker, 1996).

Geological descriptions of reservoirs is generally subjective, qualitative, conceptual-oriented, whereas geophysical and petroleum-engineering approaches tend to be more quantitative, but ignore genetic stratigraphic controls and lithofacies classifications. Those geological controls are also difficult to combine quantitatively with the geophysical and petrophysical responses of reservoir rocks.

Measured and calculated rock properties from well logs include porosity, water saturation and lithology. Seismic data can define large-scale bed geometries and physical properties such as acoustic impedance and amplitude. Because most log-derived porosity values and seismic responses are extracted from sonic velocity they are difficult to use directly to predict compositional and textural properties. The spatial distributions of geologic variations control the development of pore systems and permeability within a reservoir. There are intrinsic limitations of vertical and lateral resolution of most geophysical and petrophysical imaging and measurement tools.

Our understanding of interrelationships between genetic processes and reservoir properties remains at the beginning stage despite the work of Kerans and Tinker (1997) and Gardner (1999). More quantitative and less subjective approaches are required to interpret geological controls on petrophysical properties from well log data and seismic data. Such integrated studies are required to better predict and reconstruct internal structures in reservoirs (Dorfman et al., 1990; Griffiths, 1990; Doveton and Prensky, 1992; Bucheb and Evans, 1994). Previous studies have related geological and petrological properties based on well-log response (King, 1990; Doveton, 1994a; Doveton, 1994b). It has been proposed that the permeability of sandstone could be estimated empirically of a logarithm k plot of well-log response and porosity. Using this basic concept and a series of statistical analyses between various well logs and petrophysical rock properties observed in core (e.g., texture, facies, porosity, and permeability), genetic well log lithofacies (i.e., log facies) can be constructed to estimate permeability of hydrocarbon reservoirs (Jian et al., 1994; Lee and Datta-Gupta, 1999).

This research seeks to refine conceptual geological models of carbonate platform deposit to improve reservoir characterization and construction of relational database calibrated reservoir information. In order to achieve those goals, a geological-oriented hydrocarbon reservoir study must relate genetic stratigraphic divisions and petrophysical reservoir properties.

For solving the current problems of reservoir characterization this research has three major objectives: (1) construction of a genetic high resolution stratigraphic framework of carbonate platform deposits to improve reservoir characterization; (2) definition of geological controls on petrophysical properties at well locations, and (3) interpretation of geologic and petrophysical properties into a GIS-based relational database to visualize controls on reservoir quality. This study provides new insights into Queen Formation sand reservoirs, and for future studies of reservoirs in similar geologic settings. It provides a reference approach for further development of the Queen Formation and other deeper reservoirs in the Central Basin Platform in Permian basin in Texas.

FIELD HISTORY

Means Field is located five miles northeast of Andrews County, Texas. The study area spans approximately 25 mi^2 (65 Km^2) and covers the northern two-thirds of Means (San Andreas) Field (Figure 6). Means Field is part of a major productive trend on the eastern side of the Central Basin Platform. Other significant fields lying along the same eastern edge of the

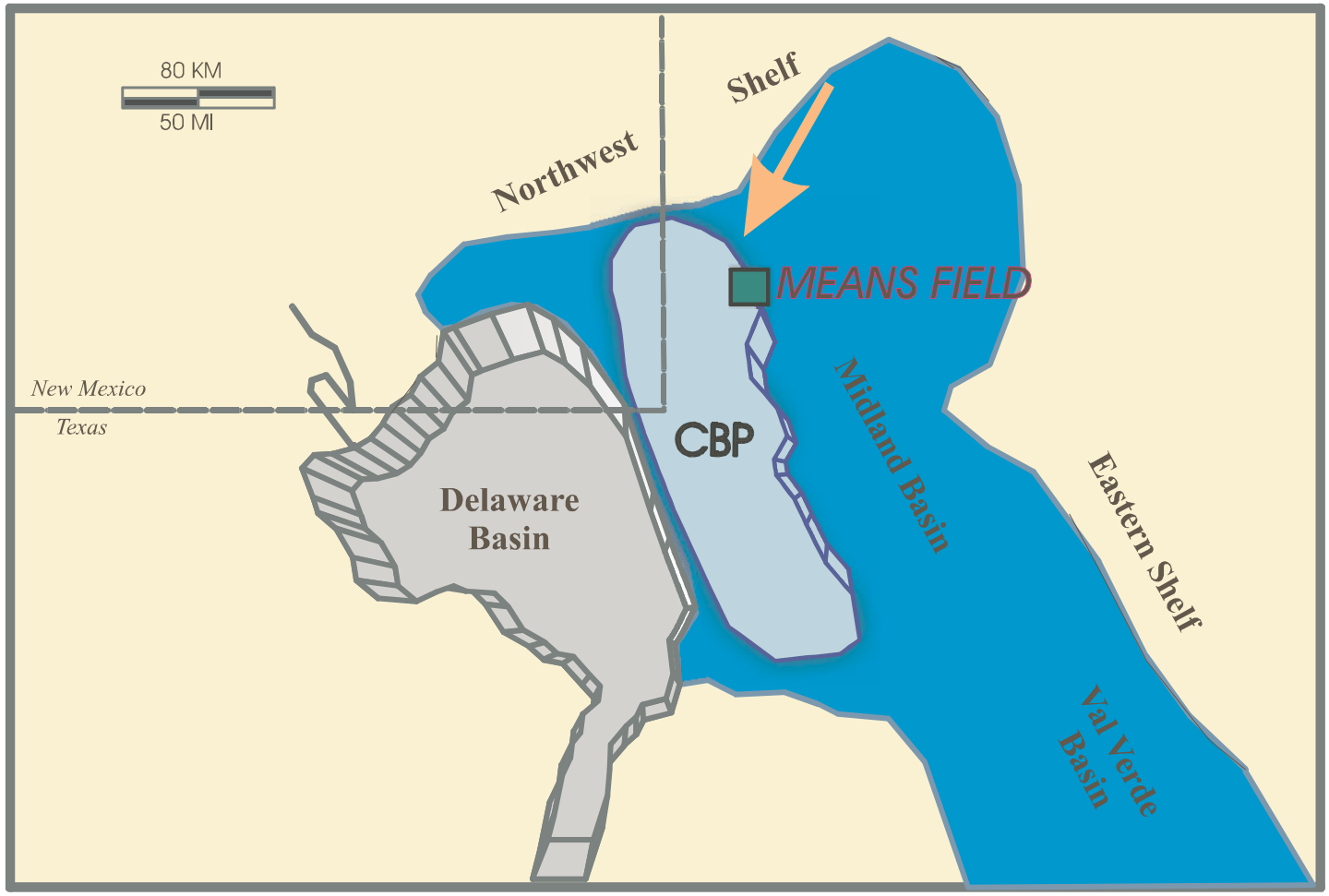

Figure 6. Map of Permian Basin of west Texas and southeastern New Mexico. Map shows the location of Means Field and other paleogeographic features. Arrow indicates paleowind direction (After, Walker, 1995a).

Central Basin Platform are Yates, McElroy, Dune, Cowden, Foster, and Goldsmith Fields. Those oil fields of eastern margin of the Central Basin Platform are mainly producing petroleum from the Grayburg and San Andres formations (Harris and Walker, 1990).

The first recorded oil show in the basal Queen sandstone in Means Field was in 1934 with a drillstem test of the J.S. Means No. 2 well (or MSAU 18-20) at a depth of 4100 to 4111 feet by the Humble Oil and Refining Company. After this first discovery and unofficial production from Queen and San Andreas Formation from these fields in 1934 and 1935 respectively, the field was drilled to 40-acre spacing. The first official Queen primary production was in 1957. During the late 1930s and early 1940s, the central part of the field was developed, while the southern region and field margins were developed in the 1950s. The field was defined as the Means San Andres Unit (MSAU) in 1963 with the first water injection.

Queen sandstone regained attention as a potential new pay zone after the results of R. M. Means No. 40 (or MSAU 9-06) well's drillstem test during the primary development of this field from 1954 to 1959. About 20 Queen wells had been completed in the end of 1954. Primary production reached a peak of 6200 BOPD in 1957, and declined to about 330 BOPD by 1959. The rapid decline of primary production of Queen sand reservoir was started to determine its original stock-tank oil in place and evaluate the economic on order to place secondary recovery by waterflooding.

The secondary recovery operation of hydraulic fracturing and peripheral water injection of Queen reservoir made production commercial in 1680 acres from 1960 to 1962. Excellent waterflooding results of Queen Formation were shown by increase oil production and decrease in the gas and oil ratio (GOR). The production of Queen reservoir increased 6500 BOPD in March 1963 with an average daily production of about 5000 BOPD. Determination of the original stock-tank oil in place (OOIP) for the area in 1959 was 72.9 Mbbls. Despite workovers for corrosion, casing failures, and frequent gypsum plugging, oil production declined to about 4650 BOPD in 1968 and water production increased. Even with a series of infilling drilling, the production results were disappointing. Means Field evaluations showed increasing net pay based on the cutoff value of permeability of 0.1 md and corresponding cutoff in porosity of 1%. After that a large-scale infill-drilling and pattern modification program was begun in 1976. By 1981, 14120-acre and 1610-acre infill wells had been drilled.

Currently about 1200 wells are located at Means Field. Of those wells, about 800 wells produce approximately 11000 BOPD from the San Andres, Grayburg, and Queen reservoirs. The

Queen reservoir includes 36 active wells and 88 inactive wells, and gross production is 275 BOPD. The ultimate recovery is estimated to be 34.3 million barrels of oil from the Means Queen reservoir-the fifth largest among Exxon-operated fields in the Mid-continent Division. The marginal Queen sand and San Andreas carbonate reservoir in this field has undergone CO_2 Tertiary recovery operation with ten-acre infill drilling since 1983 (George and Stiles, 1978; Brashear and Childers, 1984; Hoholick, 1984a; Bartel and Broomhall, 1986; George and Stiles, 1986).

The thickness of the Queen Formation in Means Field ranges from 264 to 417 feet, with an average of 351 feet (115 meters). It decreasing in thickness toward the southwestern reflecting what is assumed to be the antecedent topography at the base of the Queen Formation (Figure 7 and 8). Structure along the basal surface of the Queen Formation exhibits two main anticlinal domes (North Dome and the South Dome) separated by a structural saddle. The overall depth of the base of the Queen Formation deepens toward the east. The North Dome is structurally higher and has more prolific production than the South Dome at the San Andreas and Grayburg producing intervals (George and Stiles, 1978; Bartel and Broomhall, 1986; George and Stiles, 1986). The published regional seismic dip line through Means Field indicates an eastern thickening of the Queen Formation toward the Midland Basin to the east, and a distinct transition of parallel horizontal stratified clinoform in inner carbonate platform and downlaping clinoform in the platform margin and basin (Figure 9). The Queen Formation in Means Field was deposited on a very gentle, broad, inner carbonate platform. This lower erosional sequence boundary in Queen Formation was described by Fransen (1989) at the Guadalupian Mountains. The depth and gross thickness of the Queen Formation increase toward the northern part of the Central Basin Platform relative to the southern part of the Central Basin Platform (George and Stiles, 1978; Bartel and Broomhall, 1986; George and Stiles, 1986).

The basal Queen sandstone, the major producing interval occurs at depths of 4,000 to 4500 feet, and is called the Penrose (or McElroy) sandstone in the subsurface (Figure 8). Only the basal Queen Sandstone was cored. The basal sandstone ("Queen B sandstone" of Exxon) is easily recognized by its characteristic gamma ray, lithodensity, and neutron porosity log signature. It can be correlated laterally throughout the field and has been used as an essential reference datum for (1) determination of lithology. (2) calibration core porosity and permeability and well log porosity, and (3) calibration between well log data and compositional and textural properties.

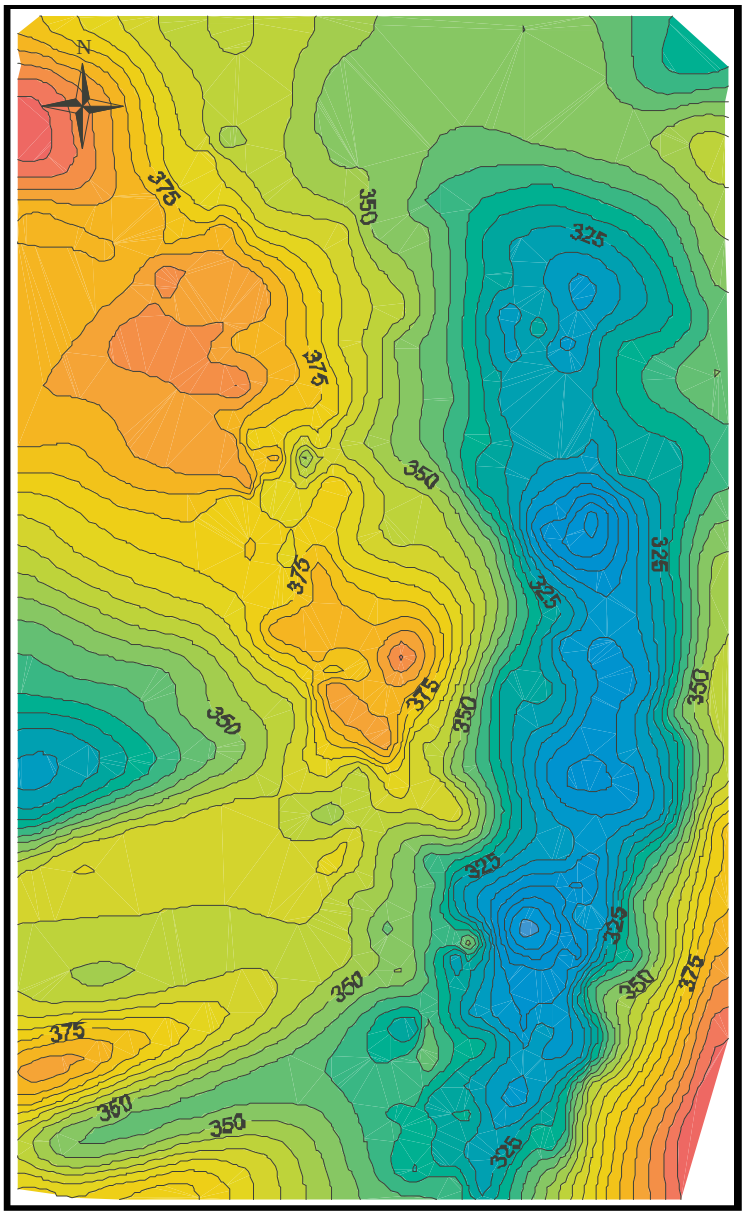

1 inch = 1.78 miles

Figure 7. Isopach map of Queen Formation. Note its decreasing thickness toward the south-western part of Means Field. Contour interval is 5 feet.

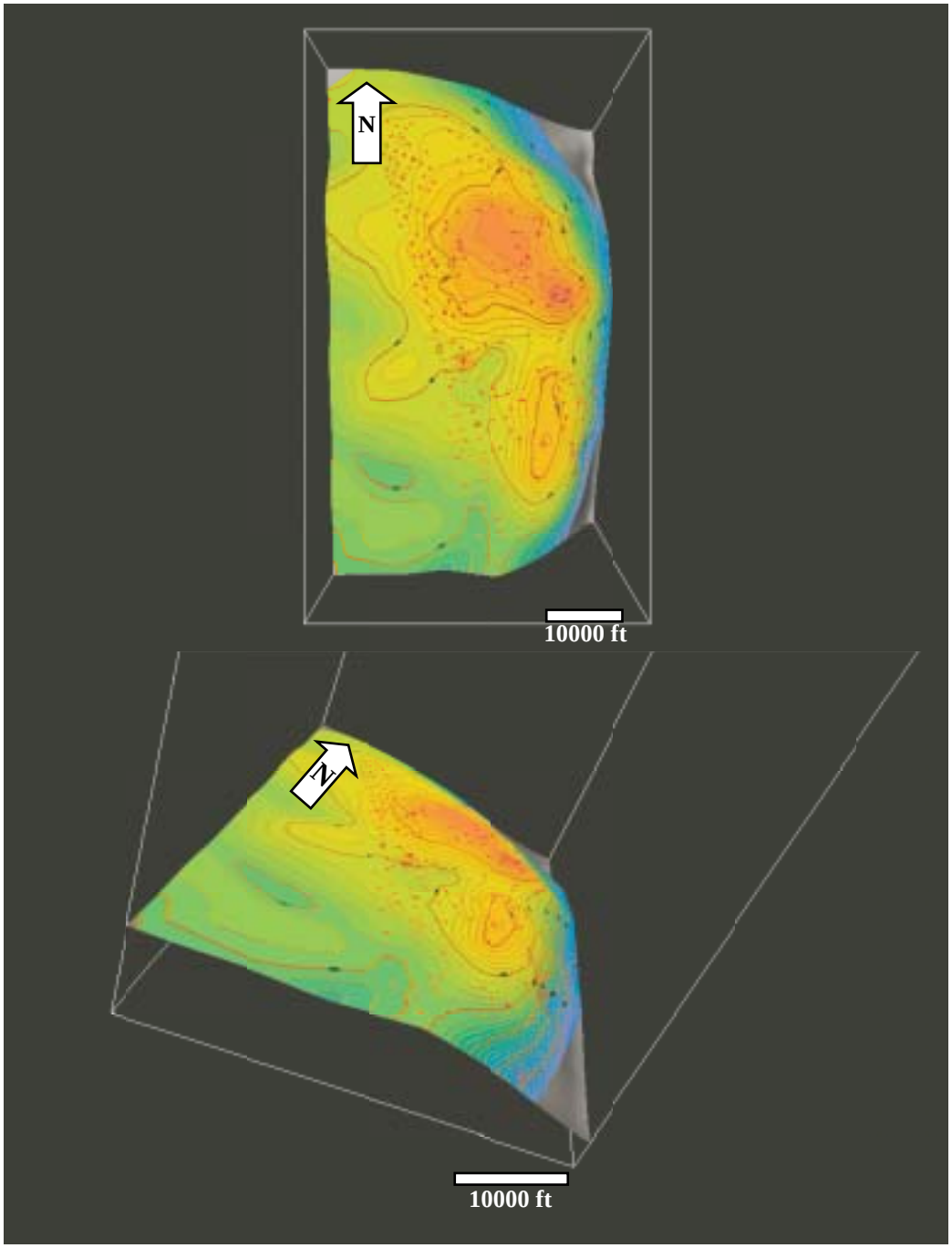

Figure 8. Three dimensional perspective views of the base of the Queen Formation.

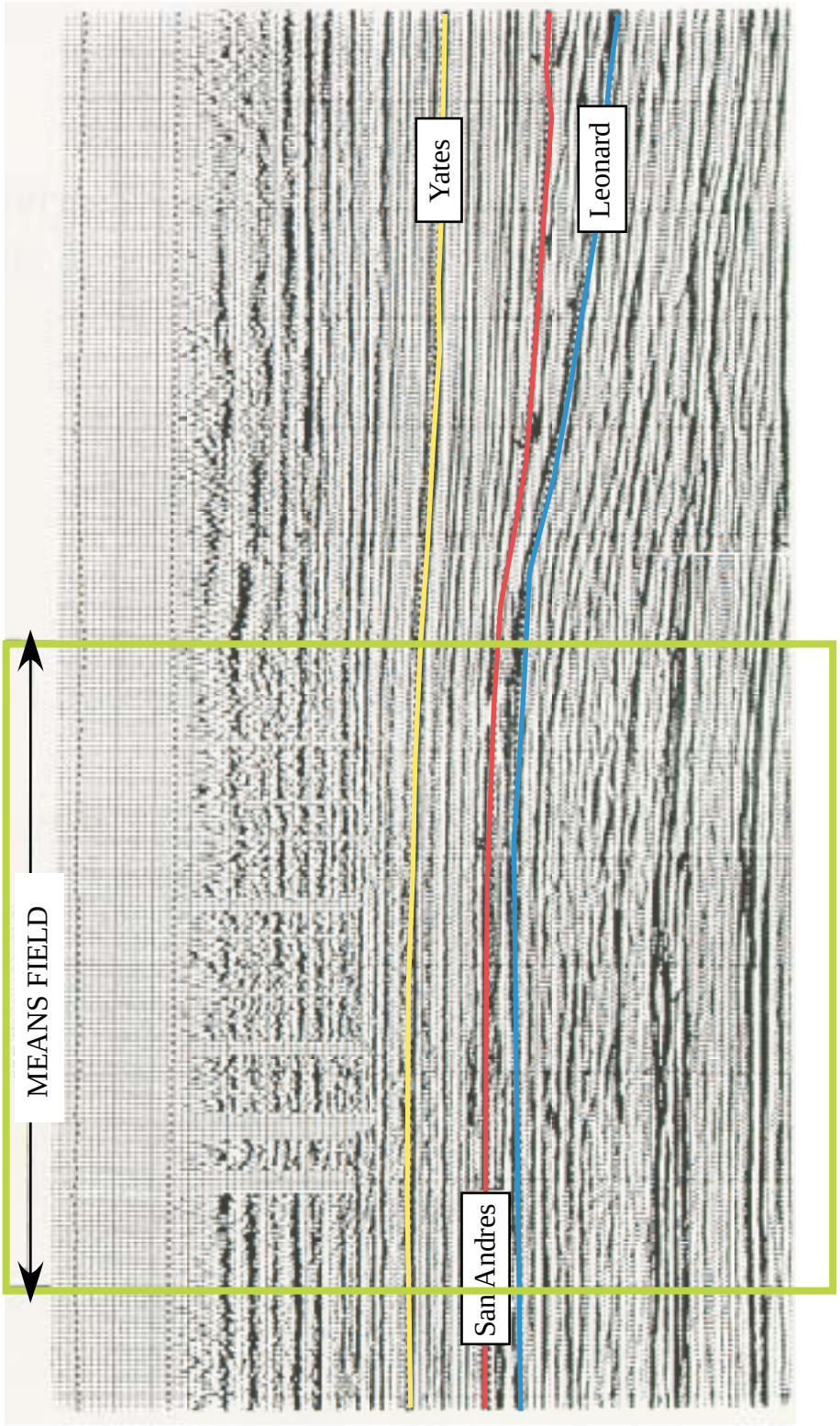

Figure 9. Dip seismic line of the Means Field (After, Bartel and Broohill, 1986).

Methodology

Data Base and Quality

This study examined cores and well log data from a well-developed reservoir in Means Field, west Texas. Data sets granted by Exxon, came from the Queen Formation reservoir sandstone in Means Field, Andrews County, in the northern part of the Central Basin Platform. The data consisted of 13 cored wells (1501 ft total), 350 thin sections, 100 petrophysical core analysis data, and 950 digital and analogue well-logs including gamma ray (GR), lithodensity (RHOB), neutron porosity logs (PHIN), and a few sonic (DT) and resistivity logs. Analogue well logs and petrophysical data sets were converted into digital data sets by digitizing constructing of the relational database.

Nine hundred and fifty well data sets were classified by well log types and ages (Table 1 and Figure 10). Of the total well data set available, data from 454 wells were chosen for examination in this study. Well density was 18.16 wells/mi^2 (6.97 wells/Km^2). Most well log data did not have log header information for borehole environments (e.g., resistivity of mud filtrate, mudcake, and drilling mud for environmental correction) except for Class 1 wells.

Work Flows

This study followed an iterative three-step workflow (Figure 11): (1) Petrophysical, sedimentological and petrological study started with the study of cored intervals. Well log responses were compared to petrophysical properties, thin-section, and core analysis data observed in core. Lithofacies, ideal vertical lithofacies successions, and stratigraphic cycles were defined. Textural and compositional properties in each lithofacies were determined by point counting and image analysis of thin sections. All available sedimentological, petrological, and petrophysical data at each wellbore location were complied in a relational database. Extensive error correcting was undertaken to assure accurate compolation; (2) Cross sections and maps of a hierarchy of geologic units and their internal petrophysical attributes were constructed; and (3) Visualizations of important geological and petrophysical properties in each stratigraphic unit and reservoir zone were examined. The observed geologic and petrophysical variability was interpreted in terms of genetic processes, and quantified by developing statistical summaries of different scales of heterogeneities.

Resources

Resources consisted of a digital camera attached microscope for image analysis and software of Media Cybernetic Inc. for image analysis, geological database software from

Table 1. Summary of well data in Means Field.

Types	Core	Well logs	Petrophysical data	Number	Characteristics
Class 1	Yes	Gamma ray, Caliper Neutron porosity Lithodensity Sonic Resistivity	Yes	12	Paper section Various vintage Mixed old and modern unit gamma ray and neutron porosity Whole Queen interval
Class 2	N/A	Gamma ray Neutron porosity Lithodensity	N/A	19	Digital format Modern unit gamma ray Modern unit neutron porosity Whole Queen interval
Class 31	N/A	Gamma ray Neutron porosity	N/A	193	Digital format Mixed old and modern unit gamma ray and neutron porosity Whole Queen interval
Class 32	N/A	Gamma ray Neutron porosity	N/A	230	Digital format Mixed old and modern unit gamma ray and neutron porosity Queen producing interval
Class 41	N/A	N/A	Yes	100	Queen producing interval

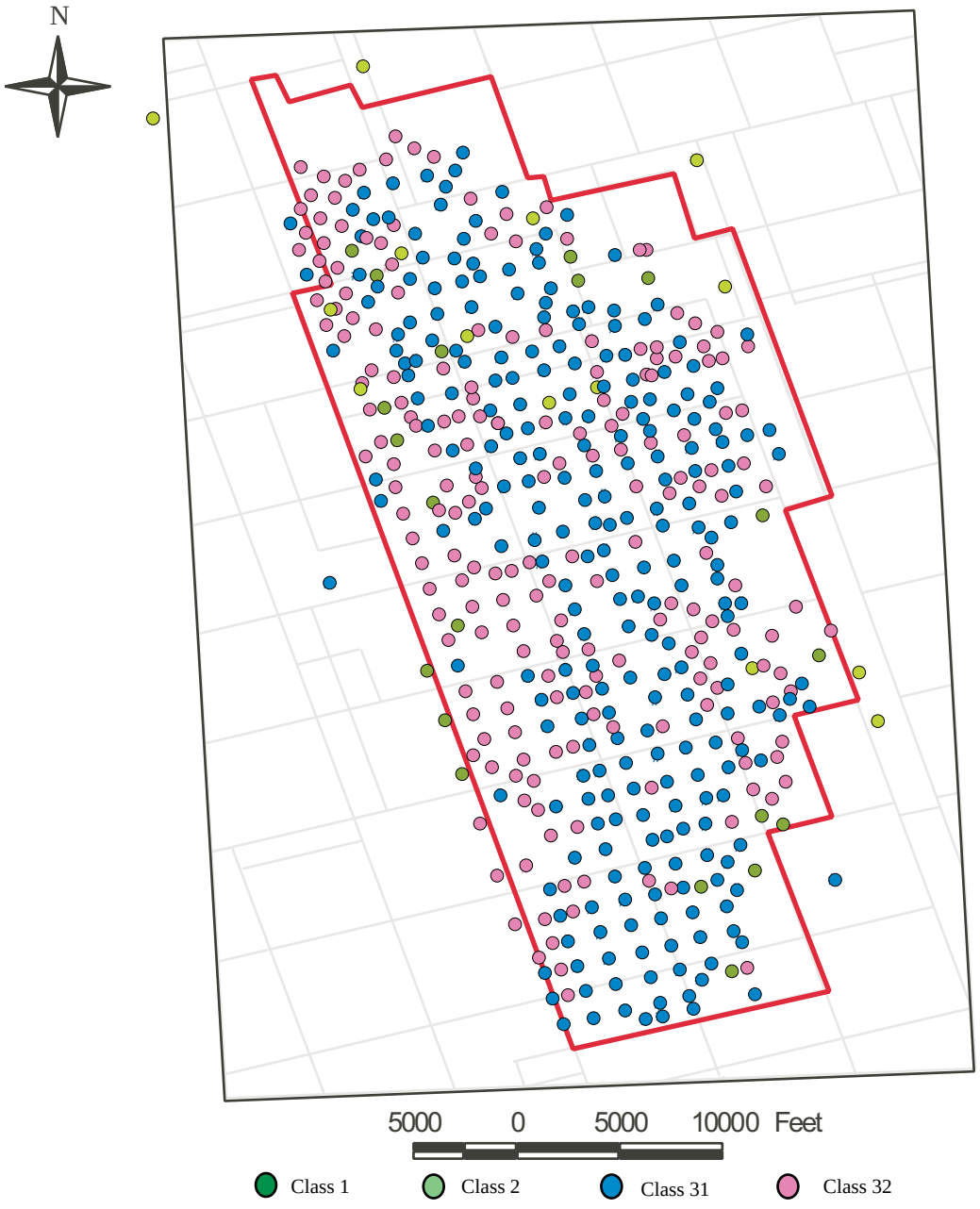

Figure 10. Well location map in study area showing Class 1, 2, 31 and 32 wells.

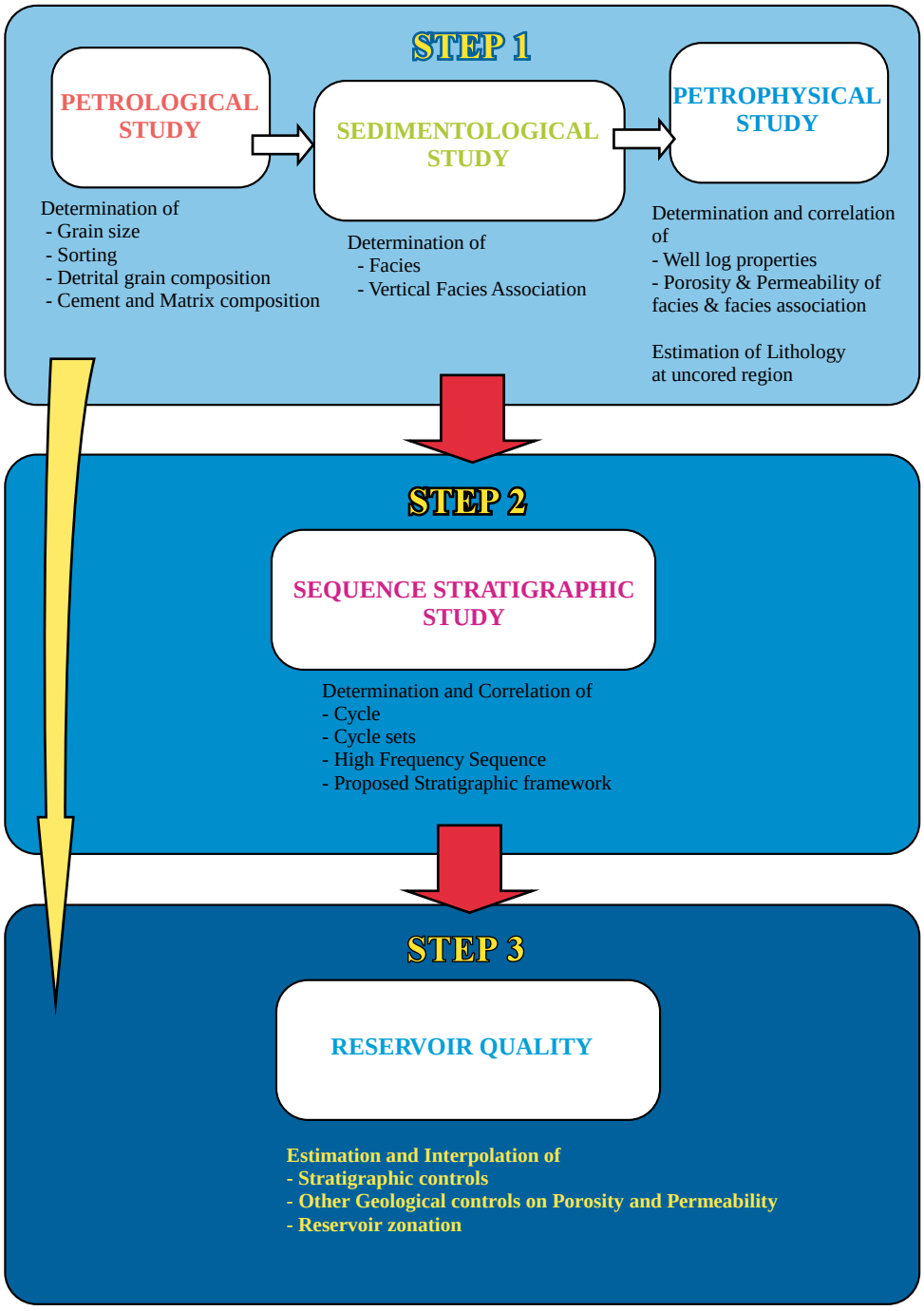

Figure 11. Generalized work flows and expected results.

Rockware Inc., a GIS relational data base system Arcinfo v.7, and Arcview v. 3.2 software of ESRI Inc., statistical software SAS v.8 of SAS institute, and petrophysical and well log interpretation software of GES Explorer, Geographix Inc.

FACIES

LITHOFACIES

Three lithofacies groups and 10 lithofacies are identified from the lower part of the Queen cored interval based on lithology, sedimentary structures, mineralogy, texture, and log signature (Figure 12 and 13). The four siliciclastic-dominated lithofacies are: (1) massive sandstone (facies S4); (2) cross and horizontal laminated sandstone (facies S3); and (3) bioturbated, cryptalgal wavy laminated silt- to sandstone (facies S2); and (4) laminated siltstone (facies S1). The three carbonate-dominated lithofacies comprise: (1) argillaceous dolomudstone (facies C3), (2) peloidal and skeletal dolowackestone to grainstone (facies C2), and (3) fenestral fabric dolomudstone (facies C1). The three evaporite-dominated lithofacies are: (1) mosaic bedded anhydrite (facies ECA); (2) nodular and enterolithic anhydrite (facies ES2); and (3) deformed wavy laminated silt- to mudstone (facies ES1).

Siliciclastic-Dominated Facies (Facies S)

Siliciclastic facies commonly occupied the base interval of the Queen Formation. The siliciclastic lithofacies comprise up to 30 to 40% of the Queen cored interval; its thickness ranges from approximately 10 to 40 feet (3 to 12 meters) in cores studied. The Facies S lithofacies group is one of the principal producing zones in this Means Field, along with the San Andreas and Grayburg Formations (Figure 13). Facies S deposits range in grain size from silt to very fine-grained subarkosic and arkosic sandstone with a minor amount of anhydrite and thin-bedded mudstone.

Facies S is subdivided into four major lithofacies: facies S1 of thinly laminated silt and mudstone; facies S2 of deformed wavy and cryptalgal laminated silt and very fine grained sandstone including some burrows and evaporite minerals; facies S3 of massive, planar cross-laminated, and thinly horizontal parallel laminated very fine- to fine-grained sandstone including small anhydrite nodules; and facies S4 of massive sandstone including rip-up mud clasts with scour and fill surfaces from top to bottom.

Detrital quartz grains are moderately well sorted to well sorted, with mean grain size ranging from 0.029 to 0.109 mm (with an average of 0.063 mm) and phi standard deviations of 0.49 to 0.51 (with an average of 0.5) (Table 2 and Figure 14). The largest grain size on average is 0.071 mm of facies S3, while the smallest grain size on average is 0.055 mm of facies S1. The vertical variation in grain size of the four-siliciclastic facies generally represents a slightly

Sedimentary Structure

Primary Structures

M Massive
Planar Horizontal Laminae
Planar Cross Laminae
Ripple Laminae
Wavy Laminae
Scour Surface
Cryptalgal Laminae
Rip-Up Clasts

Lithology

Lost Core
Siltstone
Sandstone
Gravelly sandstone
Argillaceous Dolomudstone
Dolomudstone
Peloidal or Skeletal Dolowackstone to Dolopackstone
Anhydrite

Secondary Structures

Deformed Wavy Laminae
Slump Structure and Contorted Bedding
Burrows
Bird' s Eye Structure
Collapse or Solution feature
Stylolite
Fractures
Pseudomorphic Anhydrite(Rosette Structure)
Nodular Anhydrite
Enterolithic Anhydrite
Chicken-wire mosaic Anhydrite
Dessication Crack

Bedding Contact

Sharp, planar
Gradational
Sharp, Wavy
— ? — Uncertain or Missing

Stacking Patterns

Base level fall
Base level rise

Figure 12. Symbols on lithostratigraphic sections.

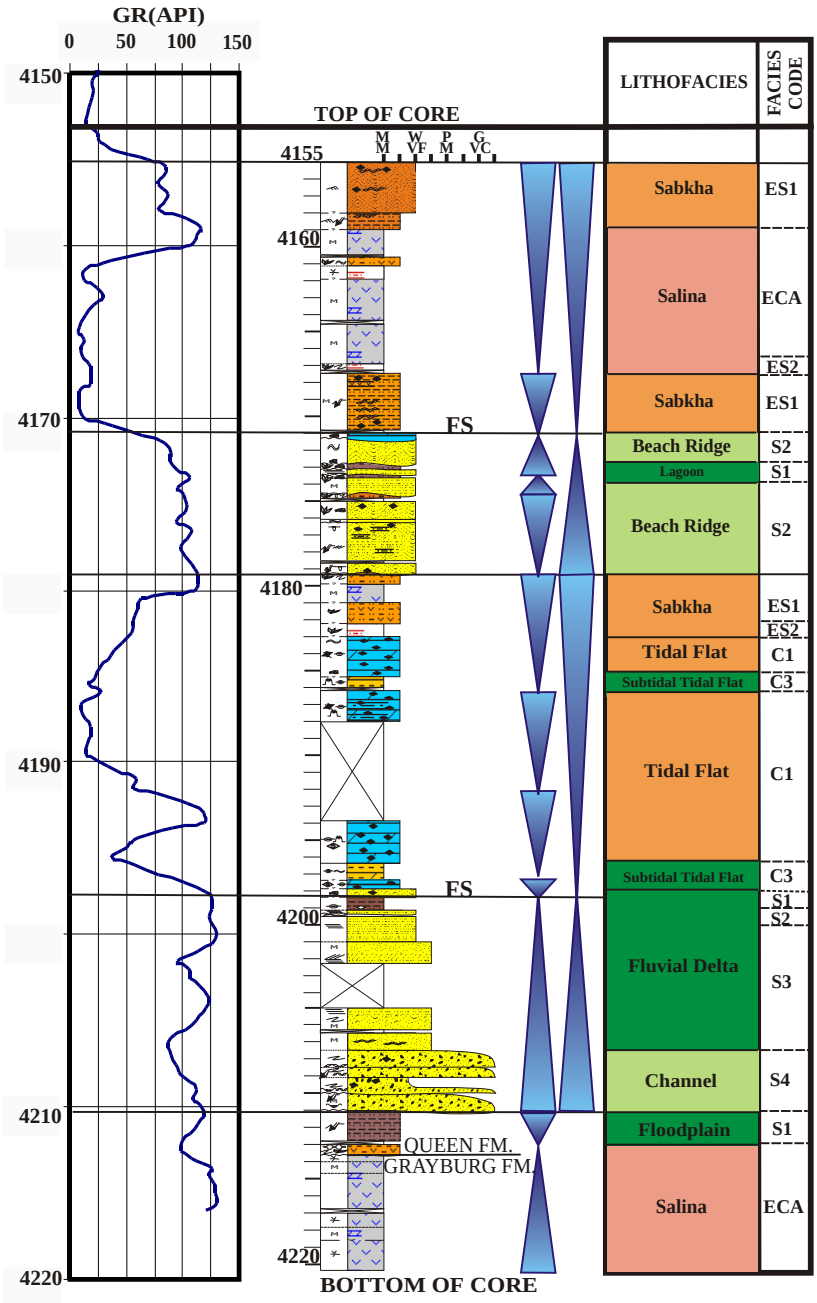

Figure 13. Lithostratigraphic log and gamma ray well log signature for Wentz 11 core. It shows the characteristics of the three lithofacies groups. Note the sharp contact between the Queen and underlying Grayburg Formation, and 2 feet depth difference between core and well log.

Table 2. Grain size analyses of siliciclastic-dominated lithofacies.

Facies	Mean Grain size (mm)	Max Grain size (mm)	Min Grain size (mm)	Mean Sorting (ϕ)	Max Sorting (ϕ)	Min Sorting (ϕ)
ES1	0.053	0.079	0.025	0.51	0.59	0.44
ES2	0.052	0.065	0.042	0.52	0.61	0.43
ECA	0.056	0.095	0.032	0.49	0.57	0.44
C1	0.062	0.107	0.029	0.54	0.73	0.43
C2	0.043	0.052	0.039	0.57	0.60	0.52
C3	0.073	0.106	0.039	0.52	0.57	0.47
S1	0.055	0.097	0.030	0.49	0.60	0.38
S2	0.067	0.109	0.040	0.49	0.77	0.38
S3	0.072	0.101	0.038	0.50	0.77	0.37
S4	0.058	0.092	0.033	0.51	0.63	0.42

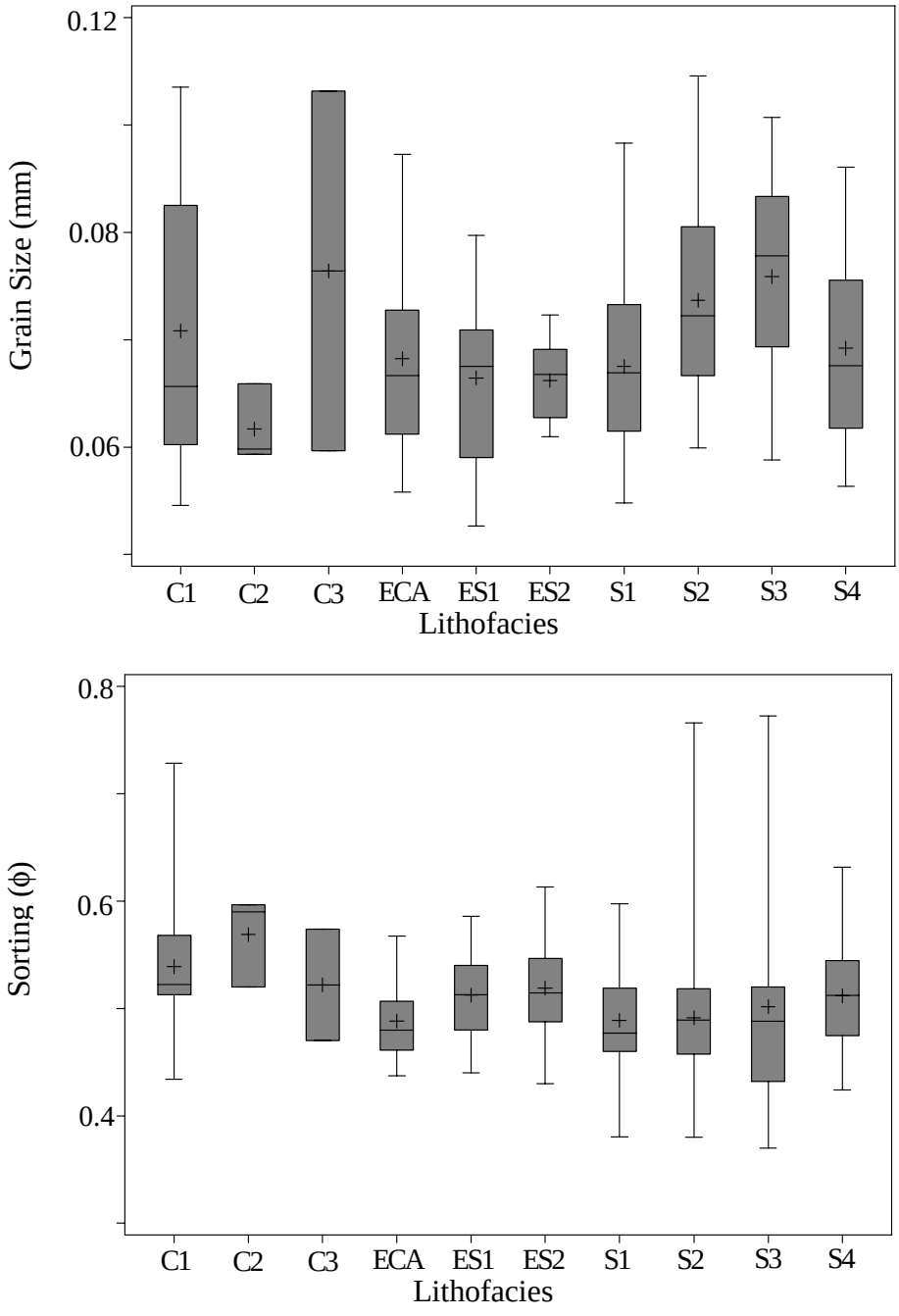

Figure 14. Grain size and sorting in lithofacies groups. The center of each box is the 50th percentile; margins of the boxes are the 25th and 75th percentiles; and whiskers denote the 0th and 100th percentiles. See Table 2 for statistical comparison of lithofacies group.

upward-fining trend from facies S3 (bottom) to facies S1 (top) of the cored interval in vertical. Clay minerals, although present throughout four siliciclastic facies, are not significant in terms of total bulk volume (Hoholick, 1984a; Pawlowicz and Bolger, 1983). Clay minerals are 5% of the Queen sandstone's composition in total bulk volume. Semi-quantitative x-ray analyses of siliciclastic lithofacies indicate the presence of four clay minerals: 44% of corrensite, 24% of kaolinite, 16% of illite, and 16% of chlorite in average. S.E.M analyses show that kaolinite and chlorite are principally pore filling authigenic clay. Illite is present in detrital shale clasts and corrensite is present as a clay mineral coating (Hoholick, 1984a; Pawlowicz and Bolger, 1983). Corrensite is an especially common magnesium-rich clay mineral in the clastic rocks of the Permian Basin, which indicates marine hypersaline environments in association with interstratified chlorite, smectite, and other evaporite minerals. The presence of a very thin (approximately one micron) veneer on all detrital framework grains has been reported.

Facies S are arkosic and subarkosic sandstones and siltstones with framework grains consisting of an average of 71% monocrystalline quartz, 24% feldspars, and 5% rock fragments. These grains are cemented by poikilotopic anhydrite and fine grained, subhedral to anhedral dolomite (Table 3 and 4, and Figure 15 and 16). Quartz content increases progressively from 64% in facies S1 to 80% facies S4. Feldspar content decreases from 32% in facies S1 to 16% in facies S4.

According to core analysis results, facies S are major producing reservoir intervals in this study area, with mean porosity ranging from 7.76 to 10.89 %, mean permeability in horizontal direction ranging from 3.42 to 22.5 md, and mean permeability in vertical direction ranging from 0.1 to 0.43 md. Of four siliciclastic lithofacies, facies S2 and S3 have higher porosity and permeability values than facies S1 and S4 (Table 5 and Figure 17).

Facies S1

Facies S1 is composed of greenish gray, dark greenish gray (5Y 3/2 to 5GY 4/1) to greenish black (5GY 2/1) thinly interbedded parallel laminated and wavy and planar cross-laminated silt- to mudstone (Figure 18). The thickness of facies S1 ranges from 1 to 5 feet (0.3 to 1.5 meter) in this study area. Individual silt-sized laminae show normal grading on a microscopic scale. Each lamina is separated by very thin, dark greenish black (5GY 2/1) clay laminae (Figure 18A, B, C and D).

Facies S1 is also disturbed by intensive bioturbation and evaporite cementation (Figure 18A, E and F). The lower, coarser part of facies S1 includes bioturbation structures but these are

Table 3. Composition of major detrital grain in Queen Formation lithofacies.

Facies	Mean Q (%)	Mean F(%)	Mean RF(%)	Max Q (%)	Min Q (%)	Max F (%)	Min F (%)	Max RF(%)	Min RF (%)
ECA	74	21	5	80	66	32	10	10	1
ES1	69	24	8	83	50	43	8	14	1
ES2	67	27	5	88	25	75	7	11	0
C1	74	20	6	80	68	26	14	12	0
C2	NA	NA	NA	NA	NA	NA	NA	NA	NA
C3	76	20	5	76	76	20	20	5	5
S1	64	32	4	86	42	54	10	12	0
S2	69	25	7	100	42	53	0	20	0
S3	70	24	6	82	59	36	12	13	0
S4	80	16	4	100	60	36	0	12	0

Table 4. Percent grains, matrix, and authigenic cements in Queen Formation lithofacies.

A. Quartz (%)

Facies	ES1	ES2	ECA	C1	C2	C3	S1	S2	S3	S4
Mean	32	21	28	31	NA	42	27	32	33	24
Maximum	41	39	38	43	NA	42	62	59	47	35
Minimum	16	1	19	7	NA	70	20	20	14	4
Standard Deviation	0.08	0.14	0.07	0.15	NA	NA	0.16	0.11	0.08	0.13

B. Feldspar (%)

Facies	ES1	ES2	ECA	C1	C2	C3	S1	S2	S3	S4
Mean	10	6	5	7	NA	11	10	10	11	7
Maximum	17	12	10	14	NA	11	20	18	16	16
Minimum	0	1	0	0	NA	11	0	0	6	0
Standard Deviation	0.05	0.04	0.04	0.05	NA	NA	0.06	0.05	0.03	0.07

C. Rock fragments (%)

Facies	ES1	ES2	ECA	C1	C2	C3	S1	S2	S3	S4
Mean	3	2	3	3	NA	3	2	3	3	2
Maximum	6	4	4	6	NA	3	7	8	8	4
Minimum	1	0	1	0	NA	3	0	0	0	0
Standard Deviation	0.02	0.02	0.01	0.03	NA	NA	0.02	0.02	0.02	0.02

D. Cements (%)

Facies	ES1	ES2	ECA	C1	C2	C3	S1	S2	S3	S4
Mean	45	62	43	23	NA	45	38	39	32	45
Maximum	60	88	65	47	NA	45	86	97	63	69
Minimum	25	39	0	0	NA	45	0	0	17	35
Standard Deviation	0.10	0.21	0.22	0.18	NA	NA	0.28	0.20	0.13	0.16

E. Clay (%)

Facies	ES1	ES2	ECA	C1	C2	C3	S1	S2	S3	S4
Mean	10	7	16	8	NA	0	6	5	2	13
Maximum	38	14	37	34	NA	0	50	39	7	23
Minimum	0	0	0	0	NA	0	0	0	0	1
Standard Deviation	0.13	0.05	0.12	0.13	NA	NA	0.14	0.08	0.02	0.11

F. Mica (%)

Facies	ES1	ES2	ECA	C1	C2	C3	S1	S2	S3	S4
Mean	2	1	2	0	NA	0	3	1	0	1
Maximum	5	3	5	1	NA	0	16	5	3	2
Minimum	0	0	1	0	NA	0	0	0	0	0
Standard Deviation	0.01	0.01	0.02	0.00	NA	NA	0.04	0.01	0.01	0.01

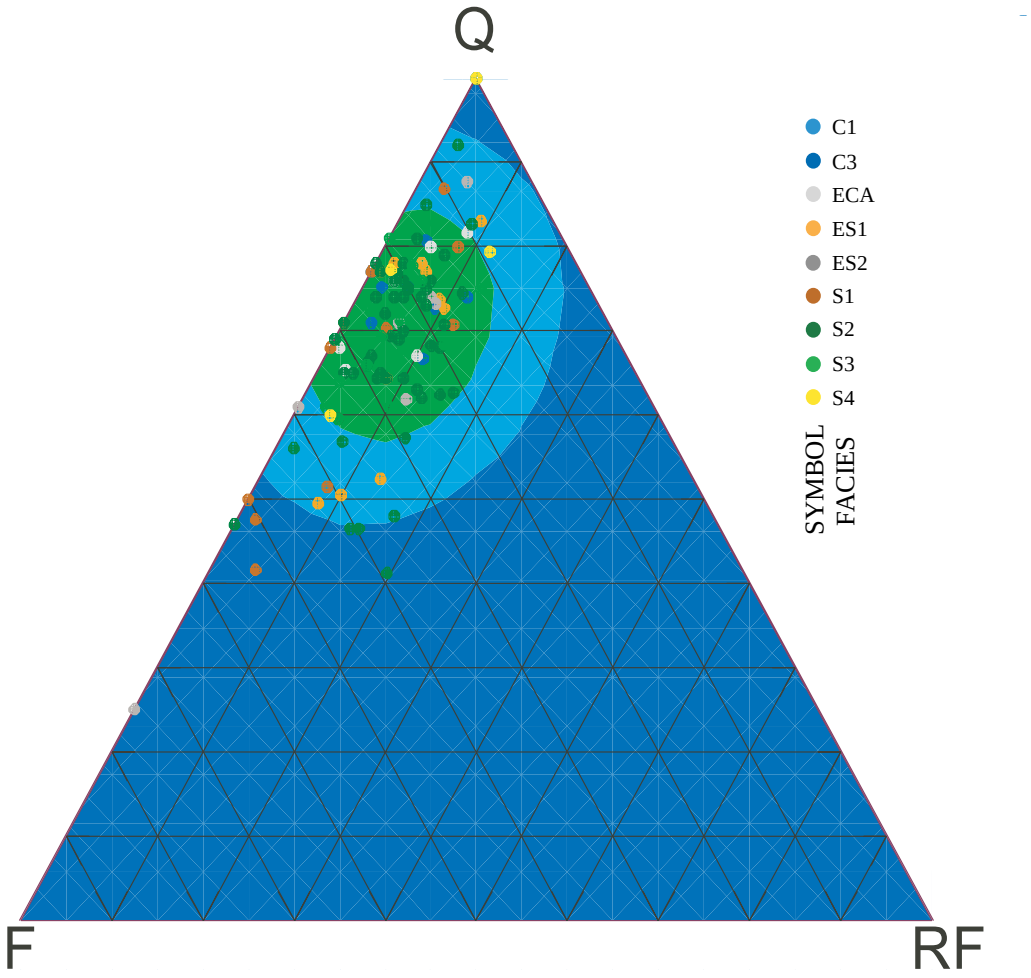

Figure 15. Petrology of Queen Formation siliciclastic lithofacies. See Table 3 for statistical comparison of lithofacies.

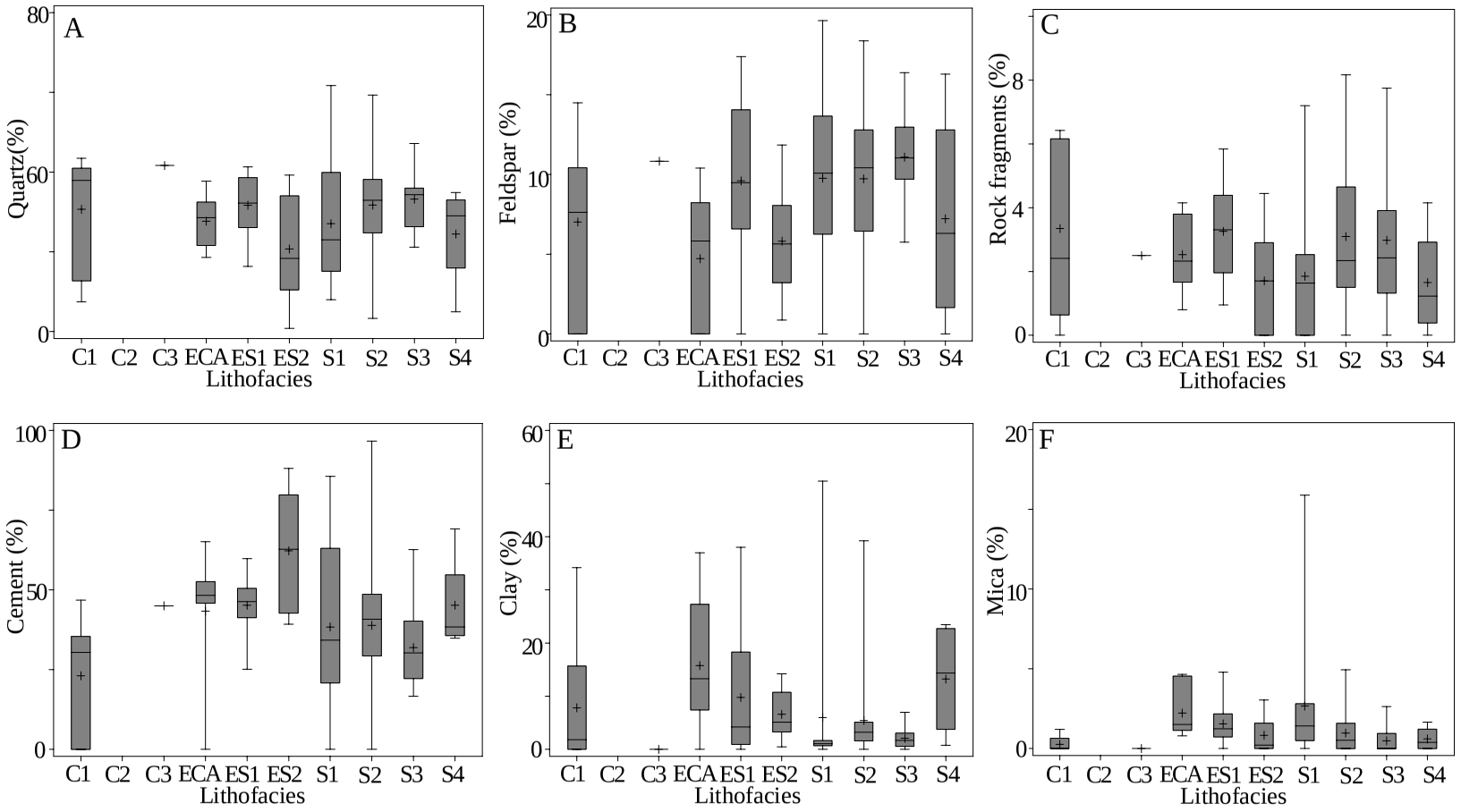

Figure 16. Properties of framework grains, matrix, and authigenic cement in lithofacies groups. The center of each box is the 50th percentile; margins of the boxes are the 25th and 75th percentiles; and whiskers denote the 0th and 100th percentiles. See Table 4 for statistical comparison of lithofacies group.

Table 5. Petrophysical properties of lithofacies .

A. Core Porosity (%)

Facies	ES1	ES2	ECA	C1	C2	C3	S1	S2	S3	S4
Mean	6.32	4.85	3.33	7.59	3.05	5.16	7.76	10.28	10.89	9.15
Maximum	11.30	10.80	9.70	15.10	5.20	8.00	21.70	25.60	21.60	22.10
Minimum	2.70	0.80	0.40	1.50	1.00	0.70	0.20	0.20	1.40	3.70
Standard Deviation	2.90	2.76	3.31	5.09	1.72	2.74	5.66	6.26	5.09	4.57

B. Core Permeability in horizontal direction (md)

Facies	ES1	ES2	ECA	C1	C2	C3	S1	S2	S3	S4
Mean	1.52	0.58	0.83	4.90	0.11	0.19	3.42	13.82	22.50	10.41
Maximum	4.80	2.90	6.10	15.00	0.16	0.55	34.00	145.00	204.00	115.00
Minimum	0.07	0.01	0.06	0.01	0.03	0.02	-0.10	-0.10	-0.10	0.10
Standard Deviation	1.75	0.80	1.71	6.05	0.06	0.22	7.84	24.20	41.96	30.33

C. Core Permeability in vertical direction (md)

Facies	ES1	ES2	ECA	C1	C2	C3	S1	S2	S3	S4
Mean	0.13	0.15	1.10	NA	NA	NA	0.26	0.21	0.43	0.10
Maximum	0.30	0.20	1.10	NA	NA	NA	0.80	0.90	1.10	0.10
Minimum	-0.10	0.10	1.10	NA	NA	NA	-0.10	-0.10	-0.10	0.10
Standard Deviation	0.21	0.07	NA	NA	NA	NA	0.34	0.25	0.61	NA

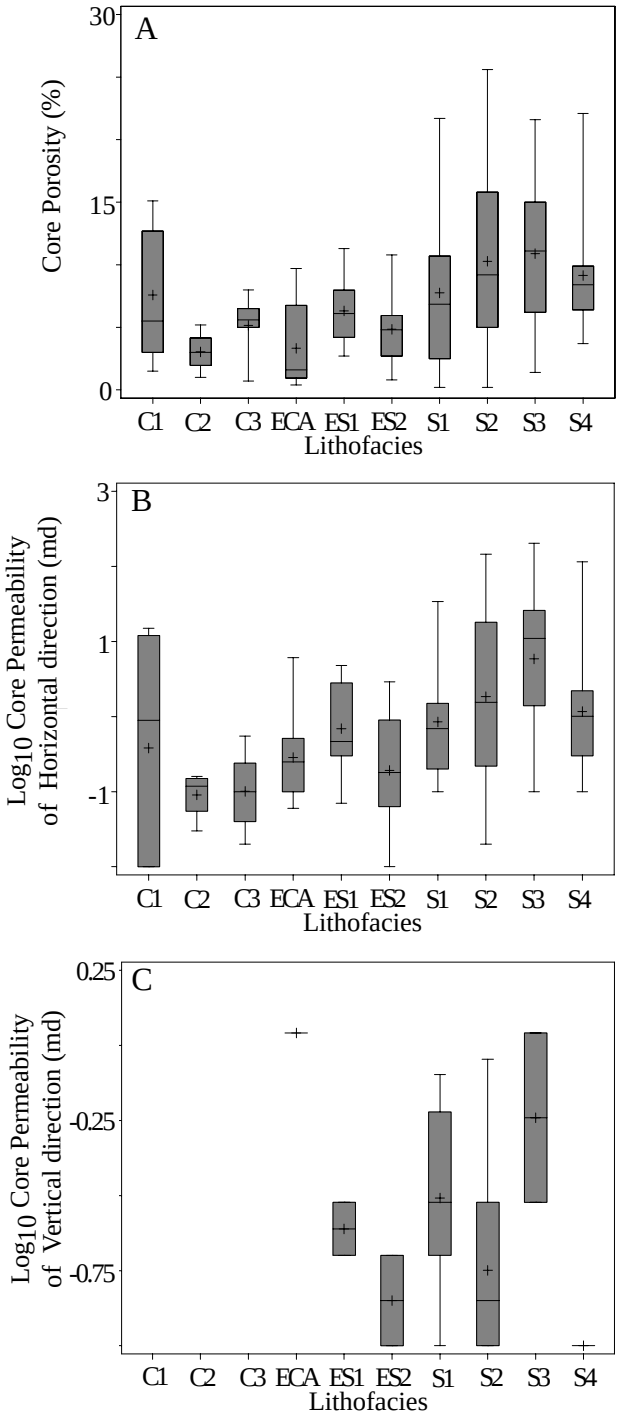

Figure 17. Petrophysical properties of lithofacies groups. The center of each box is the 50th percentile; margins of the boxes are the 25th and 75th percentiles; and whiskers denote the 0th and 100th percentiles. See Table 5 for statistical comparison of lithofacies groups.

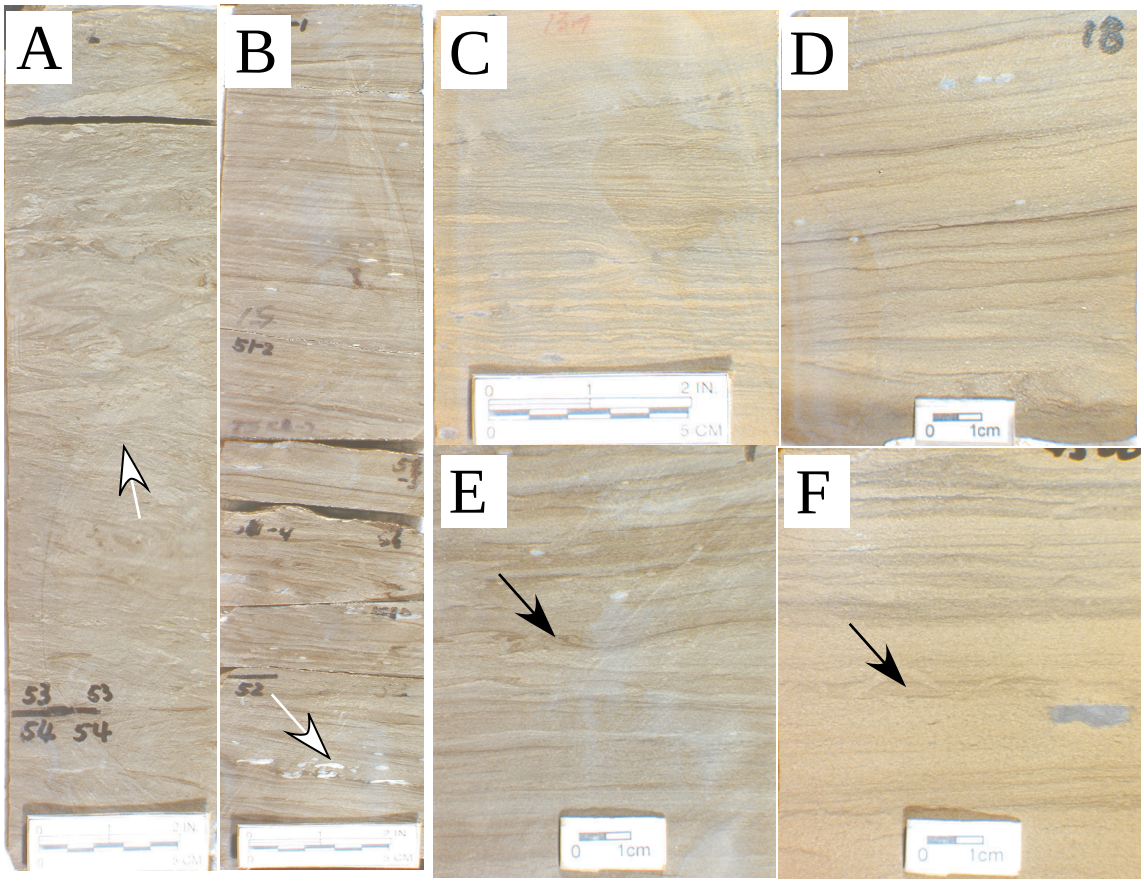

Figure 18. Sedimentary structures of facies S1. (A) JSM 300, 4553 to 4554 ft, bioturbated ripple cross laminated mudstone. Arrow indicates bioturbated structure. (B) JSM 300, 4550 to 4552 ft, parallel planar to slightly cross laminated mudstone and small anhydrite nodules (arrow). (C) JSM 23-19, 4128 ft, very thinly undulatory and planar laminated siltstone including little disturbed structures. (D) Dibrell 3, 4118 ft, slightly cross laminated siltstone including small anhydrite bleb. (E) JSM 300, 4549 ft, planar and disturbed wavy laminated mudstone to siltstone. Arrow indicates top of disturbed wavy laminae. (F) JSM 301, 4566 ft, parallel planar laminated siltstone to very fine grained sandstone. Arrow indicates burrow.

not pervasive in the whole facies S1. Some laminated facies S1 is disturbed by the growth of diagenetic anhydrite blebs, which are less than 1x1 inch (2.54x2.54 centimeters) in diameter (Figure 18B,D and E).

Facies S2

Facies S2 is composed of olive gray (5Y 5/2 to 5Y 3/2) to bluish gray (5B 7/1) bioturbated ripple cross- and wavy laminated to thinly cryptalgal-laminated silt- to very fine-grained sandstone (Figure 19). The thickness of laminae generally decreases upward. The thickness of facies S2 ranges from 1 to 8 feet (0.3 to 2.5 meters) in this study area.

Facies S2 commonly fines upward from thicker-bedded bioturbated or deformed, wavy laminated and massive very fine- to fine-grained sandstone with anhydrite nodules (Figure 19 C, D, E, F and G), thinly-bedded (0.25 to 5 centimeters) cryptalgal laminated silt-to very fine-grained siltstone and sandstone (Figure 19 H and I). A major portion of facies S2 is composed of the cryptalgal laminated deposits. Individual laminae are separated by very thin, dark greenish black (5GY 2/1) organic rich material or clay laminae. This laminated facies S2 is sometimes disturbed by syndepositional micro-faults and convolute lamination produced by liquefaction at the lower part of deformed or disturbed facies of S2 (Figure 19F and G). The cryptalgal-laminated siltstone to very fine-grained sandstone shows very thin laminae, including desiccation crack, which is not disturbed by any bioturbated activities (Figure 19H and I).

The wavy to massive basal deposits of facies S2 formed from deposition on wavy-rippled bed. The ripples and wavy-lamination were disrupted by intense bioturbation, syndepositional deformation (liquefaction), and the growth of anhydrite after gypsum at the bottom part of the facies. Sedimentary structures and bioturbation reflect deposition in a shallow subtidal to intertidal setting due to eustatic flooding or shelf submergence during relative sea level rises. These deposits are very similar to the homogenized facies of the Yates Formation (Andreason, 1992). Andreason (1992) suggested that the combined effects of seasonal marine flooding, eustatic marine flooding, and tidal pumping of the groundwater table at shallow depths formed similar disturbed facies.

The cryptalgal-laminated siltstone forming the upper part of facies S2 was not disturbed by any bioturbation, but was only deformed by heavy evaporite cementation. This resulted as water depth decreased and salinity increased, thereby decreasing the degree of bioturbation and allowing growth of halotolent microbial organism as browsing predators decreased in abundance. These evaporite-associated stromatolites and cryptalgalaminites were formed at the

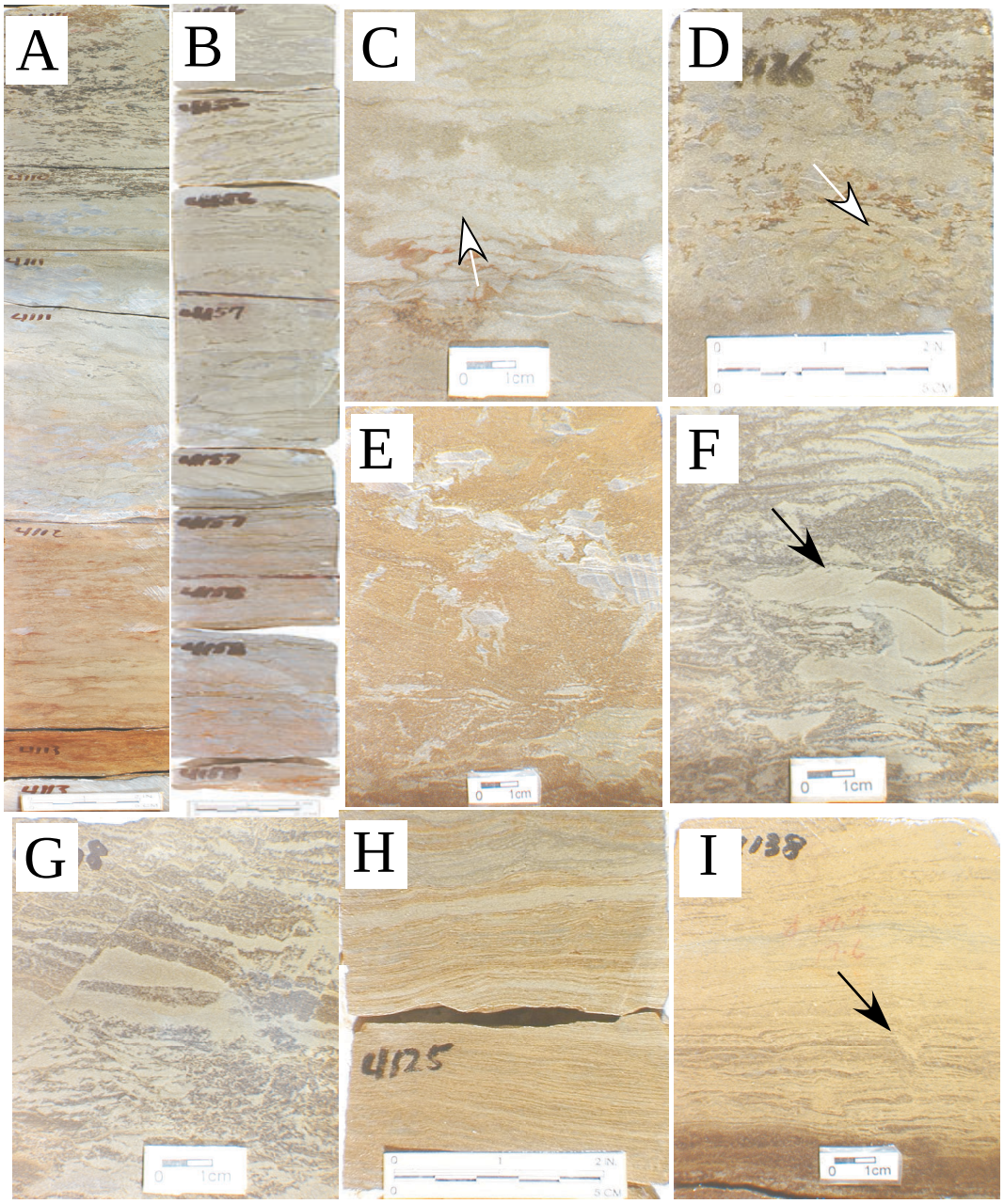

Figure 19. Sedimentary structures of facies S2. (A) JSM 23-19, 4110 to 4113 ft and (B) RMM 7-51, 4156 to 4158 ft, vertical facies transition of facies S2, showing underlying facies ES1 and ES2 with gradational or sharp bed contact. (C) Wentz 11, 4178 ft, and (D) RMM 7-51, 4126 ft, bioturbated disturbed laminated sandstone. Arrow indicates bioturbated structure. (E) JSM 23-19, 4143 ft, anhydrite filling burrow. (F) Wentz 11, 4177.1 ft, fluidized structure in disturbed laminated sandstone (arrow). (G) Wentz 11, 4177 ft, syndepositional deformed structure of facies S2 including microfault and collapsed breccia. (H) RMM 7-51, 4125 ft, very thinly cryptalgal laminated siltstone. (I) JSM 23-19, 4138 ft, thinly cryptalgal laminated siltstone including desiccation crack (arrow).

mudflat and littoral margins of saline and alkaline playas during the Phanerozoic era (Hardie and Shinn, 1986; Warren, 1999).

Facies S3

Siliciclastic facies S3 is composed of yellowish gray (5Y 7/2) to bluish white (5B 9/1) massive, cross-laminated, or planar-laminated, very-fine-grained sandstone (Figure 20). Beds thickness ranges from less than 0.5 to 1 inch, and decreases upward. Distinct bioturbated structures were not observed. The thickness of facies S3 ranges from 4 to 20 feet (1 to 6 meters).

Facies S3 fines upward slightly. A complete upward progression from massive sandstone to cross-laminated, very-fine- to fine-grained sandstone and siltstone (Figure 20A, B, C and D), or parallel-laminated silt-to very-fine-grained sandstone (Figure 20E, F and G) occurred where facies S3 is in the western part of the study area. Elsewhere incomplete successions consisting of ripple-cross-laminated and planar-laminated silt- to very-fine-grained sandstone comprise facies S3.

The massive very-fine-grained sandstones at the base of facies S3 rarely included cross lamination and commonly contained rip-up mud clasts of facies S4 (Figure 20A and B). The thickness of massive sandstone ranges from 1 to 2 feet (0.3 to 0.6 meters). Primary structures were obliterated by intense cementation. Evaporite cementation in massive sandstone facies is mainly tiny anhydrite growths, less than 0.1x0.1 inch (0.25x0.25 centimeters) in diameter.

The massive sandstone grades upward to beds of cross-laminated very-fine-grained sandstone and siltstone that are 2 to 3 feet (0.6 to 1 meters) thick (Figure 20C and D). Cross lamination has low-angle foreset dips, ranging from 10 to 20 degrees and individual sets are about 1 inch thick. This cross-laminated sandstone was deformed by pervasive evaporite cementation, and it is very similar to the deformed wavy lamination of above facies S2. Thinner bedded (0.15 to 0.3 meters) cross-laminated deposits commonly contain climbing ripple cross strata.

Beds of planar laminated sandstone at the top of facies S3 ranges in thickness from 1 to 3 feet (0.3 to 1 meters) (Figure 20A, E and F). Individual laminas is separated by very thin, dark greenish black (5GY 2/1) clay laminae, and are deformed by anhydrite nodules (Figure 20G). The clay fraction is greater in these deposits than in the massive or cross-laminated sandstones, producing a slight upward-fining trend within beds of facies S3. These less permeable silts to sandstones lack extensive evaporite cementation (Figure 20A).

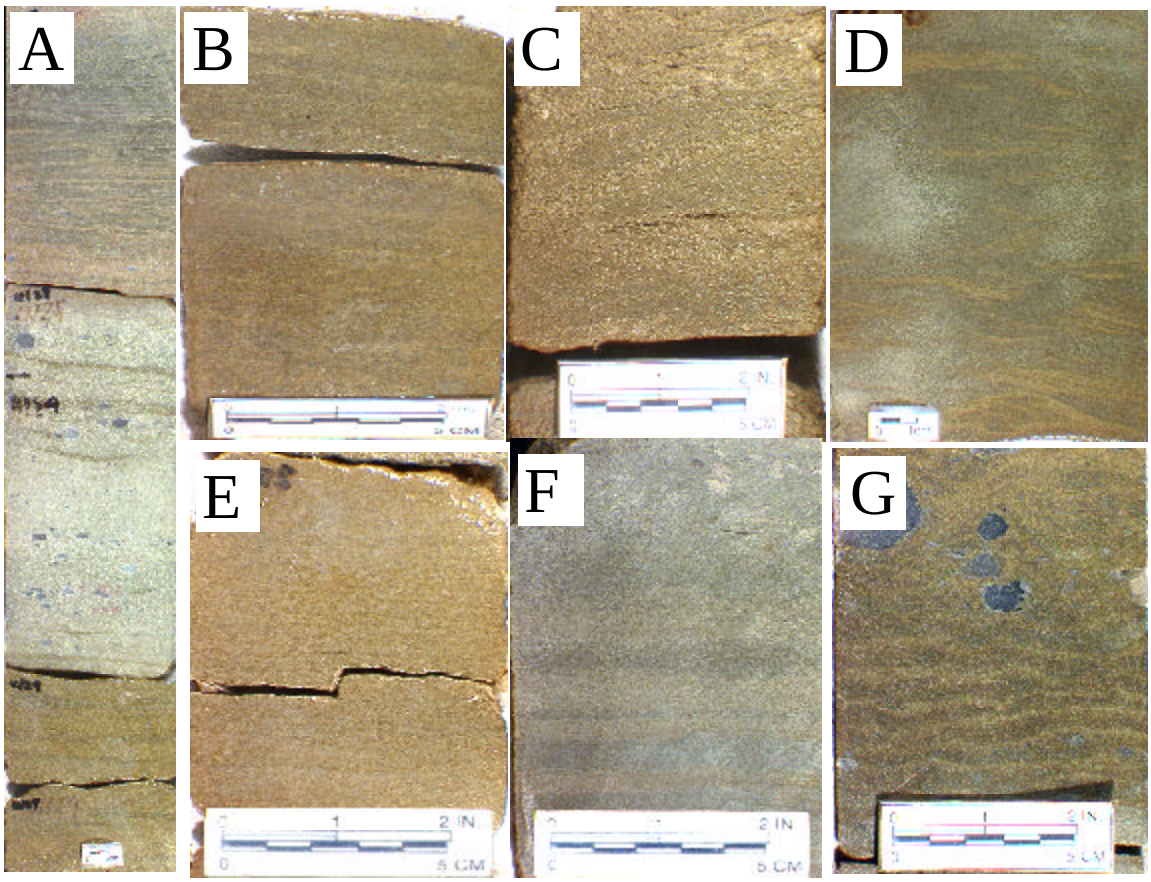

Figure 20. Sedimentary structures of facies S3. (A) JSM 23-19, 4127.5 to 4129 ft, vertical facies transition of S3, showing upward-fining trend from massive very fine-grained sandstone to thinly planar laminated siltstone. (B) Dibrell 3, 4225 ft and (C) RMM 4-25, 4579 ft, faintly cross laminated very fine grained sandstone. (D) RMM 9-25, 4269 ft, small scale ripple cross laminated very fined grained sandstone. (E) Wentz 11, 4205 ft and (F) JSM 300, 4537 ft, faintly planar laminated sandstone. (G) JSM 23-19, 4127 ft, deformed planar laminated siltstone. Note the lack of bioturbation of facies S3.

The massive sandstone was probably generated by some type of sediment gravity flow or by rapid deposition of material from suspension. The deposits of some grain flows, fluidized or liquefied flows, and debris flows may appear massive. The fact that facies S1, which includes many syndepositional structures including liquefaction sedimentary structures, commonly gradationally overlies the most massive sandstone suggested that massive sandstone was formed by rapid gravity flow. It was also deformed by intensive evaporite cementation.

Cross lamination was formed mainly by the migration of large-scale two-dimensional bedforms in incisions formed during lowstand sea level. This interpretation is supported by facies relationships with other lithofacies S groups. The more thinly-bedded cross laminated silt- to very fine-grained sandstone with climbing sets formed under rapid deposition in a high sediment input low flow regime conditions in a channel (McKee, 1965).

Thinly bedded planar laminated silt to very fine-grained sandstone forms from suspension settling of fine-size sediments of silt- or mudstone in lakes, tidal flats, subtidal shelves, or deep-sea environments or is the result of traction transport (e.g., swash and backwash on beaches, wind transport, uni-directional, upper flow currents in rivers or turbidity current flows, or sheet flow). The facies relationship with neighboring facies of S3 and the lack of inverse grading and wind ripples suggests this parallel laminated very fine-grained sandstone was deposited as dilute sheet flows or upper-flow-regimes planer beds in channels.

Facies S4

Facies S4 is yellowish gray to bluish white (5Y 7/2, 5Y 5/2, 5Y 3/2, 5B 9/1), very fine-grained, massive or chaotic laminated sandstone that contains abundant rip-up mud clasts as well as syndepositional-deformed structures and is underlain by a regional erosion surface. The thickness of facies S4 ranges from less than 1 to 4 feet (0.3 to 1.2 meters) in this study area (Figure 21). Based on the isopach map of this facies, the major depositional site of facies S4 is mainly located at the western border of the study area. Overall its distribution pattern indicates northwestern to southeastern trending dispersal patterns.

Facies S4 commonly shows a slightly fining-upward trend from base to top that is largely a reflection of decreasing mud clast size upward. Clasts range from 0.05 to 2 inch (0.13 to 5 centimeters) in diameter, are angular and may show imbrication or random orientations. Largest mud clasts are found at the base of scours, and imbrication becomes better developed upward in the scours (Figure 21A, B and C). Imbricate clasts are associated with synsedimentary folds, faults, and fluidized deformational structures (Figure 21D, F, G, H and I).

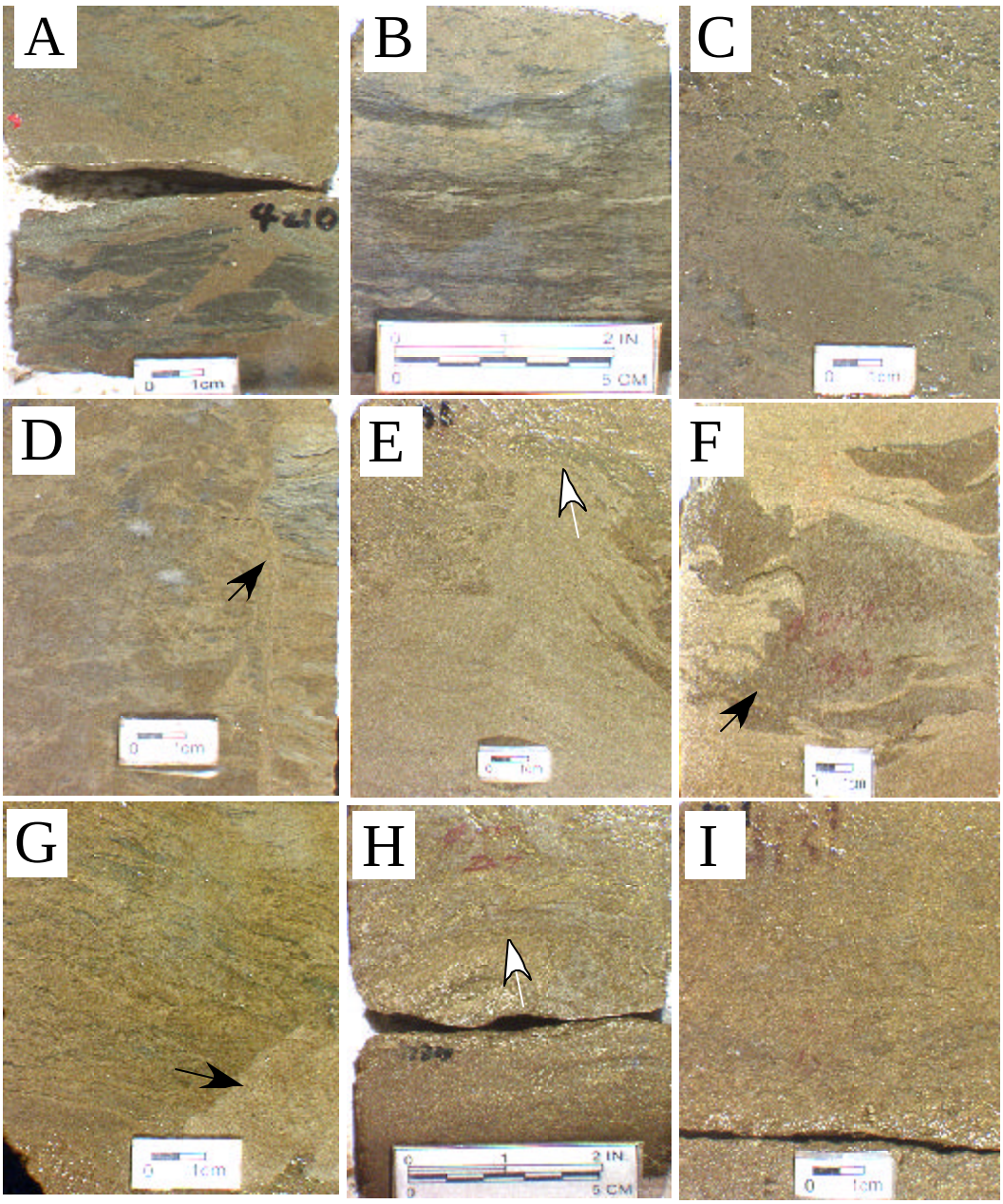

Figure 21. Sedimentary structures of facies S4. (A) Wentz 11, 4207 ft, rip-up mud clasts showing primary laminae. (B) Dibrell 3, 4232 ft, rip-up mud clasts underlying scour surface. (C) Dibrell 3, 4229 ft, imbricate rip-up clasts which overlie (B). (D) Wentz 11, 4208 ft, microfault structure showing soft deformation. Arrow indicates microfault. (E) JSM 23-19, 4136 ft and (F) 4137 ft, syndepositional fluidized deformed structures (arrow). (G) Dibrell 3, 4229.3 ft, syndepositional deformed laminae and pseudo sand balls (arrow). (H) JSM 23-19, 4134 ft, syndepositional chaotic deformed laminae (arrow). (I) JSM 23-19, 4131 ft, massive very fine-grained sandstone.

Massive sandstone containing rip-up mud clasts commonly occurs in turbidites, debris flow, and other types of sediment gravity flows and in fluvial deposits. The relationship of facies transition and regional truncation surface of base of facies S4 suggest that it was deposited at the base of fluvial incised sedimentary deposits associated with overbank collapse and liquefaction in deltaic regions. Associated synsedimentary deformational structures were produced by penecontemporaneous deformation by slumping or foundering of mud into sand.

Carbonate-Dominated Facies (Facies C)

Carbonate-dominated lithofacies occur at the middle part of the cored interval; their thickness ranges from approximately 2 to 15 feet (0.6 to 5 meters) of the Queen cored interval in this study area. As a non-producing horizon in the Means Field, it occupies the smallest portion in the study area in terms of total bulk volume (Figure 13). Facies C lithofacies comprise thin to medium-bedded yellowish gray to olive gray (5Y 4/1 to 5Y 3/2) peloidal and skeletal dolowackestone to dolograinstone with filling anhydrite cement and minor amounts of coarse silt and subarkosic sandstone materials.

Thin section study reveals the extensively dolomitized nature of the carbonate interval. The carbonate interval always includes evaporite nodules and siliciclastic materials, as do other Guadalupian carbonate strata. Most carbonate lithofacies are predominantly micrite-sized carbonate. They also contain varying amounts of allochems such as intraclasts, peloids, calcispheres, pelycopod, ostracode, and foraminifer fragments. The carbonate lithofacies includes minor subarkosic sandstone material with an average of 75% monocrystalline quartz, 20% feldspars, 5.5% rock fragments, and poikolotopic anhydrite cement in which the quartz content is generally higher than that of siliciclastic lithofacies. The detrital quartz grains in carbonate lithofacies are moderate well sorted, with grain size ranging from 0.043 to 0.073 mm (an average of 0.059 mm), and a phi standard deviations of 0.52 to 0.57 (an average of 0.53) (Table 2, 3 and 4; Figure 14, 15 and 16). The anhydrite cements in carbonate lithofacies always fill moldic and vuggy pore space produced by the dissolution of fossil fragments and formation of fenestral pores during early diagenetic event.

The carbonate dominated facies C can be subdivided into three major lithofacies: facies C1 of peloidal and dolomudstone, with fenestral pores, sheet cracks, in situ breccia and cryptalgal laminae; facies C2 of peloidal dolowackestone to dolograinstone, which contains skeletal grains; and facies C3 of argillaceous dolomudstone in descending vertical order.

Facies C1

Carbonate facies C1 is composed of yellowish gray to light bluish gray (5Y 4/1 to 5B 7/1) peloidal dolomudstone with fenestral fabrics, algal lamination, in situ breccia and desiccated sheet crack (Figure 22). The thickness of facies C1 ranges from 1 to 15 feet (0.3 to 5 meters) in this study area (Figure 13).

The fenestral fabrics are typically associated with other sheet crack and in situ angular breccia at the base of facies C1 (Figure 22A and B). Fenestrae increase in size and abundance upward within C1 deposits. Fenestrae are filled with diagenetic evaporite cement; fenestral carbonates grade up to algal laminated dolomudstone (Figure 22C, D, E and F). Algal lamination of facies C1 exhibits finely crystalline dolomicrite including crinkly and undulatory lamination and tiny voids of fenestral structures, in which algal laminae are cemented by anhydrite after gypsum.

Desiccation cracks occur throughout this facies and are filled with in situ breccia; such cracks are indicative of subaerial exposure indicators (Figure 22G). Sometimes small pseudomorphing gypsum crystals are present within algal laminae (Figure 22H). The cemented anhydrite exhibits felted crystalline structures in dolomicrite matrix at microscopic observation. These fenestral and algal laminae of facies C1 dolomudstone are very reliable indicators of supratidal conditions. They are associated with subaerial exposure features (Hardie and Shinn, 1986). Thus, facies C1 is interpreted as having formed in a supratidal and low intertidal tidal flat environment.

Facies C2

Facies C2 consists of yellowish gray to olive gray (5Y 4/1 to 5Y 3/2) peloidal dolowackestone. Skeletal dolopackstones to dolograinstones were rarely observed in this study area, mainly at the thick part of carbonate facies, along with locally thin peloidal dolopackstone. Facies C2 deposits are either massive or show faint lamination. Burrows, horsetail shaped stylolites and vertical fractures are locally observed (Figure 23). The thickness of facies C2 ranges from 0.5 to 1.5 feet (0.15 to 0.7 meters) in this study area (Figure 13).

The peloids of facies C2 are composed of pellet particles that were altered by poikilotopic anhydrite cement or subhedral or anhedral dolomite crystal, and they exhibit a lack of internal structure (Figure 23A, B, and C). The peloids generally are subspherical or elliptical in shape and are usually less than 0.2 inch (0.5 mm) in size. Minor local skeletal debris in this facies includes calcispheres, pelycopod, ostracode, and foraminifera (Figure 23D, E, F and G).

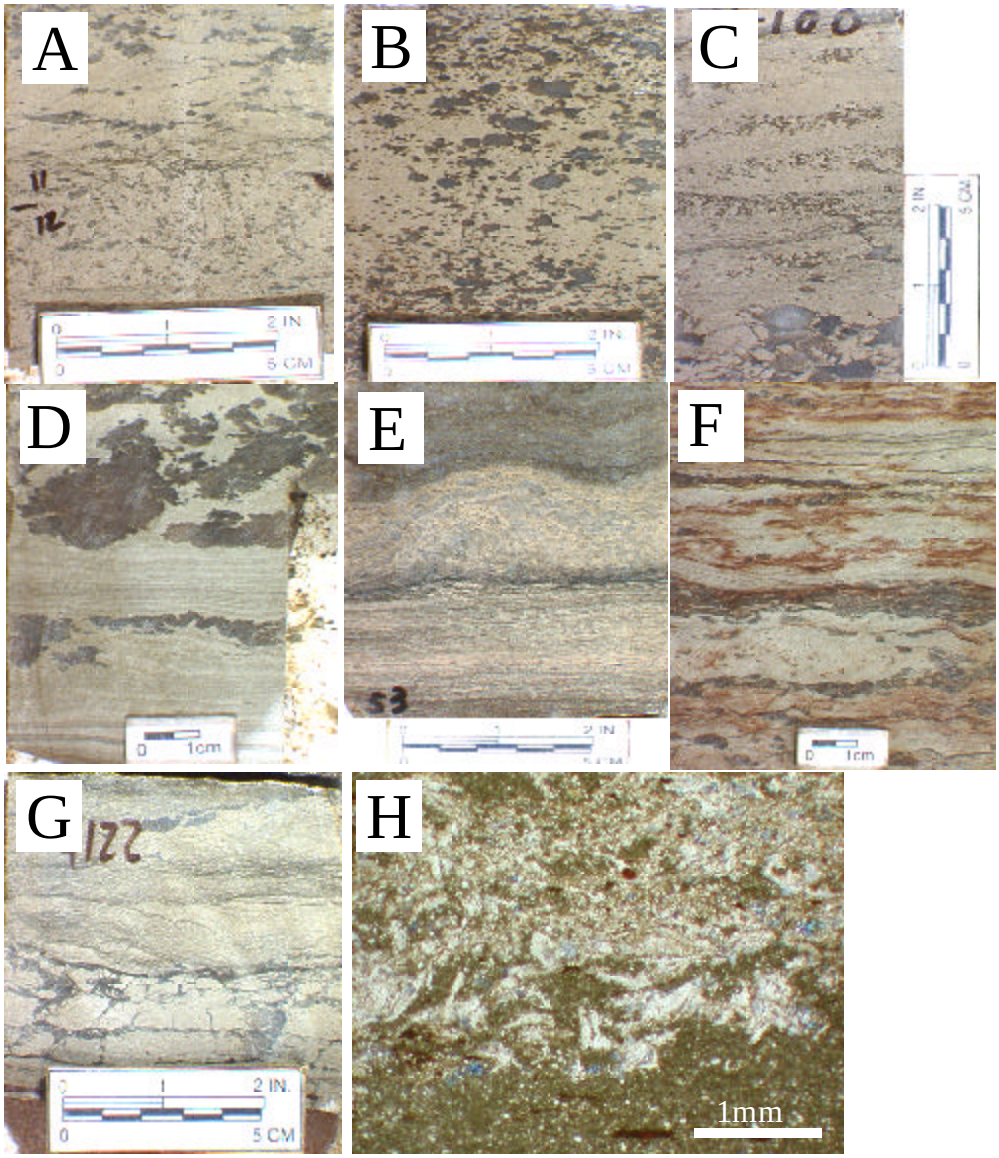

Figure 22. Sedimentary structures of facies C1. (A) Dibrell 3, 4211 ft, fenestral fabric filling with anhydrite cement. Increase the sizes of fenestral fabric and associated minor sheet crack. (B) Wentz 11, 4180 ft, anhydrite filled fenestral fabric. (C) RMM 10-51, 4100 ft, algal laminated dolomudstone. (D) Dibrell 3, 4209 ft, algal laminae and nodular anhydrite. (E) JSM 300, 4454 ft, thinly anhydrite cemented algal laminae and overlying dolomite laminated anhydrite of facies ECA. (F) JSM 300, 4477 ft, thinly algal laminated dolomudstone cemented by anhydrite. (G) JSM 23-19, 4122 ft, sheet crack including in situ breccia and overlying massive dolomudstone. (H) Dibrell 3, 4213 ft, photomicrograph of felted anhydrite cemented dolomicrite under plane polarized light. Scale bar is 1mm.

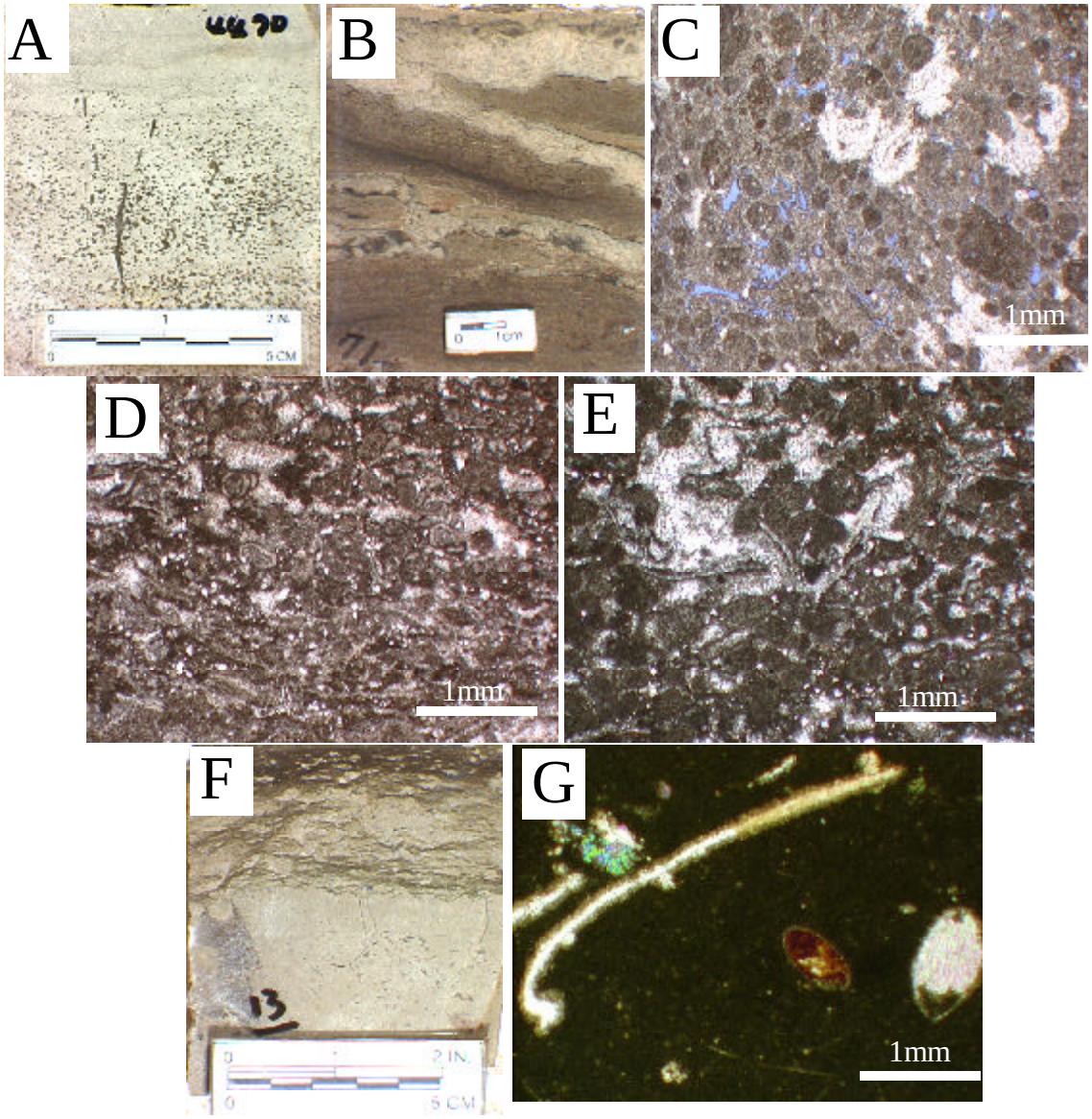

Figure 23. Sedimentary structures and other features of facies C2. (A) RMM 5-23, 4470 ft, peloidal dolopackstone cemented by anhydrite. (B) JSM 300, 4471 ft, peloidal dolopackstone and possible marine cement in desiccation crack and karst surface. (C) MSAU 59-60, 4026 ft, photomicrograph of peloidal dolopackstone of plane polarized light. Scale bar is 1mm. (D) and (E) JSM 300, 4472 ft, photomicrograph of peloidal and skeletal dolopackstone to grainstone of plane polarized light. Note foraminifera and pelecypod fragments. Scale bar is 1mm. (F) Dibrell 3, 4213 ft, skeletal dolomudstone to packstone showing sparse skeletal allochems and horsetail stylolites. (G) Dibrell 3, 4214 ft, photomicrograph of skeletal dolomudstone to packstone cemented by anhydrite of cross polarized light. Note pelecypod and ostracode fragments. Scale bar is 1mm.

Aggregates of clotted peloid and skeletal debris exhibit locally. Quartz grains are locally abundant (Figure 23E).

Based on fabric, abundance of carbonate mud, sparse skeletal allochems, lack of sedimentary structures (presumably due to intense bioturbation), lack of evaporite minerals, and the adjacent facies relationships, these peloidal and skeletal dolowackestone of facies C2 reflect a low energy setting, such as shallow, protected, or a lower intertidal to subtidal environment.

Facies C3

Carbonate facies C3 is characterized by gray (5Y 4/1 and 5Y 3/2) to black (5GY 2/1) massive or faintly laminated argillaceous dolomudstone that contains laminae of organic material and is very similar in appearance to facies S1 (Figure 24). There are also associated clay seams and stylolites. Facies C3 typically occurs at the base of carbonate cycles. The thickness of facies C3 ranges from 0.2 to 1 feet (0.06 to 0.3 meters) in this study area (Figure 13). Facies C3 commonly occurs at the thick part of carbonate facies.

The dolomudstone is composed of micritic subhedral or anhedral dolomite. Fossil fragments and burrows are rare to absent (Figure 24). Quartz grains are locally abundant and peloids are cemented by anhydrite.

Based on the fabric, quartz admixture, quartz texture, sedimentary structures, and the adjacent facies relationships, these argillaceous dolomudstones of facies C3 reflect a starvation of clastic material and carbonate sedimentation in a low energy, subtidal environment.

Evaporite-Dominated Facies (Facies E)

The evaporite-dominated lithofacies is the most dominant lithofacies in this study area, ranging from 30 to 40 feet thick, on average, in the 60 to 70 feet (18 to 21 meters) cored interval (Figure 13). Its thickness is mostly uniform across the study area.

The evaporites and evaporite-dominated lithofacies in the Queen Formation are described according to Maiklem's classification, which is based on the relationship between anhydrite and associated matrix, such as pseudomorphing crystalline and felted, nodular, nodular mosaic, and bedded massive (Maiklem et al., 1969). Using this classification and based on the thickness of evaporite beds, lithofacies E can be subdivided. The siliciclastic dominated ES1 facies is composed of reddish brown, deformed wavy mudstone and siltstone-including pseudomorphic felted and rosette structured anhydrite. Facies ES2 consists of nodular, enterolithic, mosaic, chicken wire and bedded massive anhydrite with siltstone background. The evaporite dominated ECA facies is composed of mosaic and bedded massive anhydrite with

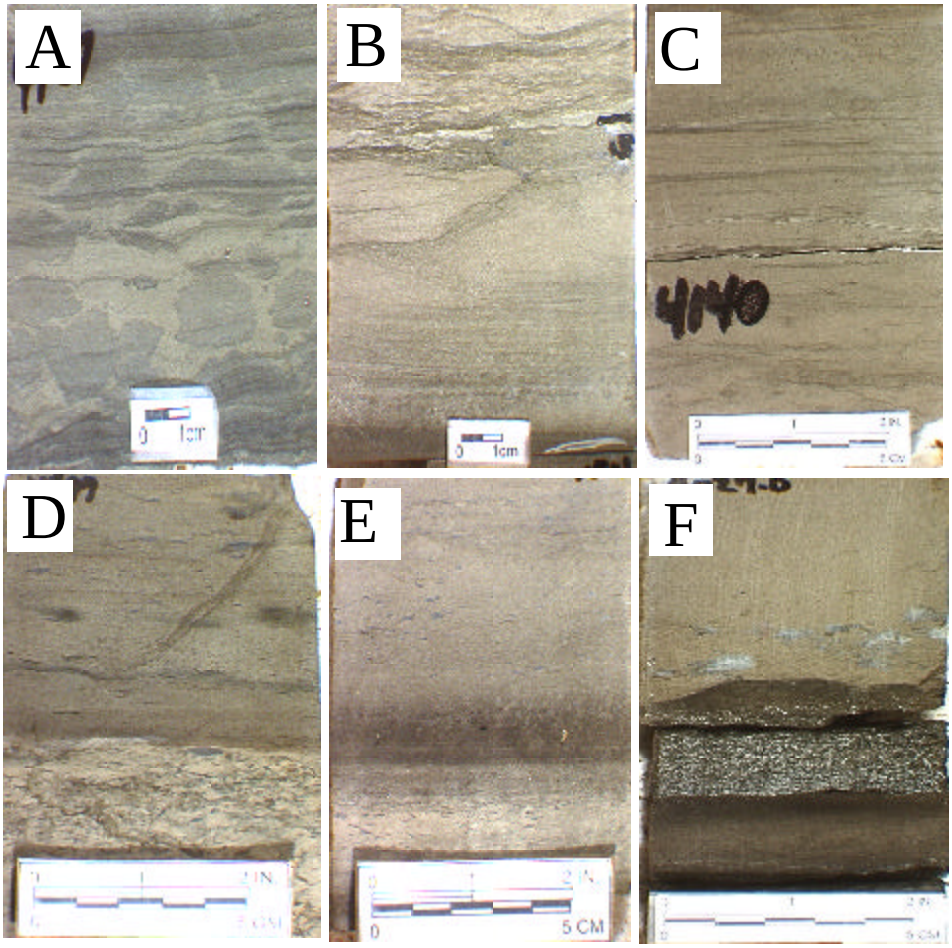

Figure 24. Sedimentary structures of facies C3. (A) RMM 95-15, 4111 ft, argillaceous dolomudstone including in situ mud breccia. (B) Dibrell 3, 4215 ft, thinly laminated argillaceous dolomudstone and horsetail stylolites. (C) RMM 7-51, 4140.5 ft, thinly laminated argillaceous dolomudstone. (D) Wentz 11, 4197 ft, and (E) Dibrell 3, 4212 ft, massive argillaceous dolomudstone overlie facies C1 including sheet crack with sharp bed contact. (F) MSAU 59-60, 4026.9 ft, massive dolomudstone and underlying argillaceous dolomudstone.

dolomite laminae, and massive anhydrite. The evaporite content generally increases from ES1 to ES2 to ECA facies. Although those three evaporite lithofacies have very subtle differences, they can be identified based on structural differences, which result from not only different primary depositional environments, but also from subsequent early diagenetic modification. Those processes result in the creation of different petrophysical characteristics in terms of hydrocarbon reservoirs.

The detrital sand composition of facies ES 1 and 2 consist of an average of 68% monocrystalline quartz, 25.5% feldspars, and 6.5% rock fragments (Table 3 and 4, and Figure 15 and 16). Quartz content ranges from 21% to 32%; facies ES1 has the highest quartz content 32% with facies ES2 containing 21%. The detrital quartz grains are moderate sorted to moderate well sorted. The grain size of ES1 facies ranges from 0.025 to 0.079 mm, with a mean grain size of 0.053 mm of coarse silt fraction (Table 2 and Figure 14). The grain size of ES2 facies ranges from 0.041 to 0.065 mm, with a mean grain size of 0.052 mm of coarse silt fraction. The detrital quartz grains are moderately to moderately well sorted in both ES facies (Table 2 and Figure 14). Feldspar content ranges from 6% in ES2 to 10% in ES1. Fine silt is more abundant in ES2 than ES1.

Facies ES1

Facies ES1 consists of thin to thick bedded, moderate to dark reddish brown deformed wavy-laminated and deformational disturbed structured mud- to very fine-grained sandstone with color mottling, microfaults, fluid escape and salt ridge structures. This facies is also characterized by the association with a relatively small amount of evaporite cementation and lack of fossils in evaporite-dominated lithofacies. The thickness ranges from 0.5 to 5 feet (0.15 to 1.5 meter; Figure 13 and Figure 25).

The deformed wavy lamination and deformational structures of facies ES1 are the most common sedimentary structures of the ES1 facies (Figure 25A, B, C, D and E). These reddish brown colored siliciclastic-rich facies are also commonly associated with small crystalline felted or rosette structured anhydrite and nodular anhydrite (Figure 25C, E, F, G and H). The deformed mudstone to sandstone of ES1 facies is disturbed to varying degrees (Figure 25A, B, C, D and E). The most common primary sedimentary structures of this deformed unit are mostly ripple cross- and wavy-lamination. The red beds of Facies ES1 also exhibit syndepositionally deformational sedimentary structures (e.g., fluid escape structures and microfaults) associated with color mottling bands, mud cracks, and rotated detrital clay (Figure 25I).

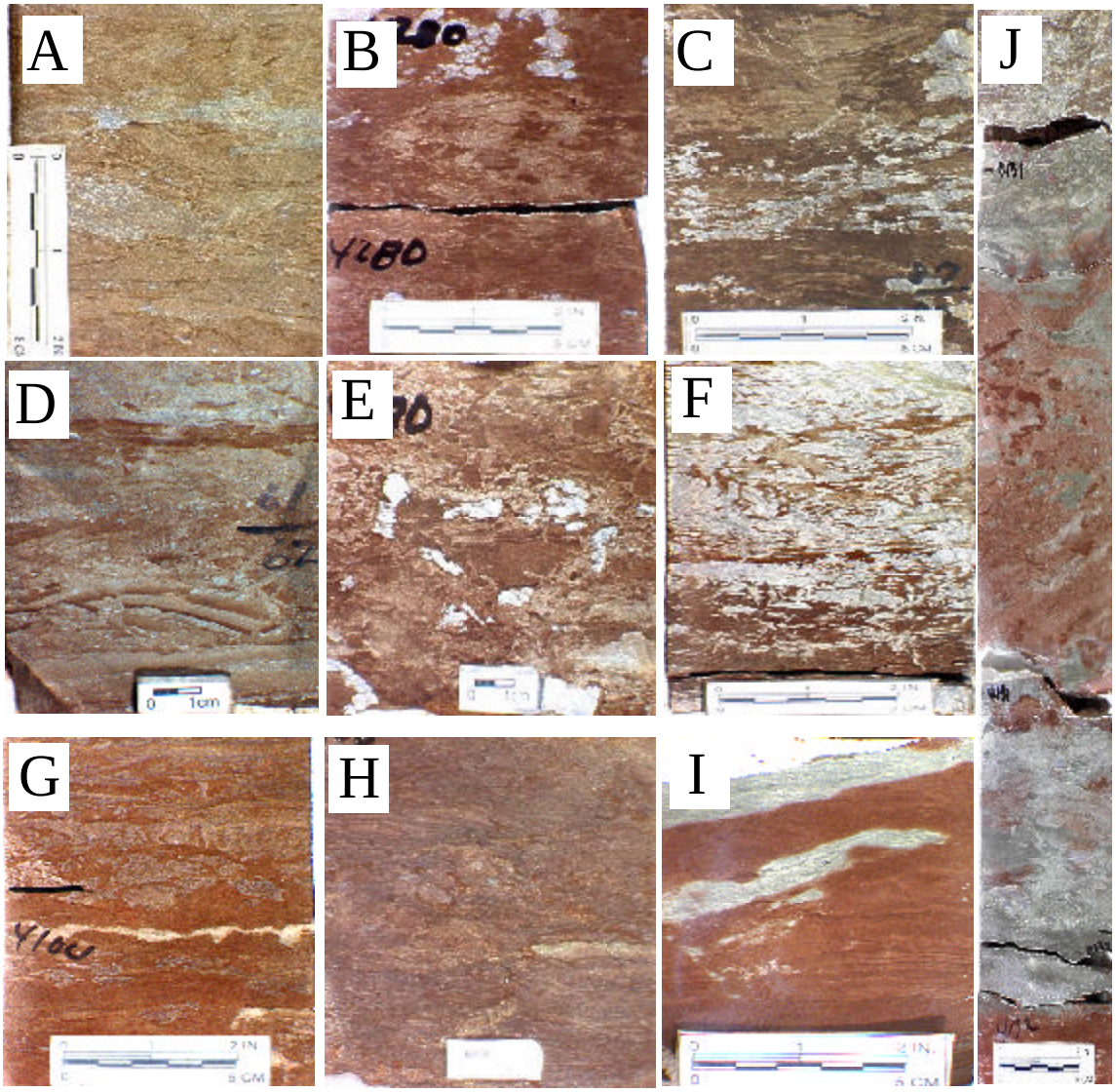

Figure 25. Sedimentary structures and other features of facies ES1. (A) RMM 5-23, 4463 ft, deformed chaotic wavy lamination and mud clasts. (B) RMM 9-25, 4279 ft, disturbed mud bed including anhydrite cemented burrow and mud clasts. (C) RMM 5-23, 4488 ft, deformed ripple laminated bed and small anhydrite nodule. (D) JSM 300, 4462 ft and (E) RMM 9-25, 4280 ft, disturbed mud bed and mud clasts. Note preserved primary structures. (F) JSM 23-19, 4142 ft, (G) RMM 95-15, 4104 ft, and (H) RMM 95-15, 4104 ft, felted crystalline anhydrite cemented reddish brown mudstone. (I) JSM 300, 4480 ft, planar laminae and light gray color mottling band. Note color mottling band which is not controlled by sedimentary structures. (J) RMM 95-15, 4131 to 4132 ft, vertical transition of ES facies. Note disturbed bed and color mottling band.

The previous works on the Shattuck Member and Yates Formation were classified into evaporite-dominated red bed or red argillaceous siltstone/sandstone facies (Borer and Harris, 1989; Borer and Harris, 1991; Mazzullo et al., 1991; Andreason, 1992; Malicse and Mazzullo, 1996). The red or reddish brown colors in facies ES1 are probably due to very fine-grained hematite and its composition of ferric iron (Figure 25). Many other previous works of the Shattuck Member of the Queen Formation and the Yates Formation mentioned this unit as red bed or red sandstone, and reported some paleosoil features such as cutan, caps, bridges, and pendants (Mazzullo et al., 1991; Andreason, 1992; Malicse and Mazzullo, 1996). In this study area, the lower part of the Queen Formation contains pedogenetic and diagenetic features such as detrital clay and color mottling bands, which include labile grain dissolution, hematitization and precipitation of authigenic species, and precipitation of major pore-filling cements. These pedogenetic soil horizons can be used as an alternative criterion of subaerial exposures in this area. Smith (1990) suggested color-mottling bands in the reddish brown mudstone could be a product of hydromorphism by repetitive wetting and drying processes under warm to hot semiarid climatic conditions.

The ES1 facies is also crystalline pseudomorphic felted, rosette crystalline structured, and contains small nodular anhydrite, which obliterates most primary sedimentary structures (Figure 25F, G and H). The size of the associated anhydrite ranges from less than 0.1 to 0.25 inches (0.2 mm to 0.5 cm). The felted and rosette crystalline structured anhydrite shows randomly oriented lath and radiating blade rosette shapes in core samples, and also exhibits radiating lath-shaped and coarse crystalline crystal in the thin section. Its crystal shape in the core and thin sections is very similar to gypsum crystal, while the small nodules are ovate and irregular lenses in shape that are equidimensional, elongate nearly parallel or random to bedding, and are supported by reddish brown to moderate brown siltstone matrix (Figure 25C and E).

The most common syndeformational structures in facies ES1 are deformed wavy and cross-lamination, and disturbed mud intraclasts facies (Figure 25A to E). Deformed laminated mud beds exhibit a faint to very well defined ripple and wavy lamination, which generally includes few mud clasts and small amounts of anhydrite bleb and nodule (Figure 25A, B, and C). The disturbed intraclasts also contain rotated mud lamination, which is generally associated with small size anhydrite blebs and an erratic shaped nodule. Sparse anhydrite cementation occurs randomly or rarely in burrows (Figure 25C).

These syndeformational structures are interpreted as salt ridge and fluid escape structures that are indicative of deposition in sabhka setting. Deformation of sedimentary structures due to anhydrite cementation was also produced by repetitive wetting and drying events. Andreason (1992) also suggested that the disturbed intraclast beds were part of a salt ridge formed by halite growth at a coastal sabhka, which were subsequently disrupted during desiccation, while Mazzullo (1991) proposed that the deformed wavy lamination of the upper Shattuck Member was formed by the growth of anhydrite nodules. In this study area, the disturbance of reddish brown mud- to sandstone is ubiquitous in facies ES1 regardless of the presence of evaporite nodule and the absence or sparseness of displacive halite. The deformation of primary wavy and ripple lamination probably results from a combination of syndeformational and early diagenetic processes, including dissolution and precipitation of anhydrite, haloturbation, and dewatering of compaction, drying and wetting during seasonal a dry mudflat rather than saline mudflat.

Based on the crystal shape and previous works on similar lithofacies of facies ES1, the anhydrite crystal of coarse silt to mud fraction in facies ES1 was formed by the alteration of primary gypsum crystal below the capillary zone of ground water table in the arid coastal sabhka region. Anhydrite blebs and small nodules in this facies were changed into nodular or coalesced nodular anhydrites of facies ES2.

Facies ES2

Facies ES2 consists of medium to thick bedded, nodular, enterolithic, coalesced nodular, mosaic, chicken-wire and bedded massive anhydrite with a reddish brown siltstone background, the thickness of which ranges from 1 to 9 feet (0.3 to 3 meter) (Figure 13 and 26). Unlike other evaporite-dominated lithofacies such as facies ECA, the matrix of facies ES2 is comprised of reddish brown siltstone to very fine-grained sandstone and dolomite background material. It has a very similar appearance to that of facies ES1, with the exception of intense evaporite cementation and the size of the evaporite bed. Facies ES2 can be recognized by faint primary gypsum crystal outlines and displacive discrete nodular shapes in reddish brown silt and light yellow dolomite backgrounds. The coalesced nodular and mosaic anhydrite in reddish brown siltstone and yellow dolomitic matrices typically exhibit very random alignment relative to bedding planes. The sizes of anhydrite nodules in evaporite-dominated ES2 facies ranges from less than 0.25 to 2 inches (0.5 to 3 cm), and is generally larger than in facies ES1.

Common vertical facies transitions reveal an upward succession of discrete nodular anhydrite, enterolithic structured anhydrite, coalesced nodular anhydrite or chicken-wire anhydrite and bedded massive anhydrite with anhydrite increasing upward (Figure 26). The thin enterolithic structured anhydrite bed exhibits some fold-like deformation structures and brittle deformed structures due to compaction, which are usually parallel to the bedding plane (Figure 26A, B and C). The coalesced nodular and chicken-wire anhydrites are ovate and irregular coalesced lenses that show the random aggregation of discrete lenticular shaped anhydrite nodules, and are supported by reddish brown to moderate brown siltstone and light yellow dolomitic matrix (Figure 26D, E and F). These anhydrites also reveal coarse crystalline textures in the thin section.

Andreason (1992) adapted Jacka and Fransco's (1974) interpretation of a transition from coastal to continental sabhka on the basis of the change from reddish brown and moderate brown mudstone to very fine grained sandstone matrix (the so called Red beds of the Permian strata), and extensive anhydrite cementation of the upper Guadalupian shelf sediments of the Permian. They suggested siliciclastic dominant red beds are proximal to the coast, where sediments retained a reduced state of iron and the accumulation rate is very high. However, anhydrite dominated facies in this study are considered as to product of evaporite diagenesis. The anhydrite-dominated facies in the Queen Formation cannot be interpreted as Andreason's interpretation of continental and coastal sabhka.

Fryberger et al. (1983) based a two-fold subdivision of sabhka facies on the amount of evaporite present: dry detrital- and saline evaporite-dominated sabhka facies. According to this scheme, the deformed wavy lamination of facies ES1 can be interpreted as having formed on a detrital dominated dry mud flat in a proximal coastal setting. Evaporite dominated mosaic and bedded massive anhydrite of facies ES1 and ES2 are interpreted as evaporite dominated saline mud flats or evaporite flats on coastal sabhka facies on the basis of dominant lithology and its sedimentary structures. Facies ES1 and ES2 were deposited in the upper supratidal and intertidal zones, in which brine level is approximately less than 5 meters in water depth (Kendall, 1992).

Facies ECA

Facies ECA consists of medium to thick bedded, mosaic and bedded massive anhydrite including anhydrite pseudomorphs of gypsum, various types yellowish gray algal dolomitic lamination, and relatively pure massive anhydrite, in which the thickness ranges from 2 to 15 feet (0.6 to 5 meters) (Figure 13 and 27). Facies ECA is very difficult to distinguish from facies

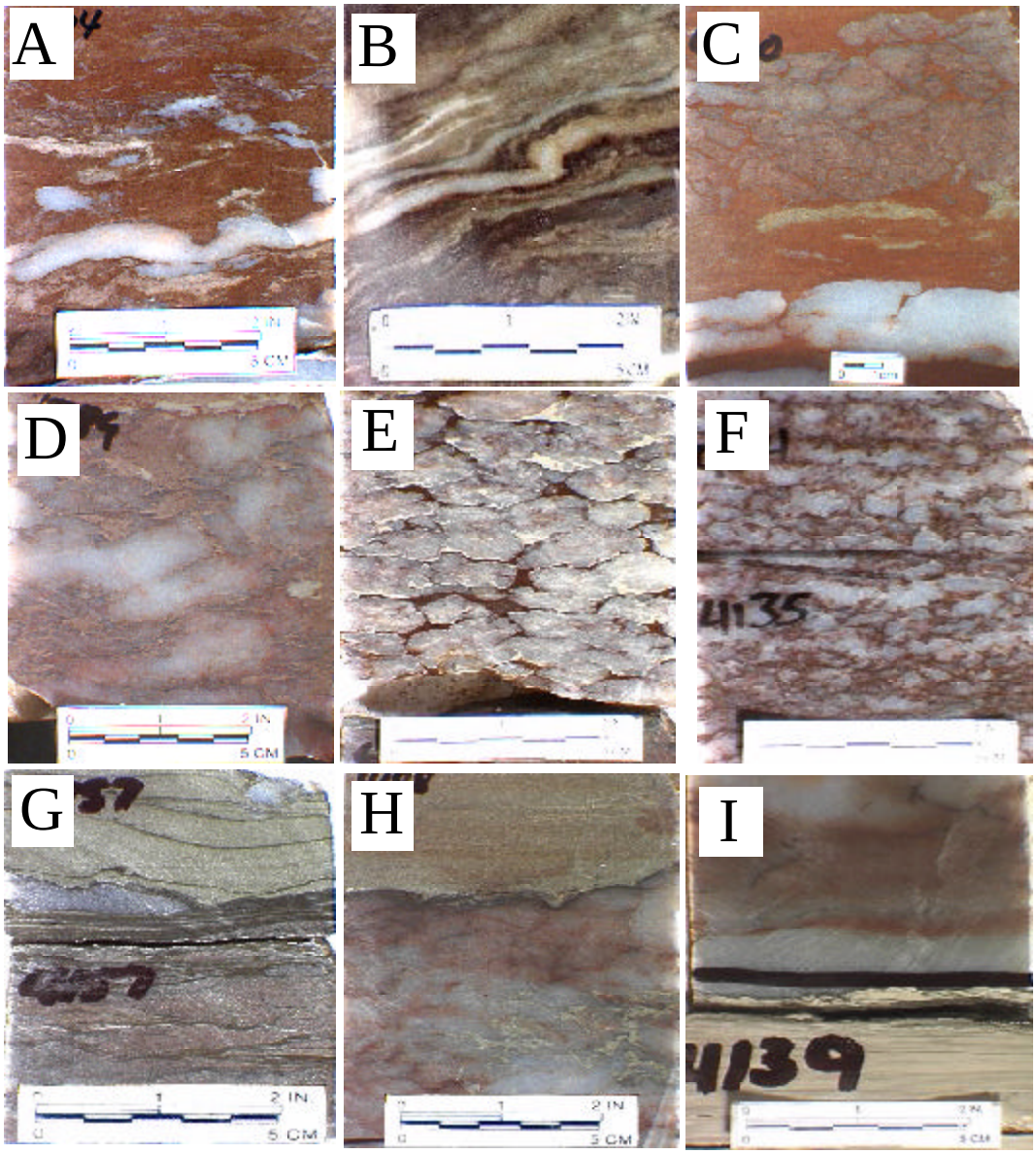

Figure 26. Sedimentary structures and other features of facies ES2. (A) RMM 95-15, 4104 ft and (B) RMM 5-23, 4464 ft, enterolithic structured anhydrite of ES2 facies. (C) RMM 9-25, 4290 ft, enterolithic anhydrite of facies ES2 and overlying color mottling band and anhydrite cement of facies ES1. (D) RMM 9-25, 4289 ft and (E) RMM 7-51, 4136 ft, coalesced nodular anhydrite with dolomite background (D) and reddish brown siltstone background. (F) RMM 7-51, 4135 ft, chicken-wire structured anhydrite. (G) RMM 7-51, 4157 ft, ES2 facies is bounded by dark colored clay or organic material of facies S2. (H) RMM 95-15, 4108 ft, Note dissolved sharp bed boundary between underlying ES2 and S2 facies. (I) RMM 7-51, 4139 ft, overlying ES2 facies is bounded by sharp, irregular bed boundary with facies C1.

ES2 except that lithofacies ECA does not include any yellow gray dolomitic laminae. The common vertical subfacies transition of facies ECA is from thinly dolomitic laminated anhydrite to anhydrite pseudomorphing after gypsum, to pure pristine bedded anhydrite.

The dolomitic laminated anhydrite contains planar and wavy dolomitic laminae and anhydrite pseudomorphs of bottom grown (based on its shape) gypsum (Figure 27). Laminae are the alternately thin and thick. One characteristic feature of dolomite laminae is dark yellowish brown dolomite laminae of anhydrite pseudomorph that are overlain by pure massive bedded anhydrite of another ECA facies and underlain by thick wavy dolomitic laminae, including bedded anhydrite. This lower dolomitic laminated facies is composed of swallowtail gypsum pseudomorphs, which exhibit a vertically oriented and elongated crystal shape (Figure 27A, B and C). No halite was found in facies ECA. Pseudomorph anhydrite crystals commonly range from 0.5 to 1.5 inch (1 to 3 cm). Same laminae show crenulations similar to algal laminated carbonate facies except for the predominance of anhydrite. Crenulated dolomitic laminae are commonly overlain by another massive bedded anhydrite and underlain by a sharp base with organic laminae and thinly laminated dolomudstone of facies C3 and deformed wavy laminated very fined-grained sandstone of facies S2 (Figure 27D, E and F).

This ECA subfacies transition represents the “brining-upward trend” proposed by Longman et al. (1983) with underlying very thinly laminated dolomudstone. This can be considered as the product of the fluctuation of the hydrologic setting and salinity, which is produced by a shoaling-upward trend from the supratidal marginal sabhka to a subtidal deposit in the arid climatic condition platform interior.

Warren and Kendall (1985) suggested these wavy and sharp lower bed boundaries are the product of shallowing cycles of salina with increasing dolomite amounts. He considered these bed boundaries as corrosion boundaries, which are developed by the difference of saturation stability between carbonate and calcium sulfates. When salina or saltern is deep, density stratification maintains gypsum saturation at the bottom and prevents the dilution by meteoric water. As the salina becomes shallower as a result of gypsum deposition, seasonal rainfall dilutes the salina, eroding gypsum and allowing carbonate deposition. According to Warren’s model, ECA facies of the Queen formation represents increasing salinity from the bottom to the top. Then, the laminated dolomudstone of C1 facies formed when meteoric water diluted the brine that was enriched in magnesium due to depletion of calcium as a result of

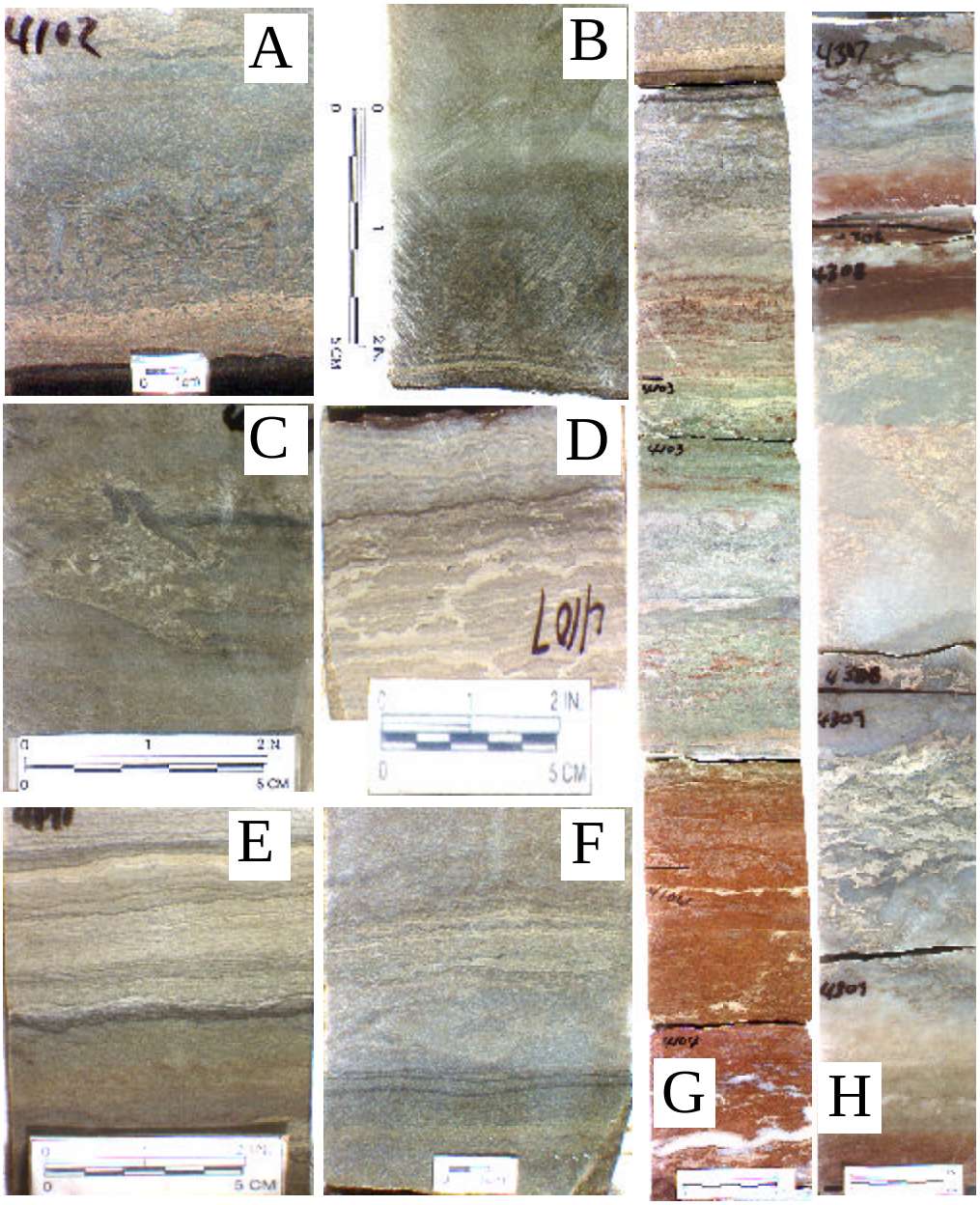

Figure 27. Sedimentary structures and other features of facies ECA. (A) RMM 95-15, 4102 ft and (B) RMM 5-23, 4453 ft, pseudomorphing anhydrite after bottom grown gypsum. Note underlying thinly laminated dolomudstone. (C) RMM 5-23, 4453 ft, possible pseudomorphing anhydrite after gypsum. (D) RMM 95-15, 4107 ft, (E) Wentz 11, 4171 ft, and (F) Dibrell 3, 4197 ft, very thinly laminated anhydrite with underlying thin laminated dolomudstone. Note dark colored organic bed boundary between laminated dolomudstone and deformed sandstone.(G) RMM 95-15, 4102 to 4104 ft, vertical facies transition of ES1, S2, C1 or C3 and very thinly laminated anhydrite of facies ECA. (H) RMM 9-25, 4307 to 4309 ft, vertical facies transition of chaotic laminated anhydrite of facies ECA and ES1.

gypsum precipitation. Because it is hypersaline brine water, it provides very unfavorable conditions for live predators of algae. Little bioturbation structures can be seen in C1 facies.

Facies ECA is interpreted as having formed in subaqueous shallow saline water body of salina, which represents upward-brining with increasing salinity and decreasing brine levels. Sabhkas of other evaporite-dominated facies would be expected to have formed on the paleotopographic highs, whereas salinas of facies ECA would be expected to be associated with the paleotopographic lows. Thus, some areas of salina ECA facies are related to local paleotopographic low area of salina after flooding events above carbonate facies.

DEFINITION OF WELL LOG FACIES

Determination of Lithology

Determination of lithology from well log data is required if cores data are not available. Several cross plot techniques and some multivariate statistical techniques (such as principal component and discriminant analysis) are generally used to interpret lithology based on well logs. Those methods consist of two or three combinations of the gamma, neutron porosity, lithodensity, sonic, and photoelectric log (PEF) (Bucheb and Evans, 1994). For this study, a combined cross plot of the neutron-density log of Schlumberger is a particularly useful tool because they can be used to distinguish between halite and anhydrite beds in the Queen. The estimation of the relative portion of halite and anhydrite in each cycle was very important in determining long-term base-level fluctuations in the Queen Formation. Based on the Class 1 and 2 well log data and the idealized vertical sedimentary cyclic succession of cored intervals, further stacking pattern analysis was performed.

As an initial step in analyzing well log data, a data quality control process was performed on core and well logging data of Class 1. The procedure included: (1) converting analog well log data into digital data format, (2) environmental correction; (3) depth matching; (4) fixing or removing bad data; (5) converting all neutron logs to the same lithology (limestone) unit; and (6) normalization and rescaling of well logs of different units and vintage by linear shifting method using maximum and minimum values of the study area and universally accepted data value ranges of gamma ray and neutron logs (Barret, 1992; Bucheb and Evans, 1994; Kerans and Tinker, 1997; Ali et al., 1999; Lee and Datta-Gupta, 1999).

Because more than 95% of well log data in this study area comprises several vintages gamma ray and neutron porosity logs with non-modern API scales from different service

companies, the depth of all input data were corrected and old gamma and neutron log data were normalized by using well known well log statistics of study and global averages for data quality control (Barret, 1992). In order to normalize old gamma ray and neutron porosity logs, the following linear shifting equation was used:

$$Y=mX+B \quad (1)$$

Where, m=(New high value–New low value)/(Old high value–Old low value);

B=New High–(m x Old high value);

Y=new derived gamma ray or neutron porosity log value in modern scale

X=old gamma ray or neutron porosity log value in old scale

New and old high and low values of neutron porosity were obtained from univariate statistics of all the modern scale and old scale neutron log data, while the new high and low value of gamma ray logs were taken as global average values of anhydrite (or halite) and shale in this study area. The reason for selecting anhydrite and shale lithologies is that anhydrite and halite have the minimum gamma ray value, while shale has the maximum gamma ray value. Through this process, new high and low neutron porosity values are selected as 33.7 percent and 1.9 percent, respectively. These new highest and lowest values of neutron logs were chosen after the removal of extremely poor quality data. In this study, the calibrated API GR of anhydrite (or halite) and shale values were 0 to 5 API units and 120 to 130 API units, respectively.

An integrated digital database was constructed using SAS and Arcview GIS databases. Well log data, core descriptions, textural and compositional measurement data, and static analyzed reservoir data (mainly porosity and permeability) were input to the database. 5 major well-log data sets were analyzed to identify the 10 lithofacies groups observed in core (Table 6 and Figure 28).

Well Log Properties

Gamma Ray Log (GR)

Gamma ray values can be divided into three categories on the basis of well log value statistics (Table 6A and Figure 28A). The four siliciclastic facies (facies S1, S2, S3, and S4) and an argillaceous dolomudstone of facies C3 have the highest average gamma ray values, are ranging from 73.82 to 110.93 API units. Facies C3 and S1 exhibit the lowest gamma values, while facies S4 show the highest gamma values. This variation probably reflects the abundance of mud content of each lithofacies according to compositional analysis. The second highest gamma ray values were observed for the relatively siliciclastic-dominated evaporite facies of

Table 6. Well log properties of lithofacies.

A. Gamma Ray (API)

Facies	ES1	ES2	ECA	C1	C2	C3	S1	S2	S3	S4
Mean	71.33	53.55	29.12	73.82	56.77	103.63	103.22	109.88	98.60	110.93
Maximum	129.29	126.64	119.81	127.44	99.79	128.49	128.61	129.75	128.38	128.66
Minimum	7.10	7.74	4.97	6.30	20.37	12.01	13.01	10.73	17.39	78.92
Standard Deviation	37.62	36.12	31.06	36.21	20.47	25.06	30.23	19.28	30.22	14.26

B. Neutron Porosity (%)

Facies	ES1	ES2	ECA	C1	C2	C3	S1	S2	S3	S4
Mean	7.17	6.61	4.43	11.90	8.90	17.46	14.74	14.70	20.69	13.77
Maximum	22.25	19.65	17.58	20.95	12.84	21.14	26.67	30.33	29.11	16.04
Minimum	-0.56	-0.56	-0.27	0.47	2.09	3.71	12.99	0.05	-0.69	2.92
Standard Deviation	6.46	4.79	4.19	4.87	2.94	2.76	10.04	8.58	7.49	2.10

C. Litho-density (g/cm3)

Facies	ES1	ES2	ECA	C1	C2	C3	S1	S2	S3	S4
Mean	2.79	2.83	2.89	2.72	2.76	2.61	2.31	2.55	2.38	NA
Maximum	2.93	2.94	2.95	2.95	2.78	2.72	2.52	2.90	2.49	NA
Minimum	2.60	2.67	2.78	2.52	2.75	2.52	2.18	2.26	2.28	NA
Standard Deviation	0.17	0.07	0.05	0.09	0.02	0.07	0.14	0.16	0.07	NA

D. Sonic (ft/sec)

Facies	ES1	ES2	ECA	C1	C2	C3	S1	S2	S3	S4
Mean	59.47	56.82	57.94	70.36	NA	66.74	63.54	63.76	68.05	65.47
Maximum	72.43	69.05	69.08	82.47	NA	73.72	69.21	80.79	84.39	68.88
Minimum	51.32	51.64	50.89	59.14	NA	62.31	55.39	51.49	51.44	59.74
Standard Deviation	6.64	4.05	5.44	8.06	NA	6.12	5.84	9.23	13.74	3.83

E. Photoelectric Absorption (barns/electron)

Facies	ES1	ES2	ECA	C1	C2	C3	S1	S2	S3	S4
Mean	5.26	4.70	4.72	3.33	3.74	3.43	2.79	3.00	2.80	NA
Maximum	5.47	5.76	5.55	4.34	4.14	3.79	3.18	5.07	3.43	NA
Minimum	5.04	2.90	2.82	2.19	3.00	2.48	2.06	1.88	1.96	NA
Standard Deviation	0.18	1.14	0.58	0.65	0.64	0.54	0.48	0.95	0.61	NA

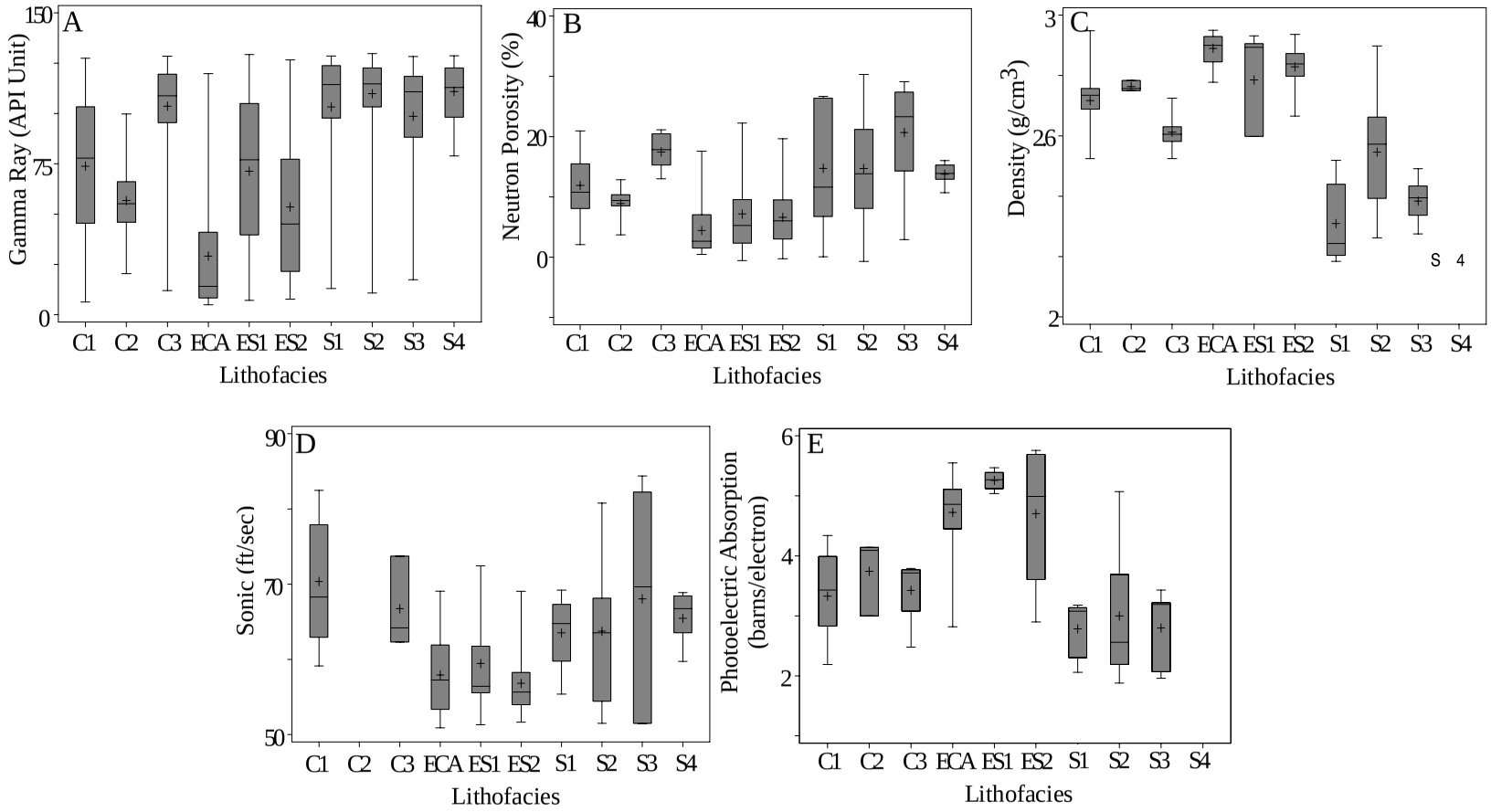

Figure 28. Well log values of lithofacies groups. The center of each box is the 50th percentile; margins of the boxes are the 25th and 75th percentiles; and whiskers denote the 0th and 100th percentiles. See Table 6 for statistical comparison of lithofacies group.

ES1 and ES2, and two carbonate-dominated lithofacies of C1 and C2. Their gamma ray values ranged from 53.55 to 73.82 API units. Facies ES2 and C2 have similar values but the variance is greater for facies ES2 than facies C2. Facies ES1 and C1 have slightly lower gamma ray values than facies C2 and ES2 and variances of gamma ray values are greater. This is to be expected as facies ES1 and C1 have greater shale content than facies ES2 and C2. The third lowest gamma ray values were observed in facies ECA, with an average of 29.12 API units. These low gamma ray values reflect the greatest evaporite content.

Neutron Log (PHIN)

Neutron porosity values were divided into 3 categories (Table 6B and Figure 28B). The highest neutron porosity log values were recorded for siliciclastic facies S1, S2, and S3 and argillaceous dolomudstone of facies C3, with average values ranging from 14.70 to 20.69 %. Of these, facies S1 and S2 show lower neutron porosity values than facies S3. Two carbonate-dominated lithofacies of C1 and C2, and one siliciclastic lithofacies facies S4 have intermediate neutron porosity values averaging from 8.9 to 13.77 %. Facies C1 and C2 have similar ranges of neutron porosity values but the variance of neutron porosity value of facies C1 is greater than that of facies C2. Due to their abundant evaporite content, lowest neutron porosity values were recorded in evaporite-dominated facies ES1, ES2, and ECA, with average values ranging from 4.43 to 7.17 %.

Lithodensity Log (RHOB)

Two categories of lithodensity log values were found (Table 6C and Figure 28C). Three evaporite-dominated lithofacies (ES1, ES2, and ECA) and two carbonate lithofacies (C1 and C2) have high average values, ranging from 2.72 to 2.89 g/cm^3. Facies ES2 and ECA have higher lithodensity values than facies ES1, C1 and C2. Facies in this high lithodensity values group have low gamma rays values and even lower neutron porosity values. This reflects the control of evaporite content on neutron porosity and lithodensity values in this study area: the higher the evaporite content the lower the neutron porosity and the higher the lithodensity values. Carbonate facies C3, and three of the siliciclastic lithofacies (S1, S2, and S3) have lower lithodensity log and also have relatively higher neutron porosity log values. The average lithodensity values of the low-value category range from 2.31 to 2.55 g/cm^3, with facies S1 and S3 having lower lithodensity values than facies S2. This reflects evaporite content (facies S2 has higher evaporite cement contents than facies S1 and S3) and porosity in the three sandstone facies. The higher value of lithodensity can be positively correlated with higher content of

evaporite in sandstone, low neutron porosity, and the high value of gamma ray values. Because this lithodensity logs are not available for the whole study area, several lithodensity logs were used only as reference data for determination of the lithology of uncored regions and intervals.

Sonic Log (DT)

Carbonate-dominated facies C1 and C3 and siliciclastic-dominated facies S1, S2, S3, and S4 have higher average sonic log values ranging from 63.54 to 70.36 feet/second (Table 6D and Figure 28D). Values for facies C1, S3, and S4 are slightly higher than for facies C3, S1 and S2. These facies show higher neutron porosity values, and lower lithodensity values. Facies ES1, ES2, and ECA have lower average sonic log values, ranging from 56.82 to 59.47 feet/second. They also show the highest lithodensity values of the 10 lithofacies. This reflects relative differences in bulk density of the 10 lithofacies, which ultimately indicates the content of evaporite cement in those three facies. Higher sonic log values are positively correlated with low evaporite content, low sonic log values are negatively correlated with higher neutron porosity and gamma ray values, and positively correlated with low lithodensity values in the 10 lithofacies. Because sonic log data exists only in a few Class 1 and 2 wells in the study area, sonic logs could be used only as supplementary reference log data in determining the lithology of uncored regions.

Photoelectric Absorption Log (PEF)

High, intermediate and low categories were identified from univariate statistics of PEF log values (Table 6E and Figure 28E). Evaporite-dominated facies ES1, ES2, and ECA show highest average values (4.70 to 5.26 barns/electron). Facies ES2 and ECA have greater variance than facies ES1. These facies also have high values in lithodensity logs. Carbonate facies C1, C2 and C3 have intermediate PEF average values (3.33 to 3.74 barns/electron). Lithodensity values for these are also intermediate but variances in PEF values of three carbonate facies are greater than lithodensity variances. Facies S1, S2, and S3 show lowest PEF average values (2.79 to 3.00 barns/electron). Higher PEF log can be correlated with lower neutron porosity log and real porosity values and is a good indicator of low porosity. Because this PEF log data exist in only a few Class 1 and 2 wells in the study area, this PEF log is also used as good supplementary reference log data for determination of lithology in uncored region.

Well Log Facies (Efacies)

Because the 10 Queen lithofacies were identified based on sedimentary and petrophysical characteristics, it was very difficult to generate a clear-cut well log signature for

each facies to use for reservoir zone delineation and stratigraphic interpretation. Designed well log lithofacies (Efacies) should express both characteristics of base-level fluctuations and the relevant variation of petrophysical reservoir properties. Many previous works on well log facies (Efacies) construction for reservoir description used purely descriptive lithofacies subdivisions in which lithofacies reflect different lithological, textural, and compositional attributes regardless of relative sequence stratigraphic evolution and the relevant petrophysical properties variations (Serra, 1984a; Serra, 1984b; Hurst and Archer, 1986; Serra, 1986; Griffiths, 1990; King, 1990; Moss, 1990; Pereira et al., 1990; Doveton and Prensky, 1992; Bucheb and Evans, 1994; Chawathe et al., 1997). However, the designed well log facies in this study were required to reflect the relative significance of base-level changes and petrophysical properties rather than simply using the 10 lithofacies.

A multi-regressive correlation procedure (Kerans and Tinker, 1997) was used. The 10 lithofacies were each assigned a coed: code 1 (facies S4), code 2 (facies S3), code 3(facies S2), code 4 (facies S1), code 5 (facies C3), code 6 (facies C2), code 7 (facies C1), code 8 (facies ECA), code 9 (facies ES2), and code 10 (facies ES1). The statistical correlation analysis showed that gamma ray, neutron porosity, and sonic logs exhibit positive correlation with the 10 lithofacies, and lithodensity and photoelectric absorption logs show a negative relationship with the 10 lithofacies, reflecting slightly decreasing porosity and increasing evaporite content from facies code 1 to 10. However, sonic logs values in this study area exhibits the least correlation result that has 0.34 in correlation coefficient value with numerical lithofacies codes, according to the correlation matrix (Figure 29). Therefore, this sonic log will be the first candidate to be excluded in further correlation steps.

The 10 lithofacies were then divided into 3 groups (Efacies) based on the statistical analysis of well log values. The 3 Efacies groups were used to determine lithology in uncored intervals, and interpret relative base-level positions and petrophysical properties (Table 7). Efacies 1 comprises four siliciclastic lithofacies S1, S2, S3, and S4 and one argillaceous dolomudstone of facies C3, which were generally deposited under base-level rise conditions of lowstand to transgressive systems tracts and have a relatively higher porosity value. Efacies 2 consists of two carbonate lithofacies (C1 and C2), which were deposited at early highstand systems tracts of turnaround points between base-level rise and fall hemicycle and have an intermediate range of porosity value. Efacies 3 includes three evaporite lithofacies (ECA, ES2, and ES1), which were deposited under base-level fall conditions of late highstand systems tracts

A

Univariate Statistics

Variable	N	Mean	Std Dev	Minimum	Maximum
NFacies	38	5.0789	2.4756	2.0000	9.0000
GR	38	74.4305	48.2892	4.9900	124.3300
RHOB	38	2.6527	0.2234	2.3537	2.9499
PHIN	38	12.9507	9.7871	1.9159	30.3256
PEF	38	3.1066	1.0212	1.8800	5.0200
DT	38	60.2814	8.8972	51.4442	78.7053

B

Correlation Matrix

	NFacies	GR	RHOB	PHIN	PEF	DT
NFacies	1.0000					
GR	-0.9069	1.0000				
RHOB	0.8624	-0.9351	1.0000			
PHIN	-0.7949	0.8359	-0.9515	1.0000		
PEF	0.8833	-0.9604	0.9188	-0.8553	1.0000	
DT	0.3415	-0.0976	0.0475	-0.0371	0.0493	1.0000

C

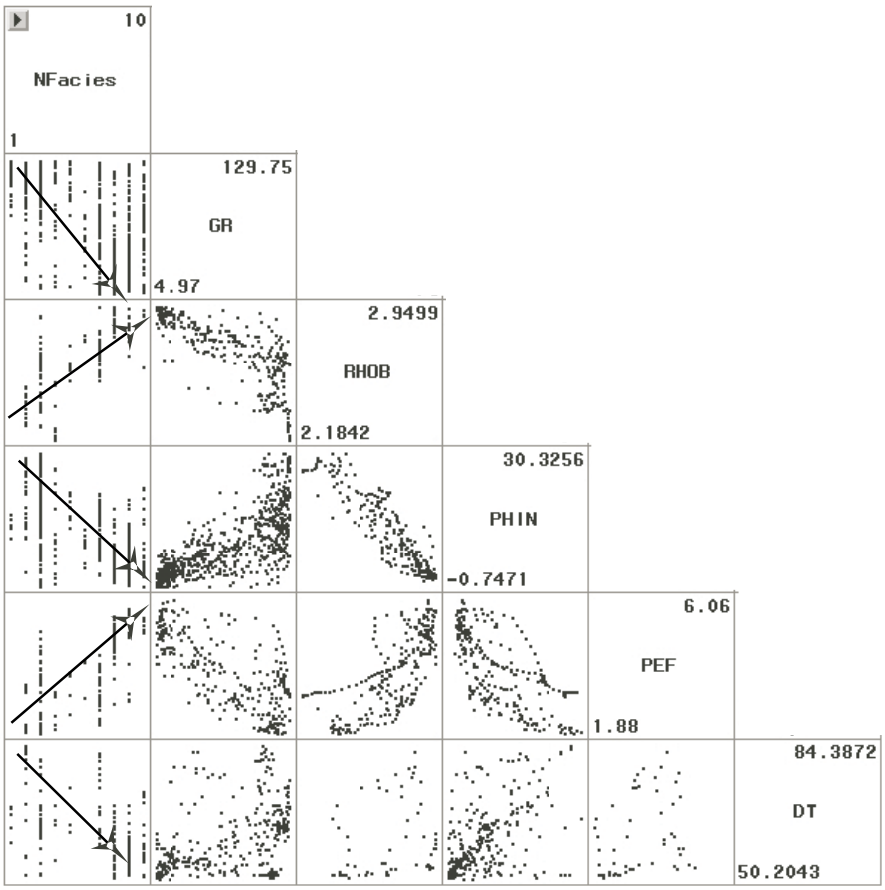

Figure 29. Summary of univariate statistics of well log values in lithofacies. (A) Univariate statistics, showing the minimum and maximum range of 5 well log data. (B) Correlation matrix indicating a lack of correlation between sonic log (DT) and facies (Nfacies). (C) Cross-plot matrix indicating positive and negative correlation (arrows) between facies and 5 well log parameters.

Table 7. Ordinal Efacies.

Efacies Codes	Existing Descriptive Lithofacies	Characteristics
3	ECA	Mosaic and massive anhydrite or halite with or without dolomite laminae
	ES2	Nodular, enterolithic, mosaic, and chicken-wire anhydrite with red brown siltstone background
	ES1	Reddish brown deformed wavy laminated and disturbed silt- to mudstone with felted and rosette structured anhydrite
2	C1	Peloidal dolomudstone with fenestral pore, cryptalgal laminae, solution breccia and sheet crack
	C2	Skeletal and peloidal dolowackestone tograinstone
1	C3	Argillaceous dolomudstone
	S1	Thin laminated silt- to mudstone
	S2	Ripple and cryptalgal wavy laminated silt- to sandstone with bioturbation
	S3	Planar cross- and horizontal -laminated sandstone with deformed wavy lamination due to the growth of anhydrite nodule
	S4	Massive sandstone with rip-up mud clasts, syndeformational, and fluid-escape structure

and have a low porosity value. Using these new subdivisions of Efacies codes, the statistical summary was performed to define their typical values of means and variance for more distinct lithology determination of Queen uncored intervals (Table 8 and Figure 30).

Gamma Ray Log (GR)

Efacies 1 gamma ray values range from 10.73 to 129.75 API units (an average of 106.92 API unit) the highest gamma ray values of the three lithofacies codes. Efacies 2 gamma ray values range from 6.3 to 127.44 API units (an average of 71.62 API units). Efacies 3 gamma ray values range from 4.97 to 129.29 API units (an average of 46.95 API units), the lowest average gamma ray values. Decreasing gamma ray values from facies code 1 to 3 reflect increasing evaporite content and decreasing shale content and porosity (Table 8A and Figure 30A).

Neutron Log (PHIN)

Efacies 1 neutron porosity values are highest ranging from –0.69 to 30.33 % (an average of 15.89 %). Efacies 2 values range from 2.09 to 20.95 % (an average of 11.50%). Efacies 3 values range from –0.56 to 22.25 % (an average of 5.85%). Decreasing values from Efacies 1 to 3 also reflects increasing evaporite content and decreasing shale content and porosity, like gamma ray log values (Table 8B and Figure 30B).

Lithodensity Log (RHOB)

Efacies 1 has lowest lithodensity values ranging from 2.18 to 2.90 g/cm^3 (an average of 2.50 g/cm^3). Efacies 2 values range from 2.52 to 2.95 g/cm^3 (an average of 2.72 g/cm^3). Efacies 3 has highest values, ranging from 2.60 to 2.95 g/cm^3 (an average of 2.86 g/cm^3). Increasing lithodensity values from Efacies 1 to 3 reflect increasing evaporite content and decreasing shale content and porosity, similar to the interpretations for gamma ray log and neutron porosity log values (Table 8C and Figure 30C).

Sonic Log (DT)

Efacies 1 has sonic log values ranging from 51.44 to 84.39 feet/second (an average of 64.90 feet/second). Efacies 2 has sonic log values ranging from 59.14 to 82.47 feet/second (an average of 70.36 feet/second). Efacies 3 values range from 50.89 to 72.43 feet/second (an average of 57.75 feet/second) (Table 8D and Figure 30D). The sonic log values of each of the three facies codes from Efacies 1 to 3 slightly reflect the direction of increasing evaporite content, but it is not a good indicator of bulk porosity-unlike other gamma ray, neutron, lithodensity and photoelectric absorption logs. The sonic log signature variation from Efacies 1 to 3 may result from development of secondary porosity and fracture in dolomitized carbonate-

Table 8. Well log properties of Efacies.

A. Gamma Ray (API)

Efacies	1	2	3
Mean	106.82	71.62	46.95
Maximum	129.75	127.44	129.29
Minimum	10.73	6.30	4.97
Standard Deviation	23.50	34.98	38.08

B. Neutron Porosity (%)

Efacies	1	2	3
Mean	15.89	11.50	5.84
Maximum	30.33	20.95	22.25
Minimum	-0.69	2.09	-0.56
Standard Deviation	8.44	4.75	5.01

C. Litho-density (g/cm3)

Efacies	1	2	3
Mean	2.50	2.72	2.86
Maximum	2.90	2.95	2.95
Minimum	2.18	2.52	2.60
Standard Deviation	0.17	0.08	0.08

D. Sonic (ft/sec)

Efacies	1	2	3
Mean	64.90	70.36	57.75
Maximum	84.39	82.47	72.43
Minimum	51.44	59.14	50.89
Standard Deviation	9.83	8.06	5.20

E. Photoelectric Absorption (barns/electron)

Efacies	1	2	3
Mean	2.97	3.36	4.78
Maximum	5.07	4.34	5.76
Minimum	1.88	2.19	2.82
Standard Deviation	0.83	0.65	0.74

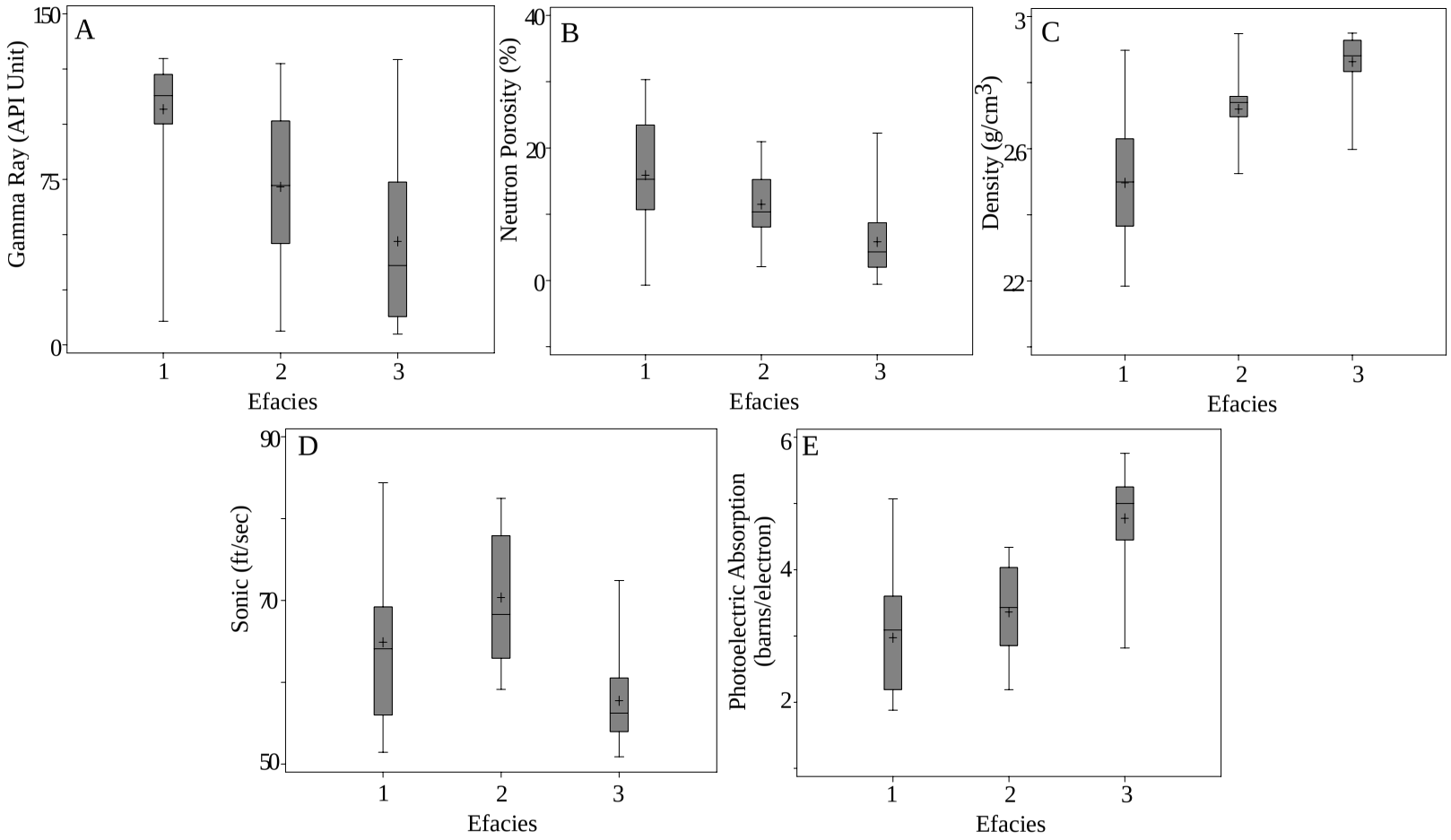

Figure 30. Well log values of Efacies. The center of each box is the 50th percentile; margins of the boxes are the 25th and 75th percentiles; and whiskers denote the 0th and 100th percentiles. See Table 8 for statistical comparison of Efacies.

dominated facies. The correlation coefficients show the least correlative between Efacies and the sonic log (Figure 31). Therefore, this sonic log will be excluded at further lithology determination processes of well log data.

Photoelectric Absorption Log (PEF)

Efacies 1 has lowest PEF log values, ranging from 1.88 to 5.07 barns/electron (an average of 2.97 barns/electron). Efacies 2 are in the intermediate range from 2.19 to 4.34 barn/electron (an average of 3.36 barns/electron). Efacies 3 are highest and range from 2.82 to 5.76 barns/electron (an average of 4.78 barns/electron). Decreasing values PEF log from Efacies 1 to 3 reflect increasing evaporite content and decreasing shale content and porosity like the lithodensity logs. Its trend shows the opposite direction from gamma ray and neutron porosity logs (Table 8E and Figure 30E).

Efacies

Lithodensity and photoelectric absorption log signatures increase from Efacies 1 to 3 while gamma ray, neutron porosity, and sonic logs increase from Efacies 3 to 1 (Figure 31). Particularly, photoelectric absorption log and lithodensity log values have higher positive correlation coefficient values (R^2 value), which are 0.91 and 0.88, respectively, while sonic logs have the least positive correlation coefficient value, which is 0.11. In the case of negative correlation coefficient values, gamma ray and neutron porosity have–0.99 and–0.77, respectively (Figure 31B).

In order to remove the least significant well log value and further lithology determination based on the only well log data characterization, multiple regressive analyses was performed between 3 Efacies codes and 5 well log signatures (Figure 31). Well log values have the smallest “F” factor in the ANOVA table, the “F” factor indicates a false probability in that correlation. In addition to this process, a correlation coefficient value was used in a qualitative sense to determine the effectiveness of that statistical process. From the first iteration of multiple regressive analyses, lithodensity, photoelectric absorption log, and sonic log have the least significant “F” values, which are 0.57, 0.7 and 0.25, respectively (Figure 32 and 33). Therefore, those three well log data were excluded from next further steps, which are the generation processes of predictive model equations of lithology determination in uncored intervals. Based on the multi regressive process between the gamma ray and neutron porosity log signature, and 3 Efacies codes, the predictive model equation of lithology determination of the Queen uncored interval

A

Univariate Statistics

Variable	N	Mean	Std Dev	Minimum	Maximum
Ecode3	38	1.7368	0.8909	1.0000	3.0000
GR	38	74.4305	48.2892	4.9900	124.3300
RHOB	38	2.6527	0.2234	2.3537	2.9499
PHIN	38	12.9507	9.7871	1.9159	30.3256
PEF	38	3.1066	1.0212	1.8800	5.0200
DT	38	60.2814	8.8972	51.4442	78.7053

B

Correlation Matrix

	Ecode3	GR	RHOB	PHIN	PEF	DT
Ecode3						
GR	-0.9415					
RHOB	0.8780	-0.9351				
PHIN	-0.7729	0.8359	-0.9515			
PEF	0.9116	-0.9604	0.9188	-0.8553		
DT	0.1116	-0.0976	0.0475	-0.0371	0.0493	

C

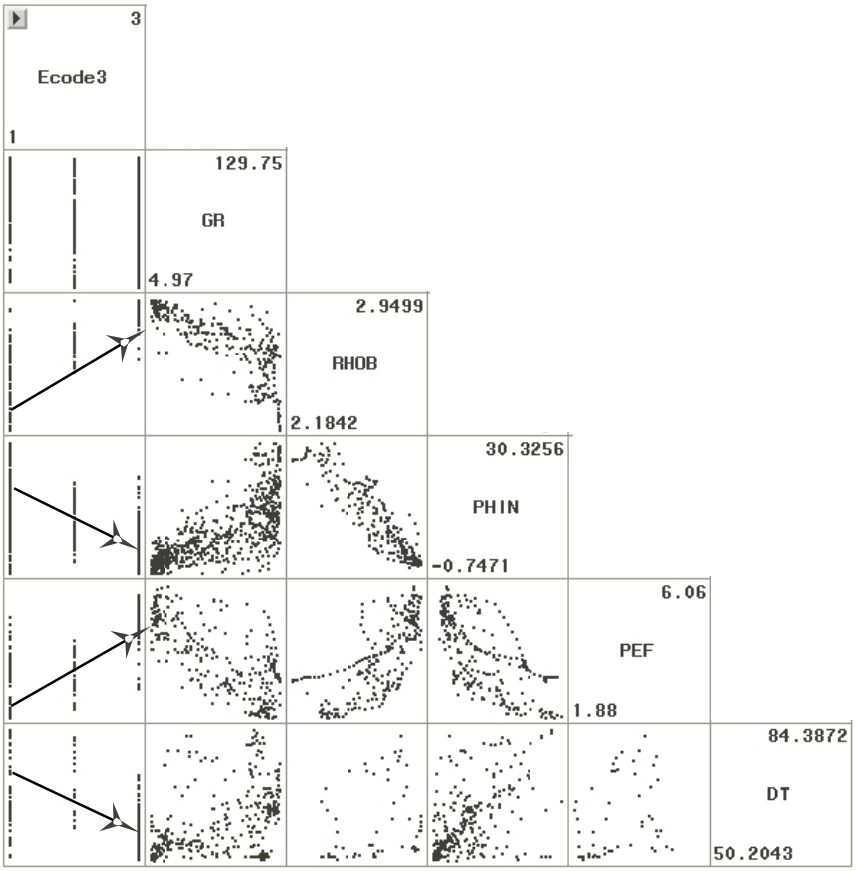

Figure 31. Summary of univariate statistics of well log values in Efacies. (A) Univariate statistics, showing the minimum and maximum range of 5 major well log data. (B) Correlation matrix indicating a lack of correlation between sonic log (DT) and Efacies (Ecode3). (C) Cross-plot matrix indicating positive and negative correlation (arrows) between facies and 5 well log parameters. It shows the better correlation than Nfacies.

A

Ecode3 = GR RHOB PHIN PEF DT
Response Distribution: Normal
Link Function: Identity

Model Equation
Ecode3 = - 1.0485 - 0.0128 GR + 1.0433 RHOB + 0.0203 PHIN + 0.1692 PEF + 0.0030 DT

Summary of Fit			
Mean of Response	1.7368	R-Square	0.8909
Root MSE	0.3165	Adj R-Sq	0.8738

Analysis of Variance					
Source	DF	Sum of Squares	Mean Square	F Stat	Pr > F
Model	5	26.1633	5.2327	52.24	<.0001
Error	32	3.2051	0.1002		
C Total	37	29.3684			

Type III Tests					
Source	DF	Sum of Squares	Mean Square	F Stat	Pr > F
GR	1	0.5510	0.5510	5.50	0.0254
RHOB	1	0.0566	0.0566	0.57	0.4577
PHIN	1	0.0919	0.0919	0.92	0.3453
PEF	1	0.0706	0.0706	0.70	0.4075
DT	1	0.0252	0.0252	0.25	0.6192

B

Ecode3 = GR PHIN
Response Distribution: Normal
Link Function: Identity

Model Equation
Ecode3 = 3.1090 - 0.0107 GR - 0.0231 PHIN

Summary of Fit			
Mean of Response	2.0143	R-Square	0.4369
Root MSE	0.6902	Adj R-Sq	0.4342

Analysis of Variance					
Source	DF	Sum of Squares	Mean Square	F Stat	Pr > F
Model	2	153.7419	76.8709	161.37	<.0001
Error	416	198.1722	0.4764		
C Total	418	351.9141			

Type III Tests					
Source	DF	Sum of Squares	Mean Square	F Stat	Pr > F
GR	1	38.3773	38.3773	80.56	<.0001
PHIN	1	6.4131	6.4131	13.46	0.0003

Figure 32. Multiple regression analysis for predicted facies in uncored intervals. (A) Prediction of facies from all well log variables. Lithodensity (RHOB), photoelectric absorption (PEF) and sonic (DT) logs have relatively lower regression coefficients than gamma ray (GR) and neutron porosity (PHIN). Thus, lithodensity (RHOB), photoelectric absorption (PEF), and sonic (DT) logs are removed at step B of the calculation of predicted facies. (B) Predictive facies equation is created, and R-square values is 0.44.

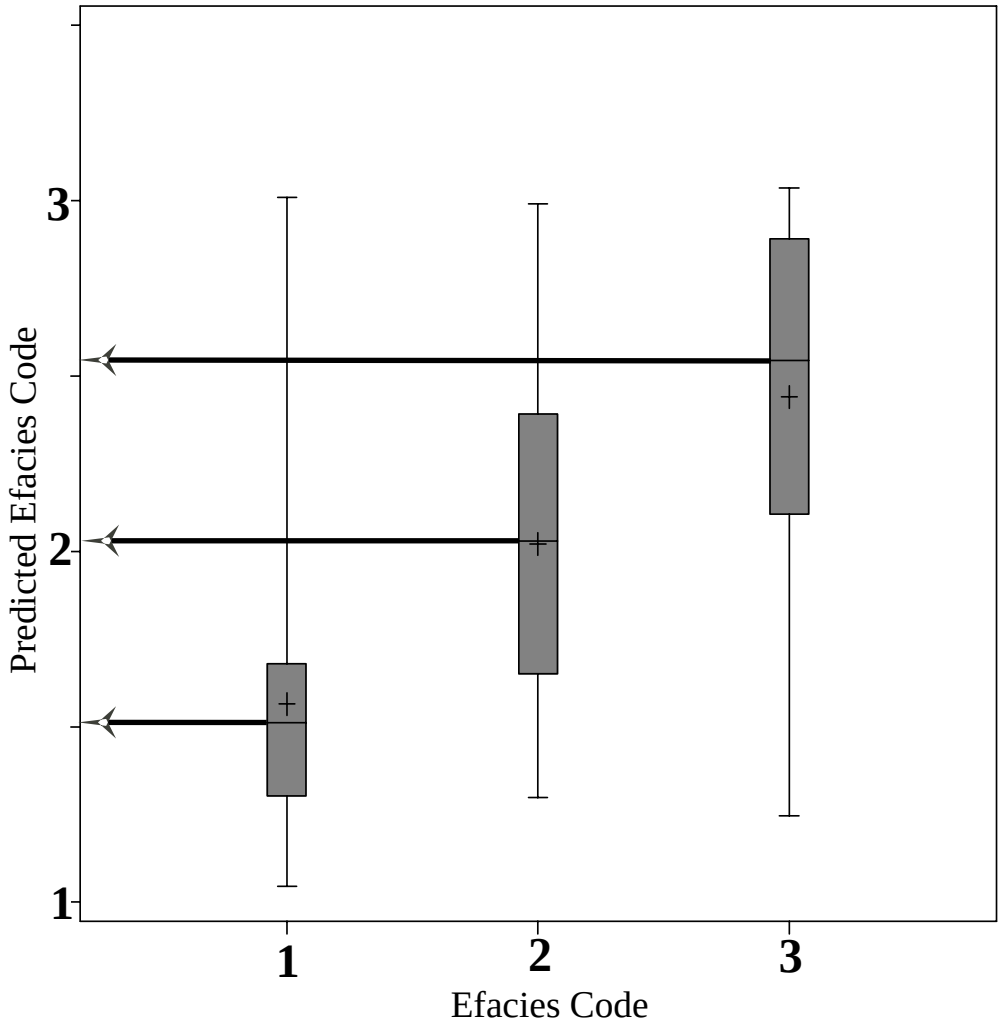

Figure 33. Representative box and whisker plot of actual and predicted Efacies. Efacies 1 is overestimated and Efacies 3 is somewhat underestimated as a function of the averaging inherent in regression analysis.

was generated, in which the regressive coefficient is 0.43. The generated predictive equation is as follows (Figure 32B):

Ecode3=3.1090–(0.0107xGR)–(0.0231xPHIN)

Where,

Ecode3=Efacies code 1, 2, and 3

GR=gamma ray

PHIN=neutron porosity

Because gamma ray and neutron porosity logs are the only available well logging data in all of the study area, this predictive equation could be the best alternate solution for lithology determination of uncored intervals. According to the comparison between actual core data and generated data, the newly generated Efacies codes from gamma ray and neutron porosity logging data show the reasonable match between them (Figure 32). Although overestimated Efacies 1 values and underestimated Efacies 3 values were generated from the equation, it was very useful in determining lithology at the Queen uncored interval (Figure 33). Analyzed core porosity and permeability shows decreasing porosity and permeability from Efacies 1 to 3 (Figure 34).

FACIES ASSOCIATIONS

The vertical organization of facies in the Queen Formation can be used to define, four types of facies associations: (1) upward-fining, fluvial-influenced delta and estuarine deposits; (2) upward-shallowing arid carbonate tidal flat deposits; (3) upward-deepening (or brining) evaporite-dominated tidal sand flat deposits; and (4) upward-shoaling evaporite salina and sabhka deposits (Table 9 and Figure 35, 36 and 37).

Core porosity and permeability measurements of these facies associations indicate upward-shallowing facies association (C12, C13, and C22) have lower porosity and permeability than upward-deepening facies association (C11 and C21; Table 10 and Figure 38).

The four types facies associations of the Queen cored interval exhibit vertical textural and compositional variations (Table 11 and Figure 39). Upward-fining facies association 1 has more texturally immature composition than other facies associations. The amount of quartz, anhydrite, dolomite cement and clay increase from facies association 1 to 2, whereas feldspar content decrease from facies association 1 to 3. Grain size and sorting of detrital grains decrease from facies association 1 to 2 and 3 to 4, respectively.

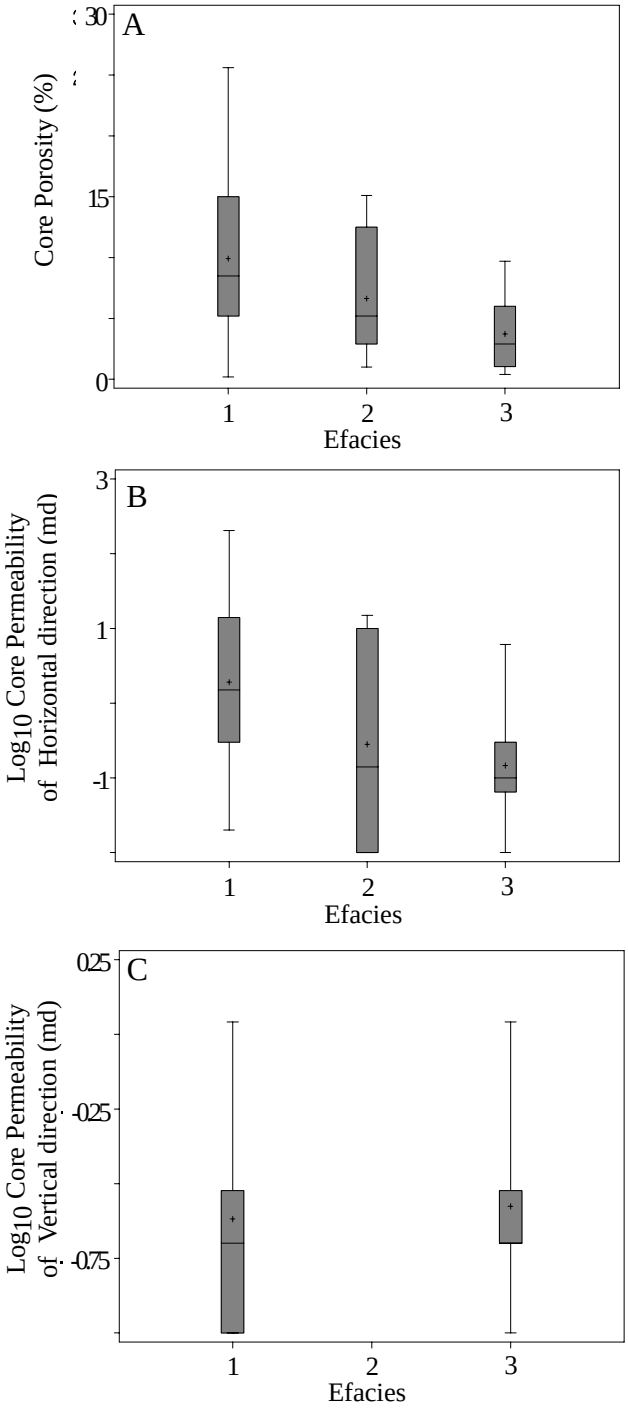

Figure 34. Petrophysical properties of Efacies. The center of each box is the 50th percentile; margins of the boxes are the 25th and 75th percentiles; and whiskers denote the 0th and 100th percentiles.

Table 9. Four types of facies associations.

Facies Association	Sedimentary Environments	Lithofacies	Characteristics
Type 4	Sabkha mudflat and salina deposits	ES1: Reddish brown deformed wavy laminated and disturbed silt- to mudstone with felted and rosette structured anhydrite ES2: Nodular, enterolithic, mosaic, and chicken wire anhydrite with red brown siltstone background ECA: Mosaic and massive anhydrite (or halite) with dolomite laminae	Upward-shallowing: C22,C912, C922, C102, C112, C122, C132, C142, C152, and C162
Type 3	Intertidal to subtidal sandflat (or beach-ridge) deposits	S2: Ripple and cryptalgal-laminated silt- to sandstone with bioturbation S3: Cross- and horizontal –laminated sandstone with anhydrite nodule	Upward-deepening or-brining: C21, C911, C921, C101, C111, C121, C131, C141, C151, and C161
Type 2	Supratidal sabkha deposits	ES1: Reddish brown deformed wavy laminated and disturbed silt- to mudstone with felted and rosette structured anhydrite ES2: Nodular, enterolithic, mosaic, and chicken wire anhydrite with red brown siltstone background ECA: Mosaic and massive anhydrite with dolomite laminae C1: Peloidal dolomudstone with fenestral pore, cryptalgal laminae, solution breccia and sheet crack	Upward-shallowing: C12, C32, C42, C521, C522, C621, C622, C72, and C82
	Inter to subtidal carbonate tidal flat	C2: Skeletal and peloidal dolowackestone to grainstone C3: Argillaceous dolomudstone	
Type 1	Bay delta or estuarine deposits	S1: Thin laminated silt- to mudstone S2: Ripple and cryptalgal-laminated silt- to sandstone with bioturbation S3: Cross- and horizontal –laminated sandstone with anhydrite nodule	Upward-fining or-deepening: C11 and C171
	Fluvial channel deposits	S4: Massive sandstone with rip-up mud clasts, syndeformational, and fluid-escape structure.	

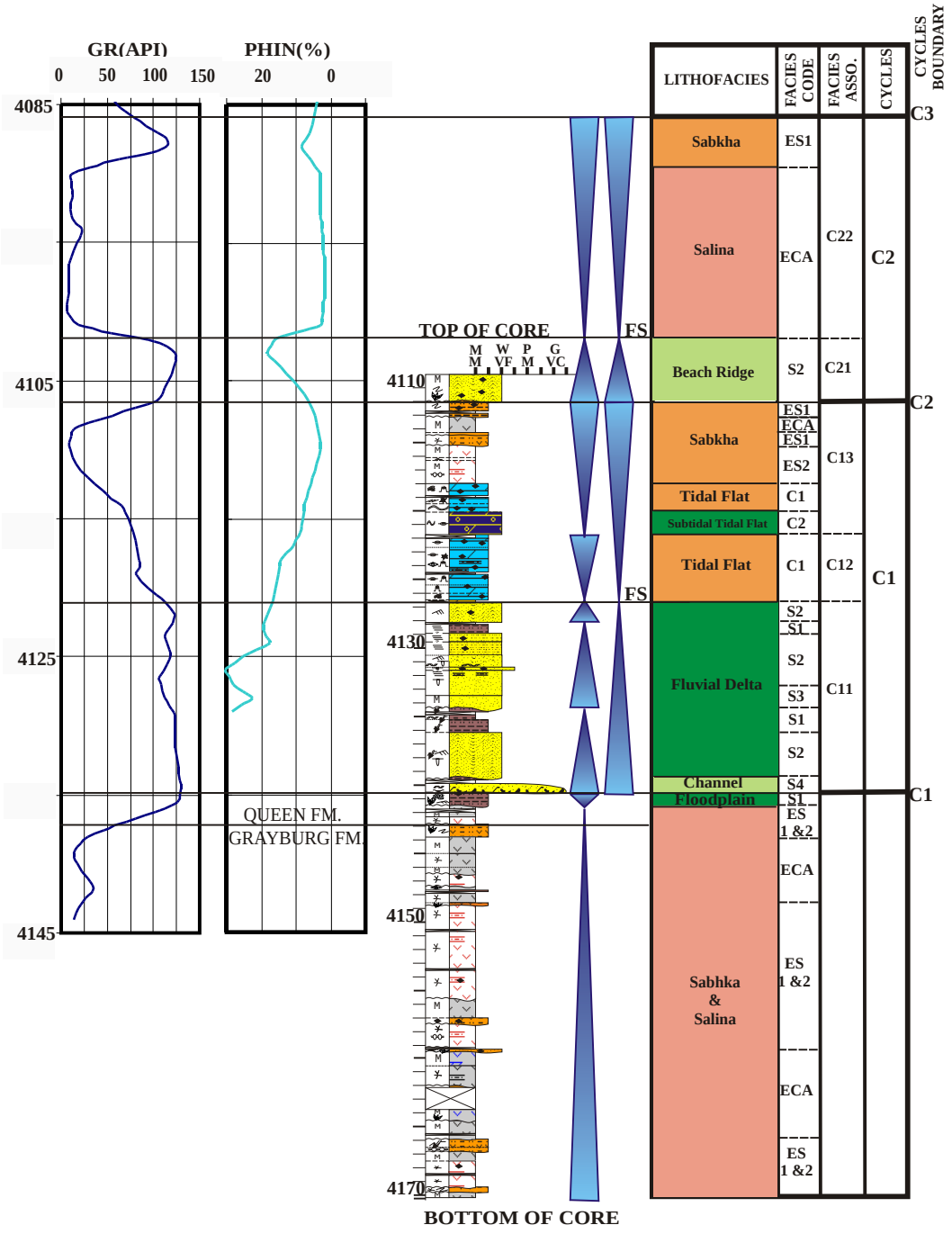

Figure 35. Lithostratigraphic, gamma ray and neutron porosity logs of JSM 23-19 shows the basal part of the Queen Formation. Contact between the Queen and underlying Grayburg Formation is sharp. Note 4 feet depth difference in scale of core and well log.

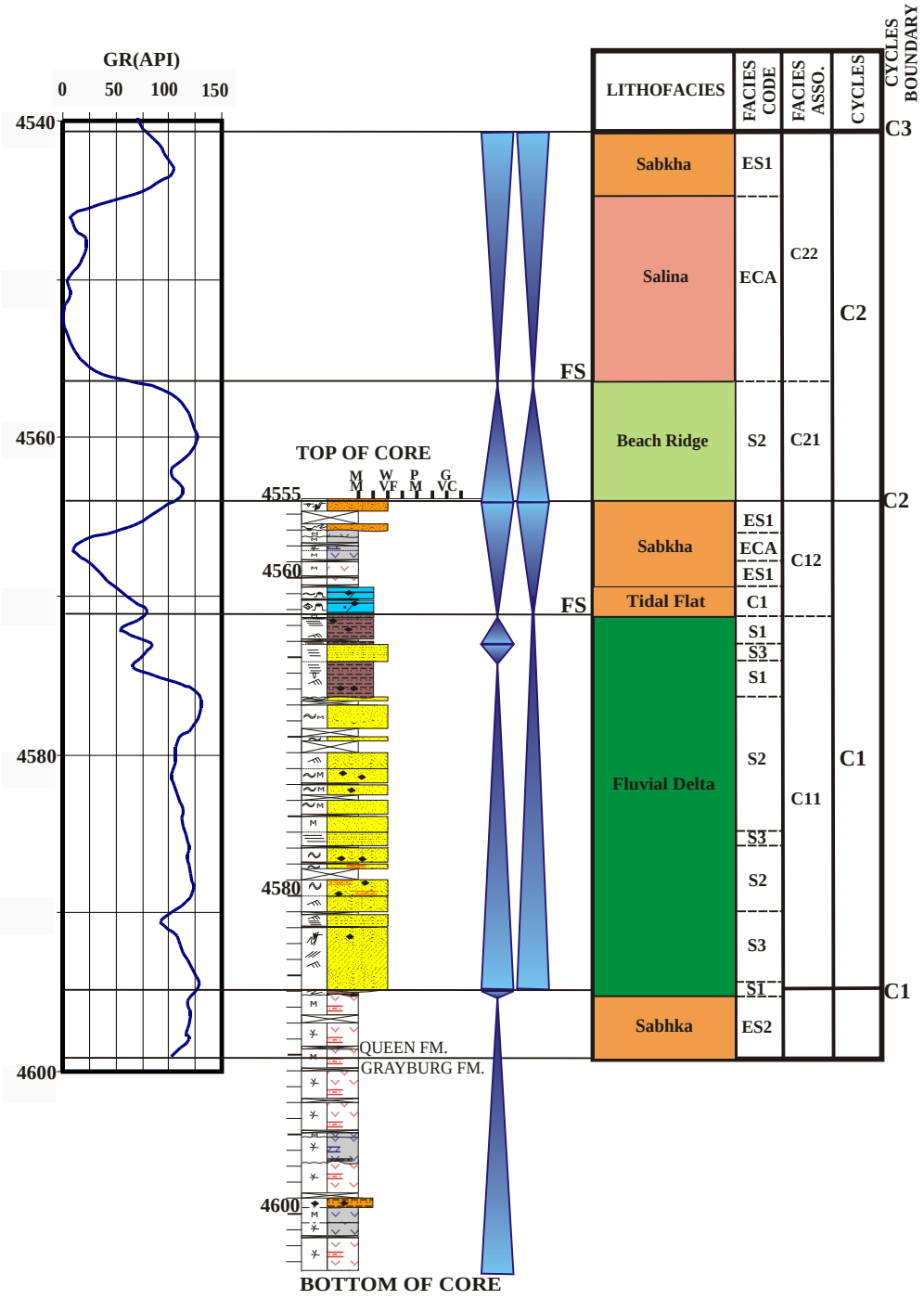

Figure 36. Lithostratigraphic and gamma ray well logs for RMM 301well shows the basal part of the Queen Formation. Contact between the Queen and underlying Grayburg Formation is sharp. Note -9 feet depth differencein scale of core and wel log. .

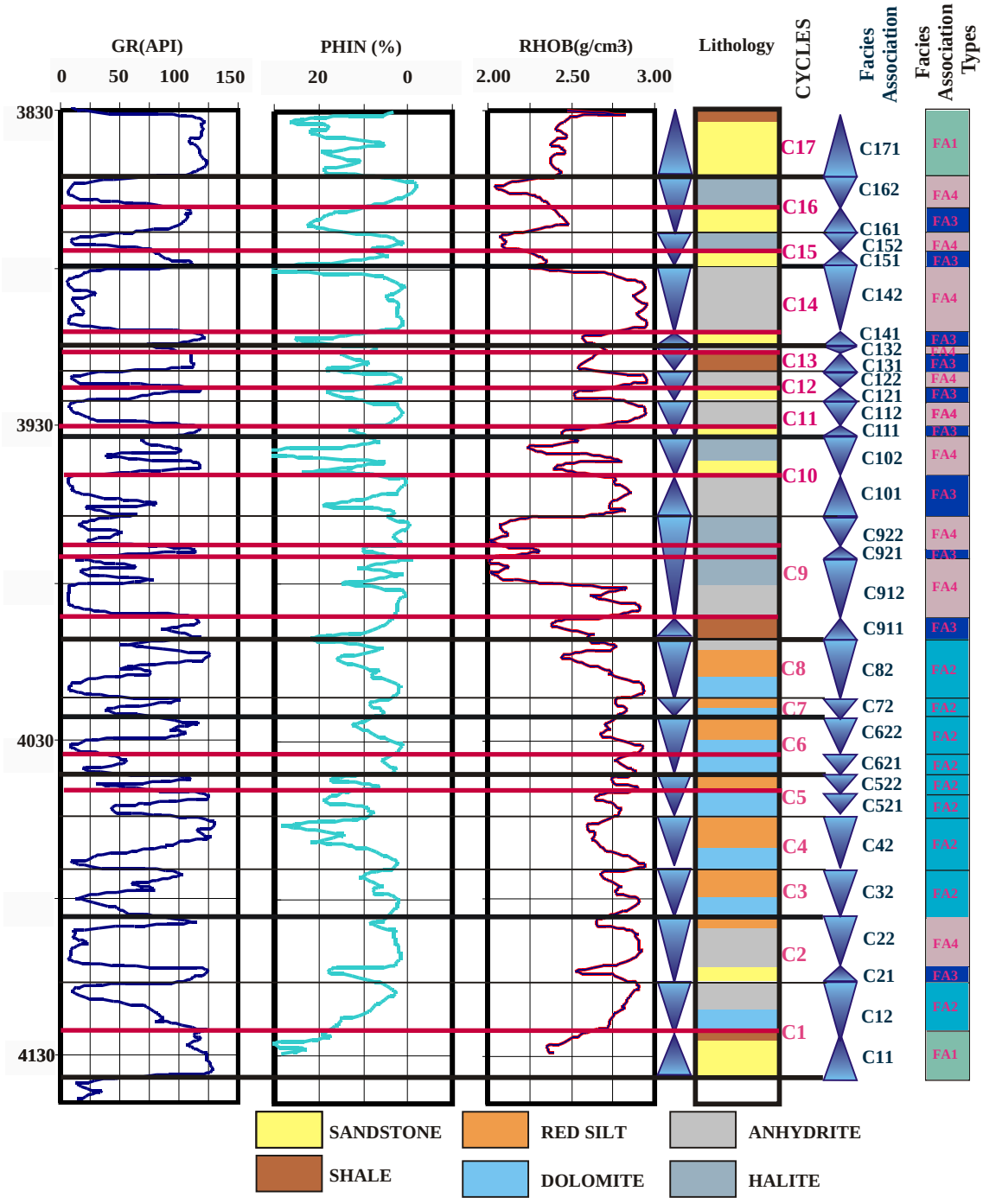

Figure 37. Type log and interpreted lithology of JSM 23-19 well generated by gamma ray (GR), neutron porosity(PHIN) and lithodensity (RHOB) well logs. 32 beds are defined within the Queen Formation. Each bed is assigned to one of four lithofacies associations. Attributes of within successive beds lithofacies defines 17 cycles. Note 4 feet offset in depth scale between the core and well log.

Table 10. Petrophysical properties facies associations.

A. Core Porosity (%)

Facies Associations	C11	C12	C13	C21	C22
Mean	11.38	5.39	5.38	7.12	2.75
Maximum	25.60	15.10	6.90	19.80	5.30
Minimum	0.20	0.40	2.90	0.20	1.00
Standard Deviation	6.01	4.34	1.56	4.47	1.43

B. Core Permeability in horizontal direction (md)

Facies Associations	C11	C12	C13	C21	C22
Mean	18.21	2.64	0.34	4.66	0.23
Maximum	204.00	15.00	1.50	66.00	0.60
Minimum	-0.10	0.01	0.01	-0.10	-0.10
Standard Deviation	31.16	4.73	0.58	12.17	0.29

C. Core Permeability in vertical direction (md)

Facies Associations	C11	C12	C13	C21	C22
Mean	0.27	NA	0.47	0.23	0.20
Maximum	1.10	NA	1.10	0.90	0.60
Minimum	-0.10	NA	0.10	-0.10	-0.10
Standard Deviation	0.35	NA	0.55	0.34	0.26

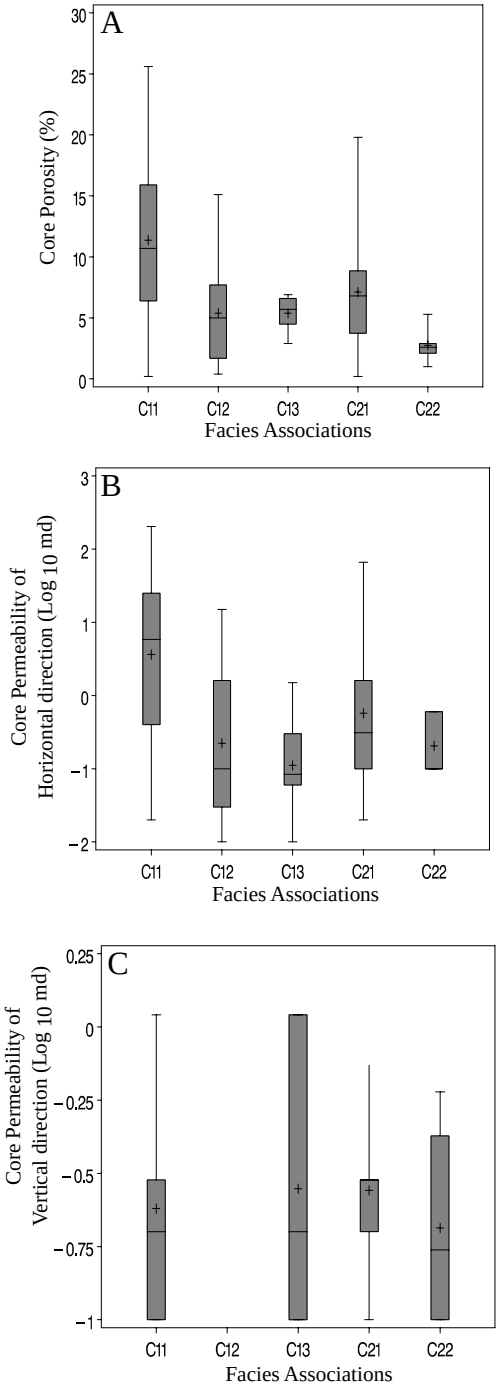

Figure 38. Petrophysical properties of facies associations. The center of each box is the 50th percentile; margins of the boxes are the 25th and 75th percentiles; and whiskers denote the 0th and 100th percentiles. See Table 10 for statistical comparison of facies associations.

Table 11. Texture of framework grains, matrix, and authigenic cements in facies associations.

A Grain size (mm)

Facies Association	Mean	Maximum	Minimum
C22	0.061	0.079	0.047
C21	0.061	0.101	0.025
C13	0.048	0.065	0.029
C12	0.060	0.107	0.033
C11	0.069	0.109	0.033

B. Sorting (ϕ)

Facies Association	Mean	Maximum	Minimum
C22	0.51	0.56	0.47
C21	0.49	0.77	0.39
C13	0.55	0.73	0.46
C12	0.53	0.64	0.43
C11	0.50	0.77	0.37

C. Quartz (%)

Facies Association	Mean	Maximum	Minimum
C22	32	62	3
C21	31	43	7
C13	28	41	1
C12	30	50	13
C11	28	41	6

D. Feldspar (%)

Facies Association	Mean	Maximum	Minimum
C22	10	18	0
C21	8	14	0
C13	2	7	0
C12	10	18	0
C11	9	14	4

Table 11. Continued.

E. Rock fragments (%)

Facies Association	Mean	Maximum	Minimum
C22	3	8	0
C21	3	6	0
C13	2	4	0
C12	3	8	0
C11	2	6	0

F. Cements (%)

Facies Association	Mean	Maximum	Minimum
C22	34	97	0
C21	32	53	0
C13	63	88	38
C12	46	75	17
C11	56	85	43

G. Clay (%)

Facies Association	Mean	Maximum	Minimum
C22	4	37	0
C21	8	34	0
C13	25	38	8
C12	5	41	0
C11	2	5	0

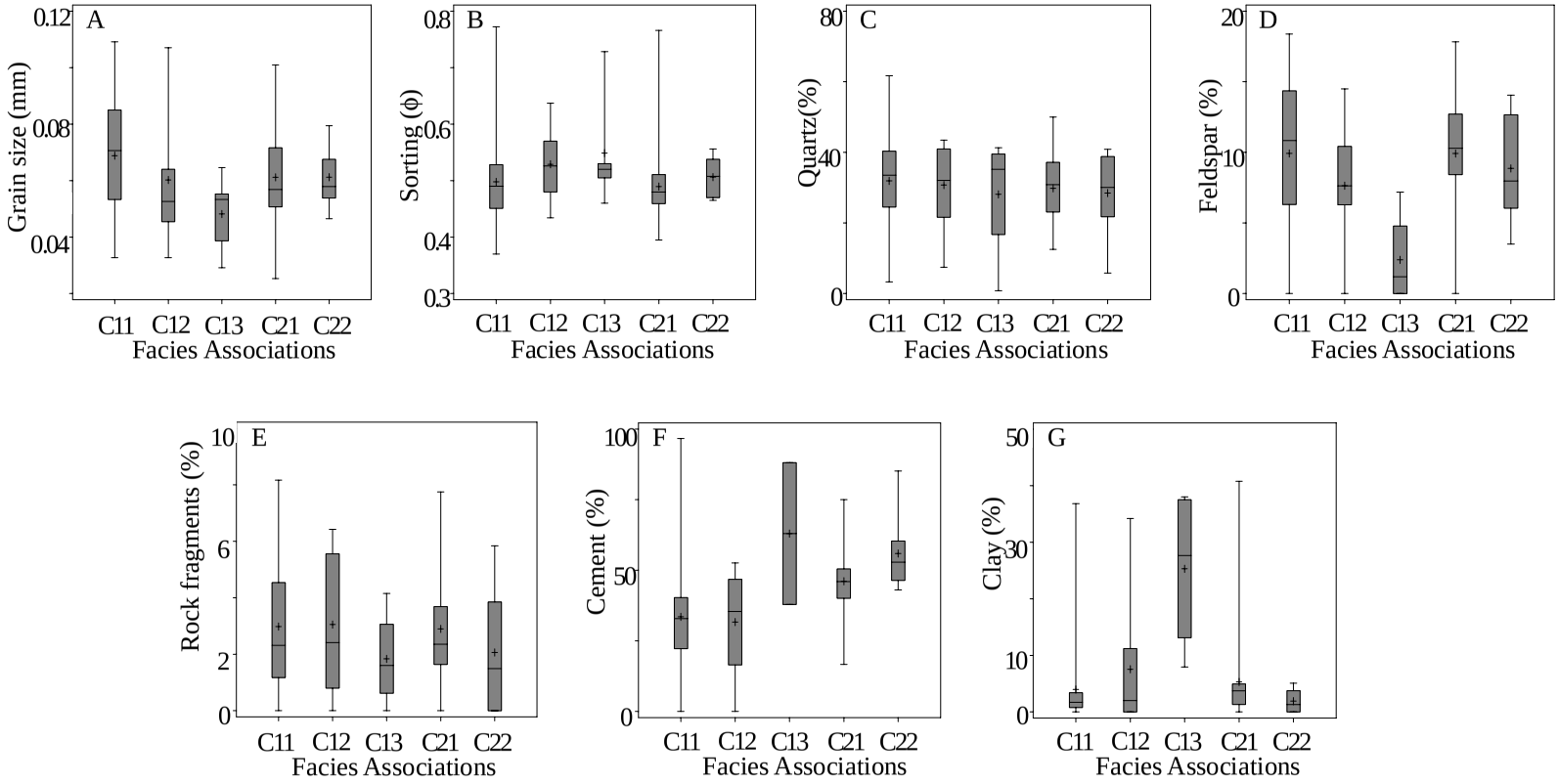

Figure 39. Texture and composition of facies associations. (A) Grain size; (B) Sorting; (C) Quartz; (D) Feldspar; (E) Rock fragments; (F) Cement; and (G) Clay. See Table 11 for tabulation of these data.

Facies Association 1 (FA1)

Lithofacies within this association are arranged in an upward-fining order: (1) small, shallow scour surfaces based beds (facies S4), (2) planar-cross stratified and horizontal laminated sandstone (facies S3), (3) ripple-laminated sandstone (facies S2), and (4) thin mud laminated sandstone (facies S1). Facies transitions within the association are gradational. The best-documented example of this facies association is 15.8 feet (4.7 meters) on an average, and has pronounced elongate patterns in plain view that extend from the western margin to the southeastern end of study area within a more uniformly-thick sheet-shaped sandstone.

Where the association is thick, there is a complete upward-fining facies succession from facies S4, S3, S2, to S1. Deposits lie along these thick zones grade downdip from sand-prone proximal fluvial-dominated deposits to mud-prone distal marine-dominated deposits. The southeastern part of the west to east trending thick zone is composed of bioturbated horizontal laminated siltstone to mudstone of facies S1. In isopach maps the association has a meandering and straight channel morphology, superimposed on a lobate thinning geometry that suggests a shoreline-attached delta (Figure 40A). The thick zone of this facies association is 8 km long, 1.2 km wide, and up to 40 feet (12 m) thick (Figure 40A). Where relatively thin deposits consist only of facies S3 and S2, which is less than 10 feet thick.

Facies association thickness trends and vertical and lateral facies patterns suggested deposits are fluvial-influenced deltas cut by shallow coastal-plain incised valley fills. Valley were cut down during lowstand and filled with relatively thin deposits of prograding deltas during transgression. This coastal plain incised valley like a facies association 1 is reported as finer-grained and having more mature deposits recycled from coastal-plain sediment than that of piedmont incised valley fills. It is bounded by flooding surfaces that exhibit starvation of clastic materials and increased bioturbation (facies S3 and S4) (Figure 35 and 36).

Deposits along thicker parts in facies association 1 show a coarse-fine-coarse vertical lithofacies pattern similar to that observed in wave-dominated incised valley fills (Dalrymple and Zaitlin, 1992). These fluvial-dominated sandy head bay deltas, pass offshore into muddy and evaporite-dominated lagoonal central basin, and a finally into wave-dominated sandy shoreface deposits (Dalrymple and Zaitlin, 1992). Distal mud-prone sections of facies association 1 can be interpreted as a distal incised valley fill deposits, while silt and sand prone section of facies association 1 can be interpreted as a proximal fluvial deposits and sheet flood deposits on adjacent floodplains after valleys had filled (Figure 35, 36 and 40A).

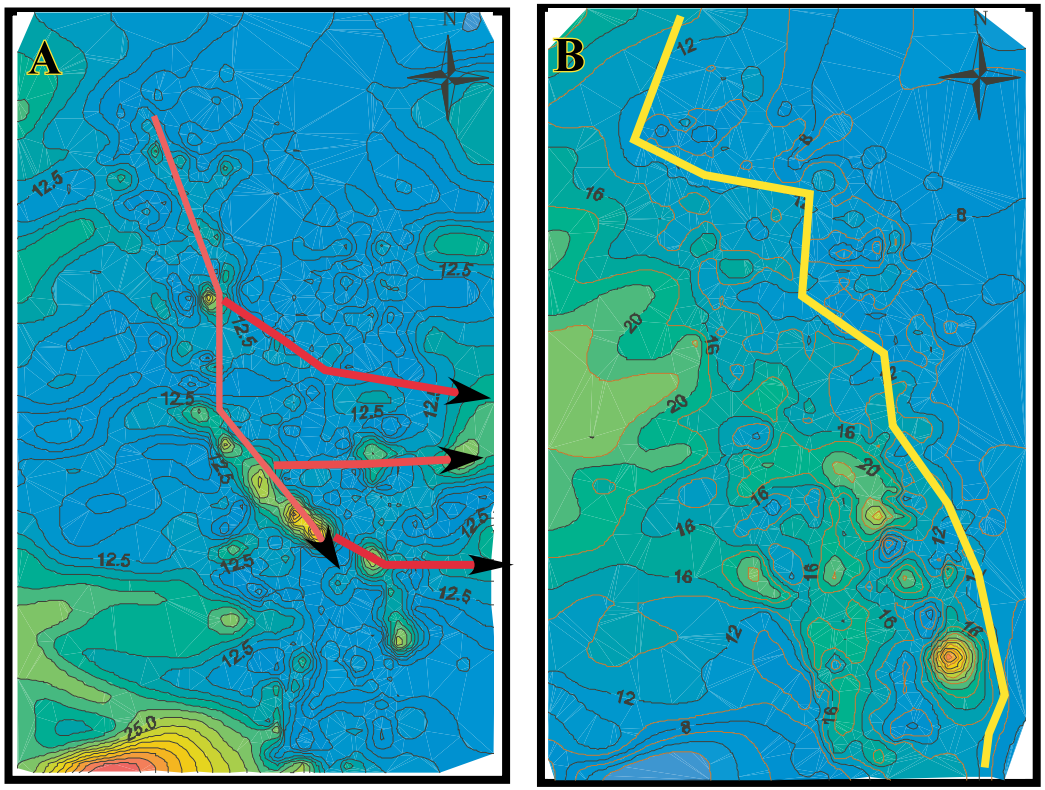

1 inch = 2.58 miles
Contour interval = 2.5 ft

1 inch = 2.58 miles
Contour interval = 2 ft

Figure 40. Isopach map of facies associations C11, C12 and C13. (A) Fluvial-dominated delta facies association of C11. Note incised fluvial channel deposits extending from northwest to southeast and thin sheet flood deposits of adjacent delta. (B) Arid carbonate tidal flat facies association of C12 and C13. Note that deposits thin to the northeast, a pattern interpreted to record decreased offshore depositional rates. Inferred coastline (yellow colored arrow) defines lithofacies transition from carbonate to shale-prone deposits.

Incised valley fills are defined as "fluvially-eroded, elongate paleotopographic low, generally larger than a single channel, which displays an abrupt basinward shift of facies at its base" (Zaitlin et al., 1994). Valleys fill during base-level rise, and in some cases also during subsequent highstands. Incised valleys are generally 100s km long and 10s of km wide, and up to hundreds meters deep. Normally fills are only ten to a few tens of meters thick. Narrow valleys generally cut into hard bottom substrates like limestone, whereas wide valleys cut into soft rock like as coal and shale (Schumm and Ethridge, 1994).

Fluvial-dominated incised fills of facies association 1 are very fine- to fine-grained sand. Low downstream slopes of the inner carbonate platform could have favored meandering rather than braided channels. During sea level rise, rapid transgression of these low gradient valleys did not provide enough time for deposition the classic valley fill succession proposed by Dalrymple and Zaitlin (1992), Zaitlin et al., (1994) and Zaitlin and Shultz (1984).

Facies Association 2 (FA2)

Where thicker this facies association comprises an upward-shallowing succession of subtidal argillaceous dolomudstone (facies C3), intertidal to subtidal skeletal and peloidal dolowackestone and dolopackstone (facies C2), fenestral fabric and desiccation structure including dolomudstone (facies C1), massive bedded anhydrite with thin dolomite laminae (facies ECA), nodular and mosaic-structured anhydrite (facies ES2), and reddish-brown siltstone to mudstone (facies ES1). Where thinner this facies association does not include facies C2 (Figure 35 and 36). The locally thicker carbonate-dominated deposits grade into shale-prone subtidal facies laterally to the northeast. This shaling of facies is approximately perpendicular to paleocoastaline and is interpreted to record a proximal to offshore facies transition. The thickness of facies association 2 averages 13.1 feet (3.9 meters) in cored interval (Figure 40B). Facies transitions in this association are generally gradational.

Facies association 2 is interpreted to be thin-bedded carbonate tidal deposits that the progression from (1) shallow restricted subtidal facies, (2) regressive fenestral fabric, (3) algal laminae supra tidal flat and (4) coastal sabhka is interpreted to record progradation. The association records increasing salinity and decreasing brine levels on the carbonate platform interior. Facies association 2 is similar to carbonate-anhydrite-halite capping cycles in the San Andres Formation, except for the presence of halite deposit in San Andres Formation (Hovorka, 1989; Hovorka, 2000). The absence of halite in the Queen Formation suggests deposition in marginal coastal environments where salinities did not reach halite saturation. Alternatively

halite may have formed as surficial crusts or layers at the top of Queen sabhkas, but was not preserved due to frequent ephemeral rains or floods.

Facies Association 3 (FA3)

Evaporite-dominated clastic deposits of facies association 3 comprise upward-deepening succession of (1) reddish brown siltstone and mudstone deposits (facies ES1), (2) ripple and wavy laminated very fine-grained sandstone deposits (facies S2), and (3) planar-cross stratified and horizontal laminated sandstone deposits (facies S3). Facies transitions in this facies association are gradational. Isopach map exhibits a uniformly thick sheet-shaped sand body. The thickness of facies association 3 average is 7.51 feet (2.25 meters) in the cored interval (Figure 41A).

The thickest part of facies association 3 is located in the western part of the study area, parallel to the northwestern to southeastern trending shoreline. There are pronounced changes in thickness perpendicular to the northwestern to southeastern oriented paleoshoreline that suggest variable sediment dispersal patterns. The paleoshoreline of facies association 3 advances in a more eastward direction than facies association 1 (Figure 40A and 41A).

Facies association 3 is interpreted to be deposits of a prograding (or aggrading) beach ridge or intertidal sand flat and wave-dominated delta deposits. It is interpreted to record a deepening upward trend with an overlying bedded anhydrite facies ECA that records brine level rise. Higher brine levels are indicated by increasing evaporite cementation, evaporite nodules and massive-bedded anhydrite in the permeable sandstone at the top of this facies association.

Facies Association 4 (FA4)

Facies association 4 consists of upward-shallowing succession of (1) bedded anhydrite or halite deposits with dolomitic laminae (facies ECA), (2) nodular and enterolithic anhydrite deposits (facies ES2), and (3) reddish-brown mud- to siltstone deposits with anhydrite nodules (facies ES1). This succession records subaqueous salina capped by supratidal coastal sabhka deposits. Facies transitions are gradational. The average thickness of this facies association is 16.9 feet (5.07 meters) in the cored interval.

Isopach maps of component facies transitions within this facies association are interpreted to reflect subtle high and low areas on partly flooded platform interior salinas and sabhkas. Lower parts of this association are bedded anhydrite with dolomitic laminae salina deposit, while the upper parts of this association are reddish-brown siltstone to mudstone coastal sabhka deposits (Figure 41B and C). The component facies in this association are similar to

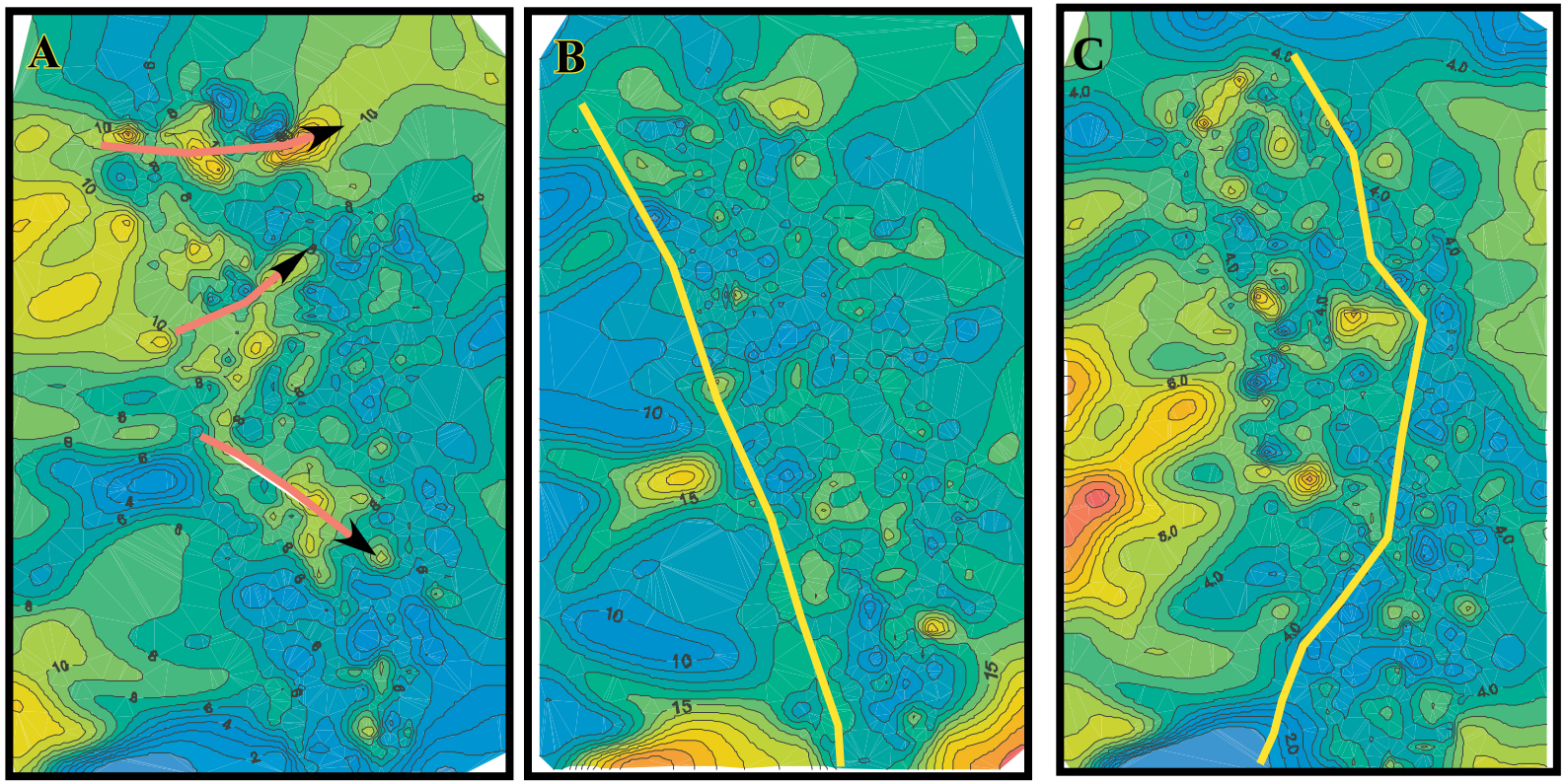

Figure 41. Isopach map of facies associations C21 and C22. (A) Prograding shoreline (or beach ridge) facies association of C21. Note progradation direction (red colored arrow) from west to east. (B) and (C) Evaporite-dominated subaqueous salina deposits and siliciclastic-dominated coastal sabhka deposits of facies association C22. Note basinward shift in shoreline from (B) to (C) records progradation of coastal sabhka and salina eastward. Yellow colored arrow line indicates inferred paleocoastline.

facies association 2, except for the presence of halite, which indicates increasing brine level and isolation of platform interiors during the development of a highstand carbonate margin. Salina environments decrease upward relative to sabhkas as lows are progressively filled. The facies association is a typical succession of upward-shoaling aggrading salina to prograding sabhka environments behind carbonate platform margins during base fall of late highstand systems tract (Warren and Kendall, 1985 and Warren, 1999).

Idealized Vertical Cycles

Facies associations are building blocks of a sequence stratigraphic architecture. Facies can be interpreted in terms of depositional environments and change in a their portion and character over time. An idealized vertical facies succession provides a template that can be used to guide stacking pattern analysis (Figure 42). The basal part of an ideal facies succession constructed for the Queen Formation contains (1) sandstone-dominated fluvial delta deposits, (2) mudstone dominant estuarine incised valley fill, (3) prodelta deposits, (4) evaporite-cemented, sandstone-dominated shoreline-attached beach ridge deposits and (5) cuspate delta deposits. Carbonate-dominated subtidal and evaporite-dominated supratidal tidal flat deposits are located at the middle part of this ideal vertical association. An interval of intense bioturbation at the top of the basal clastics and underlying the subtidal carbonates is interpreted to be a flooding surface. The upper part of the ideal vertical facies succession consists of episodic fluvial siliciclastic import into an anhydrite-halite salina facies or reddish brown mudstone-dominated coastal sabhka and evaporite mud flat facies.

The Queen Formation exhibits two such idealized facies successions, which are each interpreted to reflect a base level rise and fall hemicycle. These ideal vertical cycles record increasing evaporite content (upward-brining) and decreasing porosity upward. The base level rise hemicycle part of the cycle is composed of upward-deepening (or fining) of facies, retrograding fluvial delta and an estuarine fill, siliciclastic dominant facies associations 1 or upward-brining, prograding siliciclastic beach ridge and cuspate delta facies association 3 at the bottom. While the base level fall hemicycle is composed of overlying upward-shoaling, carbonate tidal flat facies associations 2 and evaporite mud flat and salina evaporite (halite or anhydrite) dominated facies associations 4 at the top of the succession. Two complete sedimentary hemicycles of the Queen interval comprise complete base level rise and fall cyclic variation between flooding surfaces. Transition interval between facies association 3 and 4 record subsequent rising level and salinity of brines behind highstand carbonate buildup along

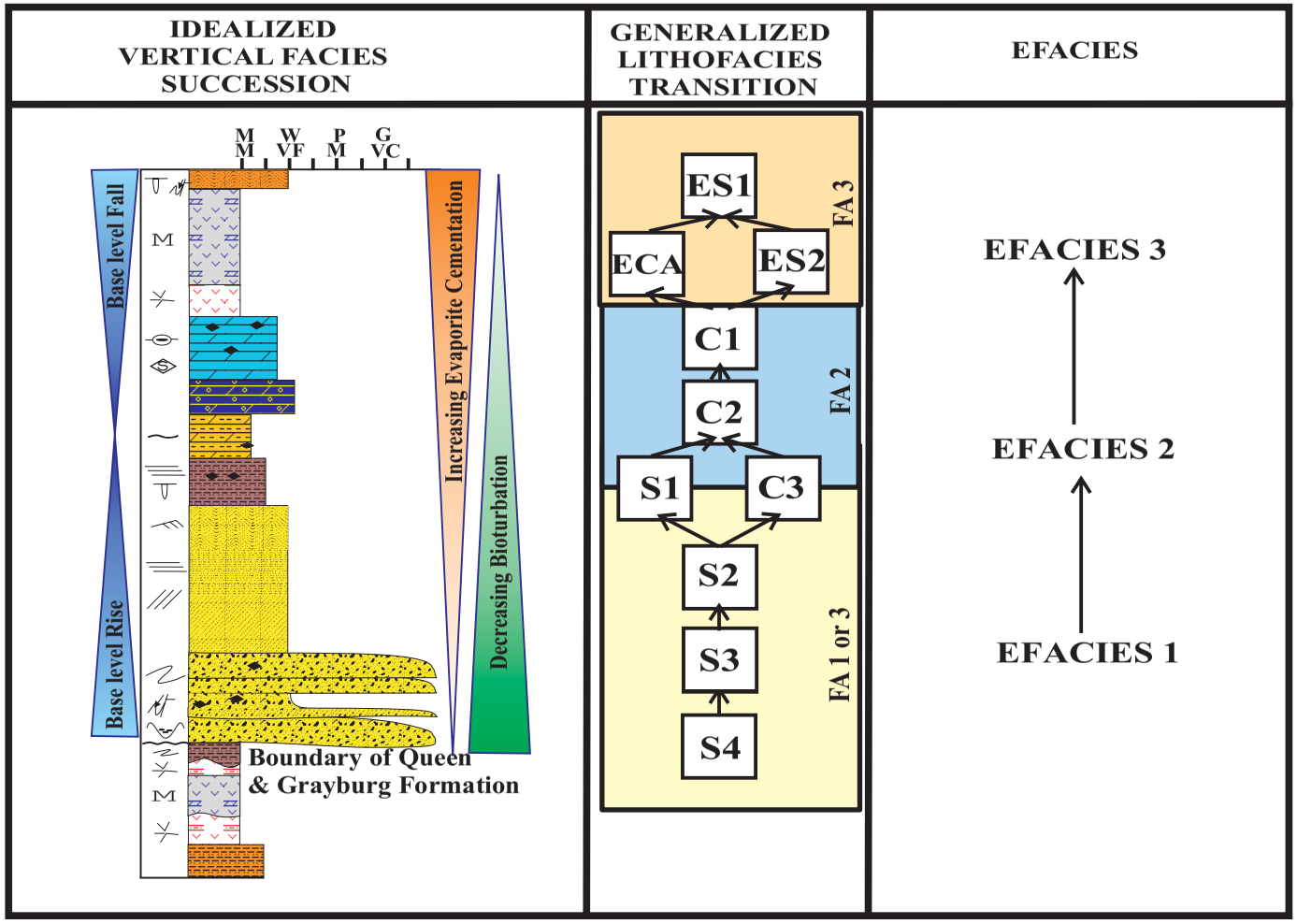

Figure 42. Idealized vertical facies associations. See Figure 12 for used symbols.

carbonate platform margins. Facies association 3 records increasing salinity and isolation of platform interiors. Facies association 4 exhibits an upward-shoaling trend from subaqueous grown anhydrite of salina facies to reddish brown siltstone and mudstone of coastal sabhka facies.

DIAGENESIS

The Queen Formation underwent two diagenetic stages: early stage eodiagenesis and late stage of mesodiagenesis. Early diagenesis reflects near surface physical and chemical modifications that were controlled mainly by interstitial water chemistry before effective burial. Porosity was formed mainly by fracturing, shrinkage, and dissolution of sedimentary grains. Late diagenesis includes dissolution and leaching of sedimentary grains and early-formed carbonate cements after burial (Schmidt and Mcdonald, 1979a; Schmidt and Mcdonald, 1979b).

Early diagenesis included 3 phases: (1) detrital clay infiltrated between detrital framework grains; (2) labile detrital grains (e.g., feldspar) were partially or completely dissolved; and (3) mechanical compaction deformed some detrital grains (e.g., mica) (Figure 43A, B and C). Pores were formed mostly by feldspar dissolution and were occluded mostly by clay infiltration and mechanical compaction along lines of weakness, such as cleavage and periphery of grains (Figure 43A, B and C). Early alteration of labile grains is supported by partially altered grains coated by detrital clay before primary pores were filled with early carbonate and anhydrite cement. In some cases early carbonate and evaporite cements completely filled voids left by dissolved grains (Figure 43D).

The second phase of early diagenesis included (1) secondary quartz and feldspar overgrowth, (2) precipitation of authigenic clays such as smectite, corrensite, and chlorite, (3) precipitation of carbonate and anhydrite cements (Figure 43A, B, E and F and 44A, B, C, and D). The rare partially dissolved secondary feldspar suggests that the silica found in cements was carried in by migrating fluids, rather than originating by pressure solution. Authigenic clay and hematite coating precipitated on altered detrital grains and quartz and feldspar overgrowth. Two major carbonate and evaporite cements can be differentiated into grain liners and primary pore filler components (Figure 43E and F and Figure 44 A, B and C). Precipitation of authigenic clay minerals after secondary quartz and feldspar overgrowth reflects a change in formation water chemistry. Authigenic clay accumulation formed detrital seams and clay cutans. Detrital labile grains became unstable, and minor quantities of detrital clay and feldspar altered to authigenic clay minerals. Ferrous ions released during the dissolution of iron rich grains oxidation and hematite, or their precursor ferric hydrates are precipitated. Most hematite precipitation probably occurred at the vadose zone, before cements completely fill intergranular pores. Hematite

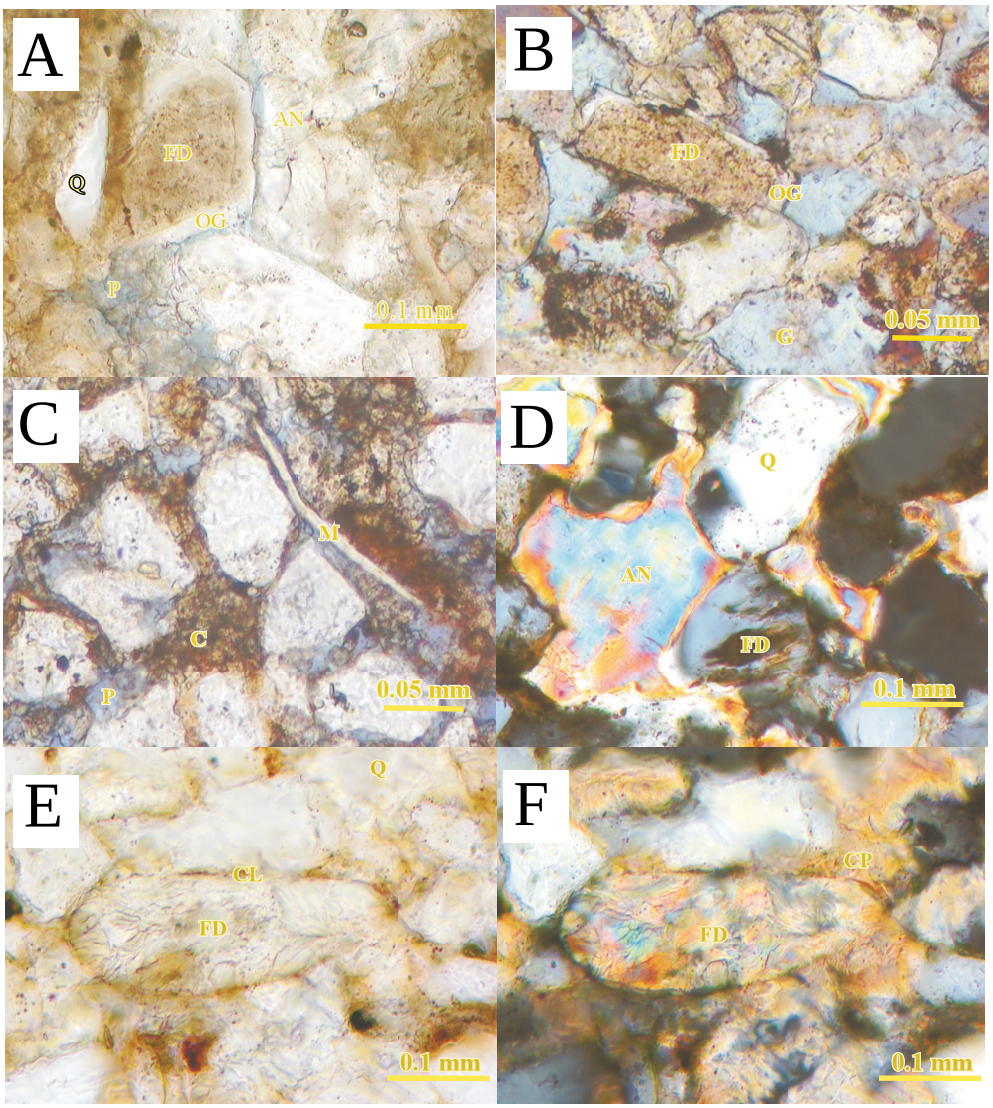

Figure 43. Early diagenetic features during the first phase. (A) Wentz 11, 4172 ft, plane-light image of detrital clay infiltration of untwined feldspar (FD) and partially dissolved carbonate in cement secondary pores (P). Note secondary overgrowth of feldspar (OG) after clay infiltration. (B) RMM 4-25, 4580 ft, polarized-light image of clay infiltrated primary feldspar (FD) and a partially dissolved overgrowth of a secondary feldspar grain. Note filling of gypsum (G) between partially dissolved detrital grains. (C) JSM 301, 4569 ft, plain-light image of mechanically compacted chloritized mica (M) and partial dissolved carbonate cement secondary pores (P) and authigenic clay (C). (D) Dibrell 3, 4198 ft, polarized-light image of anhydrite cement (AN) between detrital grains of quartz (Q) and dissolved feldspar (FD). Note secondary quartz overgrowth. (E) and (F) Dibrell 3, 4200 ft, plain and polarized-light images of clay infiltration feldspar and authigenic pore lining (CL) and pore filling (CP).

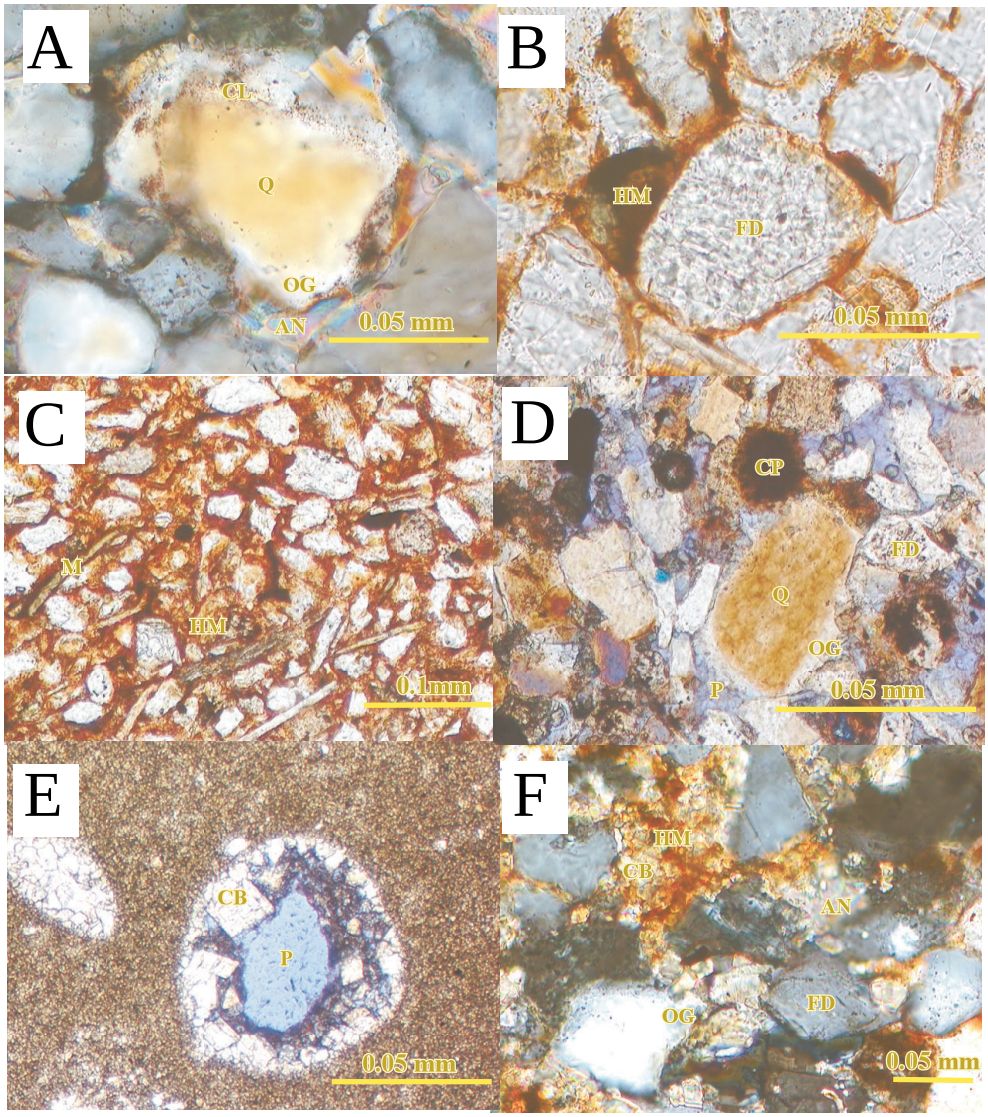

Figure 44. Early diagenetic features during the second phase. (A) Wentz 11, 4155 ft, polarized-light image of hematite coating (CL) between primary (Q) and dissolved secondary quartz (OG). Note late pore fill of anhydrite (AN). (B) Wentz 11, 4156 ft, plain-light image of green chloritized feldspar (FD) and pore filling hematite (HM). (C) RMM 7-51, 4129 ft, plain-light image of hematite pigment (HM) and chloritized mica (M). (D) JSM 301, 4574 ft, plain-light image of anhydrite and carbonate cement elongate dissolving pore (P) between quartz (Q) and dissolved feldspar (FD). Note secondary quartz overgrowth (OG) and remnant authigenic clay pore fill (CP). (E) Dibrell 3, 4214 ft, plain-light image of moldic pore and dolomite cementation (CB) after dissolution in later digenetic stage. (F) Wentz 11, 4172 ft, polarized-light images of diagenetic sequence of detrital grain clay infiltration, clay coating, secondary detrital overgrowth (OG), carbonate cementation (CB), hematite pigmentation (HM) and anhydrite cementation (AN).

cements and authigenic clays may record pedogenesis (Malicse and Mazzullo, 1996) (Figure 44 A, B and C).

The last phase of early diagenesis was precipitation of anhydrite and dolomitization of carbonate cement. Cements completely filled pores during this phase, which restricted fluid movement, and terminated the precipitation of additional authigenic cement (Figure 43D, 44 E, F, and 45A and B). Anhydrite and dolomite cements were precipitated in different times as pore fillers. Anhydrite cements predate dolomitization. Precompaction "floating" sand grains in anhydrite matrix show that anhydrite cements were earlier than dolomitization.

When gypsum is transformed to anhydrite (at temperatures above 60^{o}C and at burial depths greater than 600 meters), there is a volume loss of about 38 percent. This volume change and associated dehydration can significantly deform the deposits, whether they are evaporites or siliciclastics and carbonate with evaporite cements (Warren and Kendall, 1985). This loss of local volume also results in fractures. Anhydrite generally occurs together with dolomite. This accounts for the rarity of gypsum in Queen Formation.

Warren and Kendall (1985) described a modern analog along the Trucial Coast of evaporate sabhkas like those interpreted from the Queen Formation. The deposits there are matrix dominated and are comprised of less than 65% anhydrite. They also suggested that modern sabhkas initially have a mixed clastic and carbonate matrix, rather than an evaporite-dominated matrix. Subsequent diagenetic events formed the nodular and enterolithic anhydrites within supratidal sediments. Most primary anhydrite in supratidal sediments is formed above the water table, and gypsum is always found below the water table or on the landward side of the sabhka. The extent of the capillary zone in the sabhka area controlled the vertical and lateral extent of evaporites. Most anhydrite nodules and/or enterolithic anhydrite grow within this zone. The capillary zone level is controlled by interaction between the ground water level and seawater reflux near the shoreline. The degree of seawater reflux is probably a function of relative sea level fluctuation. Sea level rise generates hydraulic head toward less dense fresh water landward into the ground water. Anhydrite grows within these sediments by replacement of the gypsum mush. Based on this analog, most of the anhydrite beds and cementation in Queen Formation is a diagenetic product of primary gypsum and is why anhydrite are more common gypsum in the Queen siliciclastic–dominated sabhka deposits.

Shearman (1983) suggested that small nodular, coalesced nodular, mosaic chicken wire and bedded anhydrite in sabhka deposits have similar origins and that all formed beneath the

A. Anhydrite Cement (%)

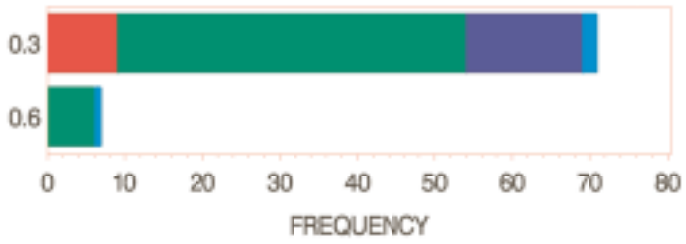

B. Dolomite Cement (%)

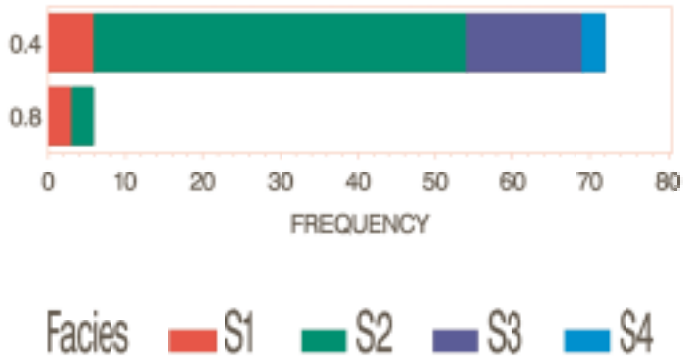

Figure 45. Anhydrite and dolomite cement types of siliciclastic lithofacies.

sediment-water interface. Shearman (1983) also suggested that gypsum crystals in sabhka deposits are mostly lenticular in shape and grow displacivly. When primary gypsum was precipitated in sediment, the primary gypsum crystals began to dissolve and formed cavernous hollows where altered tiny anhydrite crystals then precipitate. As the primary gypsum undergoes alteration to anhydrite, loose masses of anhydrite crystals pseudomorph the gypsum crystals. These anhydrite pseudomorphs of gypsum grow outward, form a nodular mass, and lose all primary structures. Shearman also suggested that anhydrite nodules may grow "by nucleation of new crystals inside the framework of the nodules, so that they expand like an inflated balloon." These anhydrite nodules grow in close proximity to one another and coalesce, and the displaced surrounding sediments become partitions between the nodules. By this process a mosaic of massive anhydrite or chicken wire fabric, anhydrite form. Both nodules of mosaic and coalesced nodule anhydrite tend to align parallel to the bedding and form continuous or discontinuous bedded nodular anhydrite. The continued growth of these coalesced nodules within the bed need more space to expand, and eventually the bed is forced to fold and contort. This results in the formation of enterolithic structures.

The extent of early diagenesis and the relative abundance of different types of cements change between facies and different location within stratigraphic cycles. Diagenetic changes affect reservoir quality of high permeability clastic facies and can be related to depositional setting. Anhydrite and dolomite cements are more abundant in facies S2 relative to facies S3 and S4 (Figure 45). Facies S2 was deposited in beach ridge or shoreline environments during highstand of cycle sets at the landward side of evaporite-dominated salina facies. There dense brine water, supersaturated calcium sulfate, percolated through permeable facies S2 sandstones. Large quantities of gypsum cement precipitated depleting calcium in the sinking brine water. Calcium depletion enriched magnesium in brine water and production favorable conditions for dolomite precipitation (Warren, 1982a and b). Dolomite also occurs as small euhedral or anhedral rhombic crystals between detrital sand grains (Figure 44E and F).

Fluvial-dominated delta and estuarine siliciclastic lithofacies (S3 and S4) deposited under normal saline seawater or blackish groundwater. Overlying tidal flat carbonate facies formed during lowstands of the cycle sets may have acted as a flow barrier to sinking supersaline fluids from subsequent salina. Therefore, facies S3 and S4 has less anhydrite and dolomitic cements.

Different evaporite cementation in facies may result from variation of permeability and grain size in facies. Shearman and Fuller (1969) proposed the extent of anhydrite cementation is dependent of matrix permeability in terms of nodule size. The chicken wire and enterolithic structures form in deposits with a permeable matrix, whereas relatively impermeable beds favor the formation of smaller nodules.

Late diagenesis of the Queen Formation included formation of secondary porosity by decarbonatization and dissolution of early cements, authigenic minerals, and labile grains. Carbon dioxide bearing acidic water resulted from decarboxylation as organic matter in intercalated shale matured (Schmidt and Mcdonald, 1979a). Leaching of pore-filling anhydrite and dolomite cements creates most of the secondary oversized and elongate porosity in Queen sand reservoirs. Moldic, honeycombed, and corroded pores of labile grains of secondary porosity are observed. Most porosity in Queen sand reservoirs is of late stage secondary origin. Malicse and Mazzullo (1990) related secondary porosities in the Shattuck Member of the Queen Formation to the generation of organic acids during kerogen maturation. Secondary porosity is recognized in thin sections by: (1) partially dissolved pores of labile grain and corroded edges of remnant cement (Figure 46E); (2) labile grain moldic pores (Figure 46F); (3) elongate pores (Figure 47A); (4) inhomogeneous packing and floating grains (Figure 47A); (5) oversized pores (Figure 47B); (6) corroded grains of labile grain overgrowth (Figure 47C); (7) honeycombed labile grains (Figure 47D and 47E); and (8) fracture grains (Figure 47F). Partially dissolved pores and elongated pores dominant in Queen sandstones. Coarser grained fluvial-dominated delta and estuary sandstones facies S3 have more elongate and oversized secondary pores than is observed in finer grained siliciclastic lithofacies (S1 and S2; Table 12 and Figure 48).

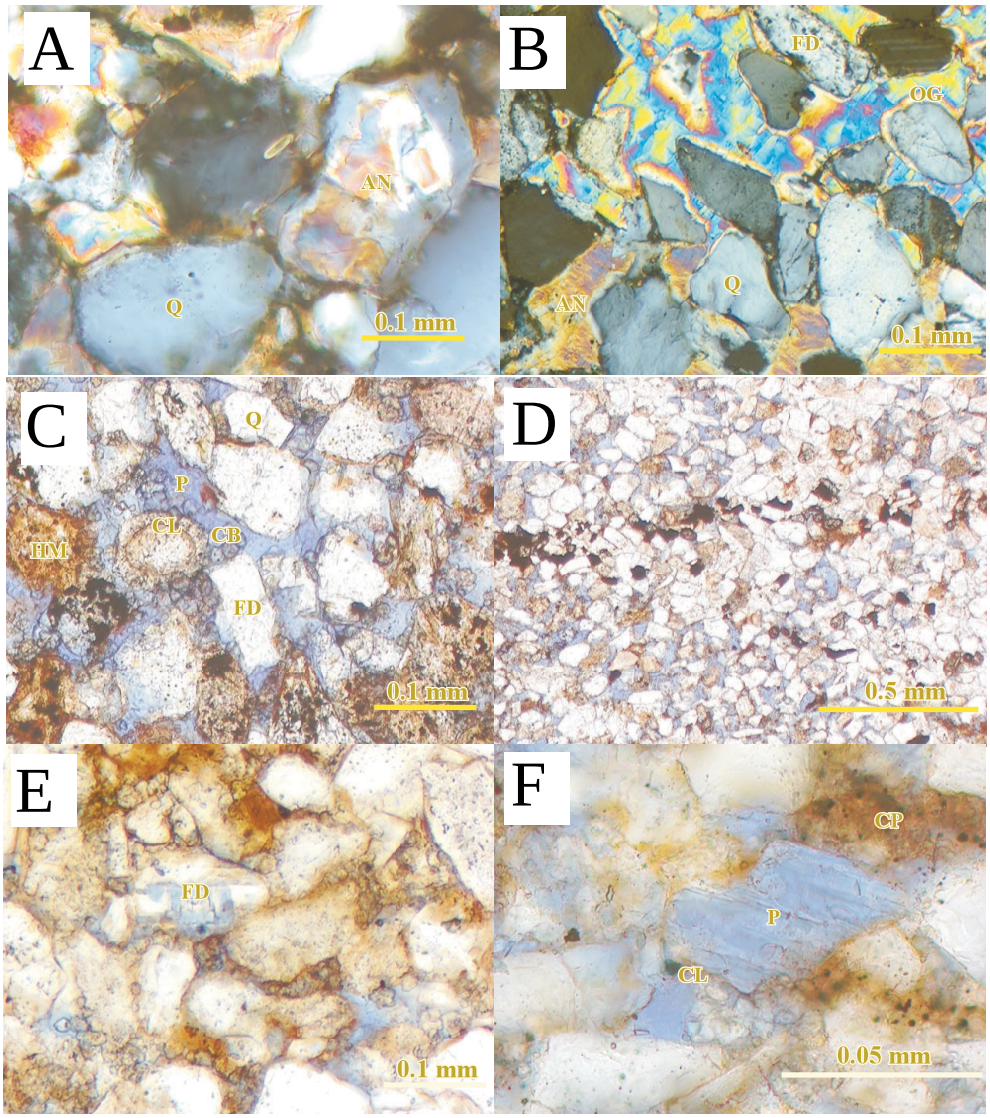

Figure 46. Early and late diagenetic features and secondary porosity. (A) Dibrell 3, 4198 ft, polarized-light image of anhydrite cement (AN) inside dissolved feldspar grain and filling pores between detrital grains. (B) Wentz 11, 4202 ft, polarized-light image of anhydrite (AN) cement of pores and quartz and feldspar overgrowths (OG). (C) JSM 301, 4569 ft, plain-light image of elongate pores (P) formed by dissolution of anhydrite and carbonate cements. Note dolomitized remnant (CB) remains in pores and hematite pigment (HM). (D) Dibrell 3, 4233 ft, plain-light image of elongate pore formed by late dissolution. (E) Wentz 11, 4209 ft, plain-light image of partial dissolved pores of feldspar grain (FD). (F) Wentz 11, 4199 ft, plain-light image of feldspar moldic pores (P), remnant clay lining (CL) and pore filled clay (CP).

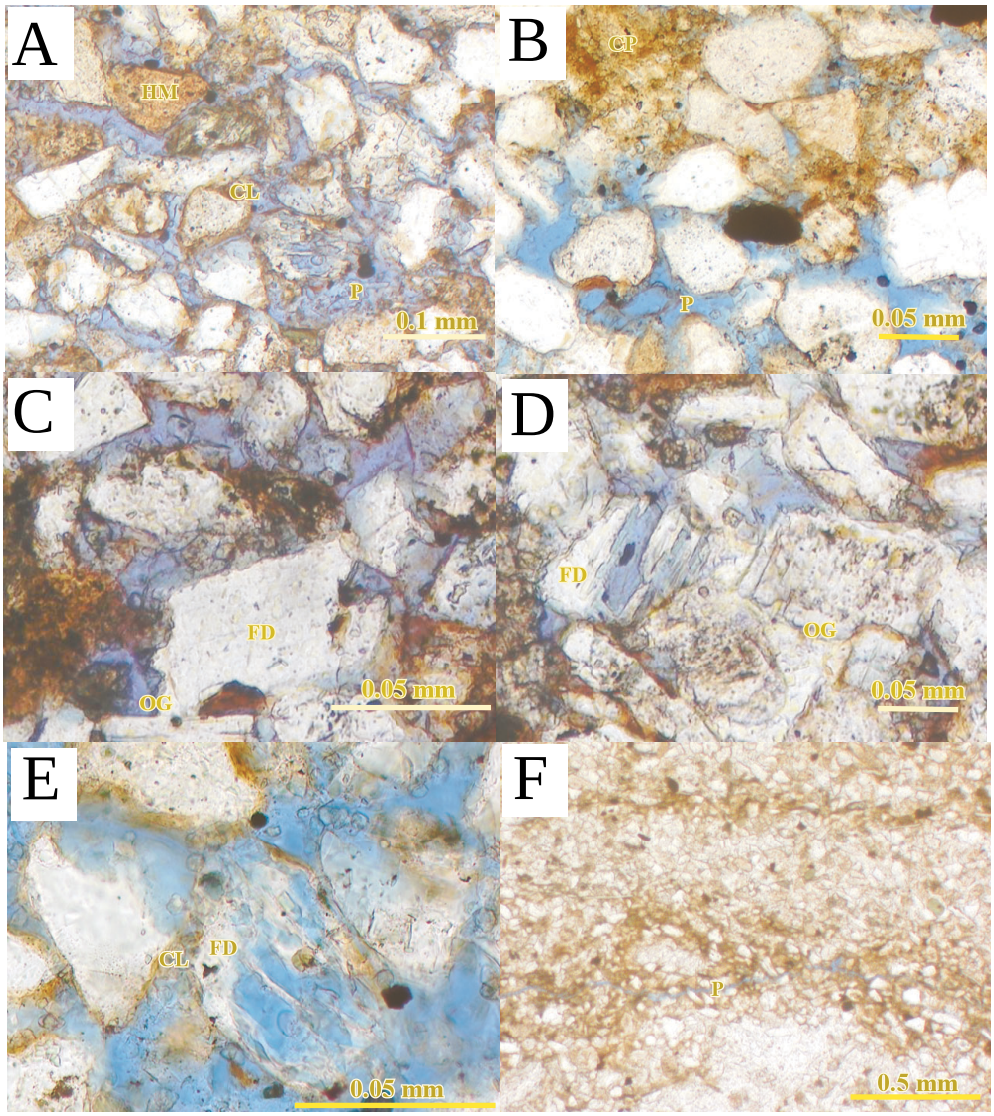

Figure 47. Secondary porosity in the Queen sandstone reservoir. (A) Wentz 11, 4202 ft, plain-light image of elongate pores (P). Note hematite altered grain (HM), clay liner (CL) and inhomogeneous pack grains. (B) Wentz 11, 4202 ft, plain-light image of oversized pore enlarged by dissolution of labile grains (P). (C) JSM 301, 4572 ft, plain-light image of corroded feldspar overgrowth (OG). (D) JSM 301, 4569 ft, plain light image of honeycomb pore adjacent to feldspar and clay altered feldspar overgrowth (OG). (E) Wentz 11, 4202 ft, plain-light image of honeycomb pore and dissolved feldspar grain (FD). (F) Wentz 11, 4174 ft, plain-light image of fracture pore (P).

Table 12. Abundance of secondary pore types in lithofacies.

Facies	Partial Dissolution (%)	Molds (%)	Inhomogeneity of Packing (%)	Oversized Pores (%)	Elongate Pores (%)	Corroded Grains (%)	Honeycombed Grains (%)	Fractures (%)
ES1	83	0	0	0	0	17	0	0
ES2	79	0	0	0	0	0	0	21
ECA	100	0	0	0	0	0	0	0
C1	45	2	0	23	26	4	1	0
C3	34	3	0	16	38	6	3	0
S1	53	6	0	1	5	8	5	21
S2	56	3	1	9	21	5	2	3
S3	33	7	3	32	17	5	2	0
S4	78	0	0	1	7	5	2	10

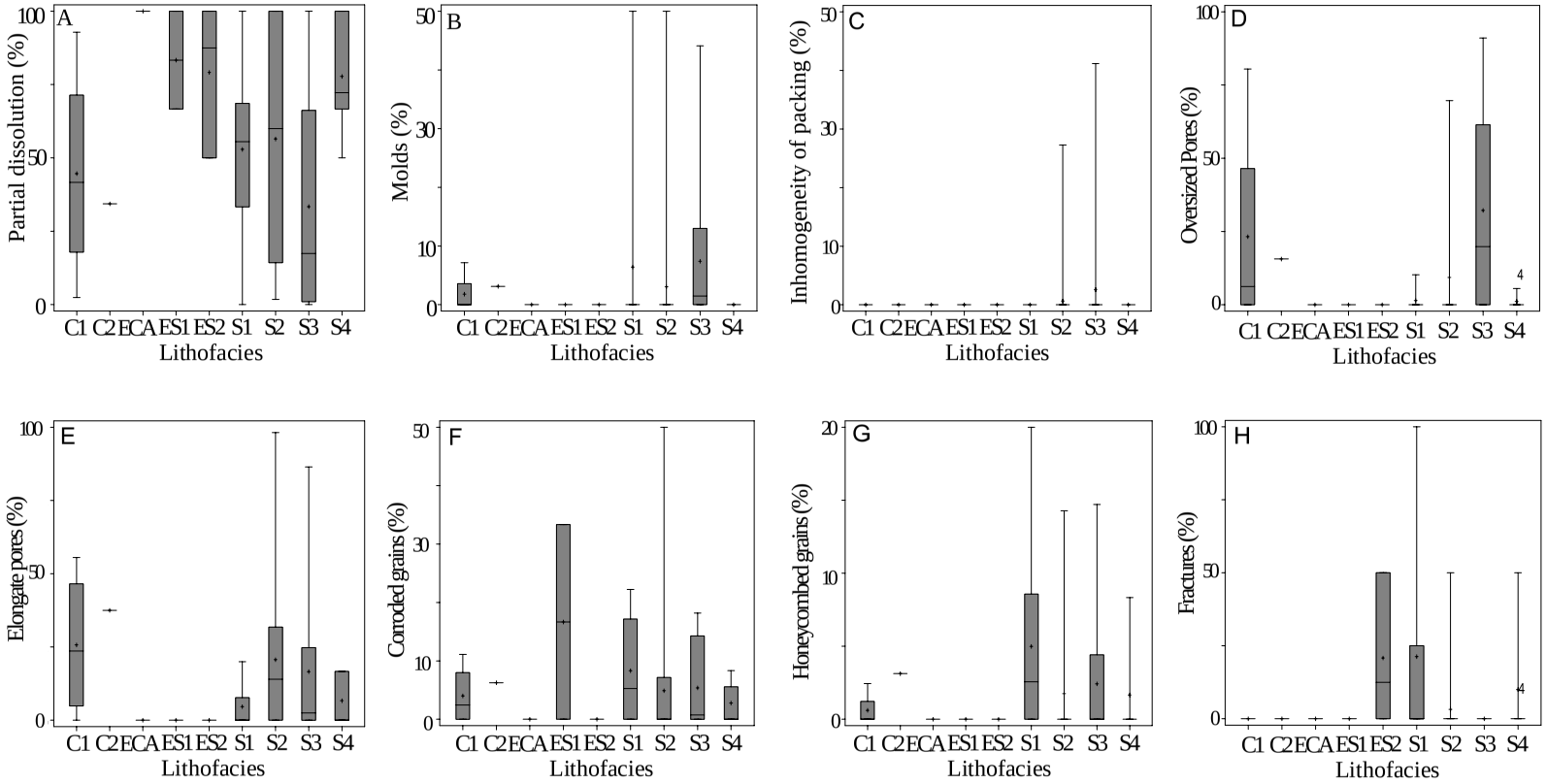

Figure 48. Abundance of secondary porosity types observed in each lithofacies. The center of each box is the 50th percentile; margins of the boxes are the 25th and 75th percentiles; and whiskers denote the 0th and 100th percentiles. See Table 12 for tabulation of these average values.

STACKING PATTERN ANALYSIS

RECOGNITION OF CYCLIC STACKING PATTERNS

Four scales of cyclic sedimentary successions are recognized in the Queen Formation based on vertical facies character and abrupt vertical facies offsets; cycles, cycle sets, sequences, and long-term accommodation trends (Figure 49 and 50). Cycles record the smallest-scale and defined by the vertical facies associations described previously, these are interpreted as base-level rise or fall hemicycles. A set of base-level rise hemicycles consists of an upward-fining (or deepening) vertical facies succession; for example the upward progression from fluvial influenced delta and estuarine deposits (facies association 1) to evaporite-dominated tidal sand flat deposits (facies association 3). Such base-level rise hemicycles occur at the lower half of the cored interval and at the top part of Queen uncored interval. Base-level fall hemicycles are composed of upward-shallowing vertical facies succession; for example the upward progression from carbonate tidal flat deposits (facies association 2) to evaporite-dominated salina and sabhka deposits (facies association 4). Such base-level fall hemicycles occur in the middle and the upper half part of the Queen Formation. Cycle boundaries define the turn-around from base-level fall to rise hemicycle. Kerans suggested that cycles provide essential chronostratigraphic units for high-resolution correlation, mapping of lithofacies, and facies interpretation (Kerans, 1994; Kerans and Tinker, 1997).

Cycle sets define from the thickness variations that are interpreted to reflect variations in relative accommodation and sediment supply (A/S) ratio (Figure 50). Upward-thickening cycle sets record retrogradational and aggradational of cycles during base level rise (e.g., CS1, 3, 5 and 7). Upward-thinning cycle sets record progradational of cycles during base level fall (e.g., CS2, 4, 6 and 8). Retrogradational, base-level rise, cycle sets include transitions from fluvial-deltaic siliciclastic-dominated deposits to carbonate-dominated tidal flat or subaqueous evaporite-dominated deposits. Progradational (or aggradational), base-level fall, cycle sets include transitions from carbonate-dominated tidal flat or evaporite-dominated salina deposits to supratidal sabhka or fluvial siliciclastic-dominated deposits. Cycle set boundaries define the turn-around from retrogradational to progradational (or aggradational) cycle set.

Kerans and Tinker (1997) proposed the bounding surfaces of high-frequency sequences are: (1) subaerial unconformities; (2) a turnaround from progradational to retrogradational cycles; (3) a major basinward shift in facies; and (4) analysis of systematic important rates in

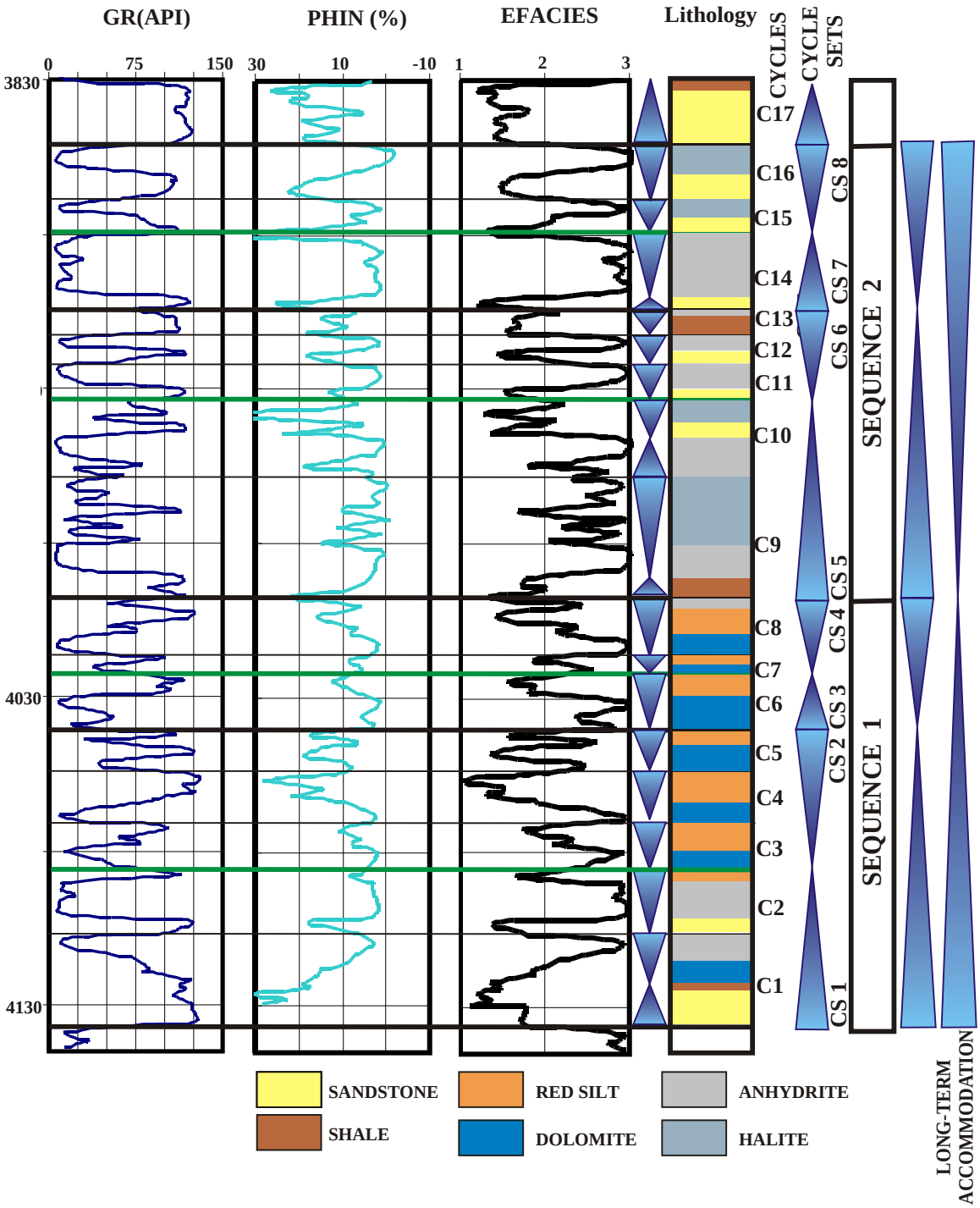

Figure 49. Type log of JSM 23-19 well. Note good match between two generated lithologies of uncored intervals and cycles, cycle sets, and high frequency sequences.

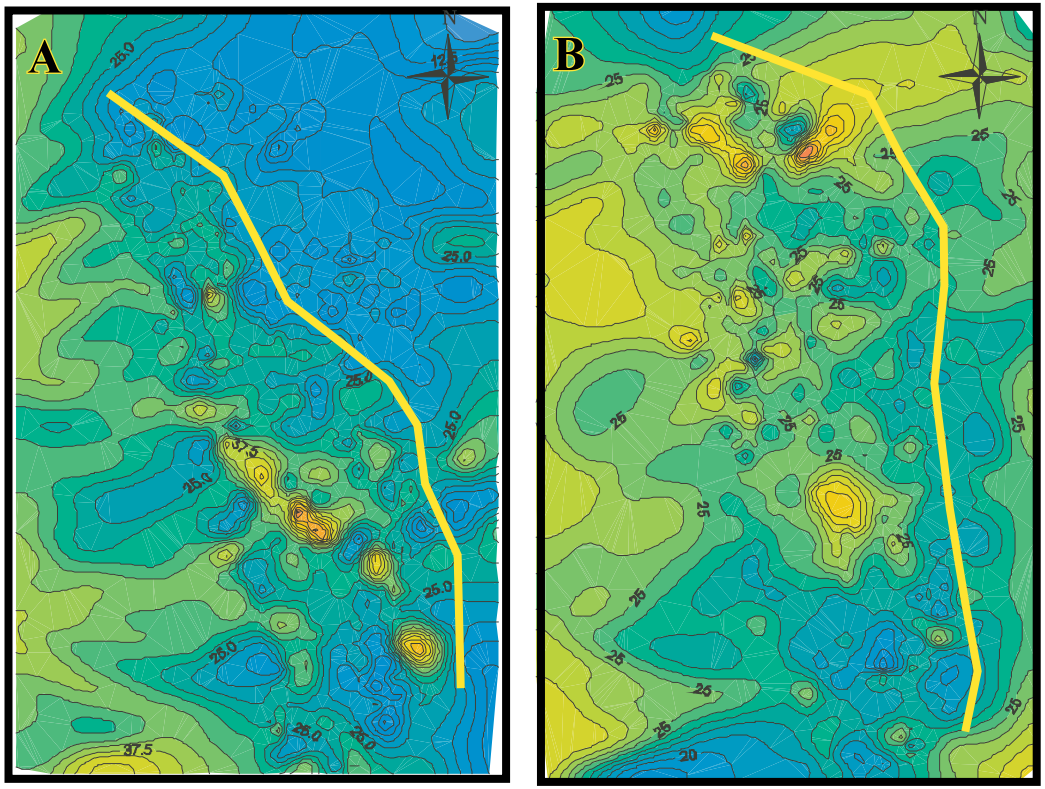

Figure 50. Isopach map of cycle set CS1. (A) Cycle C1. (B) Cycle C2. Prograding coast line between cycle C1 and C2 records relative sea level fall and eastward progradation during cycle set CS1.

trends of cycle thickness and internal lithofacies proportion. Sequence boundaries and inferred maximum flooding surfaces (MFS) were also assumed by the plot between cycle thickness and each cycle (Table 13 and Figure 51). Sequences boundaries are defined at the thinnest cycle and maximum flooding surfaces (MFS) are located at top of the thickest cycle.

SEQUENCE STRATIGRAPHIC ARCHITECTURES

Cycles and Cycle Sets

Sixteen cycles were defined in the Queen Formation. Cycles are 8.69 to 45.76 feet (2.6 to 13.7 meters) thick. Cycles were defined by a variety of criteria, including: (1) complete symmetrical or incomplete asymmetrical siliciclastic-dominated cycle, (2) incomplete asymmetrical carbonate-dominated cycle, and (3) complete symmetrical or incomplete asymmetrical evaporite-dominated cycle (Figure 50). Cycle tops are sharp, recording a period of subaerial exposure and/or nondeposition. Most cycles record upward-shallowing cycle. In well logs cycles are recorded by a succession from Efacies 1 to 3 (Figure 50).

The 16 cycles can be grouped into 8 retrogradational and progradational (or aggradational) cycle sets by the thickness variations of cycles (Figure 50). Average cycle sets thickness range from 28.30 to 74.20 feet (8.49 to 22.26 meters).

The siliciclastic-dominated cycle set at the basal part of the Queen Formation comprises cycles C1 and C2. Cycle C1 is defined by an upward-fining from fluvial to estuarine sandstone of incised valley fill facies association 1, and upward-shallowing arid carbonate tidal flat origin dolomite facies association 2. The cycle C2 consists of upward-brining shoreline sandflat sandstone of beach ridge facies association 3, and upward-shallowing evaporite salina and mud flat anhydrite and reddish brown mudstone facies association 4. These two cycles define a symmetrical base level rise and fall cycle sets. Isopach maps of cycle C1 and C2 show successively progradational supratidal tidal deposits formed during base-level rise (Figure 52). The northwestern-southeastern trending paleoshoreline advances slightly to the east (Figure 52B). There is followed by overlying upward-shallowing carbonate-dominated cycles of the base level fall.

The grain size and detrital composition maturity of cycle C1 is greater than cycle C2, whereas the sorting and amount of cement of cycle C1 is less than cycle C2 (Table 14 and Figure 53). This indicates fluctuation of the siliciclastic source area, a relative sea level rise, and increasing early evaporite cementation and salinity. Increasing salinity recorded by cementation

Table 13. Thickness of cycles, cycle sets and sequences.

A. Cycles

Cycles	Mean (feet)	Minimum(feet)	Maximum(feet)
16	16.87	6.25	26.78
15	13.35	8.33	20.84
14	28.30	22.91	32.29
13	8.69	0.50	12.53
12	10.79	7.30	16.66
11	13.93	9.87	20.31
10	28.44	13.02	38.02
9	45.76	25.52	58.65
8	21.11	14.58	29.32
7	11.53	4.16	20.31
6	25.44	13.54	37.60
5	13.77	0.52	25.20
4	17.02	9.90	29.70
3	14.80	7.30	25.50
2	24.38	9.37	56.17
1	24.63	15.63	34.38

B. Cycle sets

Cycle sets	Mean (feet)	Minimum(feet)	Maximum(feet)
8	30.22	14.58	47.62
7	28.30	22.91	32.29
6	33.41	17.67	49.50
5	74.20	38.54	96.67
4	32.64	18.74	49.63
3	25.44	13.54	37.60
2	45.59	17.72	80.40
1	49.01	25.00	90.55

C. Sequence

Sequences	Mean (feet)	Minimum(feet)	Maximum(feet)
2.5	58.52	37.49	79.91
2	107.61	56.21	146.17
1.5	58.08	32.28	87.23
1	94.60	42.72	170.95

* 1.5 and 2.5 indicate the upper part of HFS 1 and 2.

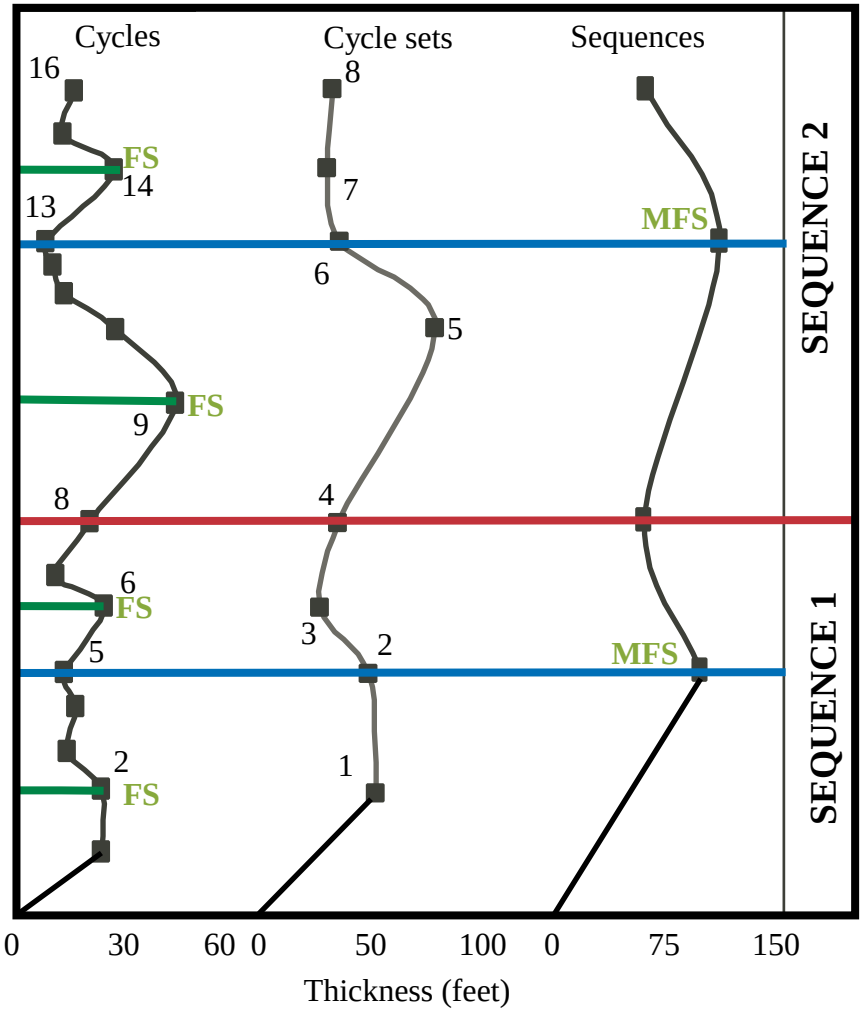

Figure 51. Thickness of cycles, cycle sets and sequences. The minimum thickness of cycles coincides with sequences boundaries. MFS stands for proposed maximum flooding surfaces. See Table 13 for statistical summary of cycles, cycle sets, and sequences.

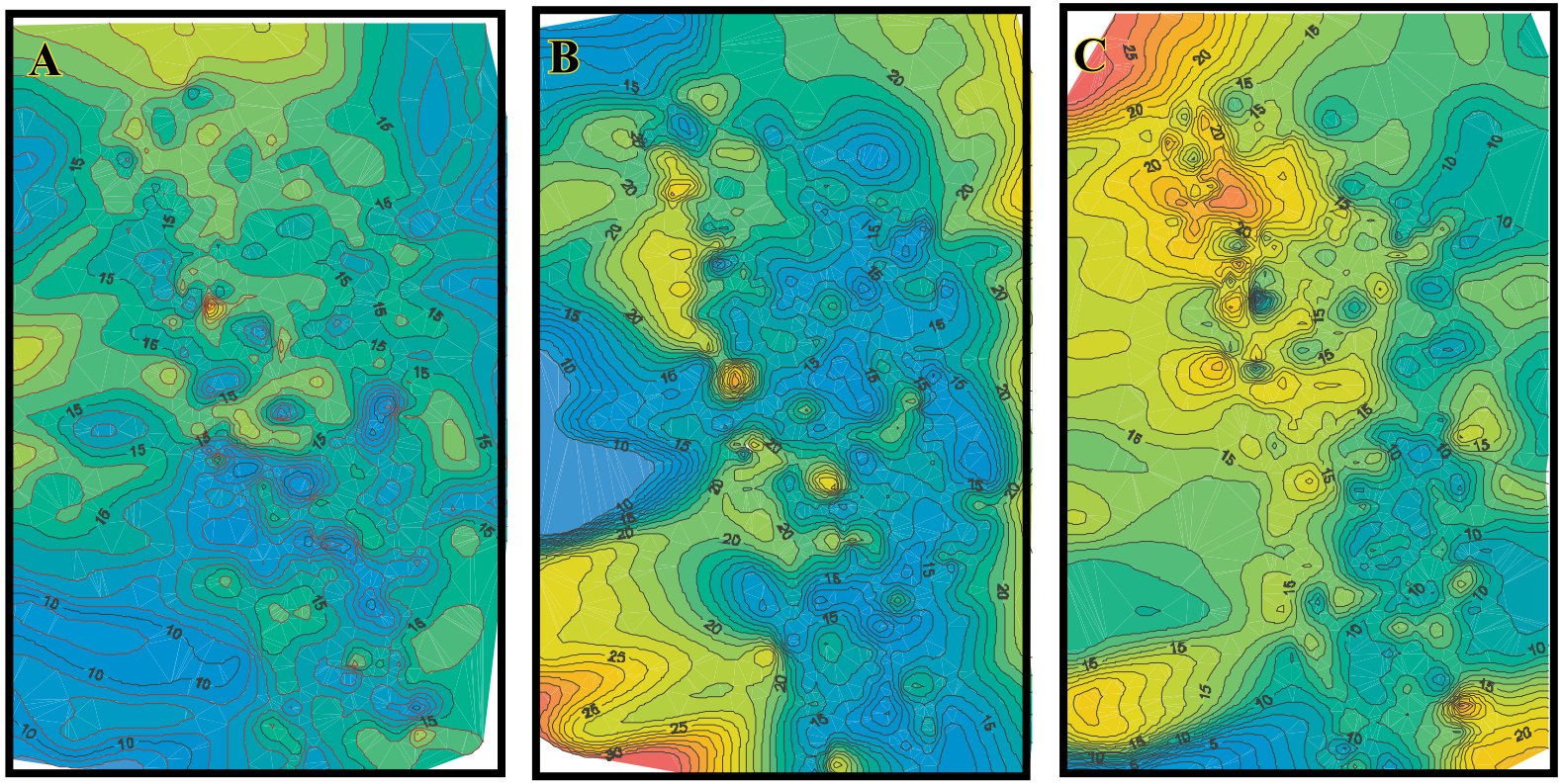

Figure 52. Isopach map of cycle set CS2. (A) Cycle C3. (B) Cycle C4. (C) Cycle C5. Note prograding-retrograding-prograding carbonate tidal flat of cycle set CS 2 during relative sea level fall from the eastern to western parts of the study area.

Table 14. Texture and composition of framework grains, matrix, and cements for the two cycles.

A. Grain size (mm)

CYCLE	Mean	Maximum	Minimum
C2	0.061	0.101	0.025
C1	0.066	0.109	0.029

B. Sorting (ϕ)

CYCLE	Mean	Maximum	Minimum
C2	0.49	0.77	0.39
C1	0.51	0.77	0.37

C. Quartz (%)

CYCLE	Mean	Maximum	Minimum
C2	31	62	1
C1	29	50	5

D. Feldspar (%)

CYCLE	Mean	Maximum	Minimum
C2	9	18	0
C1	10	18	0

E. Rock fragments (%)

CYCLE	Mean	Maximum	Minimum
C2	3	8	0
C1	3	8	0

F. Cements (%)

CYCLE	Mean	Maximum	Minimum
C2	34	97	0
C1	49	95	17

G. Clay (%)

CYCLE	Mean	Maximum	Minimum
C2	6	38	0
C1	5	41	0

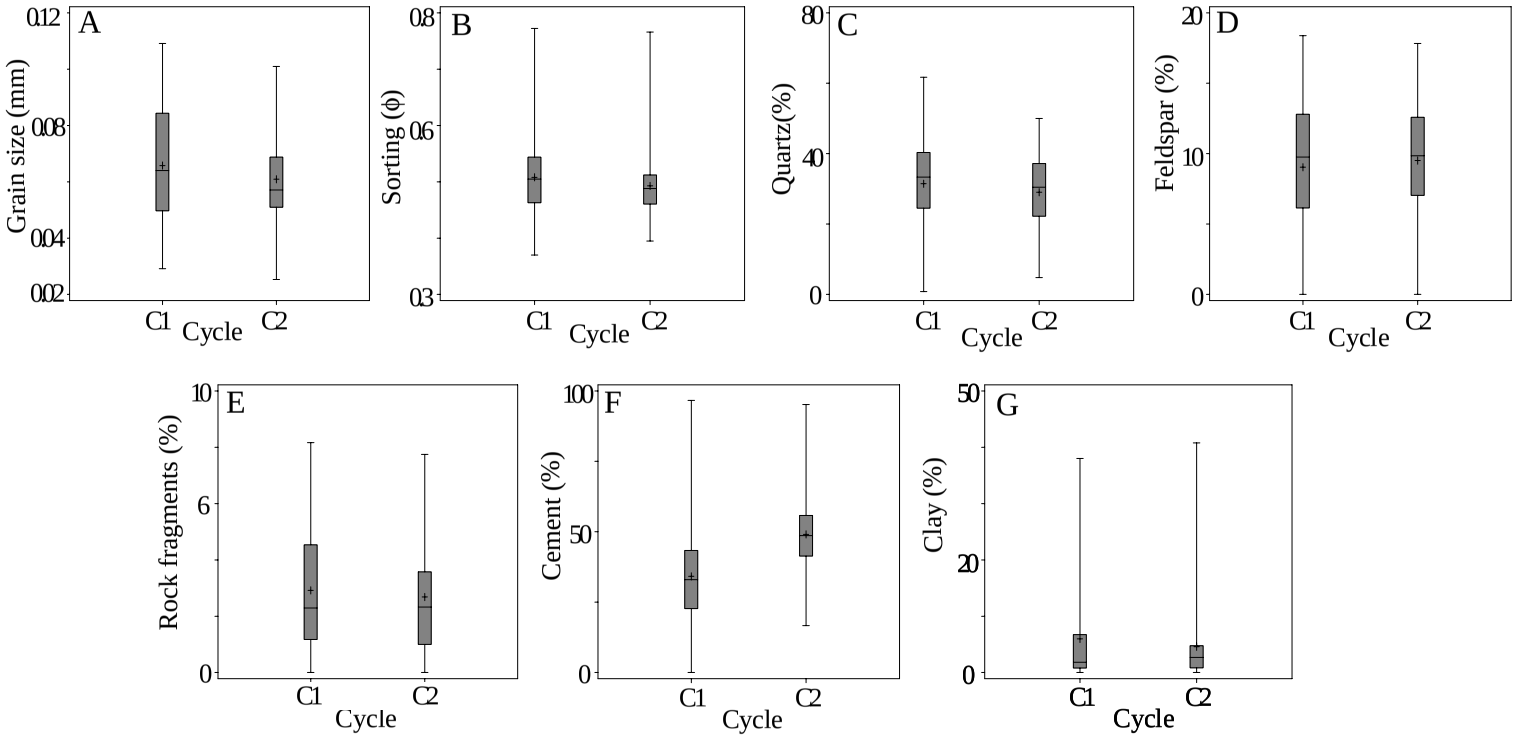

Figure 53. Texture and composition of the two cycles observed in core. (A) Grain size; (B) Sorting; (C) Quartz; (D) Feldspar; (E) Rock fragments; (F) Cement; (G) Clay. See Table 14 for statistical comparison of cycles.

of cycle C2 suggests isolation of carbonate platform interiors by an aggrading or prograding carbonate build-up of carbonate platform margins during transgressive and highstand sea levels. Cycle C1 and C2 in producing interval shows decreasing porosity and permeability upward during base-level rise (Table 15 and Figure 54).

Carbonate-dominated cycles are defined by regressive upward-shallowing carbonate tidal flat and evaporite sabhkas cycles. Isopach maps of six cycles show prograding carbonate tidal flat and sabhka successions (Figure 52 and 55). These 6 cycles from C3 to C8 can be grouped into 3 cycle sets (CS2, CS3 and CS4). The prograding cycle set CS2, which consists of cycle C3, C4, and C5. After that minor portion of retrograding cycle set CS3 was followed. The CS3 is composed of cycle C6. Lastly, the prograding cycle set CS4 of cycle C7 and C8 was deposited in this area. These prograding carbonate-dominated cycle sets indicate that the successive decreasing accommodation space resulted in the deposition of upward-thinning and shallowing carbonate tidal flat cycles by the beginning of cycle C9. At this time, the carbonate platform margin had undergone a high rate of progradation (or aggradation) and began to provide successive isolation and decreasing base level inside the carbonate platform area.

Upward-brining evaporite cycles include cycles 9 to 16. The basal shale bed in cycle C9 probably indicates a long-term maximum increasing base level rise that might be a maximum flooding surface in this area based on the plot between cycle thickness and each cycle (Table 13 and Figure 51). The eight evaporite-dominated cycles are composed successions of repetitive lagoonal shale with intermittent fluvial sandstones, and evaporite salina anhydrite and halite deposits that record an upward-brining trend.

Halite in the upper Queen Formation reflects a major change in brine-level. The 25 feet (8.3 meters) thick halite horizon was easily identified by lithodensity and neutron porosity curves and is very distinct and continuous across the study area. The lateral continuity and thickness of this halite bed suggests it was deposited in a marginal platform sea rather than on a continental salt fan. A dry climate, less than 76% humidity and brine-level depth less than 2m is required for halite precipitation (Tucker, 1991 and Warren, 1999).

The eight evaporite-dominated cycles can be grouped into two cycle sets. The first, a retrograding cycle set (C9 and C10) CS5 records expansion of salt-dominated giant salina behind the carbonate platform margin (Figure 51). The brine source of halite bed, was probably from the open sea (Midland Basin) which supplied waters through highstand permeable carbonate margin buildup. The brine-level was lowered by a progradational highstand carbonate buildup of

Table 15. Petrophysical properties of cycles observed in core.

A. Core Porosity (%)

Cycles	C1	C2
Mean	9.71	6.55
Maximum	25.60	19.80
Minimum	0.20	0.20
Standard Deviation	6.14	4.45

B. Core Permeability in horizontal direction (md)

Cycles	C1	C2
Mean	13.77	4.08
Maximum	204.00	66.00
Minimum	-0.10	-0.10
Standard Deviation	27.47	11.43

C. Core Permeability in vertical direction (md)

Cycles	C1	C2
Mean	0.31	0.22
Maximum	1.10	0.90
Minimum	-0.10	-0.10
Standard Deviation	0.38	0.30

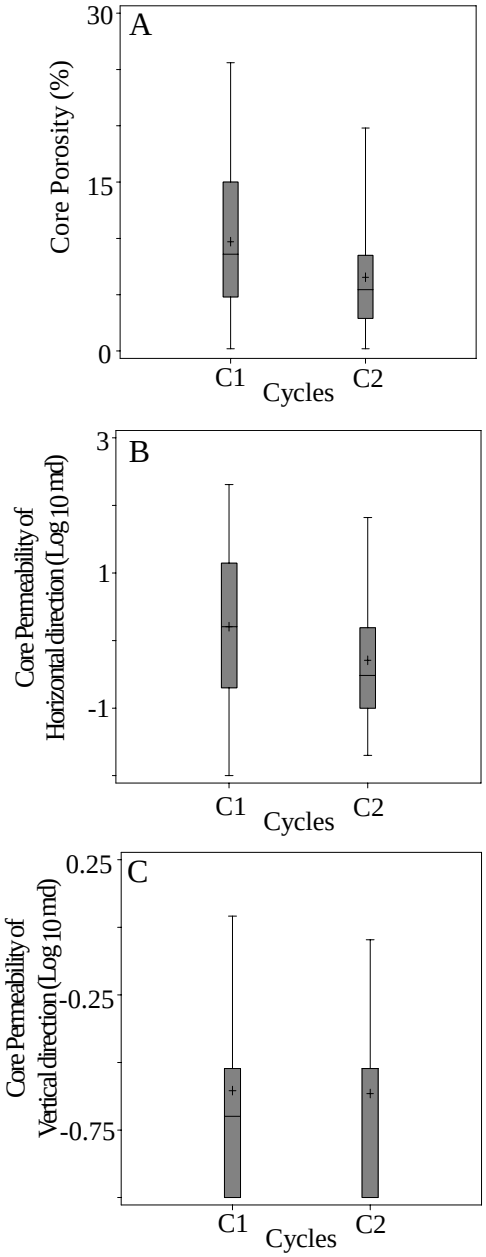

Figure 54. Petrophysical properties of two cycles observed in core. The center of each box is the 50th percentile; margins of the boxes are the 25th and 75th percentiles; and whiskers denote the 0th and 100th percentiles. See Table 15 for statistical comparison of cycles.

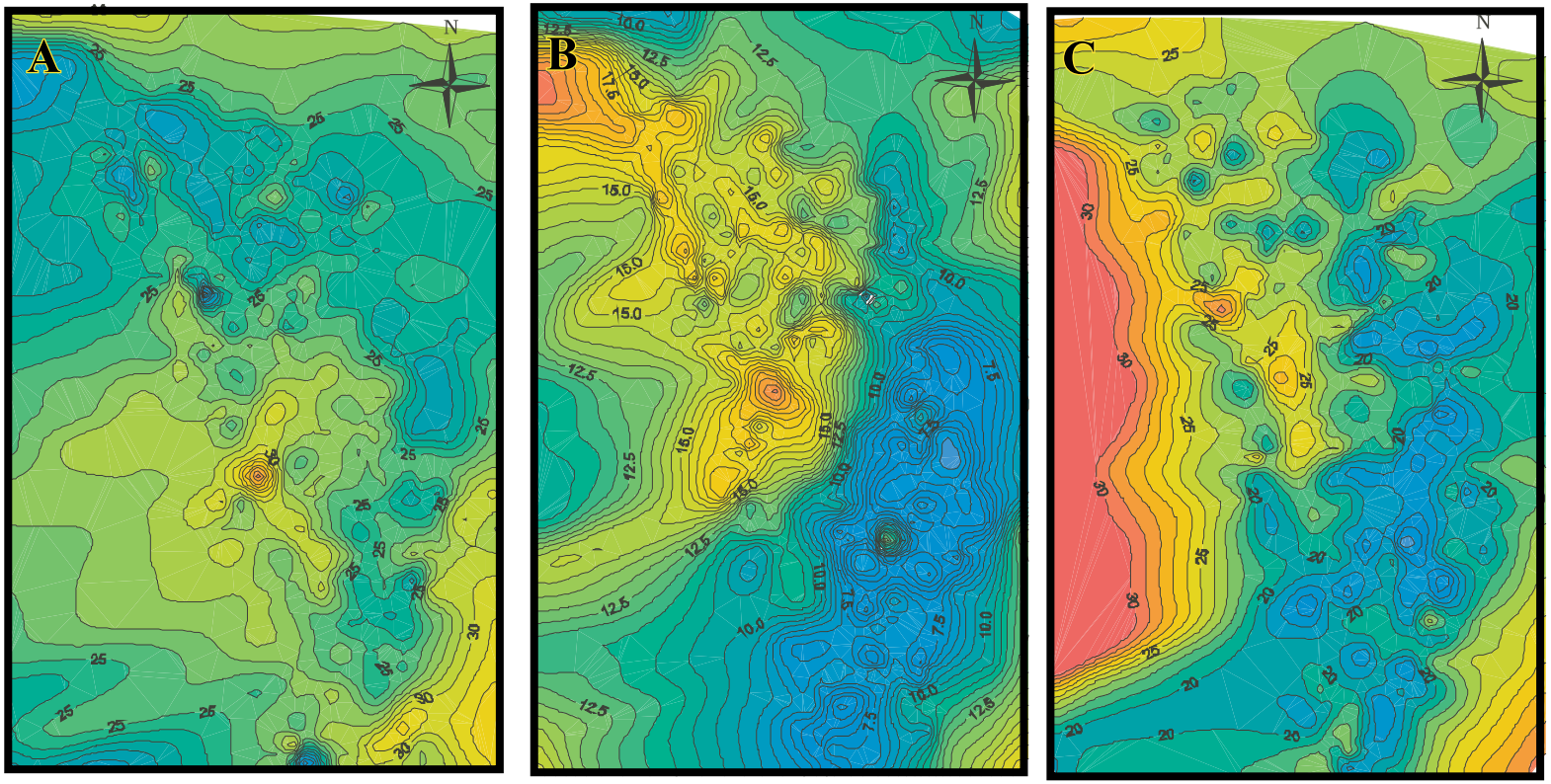

1 inch = 2.58 miles
Contour interval = 1 ft

1 inch = 2.58 miles
Contour interval = 0.5 ft

1 inch = 2.58 miles
Contour interval = 1 ft

Figure 55. Isopach map of cycle set CS3 and 4. (A) Cycle C6. (B) Cycle C7. (C) Cycle C8. Retrograding carbonate tidal flat deposits (cycle C6 and C7) records relative sea level rise and prograding coastal sabhka deposits records sea level fall during cycle set CS3 and 4.

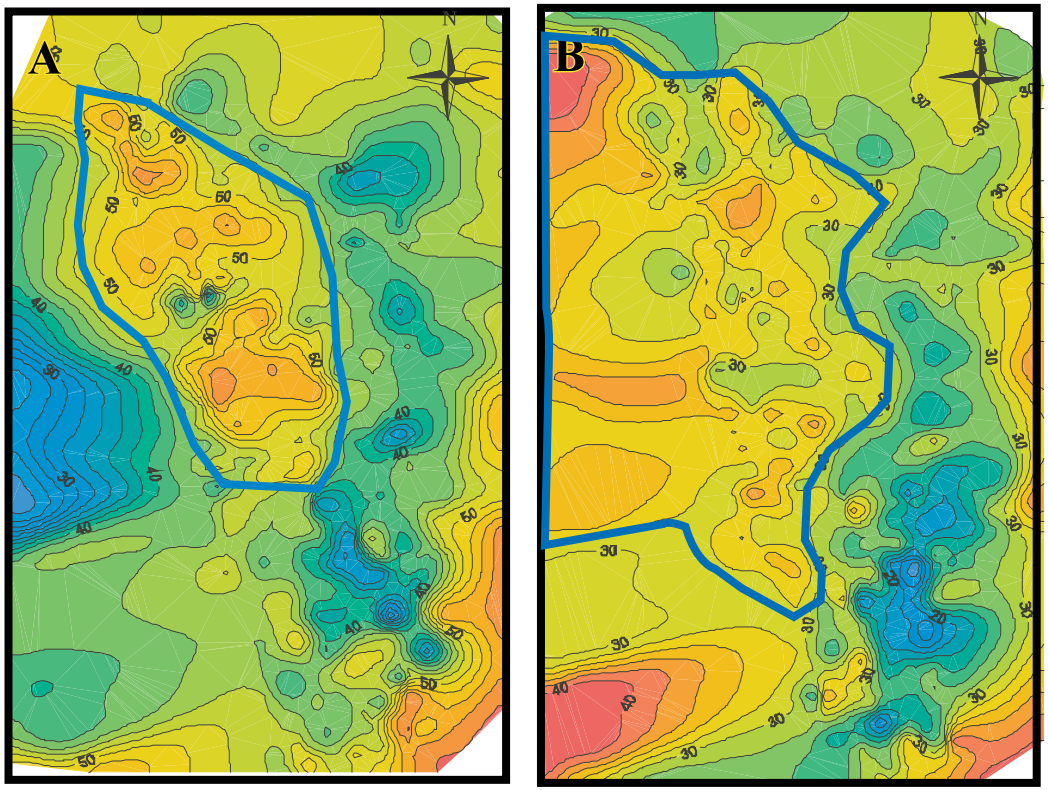

Figure 56. Isopach map of cycle set CS5. (A) cycle C9. (B) cycle C10. Increasing size of halite-dominated salina behind highstand carbonate platform records brine level fall at the end of cycle C11. Blue colored circles indicate inferred salina deposits.

platform margins. After that, upward-brining of alternated fluvial sandstone to evaporite-dominated salina anhydrites deposits of cycles C11, 12 and 13 were deposited during the base-level fall of the cycle set CS6 (Figure 57). The occurrence of an anhydrite bed instead of halite in these cycles of C11, 12, and 13 reflects the dilution of brine water due to influx fluvial sediment or a resumed connection to the open sea during late highstand. Three regressive prograding anhydrite-dominated salina cycles in cycle sets CS6 were deposited during base-level fall. The upper part of upward-shallowing of the thin bed halite dominated cycle comprises cycles C14, 15, and 16. Of the three cycles in cycle sets CS7 and 8, cycle C14 is an anhydrite-dominated cycle, which reflects dilution of brine during base level rise of cycle set CS7 and grades up to halite predominant cycles 15 and 16 of the base-level fall period in a cycle set CS8 (Figure 58A). Cycles C15 and 16 in CS8 represent the last infilling of salt-dominated salina giant and relevant prograding episodic fluvial origin deposits during base-level fall (Figure 58B and C). This cycle set of the upper part of the Queen Formation not only represent upward-brining with increasing isolation and salinity of carbonate interior, but also infilling inner carbonate platform by successively shallowing and decreasing long-term accommodation space (Figure 49).

The Queen Formation comprises complete and incomplete sedimentary cycles on the basis of generalized ideal vertical cycle and relevant full base-level change. Most cycles in the Queen Formation are composed of progradational upward-shallowing deposits that record base-level fall, and they can form few deposits formed during subsequent base-level rise, which has very little portion of the retrogradational upward-deepening part of cycle. The complete cycles during long-term base-level rise comprise the full spectrum of upward-fining of fluvial and estuarine siliciclastic deposits of facies association 1 and 3, and upward-shallowing of carbonate tidal flat deposits of facies association 2, and evaporite-dominated salina and mud flat deposits of facies association 4 within a cycle. The complete cycles commonly occurred at the beginning part of cycle sets. The incomplete cycles during long-term base-level fall do not include sedimentary deposits of base-level rise portions in complete cycle. That incomplete cycles consist of a partial record of upward-shallowing of carbonate tidal flat and evaporite mud flat deposits of facies association at the lower part of Queen Formation, or upward-brining of fluvial and salina deposits of facies association 3 and 4 at the upper part of Queen Formation.

Lithofacies and cycle thickness reflect the depositional location on the platform and relative accommodation and sediment supply (A/S) ratio. Sedimentation rate of component lithofacies and their relevant depositional settings could be important factors in controlling the

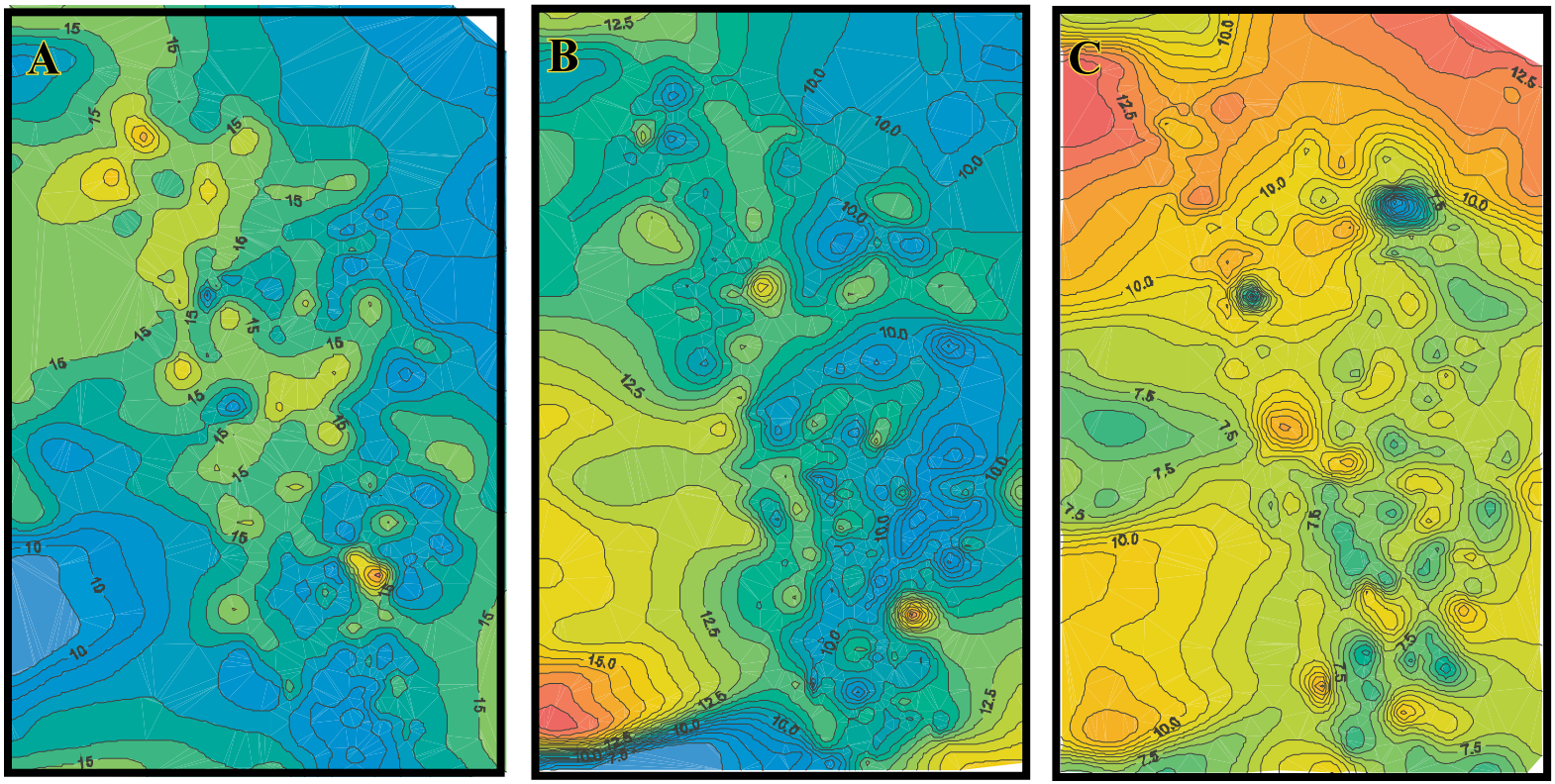

Figure 57. Isopach map of cycle set CS6. (A) cycle C11. (B) cycle C12. (C) cycle C13. Aggrading, upward-shallowing anhydrite-dominated saltina behind carbonate platform records relative sea level fall and brine level fall during cycle set CS6.

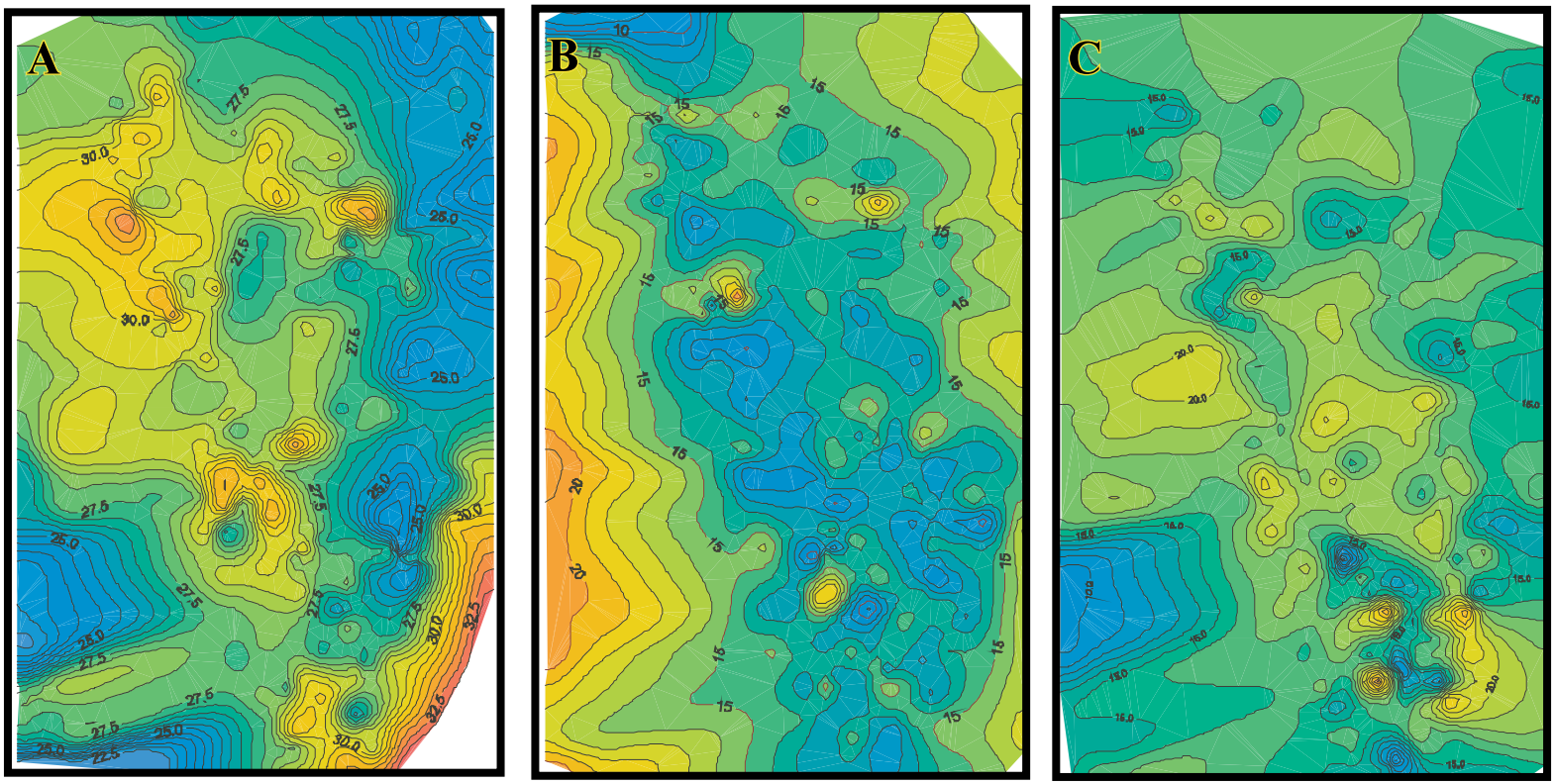

Figure 58. Isopach map of cycle set CS7 and 8. (A) cycle C14. (B) cycle C15. (C) cycle C16. Aggrading, upward-shallowing halite-dominated salina records relative sea level and brine level fall during CS7 and 8.

preservation potential and thickness of cycles. A long-term base-level rise (increase A/S ratio) indicates a decrease in sediment reworking and bypass, and an increase in sediment preservation potential that will produce retrogradational sedimentary cycles, whereas a long-term base-level fall (decrease A/S ratio) reflects an increase in sediment reworking and bypass (increase in amalgamation), and a decrease in sediment preservation potential that results in progradational or aggradational sedimentary cycles.

Base Level Cycles

Retrogradational units reflect increasing A/S ratios or base-level rise, whereas progradational (aggradational) units indicate following A/S ratios or base-level fall. The Queen Formation reflects deposition in low, accommodation shallow-water inner carbonate platform under these conditions tend depositional cycles to be asymmetric, mostly progradational. The climate was dry, so falling base level lead to decreasing brine level and increasing salinity. Changes in salinity and A/S ratio in the Queen platform interior were provided by aggradation or progradation of carbonate platform margins during the short-term low amplitude and high frequency base-level rise of greenhouse time and subsequent isolation and ponding of inner carbonate platforms.

Sequences (HFS)

Two sequences and maximum flooding surfaces were defined by a turnaround from progradational to retrogradational cycles, and analysis trend of cycle thickness and internal lithofacies proportion (Table 13 and Figure 49 and 51). Sequence 1 comprises fluvial and deltaic siliciclastics that grade upward into carbonate tidal flat. This siliciclastic to carbonate sequence records long-term base level rise. Sequence 2 is composed of salina deposits with some fluvial sandstone record long-term base level fall (Figure 49 and 51). Sequences are continuous through the study area. Sequences are average 58.52 and 107.61 feet (17.6 to 32.28 meters) thick, respectively. The base-level rise parts of sequence are average 94.60 and 107.61 feet (28.38 to 32.28 meters) thick, respectively. The base-level fall parts of sequence are average 58.08 (17.42 meters) and 58.52 (17.53 meters) thick, respectively (Table 13 and Figure 51). The lithofacies proportion variation indicates increasing salinity and decreasing base-level from sequence 1 to 2. These decreased accommodation space were marked by upper part halite dominant sequence 2.

Proposed Paracyclic Evolution

The Queen/Grayburg boundary defines a sea level lowstand when the shelf was exposed, fluvial channels incised into the platform edge and carried siliciclastic sediments into intra platform areas, and eolian processes rework interfluve areas (Figure 59A).

Transgressive estuarine deposits formed during subsequent base level rise and as the shelf was flooded siliciclastic deposits became restricted to move proximal areas (Figure 59B). Base level rise deposits became more bioturbated as waters deepened. Mudstones record siliciclastic starvation and a lag carbonate production during early transgression. Once carbonate production was initiated at the first flooding surface, upward-shoaling supratidal to subtidal carbonate tidal flat dolomudstone to dolopackstone and reddish brown siltstone were deposited in shallow subtidal, protected lagoons behind the carbonate platform interior. Coastal evaporite mud flats prograded into the basin in semiarid to arid climatic conditions. Prograding to aggrading shoreline parallel beach ridge and cuspate deltas formed during late lowstand to transgressive periods (Figure 59A). The latter prograding (or aggrading) shoreline sand deposits do not bypass the shelf was rising relative sea level produced accommodation on the platform during transgression. Muddy fine-sand transgressive deposits record fluctuation of the siliciclastic sources and gradual hinterland shift in deposition during long-term base level rise.

With increasing isolation of inner carbonate platform area during early to late highstand sea level periods, the salinity of the brine water began to increase, and brine levels started to decrease due to prograding highstand carbonate build up (Figure 59C). Inner carbonate platform became more emergent and transformed into a shallower isolated inner shelf. This could be a favorable condition for subaqueous evaporite sedimentation to begin in this semiarid to arid climatic Queen inner carbonate platform. This inner carbonate shelf was gradually changed into hypersaline salina (or saltern) behind the carbonate platform margin in which bottom-grown gypsum (present anhydrite) started to form above finely laminated dolomudstone and cryptalgal dolomitic laminated anhydrite. The salina was progressively filled with pure pristine sulfate and then evolved into evaporite and clastic dominated mud flat (sabhka) that was frequently interrupted the fluvial sandstone facies by episodic fluvial activities from hinterland.

This complete halite basin-fill provides the next phase siliciclastic bypass of the upper Queen sand member to basin at early lowstand. This upper Shattuck Sandstone Member was probably deposited after halite fill of inner carbonate platforms during another cycle of base level fall, and represents the beginning of another lowstand system tract.

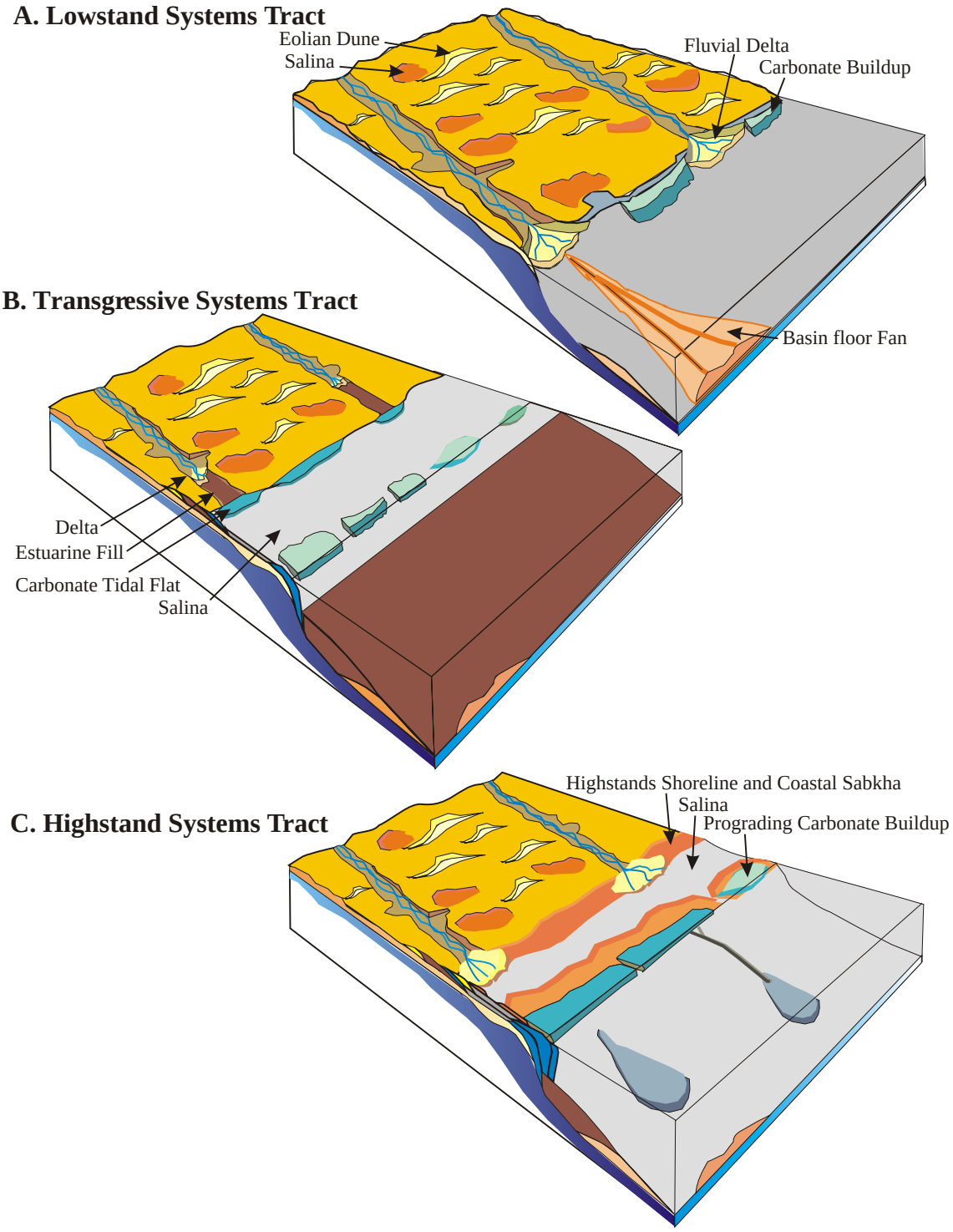

Figure 59. Paracyclic evolution of the Queen Formation (A) Lowstand systems tract, (B) Transgressive systems tract, and (C) Highstand systems tract.

RESERVOIR PROPERTIES

STATISTICAL CORRELATION ANALYSIS

A statistical correlation analysis was performed to relate petrophysical and geologic properties and better predict Queen sand reservoir quality. An integrated relational database included: (1) Raw and calculated data of lithofacies, facies association, cycle, texture, composition, porosity, permeability, and well logging properties; (2) core descriptions, petrophysical analysis and statistical analysis. The database was completed in Access 2000, SAS v.8 and GES explorer software.

Porosity

Generated Porosity

Neutron porosity was related to core porosity using the following equation (Figure 60). R-square value) is 0.47.

$$EPHI=1.0584+(0.4974xPHIN)$$

Where, EPHI=Generated neutron based porosity (%)

PHIN=Neutron log porosity (%)

A log determined by transforming neutron porosity log using this equation was named "EPHI". This is equation was found to explain 47% of this relationship.

Based on the generated porosity value (EPHI), Efacies codes from generated equations of facies analysis (NEcode1), numerical coded facies associations (NFA) and cycles (Ncycle), series of statistical correlation analysis were performed in order to estimate the relative effects of stratigraphic controls in macro-scale on reservoir quality quantitatively at the Queen cored interval.

Stratigraphic Control

Multiple regression analysis was also performed to determine if different scales of stratigraphic cycles defined distinct groups of porosity. Correlation between genetic stratigraphic constraints and estimated porosity from well logs shows lithofacies types has the most significant statistical correlation, while facies associations and cycles are less significant (Figure 61). Multi-regressive analysis suggested that facies association is the least significant influential parameter. The regression coefficient is 0.76 (R square value) in the first multi-regressive process. This analysis shows that porosity depends upon lithofacies. The boundaries of relevant cycle are already defined and mapped by sequence stratigraphic analysis in which cycle

A

PHI = PHIN
Response Distribution: Normal
Link Function: Identity

Model Equation
PHI = 1.0584 + 0.4974 PHIN

Summary of Fit			
Mean of Response	9.3170	R-Square	0.4750
Root MSE	4.0583	Adj R-Sq	0.4689

Analysis of Variance					
Source	DF	Sum of Squares	Mean Square	F Stat	Pr > F
Model	1	1281.7661	1281.7661	77.82	<.0001
Error	86	1416.4184	16.4700		
C Total	87	2698.1844			

Type III Tests					
Source	DF	Sum of Squares	Mean Square	F Stat	Pr > F
PHIN	1	1281.7661	1281.7661	77.82	<.0001

B

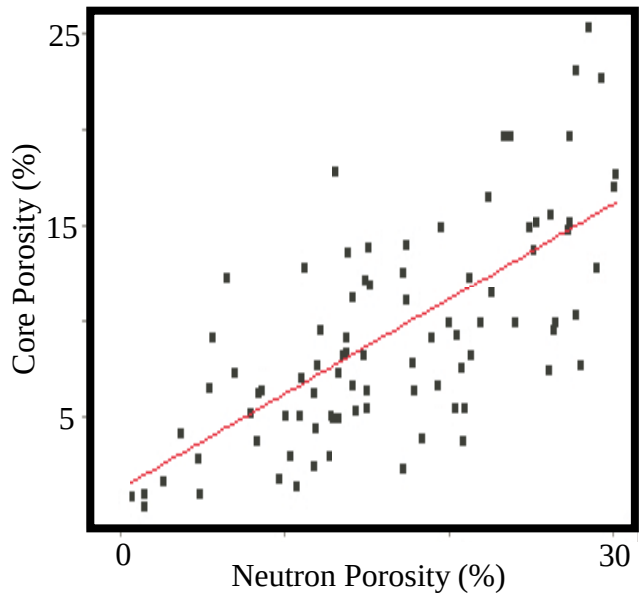

Figure 60. Predicted porosity normalized neutron porosity well log data. (A) Prediction of porosity from neutron porosity well log variables and generated equation of neutron porosity based porosity at uncored regions. (B) Scatter plot between core porosity and neutron porosity. R-square value is 0.47.

A

Univariate Statistics

Variable	N	Mean	Std Dev	Minimum	Maximum
EPHI	625	5.6269	3.6926	0.7849	15.8862
NEcode1	625	2.1671	0.6310	1.0457	3.0724
NFA	625	1.3200	0.4668	1.0000	2.0000
NCycle	625	1.5600	0.4968	1.0000	2.0000

B

Correlation Matrix

	EPHI	NEcode1	NFA	NCycle
EPHI	1.0000			
NEcode1	-0.8545	1.0000		
NFA	-0.0948	0.1644	1.0000	
NCycle	-0.3658	0.2559	-0.5942	1.0000

C

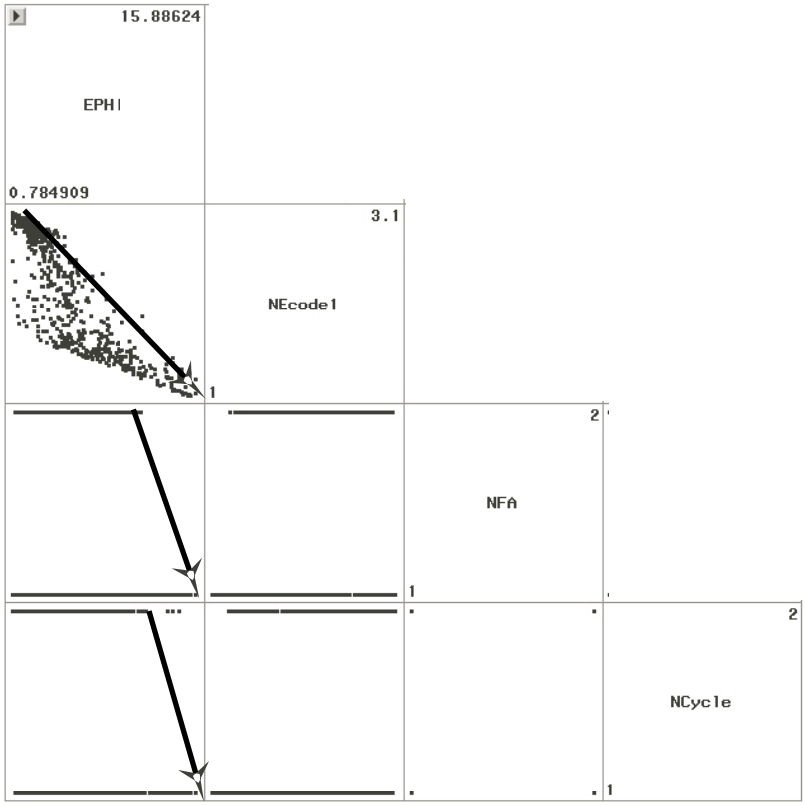

Figure 61. Summary of univariate statistics of neutron porosity log based porosity. (A) Summary of univariate statistics show the minimum and maximum range of porosity in Efacies (NEcode1), facies associations (NFA), and cycles (Ncycle). (B) Correlation matrix shows the relationships between Efacies, facies associations and cycles and porosity. (C) Cross-plot matrix indicates positive and negative correlation (arrows) between porosity and Efacies (NEcode1), facies association (NFA) and cycles (Ncycle).

boundaries are used for the first pass subdivisions of reservoir zones in this study. In order to visualize spatial porosity variation, the following equation is generated excluding the most redundant facies association (Figure 62).

$$EPHI=16.4632–(5.0003xNEcode1)$$

Where, EPHI= Generated porosity

NEcode1= Efacies codes

Textural and Compositional Control

Porosity estimations were compared to textural and compositional properties like grain size, sorting, abundance of different types of framework grains (quartz, feldspar, rock fragment), and cement and matrix (authigenic dolomite and anhydrite cement, and clay). Grain size, sorting, and the amount of authigenic cement significantly predict porosity (Figure 63).

Permeability

Generated Permeability

Regressive analysis of core permeability and neutron log defined porosity (EPHI) predicts the following equation. This equation is generated for predicting permeability in uncored region of the study area:

$$LogKH=-1.3118+(0.1408xEPHI)$$

Where, LogKH=logarithmic scale core permeability in horizontal direction

EPHI=neutron generated porosity

Using this generated predictive equation of permeability, the variation of permeability development at different stratigraphic zones can be estimated with other important geological parameters and porosity in this study area.

Stratigraphic Control

Both core and neutron-log based porosity estimation are correlated with permeability. Lithofacies and facies association have a strong correlation result with permeability development in this study area, while cycles do not have significantly correlation with permeability (Figure 64).

Lithofacies codes divided porosity values into distinct group better than the larger stratigraphic units (Figure 65). Upward-deepening base-level rise and the upward-shallowing base-level fall part of hemicycles control permeability distribution. Facies associations are very important defining reservoir zones in terms of permeability.

A

EPHI = NEcode1 NFA NCycle
Response Distribution: Normal
Link Function: Identity

Model Equation
EPHI = 19.1960 - 4.5644 NEcode1 - 0.7985 NFA - 1.6817 NCycle

Summary of Fit			
Mean of Response	5.6269	R-Square	0.7589
Root MSE	1.8176	Adj R-Sq	0.7577

Analysis of Variance					
Source	DF	Sum of Squares	Mean Square	F Stat	Pr > F
Model	3	6456.7690	2152.2563	651.48	<.0001
Error	621	2051.5528	3.3036		
C Total	624	8508.3218			

Type III Tests					
Source	DF	Sum of Squares	Mean Square	F Stat	Pr > F
NEcode1	1	4036.2636	4036.2636	1221.77	<.0001
NFA	1	46.7949	46.7949	14.16	0.0002
NCycle	1	225.7709	225.7709	68.34	<.0001

B

EPHI = NEcode1
Response Distribution: Normal
Link Function: Identity

Model Equation
EPHI = 16.4632 - 5.0003 NEcode1

Summary of Fit			
Mean of Response	5.6269	R-Square	0.7302
Root MSE	1.9196	Adj R-Sq	0.7298

Type III Tests					
Source	DF	Sum of Squares	Mean Square	F Stat	Pr > F
NEcode1	1	6212.6961	6212.6961	1686.04	<.0001

Figure 62. Predicted porosity using generated Efacies. (A) Prediction of porosity from Efacies codes (NEcode1), facies associations (NFA) and cycles (Ncycle). Facies associations (NFA) have relatively lower regression coefficient than Efacies codes (NEcode1) and cycles (Ncycle). Cycles were already defined by stacking pattern analysis. Thus, facies associations and cycles are removed at step B of the calculation of predicted porosity from macro-scale geologic constraints. (B) Predictive porosity equation using Efacies is created, and R-square values is 0.73.

A

Univariate Statistics

Variable	N	Mean	Std Dev	Minimum	Maximum
PHI	75	9.1000	5.4446	0.2000	23.3000
GSMEAN	75	67.4694	18.2772	33.0337	109.1200
SORTING	75	0.4994	0.0691	0.3962	0.7724
QTZ	75	0.3076	0.1138	0.0333	0.6173
TFD	75	0.1011	0.0472	0	0.1839
RF	75	0.0280	0.0225	0	0.0816
TCMT	75	0.3911	0.2022	0	0.9667
CLAY	75	0.0355	0.0581	0	0.3683

B

Correlation Matrix

	PHI	GSMEAN	SORTING	QTZ	TFD	RF	TCMT	CLAY
PHI	1.0000							
GSMEAN	0.4462	1.0000						
SORTING	-0.0422	-0.2007	1.0000					
QTZ	0.3627	0.5427	0.0656	1.0000				
TFD	-0.0226	0.0992	-0.1532	0.0092	1.0000			
RF	0.3191	0.5898	-0.1696	0.3388	0.3057	1.0000		
TCMT	-0.7349	-0.4957	0.0188	-0.6417	0.0524	-0.3593	1.0000	
CLAY	0.1280	-0.0282	-0.0673	0.0011	-0.4267	-0.1738	-0.2037	1.0000

C

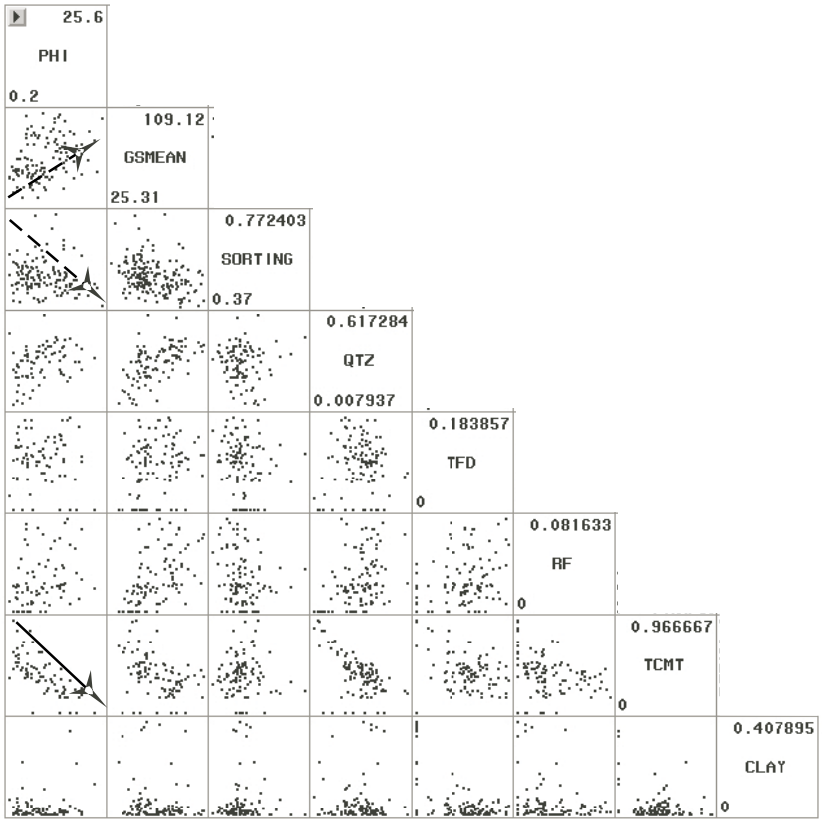

Figure 63. Summary of univariate statistics of composition, texture and porosity. (A) Summary of compositional and textural properties, and porosity. (B) Correlation matrix shows some significance authigenic cement content (TCMT), grain size (GSMEAN) and sorting (SORTING). (C) Cross-plot matrix indicating positive and negative correlation (arrows) between porosity and seven compositional and textural parameters.

A

LogKH : PHI EPHI NEcode1 NFA NCycle

Univariate Statistics

Variable	N	Mean	Std Dev	Minimum	Maximum
LogKH	88	-0.0137	1.1692	-2.0000	2.1614
PHI	88	9.3170	5.5690	0.4000	25.6000
EPHI	88	9.2182	3.7507	1.5238	15.8862
NEcode1	88	1.6705	0.5010	1.0457	3.0101
NFA	88	1.3864	0.4897	1.0000	2.0000
NCycle	88	1.2841	0.4536	1.0000	2.0000

B

Correlation Matrix

	LogKH	PHI	EPHI	NEcode1	NFA	NCycle
LogKH	1.0000					
PHI	0.7972	1.0000				
EPHI	0.4517	0.6892	1.0000			
NEcode1	-0.4442	-0.6470	-0.8247	1.0000		
NFA	-0.4565	-0.4863	-0.4980	0.5978	1.0000	
NCycle	0.0099	-0.0156	-0.0156	-0.1261	-0.4999	1.0000

C

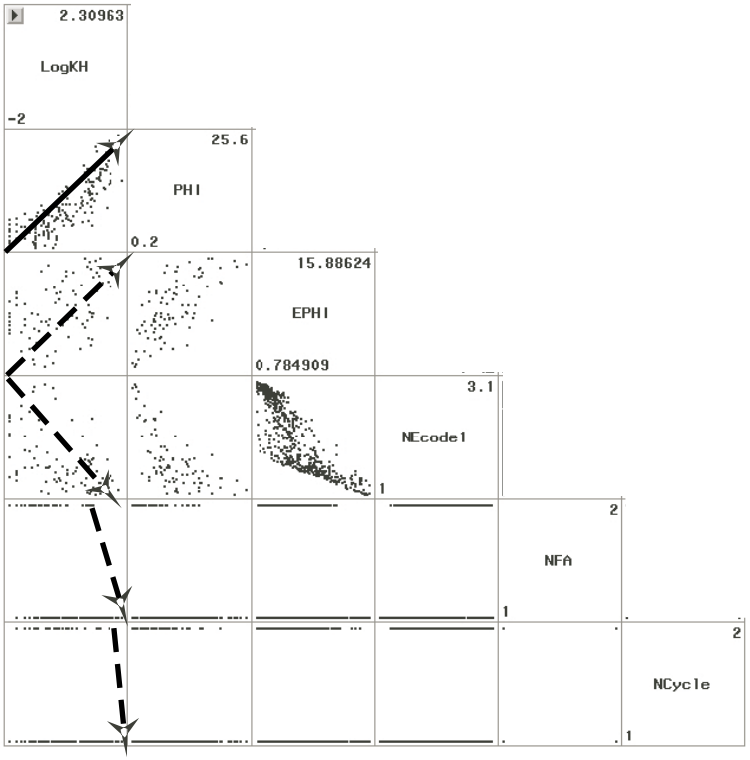

Figure 64. Summary of petrophysical properties and sequence stratigraphic divisions. (A) Summary of 5 petrophysical properties and sequence stratigraphic divisions of core porosity (PHI), generated neutron porosity (EPHI), Efacies (NEcode1), facies associations (NFA), and cycles (Ncycle). (B) Correlation matrix indicates some significance core porosity, generated neutron porosity, Efacies, and facies associations. (C) Cross-plot matrix indicates positive and negative correlation (arrows) between petrophysical properties and sequence stratigraphic divisions.

A

LogKH = EPHI NEcode1 NFA NCycle	
Response Distribution:	Normal
Link Function:	Identity

Model Equation

LogKH = 1.8586 + 0.0562 EPHI - 0.1431 NEcode1 - 1.0426 NFA - 0.5498 NCycle

Summary of Fit

Mean of Response	-0.0137	R-Square	0.3060
Root MSE	0.9973	Adj R-Sq	0.2725

Analysis of Variance

Source	DF	Sum of Squares	Mean Square	F Stat	Pr > F
Model	4	36.3921	9.0980	9.15	<.0001
Error	83	82.5444	0.9945		
C Total	87	118.9365			

Type III Tests

Source	DF	Sum of Squares	Mean Square	F Stat	Pr > F
EPHI	1	1.1546	1.1546	1.16	0.2844
NEcode1	1	0.1222	0.1222	0.12	0.7269
NFA	1	10.1851	10.1851	10.24	0.0019
NCycle	1	3.5521	3.5521	3.57	0.0623

B

LogKH = EPHI	
Response Distribution:	Normal
Link Function:	Identity

Model Equation

LogKH = - 1.3118 + 0.1408 EPHI

Summary of Fit

Mean of Response	-0.0137	R-Square	0.2041
Root MSE	1.0492	Adj R-Sq	0.1948

Type III Tests

Source	DF	Sum of Squares	Mean Square	F Stat	Pr > F
EPHI	1	24.2711	24.2711	22.05	<.0001

Figure 65. Predicted permeability using estimated porosity and stratigraphic units. (A) Prediction of permeability from estimated porosity (EPHI), Efacies codes (NEcode1), inferred facies associations (NFA), and cycles (Ncycle). Efacies (NEcode1) has a relatively lower regression coefficient. Facies associations (NFA) and cycles (Ncycle) were already defined by stacking pattern analysis. Thus, Efacies, facies associations, and cycles are removed at step B of calculation of predicted permeability. (B) Predictive permeability equation using estimated neutron porosity is created, and R-square values is 0.20.

Textural and Compositional Control

The relative effects of composition and texture on reservoir permeability development are examined (Figure 66). According to those analyses between permeability and seven textural and compositional constraints, grain size and total cement amount in Queen sandstones has a strong relationship with permeability development. The effect of two properties on reservoir quality is already known (Rittenhouse, 1971; Beard and Weyl, 1973; Pettijohn et al., 1973; Lake, 1995; Evans et al., 1997; Primmer et al., 1997). Cement amount and sandstone grain size main controls in permeability distribution in the Queen Formation (Figure 66A). Using two statically chosen textural and compositional micro-scale constraints, the predictive permeability equation was generated and "F stat value" of both properties was calculated. The "F stat value" of grain size is 0.0011, while that of the cement content is less than 0.0001. Thus, cement content in the Queen sandstone of this study is significantly related to permeability distribution in micro-scale, like porosity (Figure 66B). Cement is strongly related to base-level changes during deposition in inner carbonate platforms. It is controlled by upward-brining trends.

An equation to predict total authigenic cement content from gamma ray and neutron porosity wireline logs signature was created by multiple regression analysis (Figure 67). Neutron porosity log has a strong relationship with the total authigenic cement content on the basis of "F stat value" in gamma ray and neutron porosity logs. The second step analysis for generation of predictive equations of total cement amount used only neutron porosity log data. Using neutron porosity logs, the predictive equation was created as follows.

$$TCMT=0.6047–(0.0151xPHIN)$$

Where, TCMT=Total authigenic cement

PHIN=Neutron porosity log

This predictive equation will be utilized for determination of the relationship between permeability and porosity spatial patterns and subdivision of reservoir horizons at each different base-level sequence stratigraphic constraint.

RESERVOIR ARCHITECTURES

Facies associations and cycles are laterally continuous and have a relatively uniform thickness across the study area (Figure 68, 69, 70, and 71). Abrupt thickness variations are observed at the base of cycle C1 that reflects delta progradation, fluvial incision, and subsequent estuarine fill. Interwell correlation along strike clearly shows three to four fluvial incisions of

A

LogKH = GSMEAN SORTING QTZ TFD RF TCMT CLAY	
Response Distribution:	Normal
Link Function:	Identity

Model Equation

LogKH = - 0.4225 + 0.0225 GSMEAN + 0.9934 SORTING - 2.1919 QTZ
+ 3.3934 TFD - 0.2490 RF - 2.7919 TCMT + 0.5398 CLAY

Summary of Fit

Mean of Response	0.1927	R-Square	0.5208
Root MSE	0.7130	Adj R-Sq	0.4700

Type III Tests

Source	DF	Sum of Squares	Mean Square	F Stat	Pr > F
GSMEAN	1	5.5492	5.5492	10.92	0.0015
SORTING	1	0.2994	0.2994	0.59	0.4456
QTZ	1	2.1731	2.1731	4.27	0.0426
TFD	1	1.3915	1.3915	2.74	0.1028
RF	1	0.0013	0.0013	2.554E-03	0.9598
TCMT	1	11.4507	11.4507	22.53	<.0001
CLAY	1	0.0534	0.0534	0.11	0.7469

B

LogKH = GSMEAN TCMT	
Response Distribution:	Normal
Link Function:	Identity

Model Equation

LogKH = - 0.1939 + 0.0183 GSMEAN - 2.1966 TCMT

Summary of Fit

Mean of Response	0.1927	R-Square	0.4666
Root MSE	0.7253	Adj R-Sq	0.4516

Type III Tests

Source	DF	Sum of Squares	Mean Square	F Stat	Pr > F
GSMEAN	1	6.0614	6.0614	11.52	0.0011
TCMT	1	9.9683	9.9683	18.95	<.0001

Figure 66. Predicted permeability using composition and texture. (A) Prediction of permeability from grain size (GSMEAN), sorting (SORTING), quartz (QTZ), feldspar (TFD) rock fragment (RF), cement (TCMT), and clay (CLAY). Grain size and cement content have higher probability (low value of F factor). Thus, grain size and total cement content is used at step B of calculation of predicted permeability from micro-scale geologic controls. (B) Predictive permeability equation using grain size and cement content is generated. According to 'F factor' of type 3 test, cement content has significant relationship with permeability development. R-square values is 0.47.

A

TCMT = PHIN GR	
Response Distribution:	Normal
Link Function:	Identity

Model Equation

TCMT = 0.6717 - 0.0125 PHIN - 0.0010 GR

Summary of Fit

Mean of Response	0.3673	R-Square	0.3323
Root MSE	0.1758	Adj R-Sq	0.3061

Type III Tests

Source	DF	Sum of Squares	Mean Square	F Stat	Pr > F
PHIN	1	0.3388	0.3388	10.97	0.0017
GR	1	0.0415	0.0415	1.34	0.2519

B

TCMT = PHIN	
Response Distribution:	Normal
Link Function:	Identity

Model Equation

TCMT = 0.6047 - 0.0151 PHIN

Summary of Fit

Mean of Response	0.3673	R-Square	0.3147
Root MSE	0.1764	Adj R-Sq	0.3015

Type III Tests

Source	DF	Sum of Squares	Mean Square	F Stat	Pr > F
PHIN	1	0.7427	0.7427	23.88	<.0001

Figure 67. Predicted cementation using well logs. (A) Prediction of cementation from gamma ray (GR) and neutron porosity log (PHIN). Gamma ray logging values have lower probability (high value of F factor). Thus, the neutron porosity log (PHIN) uses at step B in the calculation of predicted cementation in Queen sandstone reservoir. (B) Predictive cementation equation using neutron porosity log (PHIN) is generated, and R-square values is 0.31.

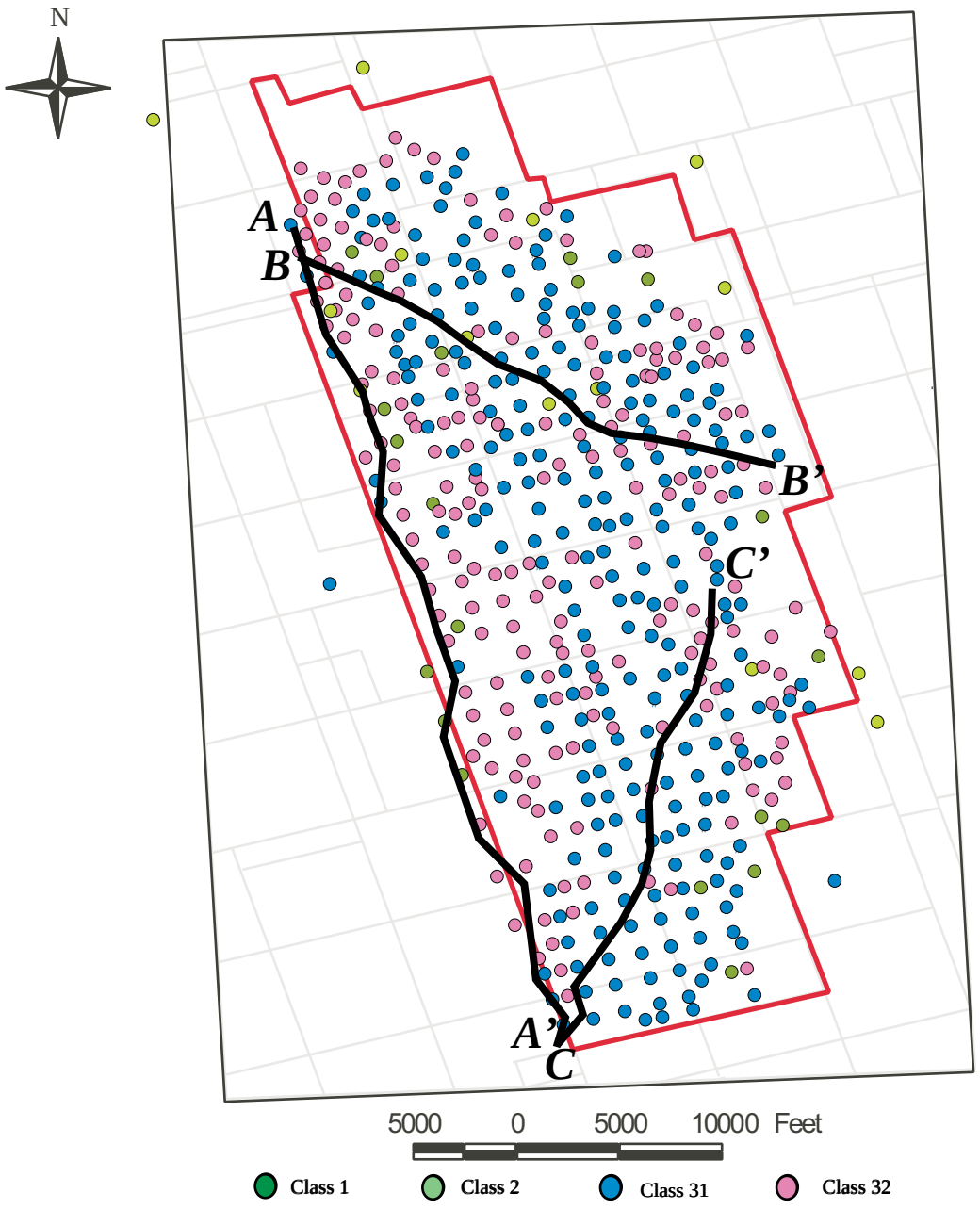

Figure 68. Index map of study area showing locations of cross sections. All isopach maps in this study area are based on geophysical log correlations from 454 wells across the study area. Different colored circles indicate different well components of Class 1, 2, 31 and 32 wells.

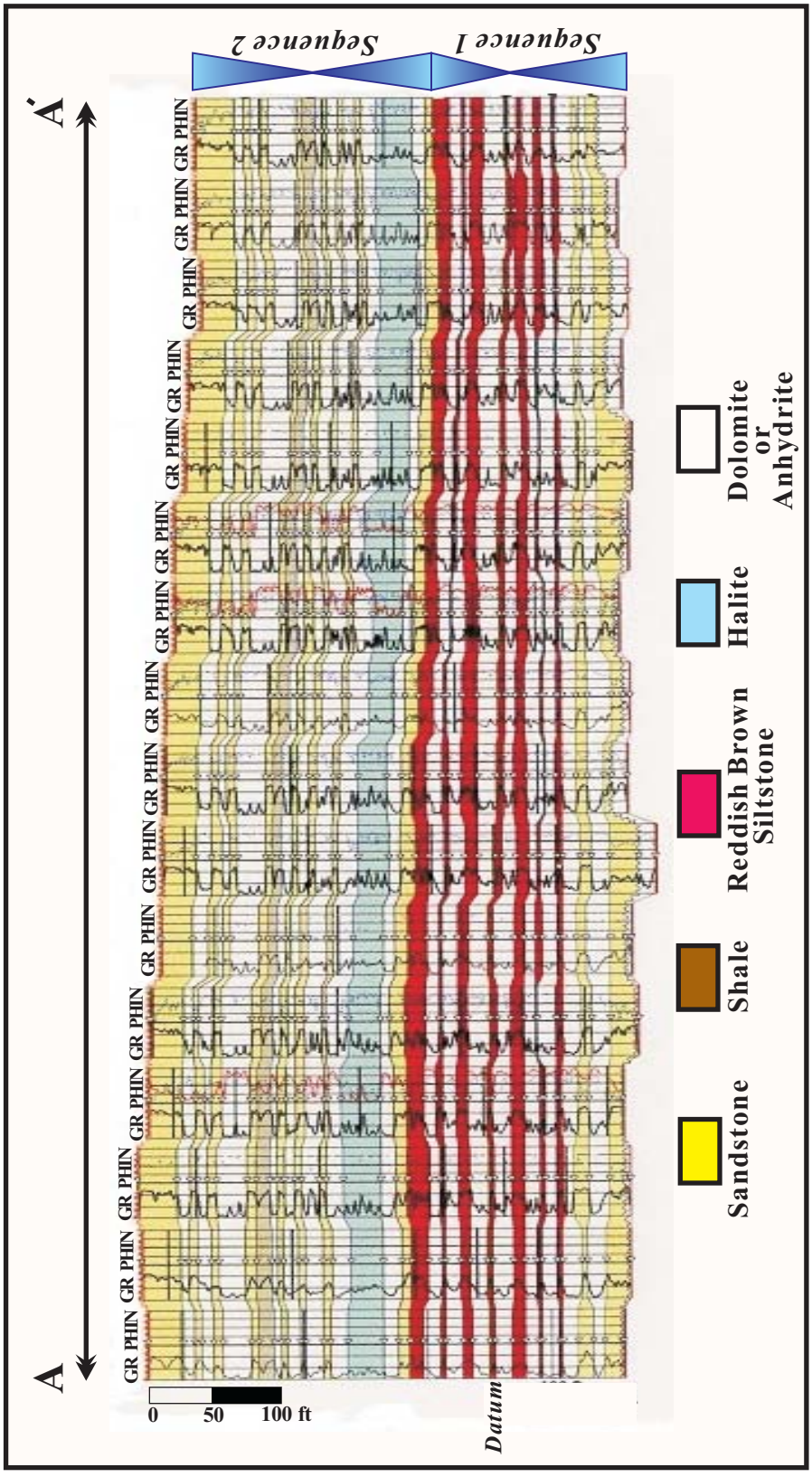

Figure 69. Cross Section A-A'. Locations of the cross section are shown in Figures 68.

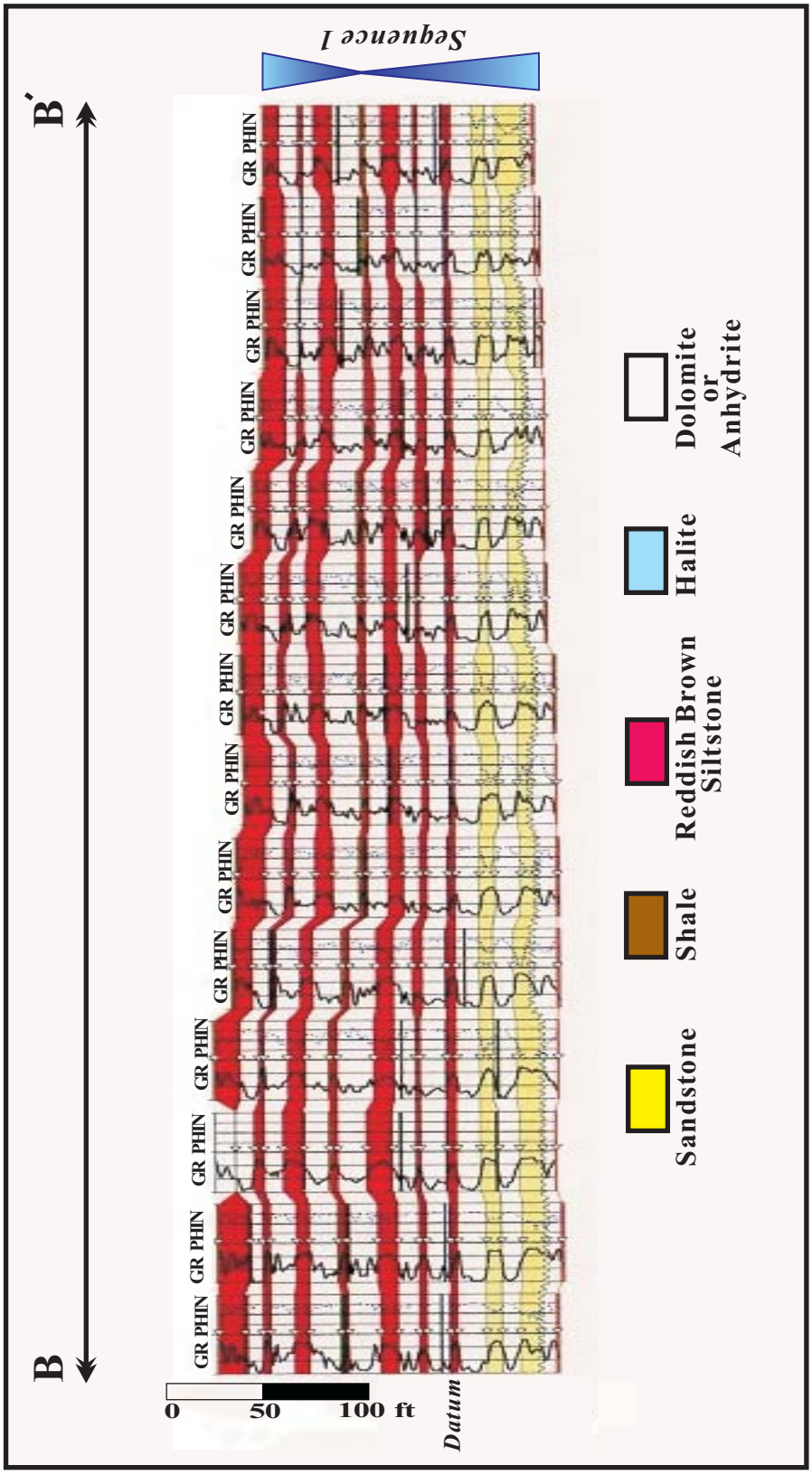

Figure 70. Cross Section B-B'. Locations of the cross section are shown in Figures 68.

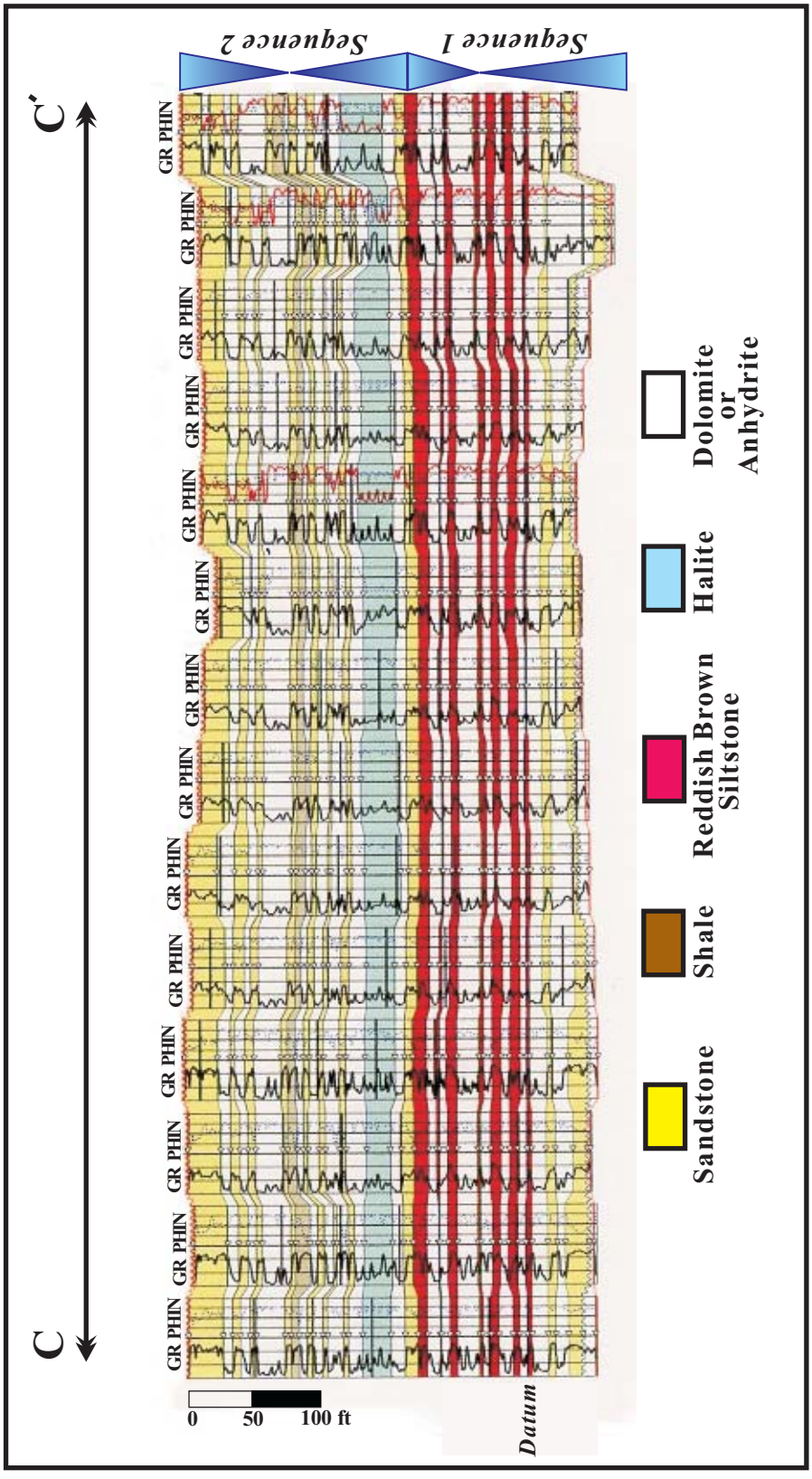

Figure 71. Cross Section C-C'. Locations of the cross section are shown in Figures 68.

cycle C1 and a very uniform thickness in the rest of the cycle. The dimension of incision exhibits decreasing width and increasing depth toward the distal (southeastern) part of the study area (Figure 69). The dip-direction cross sections show thickening of the shale bed and thinning of the fluvial sandstone and reddish brown evaporite mud flat toward the eastern proximal part of the study area (Figure 70 and 71).

On the basis of sand continuity, three geological bed architectures were proposed: (1) layer-cake formation shows good sand continuity, (2) jig-saw puzzle types are sand-rich, but show significant lateral permeability variation, and (3) labyrinth reservoirs are usually discontinuous, with complex sand arrangement and difficult interwell correlation (Figure 72) (Weber and Geuns, 1990). Based on the well-to-well correlation, the Queen Formation consists of less continuous fluvial dominated siliciclastic origin “labyrinth” reservoir geometry at the base, and evaporite- and carbonate-dominated “layer-cake” type bed geometry. Fluvial-dominated “labyrinth” bed geometry results from autocyclic processes such as delta progradation, fluvial channel filling and migration, and siliciclastic and carbonate shoal accretion during base-level rise (lowstand to transgressive periods), while carbonate and evaporite “layer-cake” bed geometry reflects typical inner platform evaporites during the base level fall (highstand periods).

Warren (1999) suggested that low-amplitude sea level fluctuations that characterize greenhouse periods favored large, highly restricted inner platform areas on carbonate platforms. Carbonate platform interiors during greenhouse periods include (1) dominantly high frequency carbonate cycles of less than 20 k.y. duration by low amplitude precessionally driven sea-level changes; (2) aggraded and flat-topped carbonate platforms; (3) dominant sub-seismic scale peritidal meter scale cycles or parasequences with tidal flat caps; (4) an absence of high relief carbonate buildups; (5) a layer cake stacking pattern of parasequences; (6) thick bedded limited laterally marginal reef/grainstone facies; (7) poorly developed cycle capping disconformities; and (8) pervasive early dolomitization of the platform interior due to the seaward migrating brine body during progradation in arid climatic conditions (Read et al., 1991).

Carbonate platform margins can grow fast enough to keep up with low amplitude base-level rises, as margin built upward wide and flat inner carbonate platforms lagoonal areas. During low-amplitude base-level falls these lagoons would become pond and could form evaporite. Thus, stacked successions of lagoon areas and saline infill evaporite very rapidly due to the relative high rate of evaporite sedimentation rate during greenhouse times. Most evaporite

A. Layer Cake

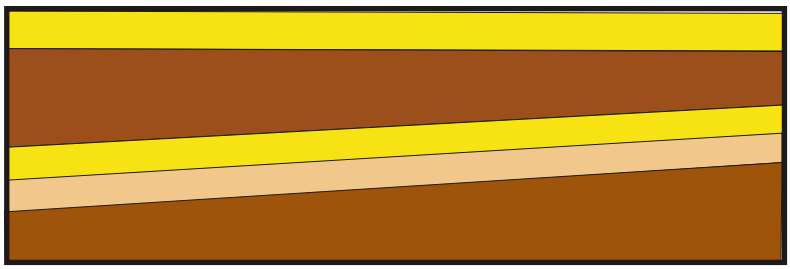

B. Jigsaw Puzzle

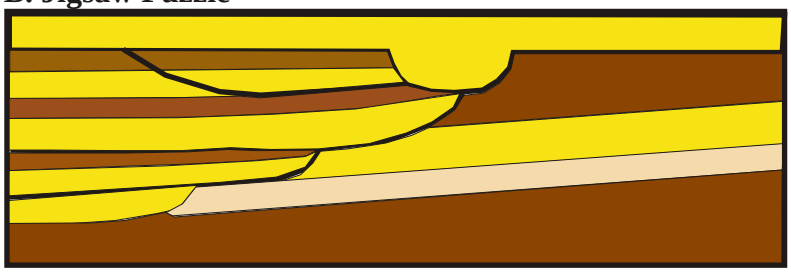

C. Labyrinith

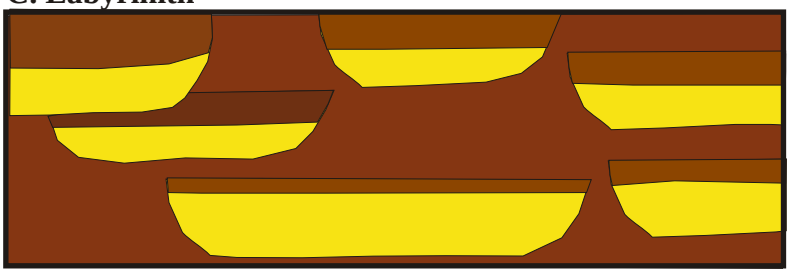

Figure 72. Three types of geological reservoir architecture (After, Weber and van Geuns, 1990).

has a very high rate of sedimentation in which evaporite sediment is part of TST, but only precipitates during the relatively short time intervals of higher-order low amplitude sea level falls (Warren, 1999).

Reservoir Zones

Previous studies on the effect of major geologic controls on reservoir quality suggested A/S ratio changes controlled facies boundaries and patterns, and the dimensions of reservoir units (Evans et al., 1997; Knox and Barton, 1999; Ye et al., 1999). In this study area, high-frequency sequence stratigraphic constraints of the cycle sets, cycles, facies association and lithofacies and diagenetic cementation control the porosity and permeability in Queen sandstone reservoirs, to different degrees.

Cycle sets, cycles, and facies association defined lateral and vertical lithofacies distribution. Diagenetic modification of authigenic cement also controls Queen reservoir quality. Variability of cycles within a cycle sets define reservoir zone boundaries and quality. Base-level rise of cycle sets generally decrease in permeability and porosity in the Queen sandstone reservoir (Table 16). However, short-term base-level hemicycle part of cycles shows better quality reservoirs.

The Queen sandstone reservoir can be subdivided into four reservoir zones of R11, R12, R21, and R22 in which reservoir zones are strongly related to the boundaries of cycles and facies associations within the same cycle set CS1. In order to determine spatial variation of Efacies, porosity, permeability, and degree of cementation, the generated Efacies code, neutron log based porosity and permeability, and degrees of cementation were mapped for the reservoir intervals (Figure 73, 74, 75, and 76).

Reservoir R11is the best reservoir horizon. Reservoir quality is distinctly worse upward (reservoir zones of R12, R21 and R22). The base-level rise facies association of R11 has better quality of static reservoir properties (porosity and permeability) than that of R12 in the study area. That means lithofacies and degree of cementation in same reservoir intervals mainly control porosity and permeability. Generally, the best reservoir interval mainly consists of siliciclastic Efacies 1, which is associated with the lowest cementation in microscopic scale in this study area (Figure 73, 74, 75 and 76).

Table 16. Summary of Queen reservoir characteristics.

Cycle sets	Cycles	Facies associations	Base-level	Porosity (%)	Permeability (md)	Proposed reservoir zone
CS1	C2	C22	Fall	2.2	0.37	R22
		C21	Rise	1.7	0.34	R21
	C1	C12 or C13	Fall	4.6	0.52	R12
		C11	Rise	8.3	0.87	R11

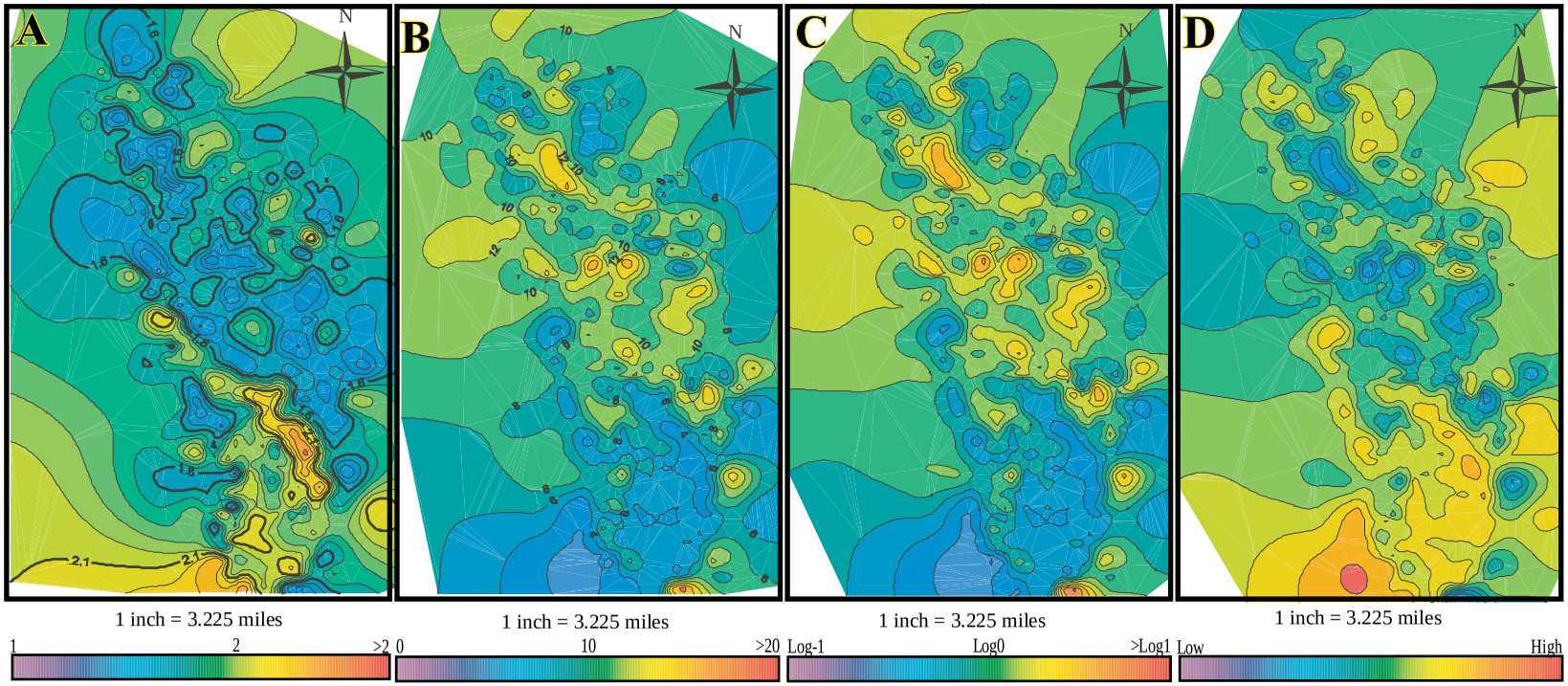

Figure 73. Queen reservoir zone R11. (A) Lithofacies, (B) Porosity, (C) Permeability, and (D) Cementation.

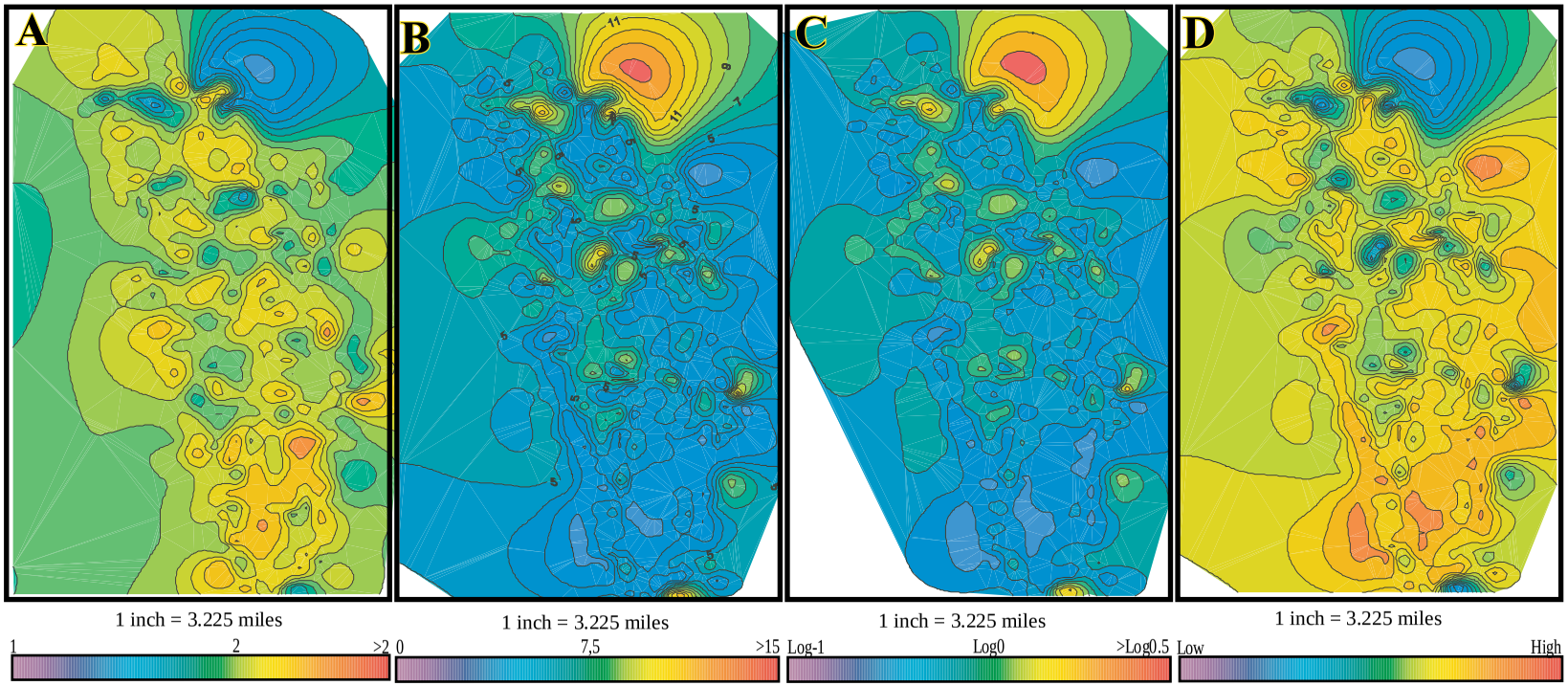

Figure 74. Queen reservoir zone R12. (A) Lithofacies, (B) Porosity, (C) Permeability, and (D) Cementation.

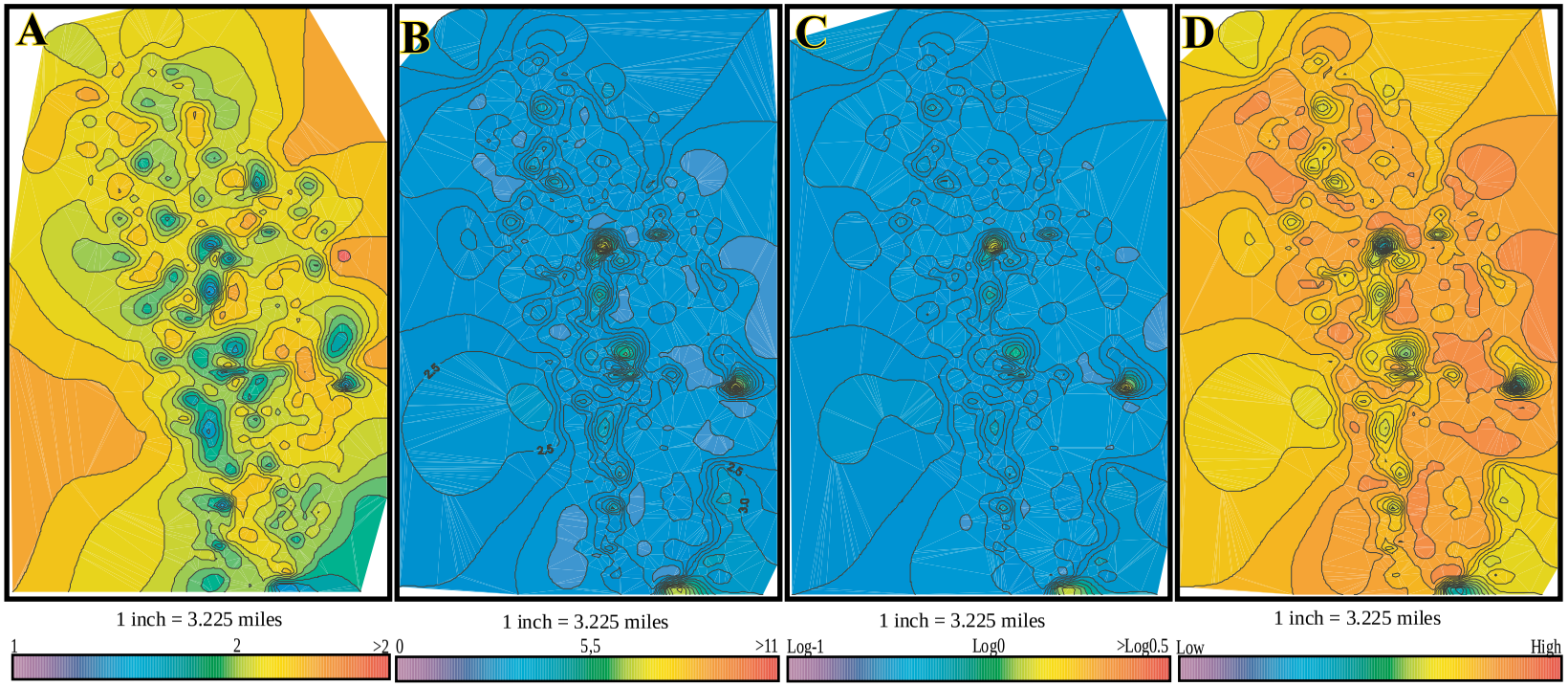

Figure 75. Queen reservoir zone R21. (A) Lithofacies, (B) Porosity, (C) Permeability, and (D) Cementation.

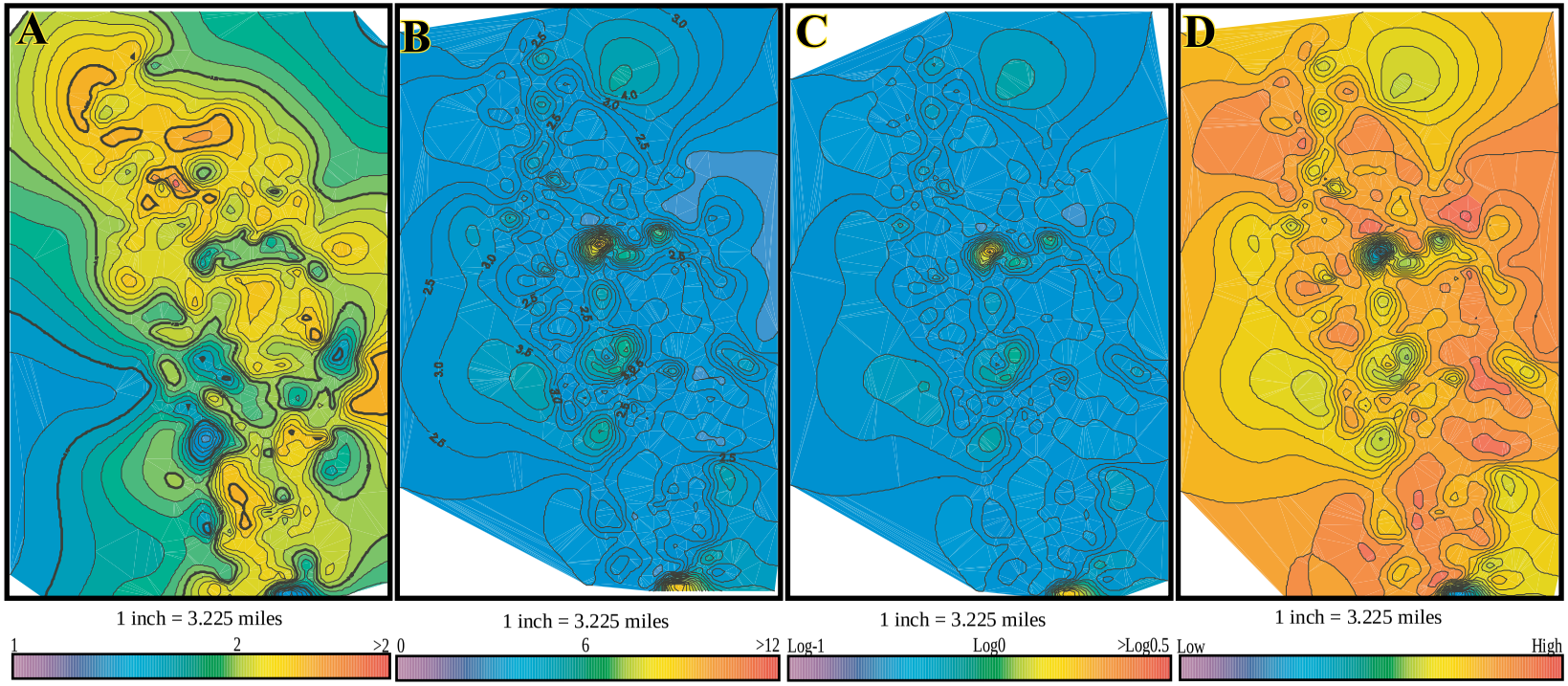

Figure 76. Queen reservoir zone R22. (A) Lithofacies, (B) Porosity, (C) Permeability, and (D) Cementation.

CONCLUSION

This study defined relationships between stratigraphic, compositional and textural variations and Queen reservoir rock properties to develop an integrated reservoir description of the Queen Formation. Studies of facies, sequence stratigraphic, petrophysical and statistical analysis defined important controls on Queen sandstone reservoir quality. Most reservoir horizons are fluvial delta and estuarine or beach ridge complex facies in the basal Queen Formation. Reservoir geometry, textual and compositional variations, and reservoir rock properties exhibit systematic changes as a function of stratigraphic position and interpreted base level changes.

Ten lithofacies from Queen cored intervals are grouped into 4 vertical facies associations on the basis of genetic facies relationship: (1) upward-fining (or upward-deepening) fluvial delta and estuarine facies in incised valley fills; (2) arid climate upward-brining (or upward-shallowing) supra- to subtidal evaporite and carbonate tidal flat; (3) upward-deepening beach ridge and evaporite sand flat facies, and (4) upward-shallowing evaporite salina and evaporite coastal sabhka mud flat facies. The 4 Queen facies associations represent mixed siliciclastic-carbonate-evaporite deposits on isolated inner parts of carbonate platforms. Deposits aggraded behind highstand, carbonate buildups at the platform margin and record low amplitude sea level fluctuations during greenhouse earth conditions.

Based on stacking pattern analysis of the Queen Formation, 16 cycles, 8 cycle sets, 2 high-frequency sequences, and a long-term accommodation increases were identified. Cycle sets 1, 2, 3, and 4 of sequence 1 are fluvial and deltaic siliciclastic deposits and carbonate tidal flat carbonate dominated upward-shallowing deposits. Cycle sets 5, 6, 7, and 8 of sequence 2 are halite and siliciclastic platform interior salina upward-shallowing deposits. From sequence 1 to 2, salinity increased from normal marine to supersaline and overall rates of accommodation increase relative to sediment supply decreased. The Queen Formation has a fluvial-dominated siliciclastic “labyrinth” reservoir geometry at the base, and a carbonate-evaporite dominated “layer-cake” type bed geometry in upper intervals.

A statistical correlation analyses was used to quantify geologic controls on reservoir quality within a sequence stratigraphic framework. Macroscopic scale controls on porosity and permeability development in Queen Formation was related to facies association, large-scale cycles and patterns of diagenetic modification. Four genetic Queen sandstone reservoir zones of

R11, R12, R21, and R22 defined by boundaries between facies association were identified. The R11 reservoir zone at the base of the Queen Formation is the best reservoir interval.

REFERENCES CITED

Ali, M., A. Chawathe, A. Ouenes, M. Cather, and W. Weiss, 1999, Extracting maximum petrophysical and geological information from a limited reservoir database, *in* R. Schatizinger, and J. Jordan, eds., Reservoir characterization: recent advances: Tulsa, Oklahoma, American Association of Petroleum Geologists, p. 191-208.

Aller, G. S., 1999, Lithologic characteristics, depositional environments and geometry of reservoir and nonreservoir facies in the Queen Formation (Guadalupian, Permian) of Moose and Virey Fields, Midland County, Texas: Master of Science thesis, Texas A&M University, College Station, Texas, 100 p.

Andreason, M. K., 1992, Coastal siliciclastic sabkhas and related evaporative environment of the Permian Yates formation, north Ward-Estes, Ward County, Texas: AAPG Bulletin, v. 76, p. 1735-1759.

Ball, S. M., J. W. Roberts, J. A. Norton, and W. D. Pollard, 1971, Queen Formation (Guadalupian, Permian) Outcrops of Eddy County, New Mexico, and their bearing on recently proposed depositional models: AAPG Bulletin, v. 55, p. 1348-1355.

Barret, D. G., 1992, Use of computers to perform old log analysis: Proceedings of the 7th Society of Petroleum Engineers Computer Conference, SPE Paper 24451, p. 267-274.

Bartel, J. R., and R. W. Broomhall, 1986, Stratigraphic potential for hydrocarbon entrapment on the east flank of the Means San Andres Field, Andrews County, Texas, *in* D. G. Bebout, and P. M. Harris, eds., Hydrocarbon reservoir studies San Andres/Grayburg Formations, Permian Basin, Midland, TX: Permian Basin Section of Society of Economic Paleontologists and Mineralogists, p. 83-87.

Beard, D. C., and P. K. Weyl, 1973, Influence of texture on porosity and permeability of unconsolidated sand: AAPG Bulletin, v. 57, p. 349-369.

Bebout, D. G., F. J. Lucia, C. R. Hocott, G. E. Fogg, and G. W. V. Stoep, 1987, Characterization of the Grayburg reservoir, University Lands Dune Field, Crane County, Texas: Austin, Texas, Bureau of Economic Geology, p. 1-97.

Bloch, S., 1991, Empirical prediction of porosity and permeability in sandstones: AAPG Bulletin, v. 75, p. 1145-1160.

Bloch, S., and J. H. McGowen, 1994, Influence of depositional environment on reservoir quality prediction, *in* M. D. Wilson, ed., Reservoir quality assessment and prediction in clastic rocks: Tulsa, Oklahoma, Society of Economic Paleontologists and Mineralogists, p. 41-57.

Boggs, S. J., 1992, Petrology of sedimentary rocks: New York, Macmillan, 707 p.

Borer, J. M., and P. M. Harris, 1989, Depositional facies and cycles in Yates formation outcrops, Guadalupe mountains, New Mexico, *in* P. M. Harris, and G. A. Grover, eds., Subsurface and outcrop examination of the Capitan Shelf margin, northern Delaware Basin: San Antonio, Texas, Society of Economic Paleontologists and Mineralogists, p. 305-318.

Borer, J. M., and P. M. Harris, 1991, Lithofacies and cyclicity of the Yates Formation, Permian Basin: Implications for reservoir heterogeneity: AAPG Bulletin, v. 75, p. 726-779.

Brashear, W. W., and D. D. Childers, 1984, A study of the Queen reservoir Means Field, Andrews County, Texas: Houston, Texas, Exxon company, Mid-continent division, USA, p. 1-23.

Bucheb, J. A., and H. B. Evans, 1994, Some applications of methods used in electrofacies identifications: The Log Analyst, v. 35, p. 14-26.

Chawathe, A., A. Ouenes, M. Ali, and W. Weiss, 1997, One core, few modern logs, and limited production data: is reliable reservoir characterization possible?: Proceedings of the Society of Petroleum Engineers SPE Western Regional Meeting, SPE paper 38260, p. 109-122.

Craig, D. H., 1990, Yates and other Guadalupian (Kazanian) oil Fields, U.S. Permian Basin, *in* J. Brooks, ed., Classic petroleum provinces: London, UK, The Geological Society of London, p. 249-263.

Crandall, K.H., 1929, Permian stratigraphy of southeastern New Mexico and adjacent parts of west Texas: AAPG Bulletin, v. 13, p. 927-944.

Dalrymple, R. W., and B. A. Zaitlin, 1992, Estuarine facies models: conceptual basis and stratigraphic implications: Journal of Sedimentary Petrology, v. 62, p. 1130-1146.

Dorfman, M. H., J. J. Newey, and G. R. Coates, 1990, New techniques in lithofacies determination and permeability prediction in carbonates using well logs, *in* A. Hurst, M. A. Lovell, and A. C. Morton, eds., Geological Society Special Publication Classics: London, UK, The Geological Society of London, p. 113-120.

Doveton, J. H., 1994a, Multivariate pattern recognition and classification methods, *in* J. H. Doveton, ed., Geologic log analysis using computer methods: Tulsa, Oklahoma, American Association of Petroleum Geologists, p. 65-96.

Doveton, J. H., 1994b, Theory and applications of time series analysis to wireline Logs, *in* J. H. Doveton, ed., Geologic log analysis using computer methods: Tulsa, Oklahoma, American Association of Petroleum Geologists, p. 97-126.

Doveton, J. H., and S. E. Prensky, 1992, Geological applications of wireline logs: a synopsis of developments and trends: The Log Analyst, v. 33, p. 286-303.

Dubrule, O., 1998, Geostatistics in petroleum geology: American Association of Petroleum Geologists continuing education course note: Tulsa, Oklahoma, American Association of Petroleum Geologists, 43 p.

Ebanks, W. J. J., 1987b, Flow unit concept-Integrated approach to reservoir description for engineering projects: AAPG Bulletin, v. 71, p. 551-552.

Eide, M., and J. Mazzullo, 1993, Facies, depositional environments and stratigraphy of the Queen formation in North Ward-Estes Field, Ward County, Texas, *in* J. Gibbs, and D. Cromwell, eds., New dimensions in the Permian Basin: West Texas Geological Society, Midland, Texas, West Texas Geological Society, p. 28-42.

ESRI, 1992, Understanding GIS: ARC/INFO method: Redlands, CA, Environmental System Research Institute, 600 p.

Ethier, V. G., and H. R. King, 1991, Reservoir quality evaluation from visual attributes on rock surfaces; methods of estimation and classification from drill cuttings or cores: Bulletin of Canadian Petroleum Geology, v. 39, p. 233-251.

Evans, J., C. A. Cade, and S. Bryant, 1997, A geological approach to permeability prediction in clastic reservoirs, *in* J. A. Kupecz, J. Gluyas, and S. Bloch, eds., Reservoir quality prediction in sandstones and carbonates: Tulsa, Oklahoma, American Association of Petroleum Geologists, p. 91-102.

Fekete, T. E., E. K. Franseen, and L. C. Pray, 1986, Deposition and erosion of the Grayburg Formation (Guadalupian, Permian) at the shelf-to basin margin, western escarpment, Guadalupe mountains, Texas, *in* G. E. Moore, and L. Wilde, eds., Lower and middle Guadalupian facies, stratigraphy, and reservoir geometries San Andres/Grayburg Formations: Tulsa, Oklahoma, Permian section, Society of Economic Paleontologists and Mineralogists, p. 69-81.

Franseen, E. K., T. E. Fekete, and L. C. Pray, 1989, Evolution and destruction of a carbonate bank at the shelf margin: Grayburg Formation (Permian), western escarpment, Guadalupe mountains, Texas, *in* P. D. Crevello, J. L. Wilson, J. F. Sarg, and J. F. Read, eds., Controls on carbonate platform and basin development: Tulsa, Oklahoma, Society of Economic Paleontologists and Mineralogists, p. 289-304.

Fryberger, S. T., A. M. Al-Sari, and T. J. Clisham, 1983, Eolian dune, interdune, sand sheet, and siliciclastic Sabhka sediments of an offshore prograding sand sea, Dhahran area, Saudi Arabia: AAPG Bulletin, v. 67, p. 280-312.

Galley, J. E., 1958, Oil and geology in the Permian Basin of Texas and New Mexico, *in* L. G. Weeks, ed., Habitat of oil: Tulsa, Oklahoma, American Association of Petroleum Geologists, p. 395-446.

Galloway, W. E., 1989, Clastic facies models, depositional systems, sequences and correlation: a sedimentologist's view of the dimensional and temporal resolution of lithostratigraphy,

in T. A. Cross, ed., Quantitative dynamic stratigraphy: New York, Prentice Hall, p. 459-477.

Galloway, W. E., T. E. Ewing, C. M. Garrett, N. Tyler, and D. G. Bebout, 1983, Atlas of major Texas oil reservoirs, Bureau of Economic Geology Special Publication, Austin, Texas, Bureau of Economic Geology, 139 p.

Garber, R. A., G. A. Grover, and H. P.M., 1989, Geology of the Capitan Shelf margin - Subsurface data from the northern Delaware Basin, *in* P. M. Harris, and G. A. Grover, eds., Subsurface and outcrop examination of the Capitan Shelf margin, northern Delaware Basin: San Antonio, Texas, Society of Economic Paleontologists and Mineralogists, p. 3-272.

Gardner, M. H., 1999, Proposal for phase III extension of multidisciplinary research on the middle Permian Brushy Canyon Formation, Delaware Basin, west Texas: Golden, Colorado, Colorado School of Mines, 11 p.

George, C. J., and L. H. Stiles, 1978, Improving techniques for evaluating carbonate waterfloods in west Texas: Journal of Petroleum Technology, p. 1547-1554.

George, C. J., and L. H. Stiles, 1986, Planning a CO_2 tertiary recovery project Means San Andres Unit: Research Conference, p. 79-82.

Goodall, I. G., G. M. Harwood, A. C. Kendall, and T. Mckie, 1992, Discussion on sequence stratigraphy of carbonate-evaporite basins: models and application to the upper Permian (Zechstein) of northeast England and adjoining North sea: Journal of the Geological Society of London, v.149, p. 1050-1054.

Griffiths, C. M., 1990, The language of rocks: an example of the use of syntactic analysis in the interpretation of sedimentary environments from wireline logs, *in* A. Hurst, M. A. Lovell, and A. C. Morton, eds., Geological applications of wireline logs: London, UK, The Geological Society of London, p. 77-95.

Hardie, L. A., and E. A. Shinn, 1986, Carbonate depositional environments: modern and ancient, part 3. Tidal flat: Colorado School of Mines Quaternary, v. 81, p. 1-74.

Harris, P. M., and S. D. Walker, 1990, McElroy Field-U.S.A., Central Basin Platform, Permian Basin, Texas, Stratigraphic Trap I: Tulsa, Oklahoma, American Association of Petroleum Geologists, p. 195-227.

Hills, J. M., 1984, Sedimentation, tectonism, and hydrocarbon generation in Delaware Basin, west Texas and southeastern New Mexico: AAPG Bulletin, v. 68, p. 250-267.

Hoholick, J. D., 1984a, Petrology and depositional environment of the basal sandstones of the Queen Formation (Permian), Means Field, Andrews County, Texas: Houston, Exxon Company U.S.A., p. 1-23.

Holley, C., 1988, The lithology, environment of deposition, and diagenesis of the Queen Formation, Mcfarland, Mcfarland North, and Magutex Fields, Andrews County, Texas: Texas A&M University, College Station, Texas, 100 p.

Holley, C., and J. Mazzullo, 1988, The lithology, depositional environments, and reservoir properties of sandstones in the Queen formation, Magutex North, Mcfarland North, and Mcfarland Fields, Andrews County, Texas, *in* B. K. Cunningham, ed., Permian and Pennsylvanian stratigraphy, Midland Basin, west Texas: studies to aid hydrocarbon exploration: Tulsa, Oklahoma, Society of Economic Paleontologists and Mineralogists Permian Basin Section, p. 55-64.

Houseknecht, D. W., 1984, Influence of grain size and temperature on intergranular pressure in a quartzose sandstone: Journal of Sedimentary Petrology, v. 54, p. 348-361.

Hovorka, S. D., 1989, Depth evolution of the Delaware basin - Castile/Salado transition, *in* P. M. Harris, and G. A. Grover, eds., Subsurface and outcrop examination of the Capitan Shelf margin, northern Delaware Basin: San Antonio, Texas, Society of Economic Paleontologists and Mineralogists, p. 441-450.

Hovorka, S. D., 2000, Deep-water to shallow-water transition in evaporites in the Delaware Basin, Texas, *in* R. F. Lindsay, R. C. Trentham, R. F. Ward, and A. H. Smith, eds., Classic Permian geology of west Texas and southern New Mexico: geo 2000: Midland, Texas, West Texas Geological Society, p. 273-299.

Hurst, A., and J. S. Archer, 1986, Sandstone reservoir description: an overview of the role of geology and mineralogy: Clay Minerals, v. 21, p. 791-809.

Jacka, A.V., and L.A. Fraco, 1974, Deposition and diagenesis of Permian evaporites and associated carbonates and clastics on shelf areas of the Permian, *in* A.H. Coogan, ed., Fourth symposium on salt, v. I: Cleveland, Northern Ohio Geological Society, p. 67-89.

Jervey, M. T., 1988, Quantitative geological modeling of siliciclastic rock sequences and their seismic expression, *in* C. K. Wilgus, H. Posamentier, J. V. Wagoner, B. S. Hastings, C. A. Ross, and C. G. S. C. Kendall, eds., Sea-level changes: an integrated approach: Tulsa, Oklahoma, Society of Economic Paleontologists and Mineralogists, p. 47-70.

Jian, F. X., C. Y. Chork, I. J. Taggart, D. M. McKay, and R. M. Bartlett, 1994, A genetic approach to the prediction of petrophysical properties: Journal of Petroleum Geology, v. 17, p. 71-88.

Kendall, A. C., 1992, Evaporites, *in* R. G. Walker, and N. P. James, eds., Facies model: response to sea level change: St. John's, Canada, Geological Association of Canada, p. 375-409.

Kendall, A. C., and G. M. Harwood, 1996, Marine evaporites: arid shorelines and basins, *in* H. G. Reading, ed., Sedimentary environments: process, facies and stratigraphy: Oxford, UK, Blackwell Science Ltd., p. 281-324.

Kerans, C., 1994, Integrated characterization of carbonate ramp reservations using Permian San Andreas Formation outcrop analogs: AAPG Bulletin, v. 78, p. 181-216.

Kerans, C., and S. Nance, 1991, High-frequency cyclicity and regional depositional patterns of the Grayburg Formation, Guadalupe mountains, New Mexico, *in* S. Meader-Roberts, M. P. Candelaria, and G. E. Moore, eds., Sequence stratigraphy, facies and reservoir geometries of San Andres, Grayburg and Queen Formations, Guadalupe Mountains, New Mexico and Texas: Tulsa, Oklahoma, Permian section, Society of Economic Paleontologists and Mineralogists, p. 53-69.

Kerans, C., and S. W. Tinker, 1997, Sequence stratigraphy and characterization of carbonate reservoirs: Society of Economic Paleontologists and Mineralogists short course notes, 130 p.

Kerans, C., W. M. Fitchen, M. H. Gardner, and B. R. Wardlaw, 1993, A contribution to the evolving stratigraphic framework of middle Permian strata of the Delaware Basin, Texas and New Mexico: New Mexico Geological Society Guidebook, v. 44th field conference, Carlsbad Region, New Mexico and west Texas, New Mexico Geological Society, 175-184 p.

King, D. E., 1990, Incorporating geological data in well log interpretation, *in* A. Hurst, M. A. Lovell, and A. C. Morton, eds., Geological Society Special Publication Classics: London, UK, The Geological Society, p. 45-55.

Knox, P. R., and M. D. Barton, 1999, Predicting interwell heterogeneity in fluvial - deltaic reservoirs: Effects of progressive architecture variation through a depositional cycle from outcrop and subsurface observations, *in* R. Schatizinger, and J. Jordan, eds., Reservoir characterization: recent advances: Tulsa, Oklahoma, American Association of Petroleum Geologists, p. 57-72.

Lake, L. W., 1995, Reservoir characterization from the laboratory to the field: Seoul, Korea, Korea Petroleum Development Corporation, 88 p.

Lee, S. H., and Datta-Gupta, 1999, Electrofacies characterization and permeability predictions in carbonates reservoirs: Role of multivariate analysis and nonparametic regression: Proceedings of the Society of Petroleum Engineers Annual Technical Conference, SPE Paper 56658, p. 409-421.

Longman, M. W., T. G.F., and J. S. Glennie, 1983, Origin and geometry of Red river dolomite reservoirs, western Williston Basin: AAPG Bulletin, v. 67, p. 744-771.

Lucia, F. J., 1983, Petrophysical parameters estimated from visual descriptions of carbonates rocks: a field classification of carbonate pore system: Journal of Petroleum Technology, v. March, 1983, p. 629-657.

Maiklem, W. R., D. G. Bebout, and R. P. Glaister, 1969, Classification of anhydrite-a practical approach: Bulletin of Canadian Petroleum Geology, v. 17, p. 194-233.

Major, R. P., and Q. Ye, 1992, Lateral and vertical reservoir heterogeneity in siliciclastic peritidal facies, Keystone (Colby) reservoir, west Texas, *in* D. H. Mruk, and B. C. Curran, eds., Permian Basin exploration and production strategies: applications of sequence stratigraphic and reservoir characterization concepts: Midland, Texas, West Texas Geological Society, p. 91-99.

Malicse, A., and J. Mazzullo, 1990, Reservoir properties of the desert Shattuck Member, Caprock Field, New Mexico, *in* J. Barwis, J. McPherson, and J. Studlick, eds., Sandstone petroleum reservoirs: New York, Springer-Verlag, p. 133-152.

Malicse, A., and J. Mazzullo, 1996, Early diagenesis and paleosol features of ancient desert sediments: examples from the Permian Basin, *in* L. J. Crossey, R. Loucks, and M. W. Totten, eds., Diagenesis and fluid flow: concepts and applications: Society of Economic Paleontologists and Mineralogists Special Publication, Tulsa, Oklahoma, Society of Sedimentary Geology, p. 151-162.

Mazzullo, J., M. Willams, and S. J. Mazzullo, 1984, The Queen Formation of Millard Field, Pecos County, Texas: its lithologic characteristics, environment of deposition, and reservoir petrophysics: Transactions of the southwest section of the American Association of Petroleum Geologists, p. 103-110.

Mazzullo, J., A. Malicse, and J. Siegel, 1991, Facies and depositional environments of the Shattuck sandstone on the Northwest shelf of the Permian Basin: Journal of Sedimentary Petrology, v. 61, p. 940-958.

Mazzullo, J., A. Malicse, D. Newsom, J. Harper, C. McKone, and B. Price, 1992, Facies, depositional environments, and reservoir properties of the upper Queen Formation, Concho Bluff and Concho Bluff North Fields, Texas, *in* D. H. Mruk and B. C. Curran, eds., Permian Basin exploration and production strategies: applications of sequence stratigraphic and reservoir characterization concepts: Midland, Texas, West Texas Geological Society Publication, p. 67-68.

Mazzullo, J., S. Dronamraju, R. Johnson, and W. Ahr, 1996, Facies and sequence stratigraphy of the late Permian Yates Formation on the western margin of the Central Basin Platform of the Permian Basin, north Ward-Estes and South Ward Fields, Ward County, Texas, *in* R. L. Martin, ed., Permian Basin oil and gas fields: Midland, Texas, West Texas Geological Society, p. 117-120.

Mazzullo, S. J., W.D. Bischoff, and C. L. Hedrick, 1989, Stacked island facies in Tansill outer-shelf platform, Dark Canyon, Guadalupe mountains, New Mexico, *in* P. M. Harris, and G. A. Grover, eds., Subsurface and outcrop examination of the Capitan Shelf margin, northern Delaware Basin: San Antonio, Texas, Society of Economic Paleontologists and Mineralogists, p. 287-294.

McKee, E. D., 1965, Experiments on ripple lamination, *in* G. V. Middleton, ed., Primary sedimentary structures and their hydrodynamic interpretation: Tulsa, Oklahoma, Society of Economic Paleontologists and Mineralogists, p. 66-83.

Meissner, F. F., 1974, Cyclic sedimentation in middle Permian strata of the Permian Basin, west Texas and New Mexico, *in* J. C. Elam, and S. Chuber, eds., Cyclic sedimentation in the Permian Basin: Midland , Texas, West Texas Geological Society, p. 203-232.

Miall, A. D., 1989, Can there be life after Facies models? The development of a framework for the quantitative description of complex, three-dimensional facies architectures, *in* T. A. Cross, ed., Quantitative dynamics stratigraphy: New York, Prentice Hall, p. 601-615.

Mitchum, R. M., and J. J. C. V. Wagoner, 1991, High-frequency sequences and their stacking patterns: sequence-stratigraphic evidence of high-frequency eustatic cycles: Sedimentary Geology, v. 70, p. 131-160.

Moran, W.R., 1954, Proposed type sections for the Queen and Grayburg Formations Guadalupian age in the Guadalupe mountains, Eddy County, New Mexico (abs.): Geological Society America Bulletin, v. 65, p. 1288.

Moss, B. P., 1990, Stochastic reservoir description: a methodology, *in* A. Hurst, M. A. Lovell, and A. C. Morton, eds., Geological Society Special Publication Classics: London, UK, The Geological Society of London, p. 57-76.

Nance, H. S., 1988, Interfingering of evaporites and red beds: an example from the Queen/Grayburg Formation, Texas: Sedimentary Geology, v. 56, p. 357-381.

Pawlowicz, R. M., and G. W. Bolger, 1983, Scanning electron microscope analysis of sandstone samples from the Queen (Permian) Formation Andrews County, Texas: Houston, Texas, Reservoir Inc., p. 1-17.

Pereira, H. G., A. C. Silva, A. Soares, L. Ribeiro, and J. Carvalho, 1990, Improving reservoir description by using geostatistical and multivariate data analysis techniques: Mathematical Geology, v. 22, p. 879-913.

Pettijohn, F. J., P. E. Potter, and R. Siever, 1973, Sand and sandstone: New York, Springer, 618 p.

Posamentier, H. W., and P. R. Vail, 1988, Eustatic controls on clastic deposition II-Sequence and systems tract models, *in* C. K. Wilgus, H. Posamentier, J. V. Wagoner, B. S. Hastings, C. A. Ross, and C. G. S. C. Kendall, eds., Sea-level changes: an integrated approach: Tulsa, Oklahoma, Society of Economic Paleontologists and Mineralogists, p. 125-154.

Posamentier, H. W., and D. P. James, 1993, An overview of sequence-stratigraphic concepts: uses and abuses, *in* H. W. Posamentier et al., ed., Sequence stratigraphy and facies association: Malden, MA, Blackwell Scientific, p. 3-18.

Posamentier, H. W., M. T. Jervey, and P. R. Vail, 1988, Eustatic controls on clastic deposition I-conceptual framework, *in* C. K. Wilgus, H. Posamentier, J. V. Wagoner, B. S. Hastings, C. A. Ross, and C. G. S. C. Kendall, eds., Sea-level changes: an integrated approach: Tulsa, Oklahoma, Society of Economic Paleontologists and Mineralogists, p. 71-124.

Primmer, T. J., C. A. Cade, J. Evans, J. G. Gluyas, M. S. Hopkins, N. H. Oxtoby, P. C. Smalley, E. A. Warren, and R. H. Worden, 1997, Global patterns in sandstone diagenesis: their application to reservoir quality prediction for petroleum exploration, *in* J. A. Kupecz, J. Gluyas, and S. Bloch, eds., Reservoir quality prediction in sandstones and carbonates: Tulsa, Oklahoma, American Association of Petroleum Geologists, p. 61-79.

Quirk, D. G., 1998, 'Base profile': a unifying concept in alluvial sequence stratigraphy, *in* J. A. Howell, and J. F. Aitken, eds., High resolution sequence stratigraphy: innovations and applications, London, The Geological Society of London, p. 37-51.

Read, J. F., L. J. Weber, J. F. Sarg, and F. M. Wright, 1991, Milankovitch sea-level changes, cycles and reservoirs on carbonates in greenhouse and ice-house worlds: Tulsa, Oklahoma, Society of Economic Paleontologists and Mineralogists, 102 p.

Rittenhouse, G., 1971, Mechanical compaction of sands containing different percentages of ductiles grains: AAPG Bulletin, v. 55, p. 92-96.

Ross, C. A., and J. R. P. Ross, 1987, Late Paleozoic sea levels and depositional sequences, *in* C. A. Ross, and D. Haman, eds., Timing and depositional history of eustatic sequences: constraints on seismic stratigraphy: New York, Cushman Foundation for Foraminiferal Research, p. 137-149.

Sarg, J. F., 1981, Petrology of the carbonate-evaporite facies transition of the Seven Rivers Formation (Guadalupian, Permian), southeast New Mexico: Journal of Sedimentary Petrology, v. 51, p. 73-96.

Sarg, J. F., 1989, Stratigraphy and sedimentology of the back-reef upper Queen-Lower Seven Rivers strata, Goat seep-Capitan reef complexes (middle-late Guadalupian, Permian), southeast New Mexico, *in* P. M. Harris, and G. A. Grover, eds., Subsurface and outcrop examination of the Capitan Shelf margin, northern Delaware Basin: San Antonio, Texas, Society of Economic Paleontologists and Mineralogists, p. 347-352.

Sarg, J. F., and P. J. Lehmann, 1986, Lower-middle Guadalupian facies and stratigraphy San Andres/Grayburg Formations, Permian Basin, Guadalupe mountains, New Mexico, *in* G. E. Moore, and G. L. Wilde, eds., Lower-middle Guadalupian facies, stratigraphy, and reservoir geometries San Andres/Grayburg Formations, Guadalupe mountains, New Mexico and Texas: Tulsa, Oklahoma, Permian Section, Society of Economic Paleontologists and Mineralogists., p. 1-35.

SAS-Institute, 1995, SAS/GIS software: Usage and reference, version 6: Cary, NC, SAS institute, 273 p.

Scherer, M., 1987, Parameters influencing porosity in sandstones: a model for sandstone porosity prediction: AAPG Bulletin, v. 71, p. 485-491.

Schmidt, V., and D. A. Mcdonald, 1979a, The role of secondary porosity in the course of sandstone diagenesis, *in* P. A. Scholle, and P. R. Schluger, eds., Aspects of diagenesis: Tulsa, Oklahoma, Society of Economic Paleontologists and Mineralogists, p. 175-207.

Schmidt, V., and D. A. Mcdonald, 1979b, Texture and recognition of secondary porosity in sandstones, *in* P. A. Scholle, and P. R. Schluger, eds., Aspects of diagenesis: Tulsa, Oklahoma, Society of Economic Paleontologists and Mineralogists, p. 209-225.

Schumm, S. A., and F. G. Ethridge, 1994, Origin, evolution, and morphology of fluvial valleys, *in* R. W. Dalrymple, R. Boyd, and B. A. Zaitlin, eds., Incised-valley systems: origin and sedimentary sequences: Tulsa, Oklahoma, Society of Economic Paleontologists and Mineralogists, p. 3-27.

Serra, O., 1984a, Fundamentals of well-log interpretation v.1: the acquisition of logging data: Developments in Petroleum Science 15a: Amsterdam, Elsevier, 423 p.

Serra, O., 1984b, Fundamentals of well-log interpretation v.2: the interpretation of logging data: Developments in Petroleum Science 15b: Amsterdam, Elsevier, 684 p.

Serra, O., 1986, Advanced interpretation of wireline logs: Montrouge Cedex, France, Schlumberger, 295 p.

Shearman, D. J., 1983, Syndepositional and late diagenetic alteration of primary gypsum to anhydrite: Proceeding of the 6th international symposium on salt, Alexandria, Virginia, p. 41-50.

Shearman, D. J., and J. G. Fuller, 1969, Anhydrite diagenesis, calcitization and organic laminates, Winnipegosis Formation, middle Devonian, Saskatchewan: Canadian Petroleum Geological Bulletin, v. 17, p. 496-525.

Smith, R. M. H., 1990, Alluvial paleosol and pedofacies sequences in the Permian lower Beaufort of the southwestern Karoo Basin, South Africa: Journal of Sedimentary Petrology, p. 258-276.

Sneider, R. M., 1990, Introduction: reservoir description of sandstones, *in* J. H. Barwis, J. G. McPherson, and J. R. J. Studlick, eds., Sandstone petroleum reservoirs: New York, Spinger-Verlag, p. 1-3.

Strohmenger, C., E. Voigt, and J. Zimdars, 1996, Sequence stratigraphy and cyclic development of basal Zechstein carbonate-evaporite deposits with emphasis on Zechstein 2 off-platform carbonates (upper Permian, northeast Germany): Sedimentary Geology, v.102, p. 33-54.

Tait, D. B., J. L. Ahlen, A. Gordon, G. L. Scott, W. S. Motts, and M. E. Spitler, 1962, Artesia Group of New Mexico and west Texas: AAPG Bulletin, v. 46, p. 504-517.

Tinker, S. W., 1996, Building the 3-D jigsaw puzzle: applications of sequence stratigraphy to 3-d reservoir characterization, Permian Basin: AAPG Bulletin, v. 80, p. 460-485.

Tucker, K. E., and R. G. Chalcraft, 1991, Cyclicity in the Permian Queen Formation-U.S.M. Queen Field, Pecos County, Texas, *in* A. J. Lomando, and P. M. Harris, eds., Mixed carbonate-siliciclastic sequences: Tulsa, Oklahoma, Society of Economic Paleontologists and Mineralogists, p. 385-428.

Tucker, M. E., 1991, Sequence stratigraphy of carbonate-evaporite basins: models and application to the upper Permian (Zechstein) of northeast England and adjoining North Sea: Journal of the Geological Society of London, v. 148, p.1019-1036.

Vail, P. R., R. M. Mitchum, and S. T. III, 1977, Seismic stratigraphy and global changes of sea level, part 3: relative changes of sea level from coastal onlap, *in* C. W. Payton, ed., Seismic stratigraphy applications to hydrocarbon exploration: Tulsa, Oklahoma, American Association of Petroleum Geologists, p. 63-97.

Van Wagoner, J. C., H. W. Posamentier, R. M. Mitchum, P. R. Vail, J. F. Sarg, T. S. Loutit, and J. Hardenhol, 1988, An overview of sequence stratigraphy and key definitions, *in* C. W. W. e. al., ed., Sea level changes: an integrated approach: Tulsa, Oklahoma, Society of Economic Paleontologists, p. 39-45.

Van Wagoner, J. C., R. M. Mitchum, K. M. Campion, and V. D. Rahmanian, 1990, Siliciclastic sequence stratigraphy in well logs, cores, and outcrops: concepts for high-resolution correlation of time and facies: American Association of Petroleum Geologists methods in exploration series, Tulsa, Oklahoma, American Association of Petroleum Geologists, 51 p.

Walker, D. A., J. Golonka, A. Reid, and S. Reid, 1995a, The effects of paleolatitude and paleogeography on late Paleozoic carbonate sedimentation in west Texas; Part II: Permian: West Texas Geological Society Bulletin, v. 34, p. 5-15.

Ward, R. F., C. G. Kendall, and P. M. Harris, 1986, Upper Permian (Guadalupian) facies and their association with hydrocarbon-Permian Basin, west Texas and New Mexico: AAPG Bulletin, v. 70, p. 239-262.

Warren, J. K., 1982a, The hydrological significance of Holocene tepees, stromatolites, and boxwork limestones in coastal salinas in South Australia: Journal of Sedimentary Petrology, v. 52, p. 1171-1201.

Warren, J. K., 1982b, Hydrologic setting, occurrence, and significance of gypsum in late Quaternary salt lakes, South Australia: Sedimentology, v. 29, p. 609-637.

Warren, J. K., 1999, Evaporites: their evolution and economics: Malden, MA, Blackwell Science, 438 p.

Warren, J. K., and C. G. S. C. Kendall, 1985, Comparison of sequences formed in marine sabhka (subaerial) and salina (subaqueous) setting-modern and ancient: AAPG Bulletin, v. 69, p. 1013-1023.

Weber, K. J., and L. C. Geuns, 1990, Framework for constructing clastic reservoir simulation models: Journal of Petroleum Technology, v. October, p. 1248-1297.

Yang, K. M., and S. L. Dorobek, 1995, The Permian Basin of west Texas and New Mexico: tectonic history of a "composite" foreland basin and its effects on stratigraphic development: Journal of Sedimentary Research, v. 52, p. 149-174.

Ye, L., D. Kerr, and K. Yang, 1999, Facies architecture of the Blue Jacket sandstone in the Eufaula lake area, Oklahoma: implications for reservoir characterization of the subsurface Bartlesville sandstone, *in* R. Schatizinger, and J. Jordan, eds., Reservoir characterization: recent advances: Tulsa, Oklahoma, American Association of Petroleum Geologists, p. 29-44.

Zaitlin, B. A., and B. C. Shultz, 1984, An estuarine-embayment fill model from the Lower Cretaceous Mannville Group west-central Saskatchewan, *in* D. F. Scott, and D. J. Glass, eds., The Mesozoic of middle north America: Canadian Society of Petroleum Geologists, v. 9, p. 455-469.

Zaitlin, B. A., R. W. Dalrymple, and R. Boyd, 1994, The stratigraphic organization of incised - valley systems associated with relative sea-level change, *in* R. W. Dalrymple, R. Boyd, and B. A. Zaitlin, eds., Incised-valley systems: origin and sedimentary sequences: Tulsa, Oklahoma, Society of Economic Paleontologists and Mineralogists, p. 45-60.

APPENDIX

Core Description
JSM #300 (API #. 420030245500)
Core Depth Interval: 4450.00–4570.00 ft
Means Field, Andrews County, Texas

DEPTH (ft/m)	THICKNESS (ft/m)	DESCRIPTION
4570.30(1393.03)	3.30(1.01)	ANHYDRITE w/ SILTSTONE; light bluish gray (5B 7/1) w/pale red (10R 6/2); mosaic, chicken wire structured anhydrite w/ pale red muddy and silty laminae remnant. The truncated surface is found at 4,567 ft; missing upper contact.
4567.00(1392.02)	0.04(0.01)	LOST INTERVAL.
4566.94(1392.00)	1.14(0.35)	ANHYDRITE w/ SILTSTONE; medium bluish gray (5B 5/1) w/ light brownish gray (5YR 6/1) and dark greenish gray (5G 4/1); mosaic and massive anhydrite w/ minor silty laminae remnant. The chicken wire structure is found at 4,166 ft and 4,565.8 ft; sharp and wavy upper contact;
4565.80(1391.66)	0.26(0.08)	ANHYDRITE w/ DOLOMITE; light bluish gray (5B 7/1) w/ yellowish gray (5Y 7/2); massive anhydrite w/ minor dolomitic laminae remnant; missing upper contact.
4565.54(1391.58)	0.38(0.12)	ANHYDRITE w/ SILTSTONE; light bluish gray (5B 7/1) w/dusky green (5G 3/2); mosaic and chicken wire structure anhydrite w/ minor silt laminae remnant; wavy and sharp upper contact.
4565.16(1391.46)	0.75(0.23)	SILTSTONE w/ ANHYDRITE; olive gray (5Y 3/2) w/ light bluish gray (5B 7/1); faintly irregular wavy laminated siltstone w/ enterolithic and nodular anhydrite; wavy and sharp upper contact
4564.41(1391.43)	0.62(0.19)	ANHYDRITE; light bluish gray (5B 7/1) w/ moderate olive brown (5Y 4/4); mosaic and clear chicken wire structure anhydrite; wavy and sharp upper contact.
4563.79(1391.04)	0.19(0.06)	ANHYDRITE w/ SILTSTONE; light bluish gray (5B 7/1) w/ olive gray (5Y 3/2); coalesced nodular anhydrite w/ faintly deformed silt laminae; gradational upper contact.
4563.60(1390.99)	0.40(0.12)	ANHYDRITE w/ DOLOMITE; light bluish gray (5B 7/1) w/ yellowish gray (5Y 7/2); mosaic w/ chaotic in minor dolomitic laminae remnant in void; wavy and sharp upper contact. **TOP OF GRAYBURG FORMATION.**
4563.20(1390.86)	1.20(0.37)	SILT- to MUDSTONE w/ ANHYDRITE; olive gray (5Y 3/2) w/ light olive gray (5Y 5/2) and light bluish gray (5B 7/1); deformed wavy laminated and faintly discontinuous planar, parallel laminated siltstone w/ pseudomorphic felted anhydrite and enterolithic structure anhydrite (12.5“) grades upward to massive anhydrite (1“); sharp and wavy upper contact.
4562.00(1390.50)	0.43(0.13)	SILT- to MUDSTONE w/ ANHYDRITE; olive gray (5Y 3/2) w/ light olive gray (5Y 5/2) and light bluish gray (5B 5/1); deformed wavy laminae w/ pseudomorphic felted anhydrite and rip-up mud clasts. The scour surface is found at 4,562.05 ft; missing upper contact.
4561.67(1390.40)	1.37(0.42)	SILT- to SANDSTONE; silt to very fine-grained; olive gray (5Y 3/2) w/ light olive gray (5Y 5/2); massive and some deformed faint discontinuous silty and sandy laminae w/ many muddy rip-up clasts. The muddy clasts show chaotic appearance; sharp and wavy upper contact.
4560.30(1389.98)	0.14(0.04)	SANDSTONE w/ Mud clasts; fine-grained; yellowish gray (5Y 7/2) w/olive gray (5Y 3/2); massive sandstone w/ chaotic muddy rip-up clasts; sharp and wavy upper contact.
4560.16(1389.94)	2.58(0.79)	SANDSTONE w/ ANHYDRITE; medium bluish gray (5B 5/1) w/ yellowish gray (5Y 7/2); ripple cross laminated sandstone (16.5“) grades upward to relatively massive and discontinuous faintly wavy laminated sandstone (5“) and stacked ripple cross laminated sandstone (10“); missing upper contact.
4557.58(1389.15)	0.08(0.02)	LOST INTERVAL.
4557.50(1389.13)	1.87(0.57)	SANDSTONE; very fine-grained; light bluish gray (5B 7/1) w/ dusky yellow (5Y 6/4); faintly stack ripple cross laminated sandstone; missing upper contact
4555.63(1388.56)	0.93(0.28)	SANDSTONE w/ ANHYDRITE; very fine-grained; dusky yellow (5Y 6/4) w/ light bluish gray (5B 7/1); faintly discontinuous parallel cross laminated and some deformed laminated sandstone by the growth of anhydrite (1.5“) is overlain by faintly discontinuous wavy laminated sandstone w/ small nodular anhydrite (4“); the above this, faintly discontinuous trough cross-laminated sandstone w/ small nodular anhydrite (4“). The sizes of nodule range from 2/10“ X 2/10“ to 1“X1“ in diameter; missing and gradational upper contact.

4554.70(1388.27)	0.50(0.15)	SANDSTONE; very fine-grained; dusky yellow (5Y 6/4) w/ olive gray (5Y 3/2); faintly discontinuous planar horizontal and cross-laminated sandstone; missing upper contact.
4554.20(1388.12)	4.75(1.64)	SILT- to SANDSTONE w/ ANHYDRITE; dark greenish gray (5GY 4/1) w/ greenish gray (5GY 6/1); ripple cross laminated sandstone (17“) is overlain by planar cross and deformed wavy laminate sandstone w/ some micro-faults, slumping structures and mud clasts between 4,552.3 ft and 4,552.63 ft (4“). It grades upward to very thin parallel cross and horizontal laminated sandstone w/ micro-fault at 4,550.80 ft and wavy laminated sandstone w/ small displacive anhydrite and loading structure (10“); the above this, very thin planar, parallel and horizontal laminated siltstone and sandstone w/ small nodular anhydrite; missing upper contact.
4548.83(1386.48)	0.23(0.07)	DOLOMUDSTONE; dolomudstone; light olive gray (5Y 5/2); ripple cross-laminated dolomite; sharp and wavy upper contact.
4548.60(1386.41)	0.70(0.21)	DOLOMUDSTONE w/ ANHYDRITE; dolomudstone; yellowish gray (5Y 7/2); cryptalgal laminated dolomite w/ minor anhydrite in fenestral pore and solution breccia; sharp and wavy upper contact.
4547.90(1386.20)	0.36(0.11)	DOLOMUDSTONE; dolomudstone; dark greenish gray (5G 4/1), massive dolomite w/ truncation surface at 4,547.9 ft; gradational upper contact.
4547.54(1386.10)	1.09(0.33)	DOLOMITE w/ ANHYDRITE; dolomudstone to dolowackestone; greenish gray (5Y 6/1); cryptalgal wavy laminate dolomite w/ anhydrite in fenestral pores, solution breccia and stylolite. Some dark wavy organic laminae are found through most parts of bed. The displacive anhydrite is filled with peloid mold between 4,546.45 ft and 4,547.25 ft. The sizes of nodules are less than ¼” in diameter; sharp and wavy upper contact.
4546.45(1385.76)	0.15(0.05)	DOLOMUDSTONE; dolomudstone; dark greenish gray (5GY 4/1); very thin organic planar laminated dolomite. The truncation surface is found at 4,546.3 ft; planar and sharp upper contact.
4546.30(1385.71)	0.66(0.20)	DOLOWACKESTONE w/ ANHYDRITE; peloidal dolowackestone; yellowish gray (5Y 6/1) w/ medium bluish gray (5B 5/1); massive peloidal dolomite w/ small displacive anhydrite w/ dissolved peloids and fractures; sharp and wavy upper contact.
4545.64(1385.51)	2.60(0.79)	DOLOMUDSTONE w/ ANHYDRITE; dolomudstone; yellowish gray (5Y 7/2) w/ medium bluish gray (5B 5/1); massive dolomite grades upward to very thin crenulated and planar laminated dolomite w/ anhydrite in fenestral. The displacive anhydrite on fenestral pores ranges from less than 1/10“ to 5/10“X1“ in diameter; sharp and wavy upper contact.
4543.04(1384.72)	0.99(0.30)	ANHYDRITE w/ SILTSTONE; pale brown (5YR 5/2) w/ grayish olive (10Y 4/2); mosaic anhydrite w/ minor silty remnant; sharp and wavy upper contact.
4542.05(1384.42)	0.25(0.08)	SILTSTONE w/ ANHYDRITE; dark reddish brown (10R3/4) w/ pale brown (5YR 5/2); very thin parallel, horizontal laminated siltstone w/ pseudomorphic felted anhydrite; missing upper contact.
4541.80(1384.34)	0.26(0.08)	ANHYDRITE w/ SILTSTONE; light brownish gray (10R3/4) w/ grayish red (10R 4/2); mosaic anhydrite w/ minor silty remnant; sharp and wavy upper contact.
4541.54(1384.26)	0.04(0.12)	SILTSTONE; siltstone; dark greenish gray (5G 4/1); massive siltstone; missing upper contact.
4541.50(1384.25)	3.50(1.07)	ANHYDRITE w/ SILTSTONE; medium bluish gray (5B 5/1) w/ dark reddish brown (5G 4/1); massive anhydrite w/ minor silty remnant (23“) is overlain by mosaic anhydrite w/ minor more silty remnant (15“) and then massive anhydrite (4“); missing upper contact.
4538.00(1383.18)	5.25(1.50)	SANDSTONE; very fine-grained; pale olive (10Y 6/2) w/ moderate reddish brown (10R 4/6); discontinuous planar horizontal laminae (8.5“) grades upward to faintly ripple cross laminae (6.5“), discontinuous planar horizontal laminae (5“), faintly planar cross laminae (6“) and discontinuous planar horizontal laminae (4“); the above this, massive sandstone w/ wavy laminae in local (1.5“); massive and faintly planar cross laminae (6.5“), and discontinuous planar horizontal laminae (15“); missing upper contact.
4532.75(1381.58)	1.25(0.38)	SILTSTONE; siltstone; greenish gray (5GY 6/1) w/ dark greenish gray (5GY 4/1); very thin parallel continuous planar laminae (5“) grades upward to very thin parallel continuous horizontal laminae (21“); missing upper contact.
4530.50(1380.90)	1.50(0.46)	SANDSTONE w/ ANHYDRITE; very fine-grained; pale olive (10Y 6/2) w/ light bluish gray (5B 7/1); ripple cross laminated sandstone w/ pseudomorphic felted anhydrite (5“) grades upward to massive sandstone due to the extensive anhydrite growth w/ pseudomorphic felted anhydrite (12.5“); missing upper contact

4529.00(1380.44)	0.21(0.06)	SANDSTONE; very fine-grained; yellowish gray (5Y 7/2); deformed wavy laminated sandstone; wavy and sharp upper contact
4528.79(1380.38)	0.37(0.11)	ANHYDRITE w/ SANDSTONE; light bluish gray (5B 7/1) w/ pale olive (10Y 6/2); displacive pseudomorphic felted anhydrite w. minor very fine-grained sandstone in void; missing upper contact.
4528.42(1380.26)	2.42(0.74)	ANHYDRITE; yellowish gray (5Y 7/2) w/ light bluish gray (5B 7/1), massive anhydrite w/ some faintly discontinuous wavy and planar silty laminae; missing upper contact.
4526.00(1379.52)	39.50(12.04)	LOST INTERVAL.
4486.50(1367.49)	1.50(0.45)	SANDSTONE; very fine-grained; very dusky red (10R 2/2) w/ pale olive (10Y 6/2); massive faintly wavy laminae due to some burrow; missing upper contact.
4485.00(1367.03)	0.42(0.13)	LOST INTERVAL.
4484.58(1366.78)	0.38(0.12)	SANDSTONE; very fine-grained; very dusky red (10R 2/2) w/ pale olive (10Y 6/2); massive faintly wavy laminae due to burrow; missing upper contact.
4484.20(1366.78)	0.60(0.18)	SILTSTONE; dusky red (10R 2/2); massive faintly wavy laminae w/ burrow at 4,484 ft; gradational upper contact.
4483.60(1366.60)	0.94(0.29)	MUD- to SILTSTONE; dusky red (10R 2/2) w/ dark greenish gray (5GY 4/1); deformed wavy laminae w/ some very thin continuous parallel wavy laminae; missing upper contact.
4482.66(1366.31)	0.20(0.06)	DOLOMUDSTONE w/ MUDSTONE; dolomudstone; yellowish gray (5Y 7/2) w/ olive gray (5Y 3/2); deformed wavy laminae w/ rip-up mud clasts; wavy and sharp upper contact.
4482.46(1366.25)	1.33(0.41)	MUDSTONE w/ ANHYDRITE; dark reddish brown (10R3/4) w/ olive gray (5Y 3/2); deformed wavy and very thin planar horizontal laminated mudstone w/ small anhydrite. The scour surface is found at 4,481.46 ft; wavy and sharp upper contact.
4481.13(1365.85)	0.67(0.20)	DOLOMUDSTONE; dolomudstone; light olive gray (5Y 5/2) w/ yellowish gray (5Y 7/2); cryptalgal laminated dolomite w/ some stylolite and solution breccia in local; gradational upper contact.
4480.46(1365.64)	0.16(0.05)	MUDSTONE w/ ANHYDRITE; dark reddish gray (10R3/4); faintly discontinuous planar muddy laminae w/ pseudomorphic felted anhydrite; missing upper contact.
4480.30(1365.60)	0.64(0.20)	DOLOMUDSTONE w/ SILTSTONE; dolomudstone; pale reddish brown (10R 5/4) w/ yellowish gray (5Y 7/2); cryptalgal wavy laminated dolomite (4“) grades upward to cryptalgal wavy laminated dolomite w/ displacive anhydrite in fenestral pores (4“); missing upper contact.
4479.66(1365.40)	0.06(0.02)	MUDSTONE; dark reddish brown (10R ¾); deformed wavy laminae; missing upper contact.
4479.60(1365.38)	3.30(1.01)	DOLOMUDSTONE w/ ANHYDRITE; dolomudstone; pale reddish brown (10R 5/4) w/ yellowish gray; cryptalgal laminated dolomite w/ less anhydrite in fenestral pores (22“) and stylolite seams grades upward cryptalgal wavy laminated dolomite w/ more fenestral pores filling anhydrite (16.5“); missing upper contact.
4476.30(1364.38)	4.17(1.27)	DOLOMUDSTONE w/ ANHYDRITE; dolomudstone; yellowish gray (5Y 7/2) w/ light bluish gray (5B 5/1); many stylolite bearing dolomite w/ many fenestral fabric and some sheet crack (29.5“) grades upward to peloidal dolomite w/ small displacive anhydrite w/ fenestral fabric and peloids (20“); sharp and wavy upper contact
4472.13(1363.11)	0.88(0.27)	DOLOWACKESTONE TO DOLOPACKSTONE w/ ANHYDRITE; peloidal and skeletal dolowackestone to dolopackstone; yellowish gray (5Y 7/2) w/ light olive gray (5Y 6/1); pisolite dolowackestone to dolopackstone. The displacive anhydrite is filled in tepee structure; missing upper contact
4471.25(1362.84)	0.05(0.02)	LOST INTERVAL.
4471.20(1362.82)	0.57(0.17)	DOLOWACKESTONE w/ ANHYDRITE; peloidal dolowackestone; yellowish gray (5Y 7/2) w/ grayish orange pink (5YR 7/2); pisolite dolowackestone to dolopackstone. The displacive anhydrite is filled in tepee structure; missing upper contact
4470.63(1362.65)	0.43(0.13)	ANHYDRITE w/ MUDSTONE; moderate reddish brown (10R 4/6) w/ light bluish brown (5B 5/1); massive anhydrite w/ crenulated wavy laminated dolomite; sharp, planar and inclined upper contact.
4470.20(1362.52)	20(0.06)	SANDSTONE; fine-grained; pale olive (10Y 6/2); massive sandstone; sharp and wavy upper contact.
4470.00(1362.46)	2.00(0.60)	SANDSTONE w/ Mud clasts; very fine-grained; dark reddish brown (10R3/4) w/ moderate reddish brown (10R 4/6); deformed wavy laminated

		sandstone w/ some chaotic muddy fragments, load casts (7“) grades upward to massive sandstone w/ many chaotic mud rip-up clasts and some pseudomorphic anhydrite. The sizes of mud clasts is usually less than 1/10“ to 1“; missing or gradational upper contact.
4468.00(1361.85)	1.50(0.46)	MUD- or SILTSTONE; dark reddish brown (10R3/4); massive mud- to siltstone (5“) grades upward to deformed wavy laminated mudstone w/ load casts (14.5“); missing upper contact.
4466.50(1361.39)	0.39(0.12)	SANDSTONE; fine-grained; pale olive (10Y 6/2) w/ dark reddish brown (10R3/4); deformed wavy laminae w/ load casts; sharp and inclined upper contact.
4466.11(1361.27)	0.19(0.06)	ANHYDRITE; pale red (10R 6/2); massive anhydrite; gradational upper contact.
4465.92(1361.21)	0.38(0.12)	SANDSTONE; fine-grained; pale reddish brown (10R 5/4) w/ grayish olive (10Y 4/2); massive sandstone; sharp and wavy upper contact.
4465.54(1361.10)	0.62(0.19)	MUD TO SILTSTONE w/ ANHYDRITE; dark reddish brown (10R3/4) w/ pale reddish brown (10R 5/4); deformed wavy laminae w/ micro-fault, desiccation crack and pseudomorphic felted anhydrite; sharp and wavy upper contact.
4464.92(1360.91)	0.55(0.17)	ANHYDRITE; yellowish gray (5Y 8/1); massive anhydrite; sharp, irregular and wavy upper contact.
4464.37(1360.74)	0.41(0.12)	SILTSTONE w/ ANHYDRITE; dark reddish brown (10 5/4) w/ yellowish gray (5Y 8/1); massive siltstone w/ pseudomorphic rosette structured anhydrite; sharp and wavy upper contact
4463.96(1360.62)	0.13(0.04)	ANHYDRITE; light bluish gray (5B 7/1); massive anhydrite; sharp and wavy upper contact.
4463.83(1360.58)	0.16(0.05)	SILTSTONE; dark reddish brown (10R 5/4); massive siltstone w/ truncation surface at 4,463.67 ft; sharp and wavy upper contact.
4463.67(1360.53)	0.67(0.20)	ANHYDRITE; light bluish gray (5B 7/1) w/ dark reddish brown (10R 5/4); massive anhydrite; missing upper contact.
4463.00(1360.32)	3.16(0.97)	MUD- to SILTSTONE w/ ANHYDRITE; moderate reddish brown (10R 4/6) w/ pale reddish brown (10R 5/4); relatively massive siltstone w/ pseudomorphic rosette structured anhydrite (1“) grades upward to faintly planar horizontal laminated siltstone w/ mud clasts (3“) and massive siltstone w/ small displacive anhydrite wavy laminae (4“); the above this, deformed wavy siltstone w. enterolithic structured anhydrite and pseudomorphic felted anhydrite (14“) grades upward to nodular anhydrite w/ minor silty remnant (6.5“); sharp wavy and irregular upper contact.
4459.84(1359.36)	0.64(0.20)	ANHYDRITE w/ DOLOMITE; light bluish gray (5B 7/1) w/ yellowish gray (5Y 7/2); relatively mosaic anhydrite w/ minor dolomitic remnant in void; sharp and wavy upper contact.
4459.20(1359.16)	1.88(0.60)	ANHYDRITE w/ MUDSTONE; light gray (N7) w/ dark greenish gray (5GY 4/1); mosaic anhydrite w/ minor chaotic muddy laminae remnant; sharp and wavy upper contact.
4457.32(1358.59)	0.32(0.10)	ANHYDRITE w/ DOLOMITE; pale red (10R 6/2) w/ yellowish gray (5Y 7/2); mosaic anhydrite w/ more silty remnant than that of upper bed; sharp and wavy upper contact
4457.00(1358.49)	0.57(0.17)	ANHYDRITE w/ DOLOMITE; light bluish gray (5B 7/1) w/ dark greenish gray (5G 4/1); mosaic anhydrite w/ wavy dolomitic remnant; gradational upper contact
4456.43(1358.32)	0.63(0.19)	ANHYDRITE w/ SILTSTONE; medium bluish gray (5B 5/1) w/ olive gray (5Y 3/2); mosaic anhydrite and chicken-wire structured anhydrite w/minor silty remnants; missing upper contact
4455.80(1358.13)	1.80(0.55)	SILTSTONE; pale olive (10Y 6/2); relatively massive siltstone (18“) grades upward to faintly parallel planar laminae w/ very tiny anhydrite (5’); missing upper contact.
4454.00(1357.58)	0.10(0.03)	DOLOMUDSTONE; dolomudstone; yellowish gray (5Y 7/2); cryptalgal wavy laminae; sharp and planar upper contact
4453.90(1357.55)	1.90(0.58)	ANHYDRITE w/ DOLOMITE; yellowish gray (5Y 7/2) w/ light bluish gray (5B 7/1); massive and mosaic anhydrite w/ minor very thin dolomitic remnants and some algal laminated dolomite (4.5“) grades upward to massive anhydrite w/ minor dolomitic remnant (16“); missing upper contact
4452.00(1356.97)	0.34(0.10)	LOST INTERVAL.
4451.66(1356.87)	0.66(0.20)	ANHYDRITE w/ DOLOMITE; light bluish gray (5B 7/1) w/yellowish gray (5Y 7/2); mosaic anhydrite w/ minor very thin dolomitic remnants; missing upper contact
4451.00(1356.66)	0.12(0.04)	LOST INTERVAL.

4450.84(1356.62) 4450.00(1356.36)	0.84(0.26)	ANHYDRITE w/ DOLOMITE; light bluish gray (5B 7/1) w/yellowish gray (5Y 7/2); mosaic anhydrite w/ minor very thin crenulated dolomitic laminae remnants; Top of core interval at upper contact

Well Name:JSM #300(Reservoir Interval)

Depth difference between core and well log: -6.5 feet in core depth

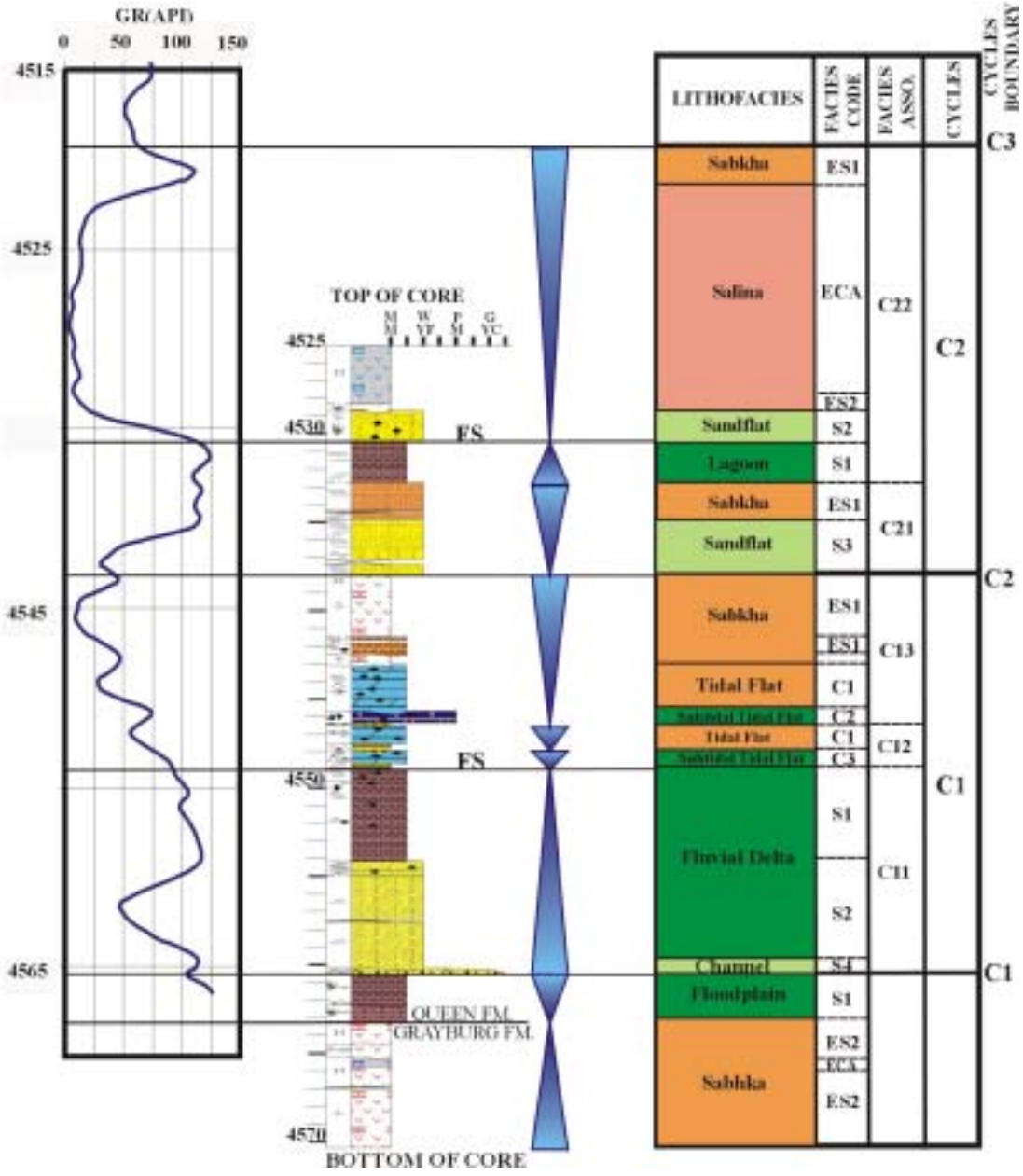

Core Description
JSM #301(API #. 420030245600)
Core Depth Interval: 4555.00–4603.00 ft
Means Field, Andrews County, Texas

DEPTH (ft/m)	THICKNESS (ft/m)	DESCRIPTION
4603.25(1403.07)	1.75(0.53)	ANHYDRITE w/ SILTSTONE; grayish red (10R 4/2); mosaic anhydrite w/ minor silty laminae remnant; missing upper contact
4601.50(1402.54)	0.10(0.03)	LOST INTERVAL. **TOP OF GRAYBURG FORMATION.**
4601.40(1402.51)	0.80(0.24)	ANHYDRITE w/ SILTSTONE; dark reddish brown (10R 3/4) w/ bluish white (5B 9/1); mosaic and chicken wire structure anhydrite w/ minor silty laminae remnant; missing upper contact.
4600.60(1402.26)	1.00(0.30)	ANHYDRITE w/ DOLOMITE; light bluish gray (5B 7/1) w/ bluish white (5B 9/1); massive anhydrite (4“) grades upward to pseudomorphic anhydrite crystals (1”) and massive anhydrite (8“); missing upper contact.
4599.60(1401.96)	0.60(0.18)	SILTSTONE w/ ANHYDRITE; dark reddish brown (10R 3/4) w/ bluish white (5B 9/1); deformed wavy laminae due to the growth anhydrite w/ small nodular anhydrite. The sizes of nodules range from 1/4X1/4“ to 1X2“. The shape of nodule is usually irregular; missing upper contact.
4599.00(1401.78)	0.25(0.08)	LOST INTERVAL.
4598.75(1401.70)	2.05(0.62)	ANHYDRITE w/ SILTSTONE; pinkish gray (5YR 8/1) w/ grayish olive (10Y 4/2); mosaic and chicken wire structure anhydrite w/ minor silty laminae remnant; missing upper contact.
4596.70(1401.07)	1.63(0.50)	ANHYDRITE w/ DOLOMITE; light brownish gray (5YR 6/1) w/ pale greenish yellow (10Y 8/2); massive and chicken-wire structure anhydrite w/ minor dolomitic remnant; sharp and wavy upper contact.
4595.07(1400.58)	1.30(0.39)	ANHYDRITE w/ SILTSTONE; pale red (10R 6/2) w/ grayish olive (10Y 4/2); mosaic anhydrite w/ minor silty laminae remnant. The truncation surface is found at 4,595.97 ft; the above this, mosaic anhydrite w/ minor silty laminae remnant and collapsed breccia (35“); sharp and wavy upper contact.
4591.57(1399.51)	0.57(0.17)	ANHYDRITE w/ SILTSTONE; light bluish gray (5B 7/1) w/ light brown (5YR 5/6); massive anhydrite w/ minor silty remnant; missing upper contact.
4591.00(1399.34)	0.20(0.06)	LOST INTERVAL.
4190.80(1399.28)	2.80(0.85)	ANHYDRITE w/ SILTSTONE; light bluish gray (5B 7/1) w/ dark greenish gray (5YR 5/6); mosaic anhydrite w/ minor silty remnant; missing upper contact.
4588.00(1398.42)	0.50(0.15)	LOST INTERVAL.
4587.50(1398.27)	0.50(0.15)	ANHYDRITE w/ SILTSTONE; light bluish gray (5B 7/1) w/ dark greenish gray (5G 6/1); mosaic anhydrite w/ minor silty remnant; missing upper contact; wavy and sharp upper contact.
4587.00(1398.12)	0.10(0.03)	SILTSTONE; dark greenish gray (5G 4/1); massive siltstone; wavy and sharp upper contact
4586.90(1398.09)	0.70(0.21)	ANHYDRITE w/ SILTSTONE; medium bluish gray (5B 5/1) w/ dark greenish gray (5G 6/1); massive anhydrite w/ minor silty remnant; wavy and sharp upper contact.
4586.20(1397.87)	0.25(0.08)	MUDSTONE w/ SANDSTONE; light olive gray (5Y 5/2) w/ olive gray (5Y 3/2); faintly deformed wavy laminae (2“) w/ thin dolomite, anhydrite, and mud clasts (2.5“); gradational upper contact.
4585.95(1397.80)	3.95(1.20)	SANDSTONE w/ ANHYDRITE; very fine-grained; dusky yellow (5Y 6/4) w/ olive gray (5Y 3/2); stacked ripple laminated and massive sandstone (12“) grade upward to massive planar cross laminated sandstone (20“) w/ several micro-faults; the above this, ripple cross laminated sandstone (15“); missing upper contact.
4582.00(1396.59)	0.20(0.06)	LOST INTERVAL.
4581.80(1396.53)	0.70(0.21)	SANDSTONE w/ ANHYDRITE; very fine-grained; dusky yellow (5Y 6/4) w/ olive gray (5Y 3/2); discontinuous planar horizontal- and ripple cross-laminated sandstone w/ small displacive anhydrite; missing upper contact.
4581.10(1396.32)	0.10(0.03)	LOST INTERVAL.
4581.00(1396.29)	2.00(0.60)	SANDSTONE w/ ANHYDRITE; very fine-grained; dusky yellow (5Y 6/4) w/ olive gray (5Y 3/2); staked ripple cross laminated sandstone (10“) grades upward to faintly discontinuous wavy laminated w/ wavy muddy laminated flake and small anhydrite (16“); missing upper contact.
4579.00(1395.68)	0.70(0.21)	LOST INTERVAL.
4578.30(1395.47)	0.30(0.09)	SANDSTONE w/ ANHYDRITE; very fine-grained; dusky yellow (5Y 6/4) w/ olive gray (5Y 3/2); discontinuous wavy laminated sandstone; missing upper contact.
4578.00(1395.37)	0.05(0.02)	LOST INTERVAL.

4577.95(1395.36)	0.95(0.29)	SANDSTONE w/ ANHYDRITE; very fine-grained; dusky yellow (5Y 6/4); low angle discontinuous wavy laminated sandstone w/ small anhydrite; missing upper contact.
4577.00(1395.07)	0.10(0.03)	LOST INTERVAL.
4576.90(1395.04)	1.90(0.58)	SANDSTONE w/ ANHYDRITE; very fine-grained; light olive gray (5Y 5/2) w/ olive gray (5Y 3/2); massive, discontinuous horizontal planar laminated sandstone w/ small anhydrite (9“) grade upward to massive sandstone (5“); missing upper contact.
4575.00(1394.46)	0.04(0.01)	LOST INTERVAL.
4574.96(1394.45)	0.96(0.29)	SANDSTONE w/ ANHYDRITE; very fine-grained; olive gray (5Y 5/2) w/ olive gray (5Y 3/2); massive sandstone w/ anhydrite; missing upper contact.
4574.00(1394.16)	0.46(0.14)	LOST INTERVAL.
4573.54(1394.01)	0.54(0.16)	SANDSTONE w/ ANHYDRITE; very fine-grained; olive gray (5Y 5/2) w/ olive gray (5Y 3/2); massive sandstone w/ anhydrite; missing upper contact.
4573.00(1393.85)	0.10(0.03)	LOST INTERVAL.
4572.90(1393.82)	1.90(0.58)	SANDSTONE w/ ANHYDRITE; very fine-grained; olive gray (5Y 5/2) w/ olive gray (5Y 3/2); massive sandstone and discontinuous nonparallel wavy laminated sandstone w/ small displacive anhydrite; missing upper contact.
4571.00(1393.24)	0.80(0.24)	LOST INTERVAL.
4570.20(1393.00)	0.20(0.06)	SANDSTONE w/ ANHYDRITE; very fine-grained; light olive gray (5Y 5/2) w/ olive gray (5Y 3/2); faintly ripple cross-laminated sandstone; missing upper contact.
4570.00(1392.93)	0.60(0.18)	LOST INTERVAL.
4569.40(1392.75)	1.40(0.43)	SANDSTONE w/ ANHYDRITE; very fine-grained; light olive gray (5Y 5/2) w/ olive gray (5Y 3/2); massive sandstone w/ remnant muddy laminae; missing upper contact.
4568.00(1392.33)	0.30(0.09)	LOST INTERVAL.
4567.70(1392.23)	0.20(0.06)	SANDSTONE w/ ANHYDRITE; very fine-grained; light olive gray (5Y 6/4) w/ olive gray (5Y 3/2); massive and faintly muddy wavy laminated sandstone; wavy and sharp upper contact.
4567.50(1392.17)	3.30(1.01)	SANDSTONE w/ ORGANIC LAMINAE and ANHYDRITE; very fine-grained; dusky yellow (5Y 6/4) w/ olive gray (5Y 3/2); massive and discontinuous slightly wavy laminated sandstone w/ small anhydrite (6“) grades up to climbing stacked ripple cross laminated sandstone (5“), discontinuous planar horizontal- and wavy laminated sandstone w/ burrow (7“); and very thin planar laminated sandstone w/ anhydrite (21“); wavy and sharp upper contact.
4564.20(1391.17)	0.20(0.06)	SILT- to SANDSTONE; silt- to very fine-grained; dark greenish gray (5GY 4/1) w/ greenish black (5GY 2/1); very thin planar horizontal and slightly wavy laminated sandstone (2“); missing upper contact
4564.00(1391.10)	0.20(0.06)	LOST INTERVAL.
4563.80(1391.05)	1.50(0.46)	SILT- to SANDSTONE; silt- to very fine-grained; dark greenish gray (5GY 4/1) w/ greenish black (5GY 2/1); ripple cross laminated sandstone (6“) grades upward to discontinuous planar and deformed wavy laminated sandstone (7“), and massive discontinuous non-parallel wavy laminated siltstone and mudstone (6“); gradational upper contact.
4562.30(1390.59)	0.90(0.27)	DOLOMUDSTONE TO DOLOWACKESTONE; peloidal dolomudstone to dolowackestone; yellowish gray (5Y 7/2) w/ light bluish gray (5B 7/1); crenulated wavy laminated dolomite w/ minor silty laminae and small collapsed dolomitic clasts (5“) grades upward to massive dolomite w/; nodular anhydrite (6“). The sizes of nodule is 5/10 X 5/10” in diameter; missing upper contact.
4561.40(1390.31)	0.10(0.03)	LOST INTERVAL.
4561.30(1390.28)	0.80(0.24)	DOLOMUDSTONE; yellowish gray (5Y 7/2); cryptalgal-laminated dolomite w/ nodular anhydrite; missing upper contact.
4560.50(1390.04)	0.04(0.01)	LOST INTERVAL.
4560.46(1390.03)	0.46(0.14)	ANHYDRITE w/ SILTSTONE; pale red (5R 6/2); massive bedded and slight laminated anhydrite w/ minor silty laminae remnant (6“); missing upper contact.
4560.00(1389.89)	0.50(0.15)	LOST INTERVAL.
4559.50(1389.74)	0.50(0.15)	ANHYDRITE w/ SILTSTONE; pale red (5R 6/2); massive bedded and slight laminated anhydrite w/ minor silty laminae remnant (6“); missing upper contact.
4559.00(1389.58)	0.25(0.08)	LOST INTERVAL.
4558.75(1389.50)	0.50(0.15)	ANHYDRITE w/ DOLOMITE; light bluish gray (5B 7/1) w/ yellowish gray (5Y 7/2); mosaic anhydrite w/ minor dolomitic laminae remnant; gradational

		upper contact.
4558.25(1389.35)	0.25(0.08)	ANHYDRITE w/ SILTSTONE; grayish red (5R 4/2); massive and faintly wavy laminated anhydrite w/ minor silty wavy laminae remnants; missing upper contact.
4558.00(1389.28)	0.15(0.05)	LOST INTERVAL.
4557.85(1389.23)	0.45(0.14)	ANHYDRITE w/ SILTSTONE; grayish red (5R 4/2); pseudomorphic felted anhydrite w/ minor silty wavy laminae; wavy and sharp upper contact.
4557.40(1389.10)	0.40(0.12)	ANHYDRITE; light bluish gray (5B 7/1); massive anhydrite; sharp and wavy upper contact.
4557.00(1388.97)	1.00(0.30)	SILT- to SANDSTONE; silt- to very fine-grained; grayish red (5R 4/2) w/ yellowish gray (10Y 4/2); ripple cross and deformed wavy laminated siltstone and sandstone; missing upper contact.
4556.00(1388.67)	0.15(0.05)	LOST INTERVAL.
4555.85(1388.62)	0.85(0.26)	SILT- to SANDSTONE; silt- to very fine-grained grayish red (5R 4/2) w/ yellowish gray (10Y 4/2); deformed wavy laminated sandstone w/ dewatering structure, micro-faults and some burrows; Top of core interval at upper contact
4555.00(1388.36)		

Core Description
Wentz #11 (API #: 420030262800)
Core Depth Interval: 4155.0–4220.17 ft
Means Field, Andrews County, Texas

DEPTH (ft/m)	THICKNESS (ft/m)	DESCRIPTION
4220.17(1286.31)	3.17(0.96)	ANHYDRITE w/ DOLOMITE; light bluish gray (5B 7/1) w/ yellowish gray (5Y 7/2); mosaic anhydrite w/ minor irregular dolomitic laminae (8“) grades upward more massive and less mosaic anhydrite (5“) and changes into massive bedded anhydrite (2“); the above this, mosaic anhydrite w/ dolomitic laminae in void; missing upper contact.
4217.00 (1285.34)	0.05(0.02)	LOST INTERVAL.
4216.95(1285.33)	3.15(0.96)	ANHYDRITE w/ DOLOMITE; light bluish gray (5B 7/1) w/ yellowish gray (5Y 7/2); mosaic anhydrite w/ dolomitic laminae in void (4.5“) grades upward to massive anhydrite (4“) and massive anhydrite (8“); gradational upper contact; **TOP OF GRAYBURG FORMATION AT 4,213 feet.**
4213.80(1284.37)	0.20(0.06)	ANHYDRITE w/ MUDSTONE; pale red (5R 6/2) w/ grayish olive (10Y 4/2); mosaic anhydrite with minor pale red remnant mudstone; sharp and wavy upper contact
4213.60(1284.31)	0.60(0.18)	MUDSTONE w/ ANHYDRITE; pale red (5R 6/2) w/ grayish olive (10Y 4/2); deformed mudstone laminae by the growth of pseudomorphic anhydrite crystals (4“) grades upward to deformed mud laminae by the growth of coalesced ellipsoidal anhydrite nodules (2“). Those sizes of nodules range from 5/10“ X 5/10“ to 2“ in diameter; missing upper contact.
4213.00(1284.12)	0.07(0.02)	LOST INTERVAL.
4212.93(1284.10)	1.75(0.53)	Interbedded MUD- to SILTSTONE w/ SANDSTONE; olive gray (5Y 3/2) w/ light olive gray (5Y 5/2); deformed wavy and ripple cross laminated mudstone and siltstone w/ many deformational structures such as load ball and pillow and convolute ripple laminae; sharp and wavy (?) upper contact.
4211.18(1283.57)	1.18(0.36)	SANDSTONE w/ MUD CLASTS; very fine-grained; yellowish gray (5Y 7/2) w/ grayish olive (10Y 4/2); massive sandstone w/ many slumping structure and mud clasts. The sizes of mud clasts are 2/10 X 2/10“ in diameter. The scour surface is found at 4,211.18 ft; sharp and inclined; gradational upper contact.
4210.00(1283.21)	3.27(0.99)	SANDSTONE; very fine-grained; yellowish gray (5Y 7/2) w/ grayish olive (10Y 4/2); massive sandstone w/ dewatering structure (5“) grade upward to massive sandstone w/ mud clasts, slumping structure and micro-faults (7“) and massive sandstone w/ dewatering structures and many mud clasts and deformed wavy laminae due to syndepositional deformation (15.5“); the above this, massive sandstone; missing upper contact.
4206.73(1282.21)	0.27(0.08)	LOST INTERVAL.
4206.46(1282.13)	5.23(1.59)	SANDSTONE; fine-grained; yellowish gray (5Y 7/2); massive sandstone w/ remnant mud rip-up clasts (10”) grades upward to planar horizontal laminated sandstone (8“), slight planar cross laminated sandstone (4“) and massive sandstone (4“); missing upper contact
4201.23(1280.53)	1.69(0.52)	SAND- to SILTSTONE; silt- to very fine-grained; yellowish gray (5Y 7/2); faintly discontinuous wavy and planar horizontal laminated sandstone; sharp and planar upper contact.
4199.54(1280.02)	0.21(0.06)	MUDSTONE; light olive gray (5Y 5/2) w/ dusky yellow (5Y 6/4); faintly discontinuous planar horizontal laminated mudstone; sharp and wavy upper contact.
4199.33(1279.96)	0.12(0.04)	SILT- to SANDSTONE w/ MUDSTONE; silt- to very fine-grained, yellowish gray (5Y 6/4) and dusky olive (5Y 7/2); faintly discontinuous planar horizontal laminated sandstone; gradational upper contact.
4199.21(1279.92)	0.50(0.15)	DOLOMUDSTONE; yellowish gray (5Y 7/2); discontinuous horizontal planar laminated dolomudstone (2“) grades upward to wavy laminated dolomite and massive dolomite (2“) and very thin wavy and planar horizontal laminated dolomudstone (1.5“); missing upper contact.
4198.70(1279.76)	0.78(0.24)	SANDSTONE w/ ANHYDRITE; very fine-grained; pale olive (10Y 6/2) w/ medium bluish gray (5B 5/1); deformed wavy laminated sandstone w/ small anhydrite nodules and load structure; missing upper contact.
4197.92(1279.53)	0.54(0.16)	DOLOMUDSTONE w/ ANHYDRITE; yellowish gray (5Y 7/2) w/ medium bluish gray (5B 5/1); very thin discontinuous planar horizontal laminated dolomite w/ small anhydrite (5“) grade upward to wavy laminated dolomite w/ fracture and solution breccia (3“); sharp and planar upper contact.
4197.38(1279.36)	0.98(0.30)	DOLOMUDSTONE w/ ANHYDRITE; argillaceous mudstone; light olive gray (5Y 5/2) w/ medium bluish gray (5B 5/1); discontinuous planar

		horizontal laminated dolomudstone w/ remnant anhydrite in fenestral fabrics (3“) grade upward to massive dolomudstone w/ anhydrite in bird’s eye structure (3“) and faintly wavy laminated w/ minor anhydrite in fenestral fabrics (6“). The sizes of anhydrite fenestral fabric range from less than 1/20“ to 1/10 X 2/10“ in diameter.; sharp and planar upper contact.
4196.40(1279.07)	2.40(0.73)	DOLOMUDSTONE w/ ANHYDRITE; dolomudstone; yellowish gray (5Y 7/2) w/ medium bluish gray (5B 5/1); massive dolomite w/ anhydrite filled in fenestral pore and many stylolite (10“) is overlain by planar horizontal, planar laminated dolomite w/ anhydrite in birds eye structure (2.5“) and very thin planar laminated dolomite w/ anhydrite in fenestral pores, many horse tail stylolites and some brecciated zone (24“). The sizes of fenestral pores range from 1/10 X 1/10“ to 1/10 X 2/10“ in diameter; missing upper contact.
4194.00(1278.33)	6.00(1.83)	LOST INTERVAL.
4188.00(1276.50)	5.00(1.52)	DOLOMUDSTONE w/ ANHYDRITE; light olive gray (5Y 7/2) w/ medium bluish gray (5B 5/1); massive dolomite w/ anhydrite in fenestral pores and stylolites. The organic thin mud laminae are found at several horizon of bed; the above this, cryptalgal laminated dolomite w/ anhydrite in birds eye structure (5“) and massive and some organic black laminae w/ fracture and anhydrite in fenestral pores (23“); missing upper contact.
4183.00(1274.98)	0.62(0.19)	SILTSTONE w/ ANHYDRITE; pale brown (5YR 5/2) w/ moderate brown (5YR 3/4); laminated siltstone with mosaic and enterolithic structured anhydrite (2“) grades upward to the association of pseudomorphic felted anhydrite (1.5“) and mosaic anhydrite (4“); missing upper contact.
4182.38(1274.79)	1.36(0.41)	ANHYDRITE w/ SILTSTONE; moderate brown (5Y 5/2) w/ pale brown (10Y 6/2); pseudomorphic felted anhydrite with deformed wavy laminated siltstone remnant due to haloturbation (3“) grades upward to mosaic anhydrite with siltstone remnant (13“); missing upper contact.
4181.02(1274.37)	1.01(0.31)	ANHYDRITE w/ DOLIMITE; medium bluish gray (5B 7/1); massive anhydrite with very thin wavy dolomitic laminae (11“) grade upward to massive anhydrite with very thin algal laminae (1“); missing upper contact.
4180.01(1274.07)	0.49(0.15)	SILTSTONE w/ ANHYDRITE; moderate brown (5YR 3/4) w/ medium bluish gray (5B 7/1); deformed wavy siltstone laminae with pseudomorphic felted anhydrite crystals (2.5“) grades upward to the association with 4/10“ thick mosaic nodular anhydrite (0.5“) and then deformed ripple (or convolute laminae) laminated siltstone with pseudomorphic laminated anhydrite (2“); sharp and wavy upper contact.
4179.52(1273.92)	0.69(0.21)	SANDSTONE w/ ANHYDRITE; very fine-grained; light olive gray (5Y 5/2) w/ light bluish gray (5B 7/1); deformed laminated sandstone w/ load structure and nodular anhydrite; missing upper contact.
4178.83(1273.71)	0.08(0.02)	LOST INTERVAL.
4178.75(1273.68)	2.57(0.78)	SANDSTONE w/ MUDSTONE; very fine-grained; light olive gray (5Y 5/2) w/ olive gray (5Y 3/2) and medium bluish gray (5B 7/1); deformed wavy and discontinuous planar laminated sandstone w/ some micro-faults (12“) grades upward to deformed cross and wavy laminated sandstone w/ micro-faults (9.5“). It is overlain by deformed wavy and ripple laminated sandstone w/ small displacive anhydrite and burrow (13.5“); wavy and irregular upper contact.
4176.18(1272.90)	0.13(0.04)	SANDSTONE; yellowish bluish gray (5Y 7/2); very fine-grained; massive sandstone; sharp and planar upper contact.
4176.05(1272.86)	1.05(0.32)	SANDSTONE w/ ANHYDRITE; very fine-grained; light olive gray (5Y 5/2) w/ olive gray (5Y 3/2) and medium bluish gray (5B 7/1); deformed wavy (or algal) and discontinuous planar laminated sandstone w/ small displacive anhydrite crystals; missing upper contact
4175.00(1272.54)	0.12(0.04)	LOST INTERVAL.
4174.88(1272.50)	0.25(0.08)	SANDSTONE w/ANHYDRITE; light olive gray (5Y 5/2) w/light bluish gray (5B 7/1); deformed wavy sandy laminae and burrow w/mosaic anhydrite; sharp and wavy upper contact.
4174.61(1272.42)	0.28(0.09)	SANDSTONE w/ MUDSTONE; very fine- to fine-grained; yellowish gray (5Y 7/2) w/ moderate brown (5Y 5/2); very thin slight wavy laminae sandstone w/ minor muddy remnant; sharp and planar upper contact.
4174.33(1272.34)	0.83(0.25)	SANDSTONE w/ANHYDRITE; light olive gray (5Y 5/2) w/light bluish gray (5B 7/1); algal wavy laminae anhydrite w/ pseudomorphic felted anhydrite; sharp and wavy upper contact.
4173.50(1272.08)	0.45(0.14)	SILT- to SANDSTONE; silt to very fine-grained; yellowish gray (5Y 7/2) w/ light olive gray (5Y 5/2); very thin planar horizontal and algal laminae; sharp and wavy upper contact.

4173.05(1271.95)	0.28(0.09)	SANDSTONE w/ANHYDRITE; yellowish gray (5Y 7/2) w/ light olive gray (5B 5/1); algal wavy laminae and silty laminae w/ pseudomorphic felted anhydrite; sharp and wavy upper contact
4172.77(1271.86)	1.44(0.44)	SANDSTONE w/ MUDSTONE; very fine-grained; yellowish gray (5Y 7/2) w/ light olive gray (5Y 5/2); faintly discontinuous planar horizontal laminated sandstone w/ remnant muddy laminae and some algal laminae (9“) grades upward to slightly wavy laminated sandstone (4.5“); sharp and wavy upper contact
4171.33(1271.42)	1.33(0.41)	DOLOMUDSTONE w/ ANHYDRITE; yellowish gray (5Y 7/2) w/ light olive gray (5B 5/1); very thin algal laminated dolomite w/ thin bedded anhydrite; missing upper contact.
4171.00(1271.32)	0.13(0.04)	LOST INTERVAL.
4170.87(1271.28)	1.21(0.37)	SILT- to MUDSTONE; silt- to mudstone; dark reddish brown (10R 3/4) w/ medium bluish gray (5B 5/1); deformed wavy laminated siltstone with elongated, ellipsoidal small displacive anhydrite between the bedding (5.5“). Those deformed wavy laminated siltstone include many small mud clasts from 4,170.5 ft, many micro-faults, fractures, and deformed mud flakes or laminae (19“); gradational upper contact
4169.66(1270.92)	1.11(0.34)	SILTSTONE w/ ANHYDRITE; medium bluish gray (5B 5/1) w/ dark reddish brown (10R 3/4); deformed wavy laminated siltstone due to haloturbation with pseudomorphic anhydrite crystals (2“) grade upward to the association with elongated, compacted, enterolithic structured anhydrite between bedding plane (3“), pseudomorphic rosette structured anhydrite (2.5”) and nodular anhydrite (3“). The size of nodules are approximately 1/8 X 1/4” in diameter; missing upper contact.
4167.45(1270.24)	0.12(0.04)	LOST INTERVAL.
4167.33(1270.20)	2.65(0.81)	ANHYDRITE w/ DOLOMITE; light gray (5B 5/1) w/ yellowish gray (5Y 7/2); relatively massive anhydrite with the remnant of deformed, planar and horizontal and algal dolomitic laminae due to the extensive anhydrite crystal growth; missing upper contact.
4164.65(1269.39)	0.07(0.02)	LOST INTERVAL.
4164.58(1369.36)	2.68(0.82)	ANHYDRITE w/ DOLOMITE; light bluish gray (5B 7/1) w/ yellowish gray (5Y 7/2); massive bedded anhydrite with the remnant deformed dolomitic laminae and mosaic anhydrite structures. Some thin interval also show small (1/10 X 1/10“ in diameter) nodular anhydrite; missing upper contact
4161.90(1268.55)	1.03(0.31)	SILTSTONE w/ ANHYDRITE; moderate brown (5YR 3/4) w/ light bluish gray (5B 7/1); deformed wavy laminated siltstone due to the growth of anhydrite, the siltstone is associated with deformed enterolithic and displacive pseudomorphic anhydrite crystals; sharp and planar upper contact.
4160.87(1268.23)	1.87(0.57)	ANHYDRITE w/ DOLOMITE; light bluish gray (5B 7/1) w/ yellowish gray (5Y 7/2), massive anhydrite with very thin slightly planar horizontal dolomitic laminae; missing upper contact
4159.00(1267.66)	1.00(0.30)	SILT- to SANDSTONE; silt to very fine-grained; moderate brown (5YR 3/4) w/ blackish red (5YR 2/2), deformed wavy and ripple laminated sandstone with fluid escape structure; missing upper contact.
4158.00(1367.36)	0.75(0.23)	LOST INTERVAL.
4157.25(1267.13)	2.25(0.69)	SANDSTONE; very fine-grained; moderate brown (5YR 3/4) w/ pale olive (10YR 6/2); faintly discontinuous wavy and ripple cross planar laminated sandstone (12“) grades upward to massive sandstone w/ several red oxidized beds horizon and some mud clasts (21“); Top of core interval at upper contact
4155.00(1266.44)		

Core Description
R.M. Means #42 (API #: 420030271000)
Core Depth Interval: 4080.00–4105.16 ft
Means Field, Andrews County, Texas

DEPTH (ft/m)	THICKNESS (ft/m)	DESCRIPTION
4105.16(1251.25)	3.16(0.96)	SANDSTONE; fine-grained; dusky yellow (5Y 6/4); massive and mottled sandstone w/ burrow; the above this, very thin planar horizontal laminated sandstone w/ micro-faults (3”); missing upper contact.
4102.00(1250.29)	0.79(0.24)	LOST INTERVAL.
4101.21(1250.05)	1.21(0.37)	DOLOMUDSTONE; dolomudstone; yellowish gray (5Y 7/2); massive dolomite w/ anhydrite in birds eye structures and stylolite; missing upper contact.
4100.00(1249.68)	12.25(3.73)	LOST INTERVAL.
4087.75(1245.95)	0.75(0.23)	SANDSTONE; very fine-grained; dusky yellow (5Y 6/4) w/ grayish yellow green (5GY 7/2); massive sandstone (2”) grades upward to cryptalgal and ripple cross laminated sandstone (6.5”); missing upper contact.
4087.00(1245.72)	0.70(0.21)	LOST INTERVAL.
4086.30(1245.50)	2.30(0.70)	SANDSTONE; very fine-grained; dusky yellow (5Y 6/4); wavy laminated sandstone (8”) grades upward to discontinuous wavy laminated sandstone (2.5”); the above this, cryptalgal and planar horizontal laminated sandstone; missing upper contact.
4083.00(1244.50)	0.83(0.25)	LOST INTERVAL.
4082.17(1244.25)	0.17(0.05)	SANDSTONE; very fine-grained; dusky yellow (5Y 6/4) w/ greenish yellow green (5GY 7/2); ripple cross-laminated sandstone; missing upper contact.
4082.00(1244.19)	0.83 (0.25)	LOST INTERVAL.
4081.17(1243.94)	0.17(0.05)	SANDSTONE w/ ANHYDRITE; dusky yellow (5Y 6/4) w/ light bluish gray (5B 5/1); discontinuous wavy laminated sandstone w/ nodular anhydrite; missing upper contact.
4081.00(1243.89)	0.63(0.19)	LOST INTERVAL.
4080.33(1243.68)	0.17(0.05)	SANDSTONE w/ DOLOMITE; yellowish gray (5Y 7/2) w/ olive gray (5Y 3/2); deformed wavy laminated sandstone w/ nodular anhydrite; sharp and wavy upper contact
4080.16(1243.63)	0.16(0.05)	DOLOMITE w/ ANHYDRITE; light bluish gray (5B 7/1) w/ yellowish gray (5Y 7/2); massive dolomite w/ anhydrite in bird’s eye structure; Top of core interval at upper contact
4080.00(1243.58)		

Core Description
Dibrell #3 (API #: 420031012500)
Core Depth Interval: 4190.0-4239.83 ft
Means Field, Andrews County, Texas

DEPTH (ft/m)	THICKNESS (ft/m)	DESCRIPTION
4239.83(1292.30)	2.63(0.80)	ANHYDRITE w/ SILT- to MUDSTONE; light bluish gray (5B 7/1) w/ grayish brown (5YR 3/2); displacive pseudomorphic anhydrite w/ deformed wavy muddy or silty laminae remnant (2“) grades upward to coalesced nodular anhydrite w/ deformed muddy laminae and mud clasts (12“) and mosaic and chicken-wire structured anhydrite w/ deformed wavy mud laminae remnant (9“); gradational upper contact; the above this, massive and bedded anhydrite; sharp and wavy upper contact. **TOP OF GRAYBURG FORMATION.**
4237.20(1291.50)	1.70(0.52)	ANHYDRITE w/ SILT- to MUDSTONE; light bluish gray (5B 7/1) w/ grayish brown (5YR 3/2); coalesced nodular anhydrite at the bottom of bed grades upward more massive bedded anhydrite w/ minor deformed wavy muddy and silty laminae remnant; sharp and wavy upper contact.
4235.50(1290.98)	2.13(0.65)	ANHYDRITE w/ SILT- to MUDSTONE; light bluish gray (5B 7/1) w/ grayish brown (5YR 3/2); coalesced nodular anhydrite w/ minor deformed wavy silty and muddy laminae remnant on the sharp and truncated surface (16“). These nodular anhydrite change into massive bedded and enterolithic structured anhydrite w/ deformed wavy mud laminae remnant (6.5“); wavy and irregular upper contact.
4233.37(1290.33)	0.42(0.13)	SILT-to MUDSTONE w/ ANHYDRITE; light bluish gray (5B 7/1) w/ dark greenish gray (5GY 4/1); deformed wavy silty and muddy laminae w/ small nodular and pseudomorphic felted anhydrite. The sizes of nodules is less than 1/20“ in diameter and parallel to laminae; missing upper contact.
4232.95(1290.20)	0.68(0.21)	SANDSTONE w/ MUDSTONE; very fine-grained; light olive gray (5Y 5/2) w/ olive gray (5Y 3/2); massive and chaotic wavy laminated sandstone w/ deformed ball and pillow structure, some gravel sized mud clasts and micro-faults; wavy and sharp upper contact.
4232.27(1289.99)	0.26(0.08)	SANDSTONE w/ MUD CLASTS; very fine-grained; light olive gray (5Y 5/2); massive and chaotic wavy laminated sandstone w/ randomly chaotic distributed gravely mud clasts; missing upper contact.
4232.01(1289.91)	0.15(0.05)	Interbedded SANDSTONE and MUDSTONE w/ MUD CLASTS; very fine-grained sandstone and mudstone; bluish white (5B 9/1) w/ olive gray (5Y 3/2); Interbedded deformed wavy muddy laminae w/ massive and chaotic sandy laminae and randomly distributed mud clasts. Some pseudomorphic felted anhydrite is found at 4,232 ft.; missing upper contact.
4231.86(1289.87)	2.68(0.82)	SANDSTONE w/ MUD CLASTS; very fine-grained w/ gravel sized mud and sand clasts; light olive gray (5Y 5/2) w/ olive gray (5Y 3/2); chaotic gravely mud clasts bearing massive sandstone. The random mud clasts are composed of angular mud and sand gravels and their size range from 1/20” to 2” in diameters. Its random mud clast bed (12“) grades upward to the imbricated mud clasts bearing sandstone w/ some ball and pillow structure (17“). The sizes of imbricated mud clasts is more than 2” and is mostly composed of very angular mud and sand; the above, deformed wavy and wavy laminated sandstone w/ small mud clasts; missing upper contact.
4229.18(1289.05)	0.68(0.21)	SILT- to MUDSTONE; silt- to mudstone; yellowish gray (5Y 7/2); massive siltstone and mudstone (2“) grades upward to wavy laminated siltstone w/ mud clasts and flame structure (6“); sharp and irregular upper contact.
4228.50(1288.84)	2.50(0.76)	SANDSTONE; silt- to very fine-grained; yellowish gray (5Y 7/2) w/ bluish white (5B 9/1); massive sandstone w/ some nodular anhydrite and faintly wavy laminae (10“) grades upward to relatively massive, faintly discontinuous bi-directional cross laminated sandstone (8“), massive sandstone (3.5“), faintly discontinuous cross laminated sandstone (2“) and massive sandstone (2.5“); missing upper contact
4226.00(1288.08)	4.25(1.30)	SANDSTONE w/ ANHYDRITE; very fine-grained; dusky yellow (5Y 6/4); faintly discontinuous cross-laminated sandstone (9.5“) is overlain by massive sandstone (26“), faintly discontinuous cross-laminated sandstone (11.5“) and massive sandstone (16“); missing upper contact.
4220.75(1280.39)	0.66(0.20)	DOLOMITE W/ SANDSTONE; argillaceous dolomite; yellowish gray (5Y 7/2) w/ light olive gray (5Y 5/2); massive and wavy laminated dolomite w/ rip-up dolomitic clasts and remnant siliceous materials; missing upper contact.
4220.09(1286.28)	0.68(0.21)	SANDSTONE w/ DOLOMITIC CLASTS and ANHYDRITE; very fine-

		grained; yellowish gray (5Y 7/2) w/ light olive gray (5Y 5/2); deformed wavy cross laminae w/ many dolomitic clasts; The size of dolomitic clasts range from less than 1/20“ to 5/10“ in diameter; missing upper contact.
4219.41(1286.07)	3.31(1.01)	SANDSTONE w/ ANHYDRITE and MUD CLASTS; very fine-grained w/ gravely sized mud clasts; yellowish gray (5Y 7/2) w/ bluish white (5B 9/1), chaotic deformed laminated sandstone w/ imbricated angular gravely mud clasts (9“) grades upward to deformed wavy laminated sandstone w/ burrow (2.5“). It is overlain by thin planar horizontal laminated sandstone due to the growth of anhydrite (19“) and thin black organic wavy laminated sandstone (4“) and very thin deformed cross laminated sandstone (3”); gradational upper contact.
4216.10(1285.07)	1.10(0.34)	MUD- to SILTSTONE w/ ANHYDRITE; olive gray (5Y 4/1) w/ light bluish gray (5B 7/1); very thin planar cross laminated siltstone (8“) grades upward to very thin planar horizontal laminae (2“) and thin-bed massive sandstone w/ ball and pillow structure (1.5“); sharp and irregular upper contact.
4215.00(1284.73)	1.00(0.30)	DOLOMUDSTONE w/ ANHYDRITE; dolomudstone; yellowish gray (5Y 8/1) w/ light bluish gray (5B 7/1); wavy laminae w/ horse tail stylolite (3.5“) grades upward to massive dolomite w/ anhydrite in fracture and solution breccia (3“) and massive dolomite w/ many horse tail stylolite (5.5“); missing upper contact.
4214.00(1284.43)	0.26(0.08)	DOLOWACKESTONE; skeletal dolomudstone and dolowackestone; yellowish gray (5Y 4/1) w/ olive gray (5Y 3/2); massive dolomite w/ shell fragment (2“) grade upward to massive dolomite w/ horsetail stylolite (1.5“); missing upper contact.
4213.74(1284.35)	1.61(0.49)	DOLOMUDSTONE; dolomudstone and argillaceous mudstone; yellowish gray (5Y 4/1) w/ olive gray (5Y 3/2); massive dolomitic mudstone w/anhydrite in fenestral pore (4“) grade upward to massive dolomudstone w/anhydrite in fracture (2“), horizontal planar laminated dolomudstone and faint discontinuous planar laminated mudstone w/ black organic material and tiny displacive anhydrite in fenestral pore (10“). The sizes of nodules are less than 1/20” in diameter; missing upper contact.
4211.00(1283.51)	1.63(0.49)	DOLOMUDSTONE w/ ANHYDRITE; peloidal Dolomudstone; yellowish gray (5Y 8/1) w/ medium bluish gray (5B 5/1); massive dolomite w/ anhydrite in fenestral pore and peloidal moldic pore (7.5“) grade upward to horizontal planar laminated dolomite w/ enterolithic anhydrite at 4,211.1 ft and very thin organic laminae 4,211.73 ft (8“); above this faintly discontinuous laminated dolomite w/ anhydrite in tiny fenestral pore and peloidal moldic pore; missing upper contact.
4210.50(1283.36)	0.67(0.20)	ANHYDRITE w/ DOLOMITE; light bluish gray (5B 7/1) w/ moderate brown (5Y 7/2); coalesced nodular anhydrite w/ minor dolomitic laminae remnant; missing upper contact.
4209.83(1283.16)	0.18(0.05)	DOLOMUDSTONE w/ ANHYDRITE; dolomudstone; yellowish gray (5Y 7/2); cryptalgal wavy laminated dolomite w/ minor enterolithic structured anhydrite; gradational upper contact.
4209.65(1283.10)	0.61(0.19)	ANHYDRITE w/ DOLOMITE; light bluish gray (5B 7/1) w/ yellowish gray (5Y 7/2); coalesced nodular anhydrite w/ minor dolomitic laminae remnant; sharp and irregular upper contact.
4209.04(1282.92)	1.59(0.48)	ANHYDRITE w/ SILTSTONE, light bluish gray (5B 7/1) w/ moderate brown (5YR 3/4), relatively massive and bedded anhydrite w/ minor moderate brown silt wavy laminae remnant; gradational upper contact.
4207.45(1279.91)	2.27(0.84)	ANHYDRITE w/ DOLOMITE; light bluish gray (5B 7/1); massive bedded anhydrite w/ minor yellowish gray thin dolomitic wavy, chaotic laminae and fracture filled dolomite remnant; missing upper contact
4204.68(1281.59)	1.68(0.51)	ANHYDRITE; light bluish gray (5B 7/1); massive bedded anhydrite; missing upper contact
4203.00(1281.07)	0.21(0.37)	SILTSTONE; grayish brown (5YR 3/2); thin deformed ripple and wavy silty laminae; sharp and wavy upper contact.
4202.79(1281.01)	0.81(0.25)	ANHYDRITE; light bluish gray (5B 7/1); mosaic and massive bedded anhydrite; sharp and wavy contact.
4202.00(1280.77)	0.08(0.02)	ANHYDRITE w/ SILTSTONE; light bluish gray (5B 7/1) w/ olive gray (5Y 3/2); displacive nodular anhydrite w/ minor massive siltstone; wavy and sharp upper contact.
4201.92(1280.75)	0.19(0.06)	ANHYDRITE; light bluish gray (5B 7/1) w/ olive gray (5Y 3/2); massive and bedded anhydrite, missing upper contact.
4201.73(1280.69)	4.16(1.27)	SANDSTONE w/ ANHYDRITE; very fine-grained; light olive gray (5Y 5/2) w/ grayish brown (5B 7/1); relatively massive, mottled and faintly wavy

		laminated sandstone w/ intensive bioturbation between 4,200.5 ft and 4,201.46 ft, some rosette structured pseudomorphic anhydrite at 4201.46" and enterolithic structured anhydrite at 4,200.21 ft (14") grade upward to faint deformed wavy and ripple muddy laminated sandstone w/ displacive nodular anhydrite at 4199.32 and between 4,197.54 to 4198 (24"). It is overlain by massive and faintly discontinuous wavy laminated sandstone w/ pseudomorphic anhydrite (5"); sharp and wavy upper contact
4197.54(1279.41)	0.25(0.08)	SILTSTONE; siltstone; moderate olive brown (5Y 4/4); cryptalgal wavy laminae; sharp and wavy upper contact.
4197.29(1279.33)	0.96(0.29)	ANHYDRITE w/ SILTSTONE; light bluish gray (5B 7/1) w/ moderate olive brown (5Y 4/4); displacive pseudomorphic felted anhydrite w/ minor moderate olive brown wavy silty laminae remnant; the above this, mosaic and massive bedded anhydrite w/ minor moderate olive brown wavy silty and very fine grained sandy laminae remnant; sharp and wavy upper contact.
4196.33(1279.04)	6.33(1.93)	ANHYDRITE w/ DOLOMITE; light bluish gray (5B 7/1) w/ yellowish gray; massive bedded anhydrite w/ minor yellowish gray wavy deformed and cryptalgal dolomitic laminae (33") grades upward to relatively massive and bedded anhydrite (2.5"); the above this, massive and bedded anhydrite w/ minor yellowish gray thin dolomitic wavy, chaotic, planar and horizontal or cross laminae; Top of core interval at upper contact.
4190.00(1277.11)		

Well Name:Dibrell 3

Depth difference between core and well log: -4.5 feet in core depth

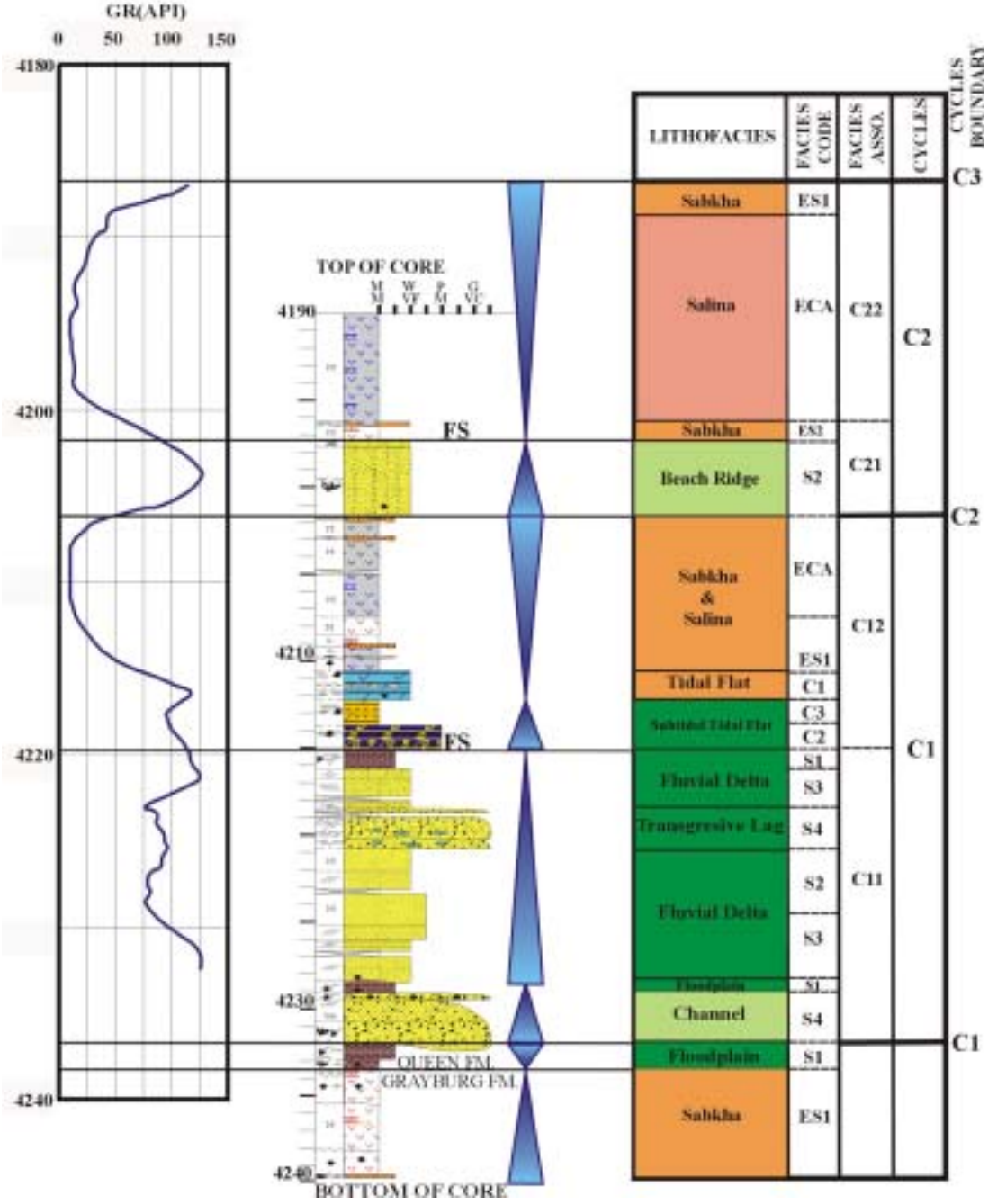

Core Description
RMM #5-23 (API #: 420031100300)
Core Depth Interval: 4448.50–4495.00 ft
Means Field, Andrews County, Texas

DEPTH (ft/m)	THICKNESS (ft/m)	DESCRIPTION
4495.00(1370.08)	0.25(0.08)	DOLOMUDSTONE w/ ORGANIC LAMINAE; dolomudstone; yellowish gray (5Y 7/2); planar horizontal organic laminated dolomudstone (2“) grades upward to algal wavy laminated dolomite (1.5”); gradational upper contact
4494.75(1370.00)	1.92(0.59)	ANHYDRITE w/ DOLOMITE; light bluish gray (5B 7/1) w/ yellowish gray (5Y 7/2); mosaic anhydrite w/ minor wavy and cryptalgal dolomitic laminae remnant (15.5“) grade upward to massive bedded anhydrite w/ minor dolomitic laminae (6.5“); missing upper contact. **TOP OF GRAYBURG FORMATION**
4492.83(1369.41)	1.13(0.34)	LOST INTERVAL.
4491.70(1369.07)	2.70(0.82)	ANHYDRTIE w/ SILTSTONE; light bluish gray (5B 7/1) w/ moderate reddish brown (10R 4/6); mosaic chicken-wire structure anhydrite w/ minor moderate reddish brown silty laminae remnant (9“) grades upward to massive anhydrite (3“); the above this distorted mosaic anhydrite w/ massive silty remnant (5“) and bedded mosaic anhydrite w/ minor silty laminae remnant (8“); missing upper contact.
4489.00(1368.25)	0.60(0.18)	LOST INTERVAL.
4488.60(1365.43)	0.20(0.06)	ANHYDRITE; light bluish gray (5B 7/1), massive anhydrite; missing upper contact.
4488.40(1368.06)	2.07(0.63)	SILTSTONE w/ ANHYDRITE; moderate reddish brown (5B 7/1) w/ dark reddish brown (10R 4/6); planar, horizontal silty laminae w/ pseudomorphic felted rosette structure anhydrite (2“). These siltstone change into deformed wavy and ripple laminae w/ deformed mud clasts and minor pseudomorphic felted anhydrite (11“); gradational or missing upper contact.
4486.33(1367.43)	1.53(0.47)	SILTSTONE; moderate reddish brown (10R 4/6); deformed wavy silty laminae w/ minor pseudomorphic felted anhydrite and many deformational structures (micro-faults and deformed mud clasts) (9.5“) grades upward to faint planar, horizontal laminated and massive siltstone (10“); gradational upper contact
4484.80(1366.97)	5.20(1.58)	ANHYDRITE w/ SILTSTONE; pale red (10R 6/2) w/ grayish red (10R 4/2); the alternation of bedded mosaic anhydrite w/ minor grayish red silty wavy laminae remnant in void (34.5“) grades upward to massive anhydrite w/ crenulated wavy silty laminae remnant in void (16“); the above this, nodular anhydrite w/ faint, discontinuous crenulated wavy silty laminae (9.5“); gradational upper contact.
4479.60(1365.38)	0.60(0.18)	SANDSTONE w/ ANHYDRITE; very fine-grained; grayish olive (10Y 4/2) w/ pale olive (5R 4/6) and moderate brown (10R 4/6); deformed wavy and chaotic laminated sandstone w/ desiccation crack at 4,479.13 ft and minor silty laminae in void; sharp and wavy upper contact.
4479.00(1365.20)	5.20(1.58)	SANDSTONE; very fine-grained; yellowish gray (5Y 7/2) w/ dusky yellow (5Y 6/4); massive sandstone w/ load, dewatering structure and scour surfaces (6“) is overlain gradationally massive and faintly discontinuous horizontal laminae and massive sandstone (20“), faintly discontinuous wavy laminated sandstone (7“), and massive sandstone w/ some burrow (16“). It is overlain by deformed wavy laminated sandstone w/ irregular oval shaped nodular and pseudomorphic anhydrite, and massive sandstone w/ pseudomorphic anhydrite (6“). The sizes of nodules is usually less than 1” in diameters; sharp and wavy upper contact.
4473.80(1363.61)	1.00(0.30)	SANDSTONE w/ ANHYDRITE; very fine-grained; light olive gray (5Y 7/2) w/ light bluish gray (5B 7/1); massive and deformed wavy and ripple laminated sandstone w/ few burrow (8“) is overlain by chaotic and some wavy algal laminated sandstone w/ load and some flame structure (4.5“); sharp and wavy upper contact.
4472.80(1363.31)	0.75(0.23)	ANHYDRITE w/ DOLOMITE; light bluish gray (5B 7/1) w/ yellowish gray (5Y 7/2); massive anhydrite w/ minor dolomitic remnant; sharp and wavy upper contact
4472.05(1363.08)	0.95(0.29)	ANHYDRITE w/ SILTSTONE; light bluish gray (5B 7/1) w/ moderate brown (5YR ¾); massive and mosaic anhydrite w/ minor cryptalgal laminated dolomite (7.5“) grades upward to nodular anhydrite w/ silty remnant in void (3“); sharp and planar upper contact.
4471.10(1362.79)	1.57(0.48)	DOLOMUDSTONE TO DOLOWACKESTONE w/ ANHYDRITE; dolomudstone to dolowackestone; yellowish gray (5Y 7/2); discontinuous

		wavy and cryptalgal laminated dolomite w/ dark organic laminae and anhydrite in peloidal moldic pores; sharp and wavy upper contact.
4469.53(1362.31)	0.53(0.16)	ANHYDRITE; light bluish gray (5B 7/1); massive bedded anhydrite; sharp and wavy upper contact.
4469.00(1362.15)	0.17(0.05)	DOLOMUDSTONE; dolomudstone; yellowish gray (5Y 7/2); cryptalgal wavy laminated dolomite w/ dark organic laminae; sharp and wavy upper contact.
4468.83(1362.10)	0.87(0.27)	ANHYDRITE w/ SILTSTONE; dusky brown (5YR 2/2) w/ light bluish gray (5B 7/1); mosaic and chicken wire structure anhydrite w/ minor deformed wavy silty laminae; sharp and wavy upper contact.
4467.96(1361.83)	0.54(0.16)	DOLOWACKESTONE w/ ANHYDRITE; peloidal dolowackestone; yellowish gray (5Y 7/2); very thin wavy dolomitic laminae; sharp and wavy upper contact.
4467.42(1361.67)	0.42(0.13)	SILTSTONE w/ ANHYDRITE; dusky brown (5YR 2/2) w/ light gray (N7); massive siltstone w/ felted rosette structured pseudomorphic anhydrite; sharp and irregular upper contact.
4467.00(1361.54)	2.30(0.70)	ANHYDRITE w/ DOLOMITE and SILTSTONE; light bluish gray (5B 7/1) w/ yellowish gray (5Y 7/2); massive anhydrite w/ faintly wavy dolomitic laminae (8“) grades upward to massive anhydrite w/ minor silty laminae remnant (15“); sharp and irregular upper contact.
4464.70(1360.84)	0.40(0.12)	SILTSTONE w/ ANHYDRITE; moderate brown (5YR 4/4) w/ light bluish gray (5B 7/1); massive siltstone w/ pseudomorphic felted anhydrite (3”) change into ripple laminated siltstone w/ small nodular anhydrite (4”); sharp and irregular upper contact.
4464.30(1370.72)	0.40(0.12)	ANHYDRITE; light bluish gray (5B 7/1) w/ moderate brown (5YR 4/4); massive anhydrite; gradational upper contact.
4463.90(1360.60)	0.87(0.27)	SILTSTONE; siltstone; moderate brown (5YR 4/4) w/ light brownish gray (5YR3/4); deformed wavy and ripple laminated siltstone. Each lamina is shown the normal grading feature; missing upper contact.
4463.13(1360.36)	0.09(0.03)	LOST INTERVAL.
4463.04(1360.33)	1.14(0.35)	SILT- to SANDSTONE; silt to very fine-grained; moderate brown (5YR3/4) w/ dusky brown (5GY 5/2); deformed chaotic wavy laminated sandstone w/ many small mud clasts and anhydrite, The primary structures was ripple laminae; gradational upper contact.
4461.90(1359.99)	4.73(1.44)	SANDSTONE w/ ANHYDRITE and MUD LAMINAE; very fine-grained; grayish yellow green (5GY 7/2) w/ dusky yellow green (5GY 5/2); deformed and chaotic wavy laminated sandstone w/ pseudomorphic felted anhydrite (5“); the above this, deformed structured and massive sandstone w/ slumping, micro-faults and loading structures (14“), deformed chaotic cryptalgal muddy laminated sandstone (10.5“), massive sandstone w/ pseudomorphic anhydrite (2“), and chaotic deformed cryptalgal and wavy muddy laminated sandstone w/ small nodular anhydrite. The sizes of nodules are 1/10 to 5/10“ in diameter; missing upper contact.
4457.17(1358.55)	0.15(0.05)	LOST INTERVAL.
4457.00(1358.49)	2.70(0.82)	ANHYDRITE w/ DOLOMITE; light bluish gray (5B 7/1) w/ dusky yellow (5Y 6/4); massive bedded anhydrite w/ minor dusky yellow crenulated wavy laminae (12.5“) grades upward to chaotic dolomitic laminae (8“) and continuous, wavy dolomitic laminae (17.5“); gradational upper contact.
4454.10(1357.61)	0.40(0.12)	ANHYDRITE w/ SILTSTONE; light brownish gray (5YR 6/1) w/ grayish olive (10Y 4/2); mosaic anhydrite w/ minor grayish olive silty laminae remnant; sharp and wavy upper contact.
4453.70(1357.49)	2.70(0.82)	ANHYDRITE w/ DOLOMITE; light bluish gray (5B 7/1) w/ yellowish gray (5Y 7/2); massive and faint deformed chaotic wavy dolomitic laminae including anhydrite w/ some solution and collapsed breccia between 4,452.9 ft and 4,453.15 ft.; missing upper contact.
4450.00(1356.36)	2.50(0.76)	ANHYDRITE w/ DOLOMITE; light bluish gray (5B 7/1) w/ yellowish gray (5Y 7/2); massive anhydrite w/ minor chaotic deformed wavy dolomitic laminae; Top of core interval at upper contact
4448.50(1355.90)		

Well Name:RMM 5-23

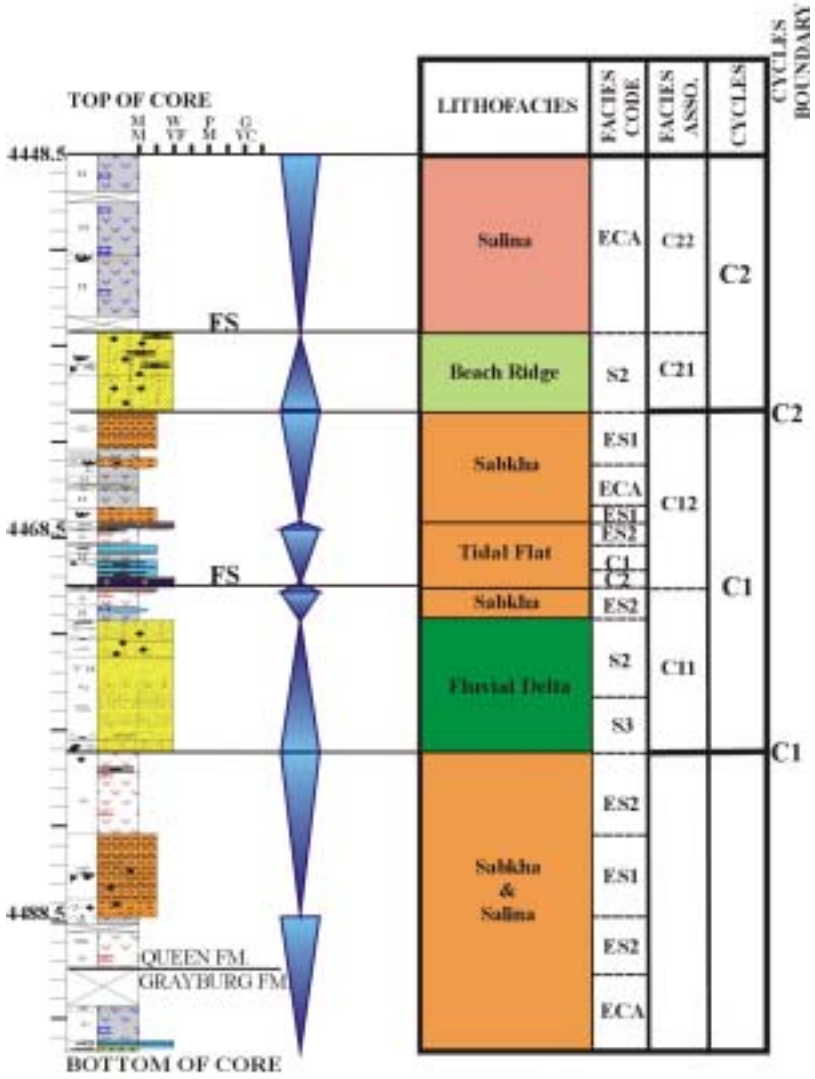

Core Description
R. M. Means # 10-51 (API #: 420033325800)
Core Depth Interval: 4078.00-4116.08 ft
Means Field, Andrews County, Texas

DEPTH (ft/m)	THICKNESS (ft/m)	DESCRIPTION
4116.08(1254.58)	2.08(0.63)	SILT- to SANDSTONE; silt to very fine-grained; pale olive (10Y 6/2) to light olive gray (5Y 5/2); deformed muddy and silty laminae due to the growth of displacive pseudomorphic anhydrite. The deformed wavy laminated mudstone grades upward to deformed wavy laminated mudstone w/ mud clasts and collapsed breccia; sharp and planar upper contact.
4114.00(1253.94)	5.95(1.82)	SANDSTONE w/ ANHYDRITE; very fine to fine-grained; pale olive (10Y 6/2) to light olive gray (5Y 5/2) w/ medium bluish gray (5B 5/1); massive and mottled sandstone w/ burrow and very small displacive anhydrite between 4114.00' and 4112.60'. The sizes of displacive anhydrite in diameter range from 1/10" X 2/10" to 3/10"; above this, faintly discontinuous wavy and ripple laminated sandstone (2.5") grades upward to faintly discontinuous and continuous planar cross laminated sandstone w/ elongated, ellipsoidal nodular anhydrite and some burrows (29"). The sizes of anhydrite nodules range from 1/20 X1/20" to 1/10 X 8/10". It is overlain by deformed wavy and ripple cross-laminated sandstone due to the growth of very tiny anhydrite and haloturbation (9"); gradational upper contact.
4108.05(1252.13)	1.05(0.32)	DOLOMUDSTONE w/ ANHYDRITE; yellowish gray (5Y 7/2) w/ medium bluish gray (5B 5/1); wavy algal laminated dolomudstone w/ displacive anhydrite in fenestral pores and collapsed breccia. The sizes of anhydrite of fenestral pore in diameter range from 2/10 X 2/10" to 1 X 3/10"; gradational upper contact.
4107.00(1251.81)	2.00(0.61)	ARGILLACEOUS DOLOMUDSTONE w/ ANHYDRITE; light olive gray (5Y 5/2) w/medium bluish gray (5B 5/1); massive dolomudstone w/ anhydrite in fenestral pores grades upward to faintly discontinuous planar horizontal laminated dolomudstone w/ small anhydrite in birds eye pores. The sizes of birds eyes range from 3/10 X 3/10" to 1 X 3/10"; sharp and planar upper contact.
4105.00(1251.20)	1.50(0.46)	DOLOMUDSTONE w/ ANHYDRITE; yellowish gray (5Y 7/2) w/ medium bluish gray (5B 5/1); wavy algal laminated dolomite w/ elongated, ellipsoidal anhydrite in fracture and some collapsed breccia; missing upper contact.
4103.50(1250.75)	0.40(0.12)	LOST INTERVAL
4103.10(1250.62)	5.39(1.64)	DOLOMUDSTONE to DOLOWACKESTONE w/ ANHYDRITE; yellowish gray (5Y 7/2) to pale olive (10Y 6/2) w/ medium bluish gray (5B 5/1); well developed wavy algal laminated dolomudstone w/ anhydrite in birds eyes structure and stylolite (30.5") grade upward to relatively massive and some wavy algal laminated dolomite w/ less anhydrite in fenestral pores (13"). The sizes of pores ranges from 1/10 X 1/10" to 6/10 X 7/10"; above this, massive dolomite w/ sparse tiny anhydrite (4") and very thin slightly wavy and planar laminated peloidal and skeletal dolowackestone w/ displacive anhydrite in moldic peloidal pores (12"); sharp and irregular upper contact.
4097.71(1248.98)	0.33(0.10)	ANHYDRITE; medium bluish gray (5B 5/1); mosaic and massive bedded anhydrite; gradational upper contact.
4097.38(1248.88)	0.38(0.12)	DOLOMUDSTONE; peloidal dolomudstone; yellowish gray (5Y 7/2) to pale olive (10Y 6/2); slightly wavy low angle cross-laminated peloidal dolomudstone w/ vertical fracture; missing upper contact.
4097.00(1248.77)	0.50(0.15)	LOST INTERVAL
4096.50(1248.61)	1.10(0.34)	ANHYDRITE w/ DOLOMITE; medium bluish gray (5B 5/1) w/ yellowish gray (5Y 7/2); mosaic anhydrite w/minor remnant dolomitic and wavy algal laminae, and some collapsed breccia in void (6") grades upward to relatively more massive anhydrite w/ wavy dolomitic algal laminae and caliche (5.5"); sharp wavy upper contact.
4095.40(1248.28)	0.58(0.18)	ANHYDRITE w/ SILTY SANDSTONE; medium bluish gray (5B 5/1) w/ dusky brown (5YR 3/2); mosaic and coalesced nodular anhydrite w/ minor thin silty wavy laminae, the coalesced nodules are similar to flowage structure. The size of nodules is 5/10 X 5/10"; sharp and wavy upper contact.
4094.82(1248.10)	0.15(0.05)	ANHYDRITE; medium bluish gray (5B 5/1) w/ yellowish gray (5Y 7/2), massive anhydrite; sharp and wavy upper contact
4094.67(1248.06)	0.80(0.24)	ANHYDRITE w/ DOLOMITE; medium bluish gray (5B 5/1) w/ yellowish gray (10Y 8/2); massive anhydrite w/ faintly discontinuous dolomitic cross-laminae (9.5") is overlain by massive anhydrite w/ faintly discontinuous cross dolomite laminae (26"); missing upper contact.

4093.87(1247.81)	0.27(0.08)	LOST INTERVAL.
4093.60(1247.73)	1.50(0.46)	ANHYDRITE w/ DOLOMITE; medium bluish gray (5B 5/1) w/ pale greenish yellow (10Y 8/2); massive anhydrite w/ minor dolomitic wavy and horizontal laminae remnant in fracture. The spacing of each lamina is about 1/10“; sharp and truncated upper contact.
4092.10(1247.27)	0.30(0.09)	SANDSTONE; very fine-grained; moderate brown (5YR 4/4); the most part of bed is composed of massive sandstone except some wavy laminae at 4,191.8 ft. The sharp scour surface is found at the bottom of bed (4,921.1 ft); sharp and wavy upper contact.
4091.80(1247.18)	0.35(0.11)	ANHYDRITE; medium bluish gray (5B 5/1); massive anhydrite w/ minor dusky brown silty laminae; missing upper contact.
4091.45(1247.07)	0.25(0.08)	LOST INTERVAL.
4091.20(1246.99)	1.10(0.34)	ANHYDRITE w/ SILTSTONE; medium bluish gray (5B 5/1) w/ dusky brown (5YR 2/2); mosaic and massive anhydrite w/ minor dusky silty laminae; sharp and wavy upper contact
4090.10(1246.66)	0.20(0.06)	SILTSTONE w/ ANHYDRITE; dusky brown (5YR 2/2) w/ medium bluish gray (5B 5/1); massive siltstone w/ irregular shaped nodular anhydrite; sharp and wavy upper contact.
4089.90(1246.60)	1.00(0.30)	ANHYDRITE w/ SILTSTONE; medium bluish gray (5B 5/1) w/ dusky brown (5YR 2/2); massive anhydrite w/ minor thin dusky brown silty laminae; sharp and wavy upper contact.
4088.90(1246.30)	0.25(0.07)	SANDSTONE; very fine-grained; moderate brown (5YR 2/2) w/ grayish brown (5B 5/1); deformed wavy laminae and wavy algal laminae; missing upper contact.
4088.65(1246.22)	1.05(0.32)	SANDSTONE w/ ANHYDRITE; very fine-grained; moderate brown (5YR 4/4) w/ grayish brown (5YR 3/2); deformed ripple and wavy laminated sandstone due to haloturbation; sharp and planar upper contact.
4087.90(1245.99)	0.85(0.26)	SANDSTONE; very fine-grained; pale olive (10Y 6/2) w/ grayish olive (10Y 4/2); massive and ripple cross-laminated sandstone; sharp and planar upper contact.
4087.05(1245.73)	0.25(0.08)	ANHYDRITE w/ DOLOMITE; medium bluish gray (5B 5/1) w/ yellowish gray (5Y 7/2); mosaic anhydrite w/ remnant dolomitic laminae; sharp and planar upper contact.
4086.80(1245.66)	1.40(0.43)	SANDSTONE w/ ANHYDRITE; very fine-grained; pale olive (10Y 6/2) w/ medium bluish gray (5B 5/1); massive and mottled sandstone w/ nodular anhydrite, The sizes of anhydrite nodules range from 2/10X2/10“ to 3/10 X 5/10“; gradational upper contact.
4085.40(1245.23)	0.40(0.12)	SANDSTONE; very fine-grained; dusky yellow (5Y 6/4) w/ pale olive (10Y 6/2); planar horizontal algal laminated sandstone; missing upper contact
4085.00(1245.11)	0.20(0.06)	LOST INTERVAL.
4084.80(1245.05)	4.95(1.51)	SANDSTONE w/ ANHYDRITE; very fine- to fine-grained; pale olive (10Y 6/2) w/ olive gray (5Y 5/2); algal and ripple laminated sandstone w/ muddy laminae and some load structure (35”) grades upward to algal wavy laminated and stacked ripple sandstone (10”) w/ small sparse anhydrite. The sizes of anhydrite is less than 1/20“; sharp and planar upper contact.
4079.85(1243.54)	1.85(0.56)	ANHYDRITE w/ DOLOMITE; medium bluish gray (5B 5/1) w/ yellowish gray (5Y 7/2); massive anhydrite w/ the alternation of very thin horizontal, slightly wavy dolomitic laminae (7“ to 12“) and thick wavy dolomitic laminae (3“); Top of core interval at upper contact.
4078.00(1242.97)		

Well Name:RMM10-51

Depth difference between core and well log: +3 feet in core depth

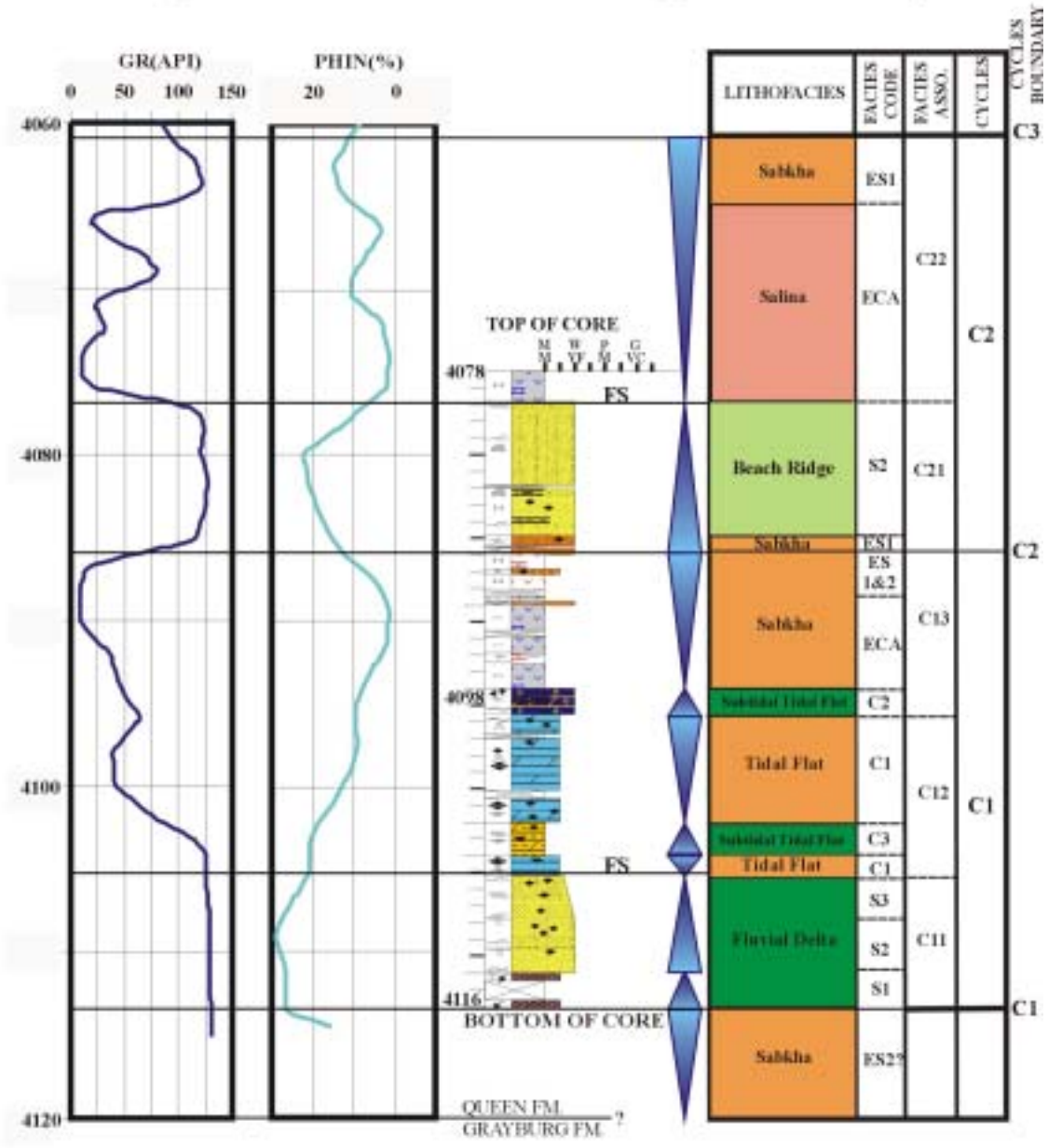

Core Description
R.M. Means #23-19 (API #: 420033334800)
Core Depth Interval: 4110.0–4170.3 ft
Means Field, Andrews County, Texas

DEPTH (ft/m)	THICKNESS (ft/m)	DESCRIPTION
4170.30(1271.11)	0.51(0.16)	ANHYDRITE; light bluish gray (5B 5/1); massive anhydrite and some wavy laminated anhydrite 4070 ft; wavy and sharp upper contact
4169.79(1270.95)	0.46(0.14)	ANHYDRITE w/ SILTSTONE; grayish orange pink (5YR 7/2) w/ moderate brown (5YR3/4); mosaic or nodular anhydrite w/ minor deformed silty remnant. The brecciated anhydrite horizon is found between 4169.63 to 4169.79 ft; wavy and sharp upper contact.
4169.33(1270.81)	0.72(0.22)	ANHYDRITE w/ SILTSTONE; grayish orange pink (5YR 7/2) w/ moderate brown (5YR 4/4); massive anhydrite (2“) grades upward to relatively mosaic anhydrite w/ minor silt remnant in fracture. The desiccation crack is found at 4,169.08 ft; missing upper contact.
4168.61(1270.59)	0.08(0.02)	LOST INTERVAL.
4168.53(1270.57)	0.96(0.29)	ANHYDRITE w/ SILTSTONE; grayish orange pink (5YR 7/2) w/ moderate brown (5YR 4/4); coalesced nodular anhydrite w/ minor moderate silty remnant (5.5“) grades upward to mosaic anhydrite w/ minor siltstone (6.5“); gradational upper contact.
4167.57(1270.28)	0.76(0.23)	ANHYDRITE; medium bluish gray (5B 7/1); relatively massive anhydrite w/ small fracture; wavy and sharp upper contact.
4166.81(1270.04)	0.86(0.26)	SILTSTONE w/ ANHYDRITE; medium bluish gray (5B 7/1) w/ moderate brown (5YR 4/4); massive siltstone w/ ellipsoid and irregular shaped nodular and enterolithic structured anhydrite, which ranges from 0.5 to 1“ in diameter (3“); the above this, discontinuous wavy laminated siltstone w/ load cast at 4,166.3 ft (1.5“). It is overlain by thin enterolithic structured anhydrite (1“) and discontinuous wavy laminated siltstone (3“); wavy and sharp upper contact
4165.95(1269.78)	0.27(0.08)	ANHYDRITE; medium bluish gray (5B 7/1); massive anhydrite; missing upper contact.
4165.68(1269.70)	0.21(0.06)	LOST INTERVAL.
4165.47(1269.64)	0.74(0.23)	ANHYDRITE w/ DOLOMITE; light bluish gray (5B 5/1); clear massive anhydrite w/ dolomitic remnant laminae (2“) grades upward to mosaic anhydrite w/ minor dolomitic remnant (10“). The size of nodule is less than 4/10“; missing upper contact.
4164.73(1269.41)	0.98(0.30)	ANHYDRITE w/ SILTSTONE; moderate brown (5YR3/4) and light bluish gray (5B 5/1); thin pseudomorphic felted anhydrite (2/10X 7/10”) w/ faintly discontinuous wavy laminated siltstone (1“) is underlain by massive anhydrite w/ minor silty remnant in fracture (2.5“); missing upper contact.
4163.75(1269.11)	1.60(0.49)	LOST INTERVAL
4162.15(1268.62)	1.73(0.53)	ANHYDRITE w/ SILTSTONE; grayish orange pink (5YR 7/2) w/ moderate brown (5YR 3/4); coalesced nodular anhydrite w/ minor silty remnant (10“) grades upward to thin-bed mosaic (10“) anhydrite w/ minor silty remnant; sharp (?) upper contact.
4160.42(1268.10)	0.07(0.02)	SILTSTONE w/ ANHYDRITE; grayish orange pink (5YR 7/2) w/ moderate brown (5YR3/4); thin massive siltstone w/ pseudomorphic felted anhydrite; gradational upper contact.
4160.35(1268.07)	0.94(0.29)	ANHYDRITE; light bluish gray (5B 5/1); massive bedded anhydrite that is more or less mosaic appearance w/ minor dolomitic remnant in fracture at 4160 ft; sharp and wavy upper contact.
4159.41(1267.80)	0.17(0.05)	SANDSTONE w/ ANHYDRITE; pale yellowish brown (10YR 6/2) w/ light bluish gray (5B 5/1); very fine-grained; massive and faint ripple laminated sandstone w/ scour surface at 4,159.41 ft; missing upper contact.
4159.24(1267.74)	0.10(0.03)	LOST INTERVAL.
4159.14(1267.71)	1.64(0.50)	ANHYDRITE w/ SILTSTONE; grayish orange pink (5YR 7/2) w/ moderate brown (5YR3/4); massive and deformed wavy laminated siltstone (1“) interbedded with thick enterolithic and coalesced nodular anhydrite w/ moderate brown silty remnant (6 to 12“). The anhydrite bed is thicker with upward. The collapsed breccia and micro-fault are found at 4,158.5 ft; sharp and wavy upper contact.
4157.50(1267.21)	0.50(0.15)	SILTSTONE w/ ANHYDRITE; moderate brown (5YR3/4) w/ light bluish gray (5B 5/1); massive and deformed laminated siltstone w/ mosaic and nodular anhydrite; gradational upper contact.
4157.00(1267.05)	1.36(0.41)	ANHYDRITE; light bluish gray (5B 5/1) w/ moderate brown (5YR3/4); massive and mosaic anhydrite; sharp and wavy upper contact.

4155.64(1266.64)	2.04(0.62)	ANHYDRITE w/ SILTSTONE; light bluish gray (5B 5/1) w/ moderate brown (5YR 4/4); thick coalesced nodular anhydrite w/ minor silty background (6 to 13“) grades upward to relatively thin bed massive anhydrite (3 to 6“). The massive anhydrite is thicker with upward; sharp and wavy upper contact.
4153.60(1266.02)	0.07(0.02)	SILTSTONE; moderate brown (5YR 4/4); massive siltstone; missing upper contact.
4153.53(1265.99)	0.20(0.06)	LOST INTERVAL.
4153.33(1265.93)	1.13(0.34)	ANHYDRITE w/ SILTSTONE; light bluish gray (5B 5/1) w/ moderate brown (5YR3/4); mosaic anhydrite w/ minor moderate brown silty remnant; sharp and wavy upper contact.
4151.38(1265.34)	0.62(0.19)	ANHYDRITE; light bluish gray (5B 5/1) w/ moderate brown (5YR3/4); mosaic anhydrite; missing upper contact.
4150.76(1265.15)	0.07(0.02)	LOST INTERVAL.
4150.69(1265.13)	1.94(0.59)	ANHYDRITE w/ SILTSTONE; light bluish gray (5B 5/1) w/ moderate brown (5YR ¾); the alternation of massive and mosaic anhydrite w/ minor moderate brown silty remnant; sharp and wavy upper contact. **TOP OF GRAYBURG FORMATION.**
4148.75(1264.54)	0.21(0.06)	ANHYDRITE w/ SILTSTONE; light bluish gray (5B 5/1) w/ moderate brown (5YR3/4); pseudomorphic felted and coalesced nodular anhydrite w/ minor massive siltstone remnant. The content of silt increase with upward; sharp and wavy upper contact
4148.54(1264.47)	0.68(0.21)	ANHYDRITE; light bluish gray (5B 5/1); thick-bed mosaic anhydrite; missing upper contact
4147.86(1264.27)	0.13(0.04)	LOST INTERVAL.
4147.73(1264.23)	0.03(0.01)	MUDSTONE; olive gray (5Y 3/2); thin-bed slight planar cross-laminated mudstone; sharp and planar upper contact.
4147.70(1264.22)	0.24(0.07)	ANHYDRITE w/ DOLOMITE; light bluish gray (5B 7/1) w/ yellowish gray (5Y 5/2); solution breccia dolomite in fracture w/ bedded massive anhydrite; sharp and wavy upper contact.
4147.46(1264.15)	0.86(0.26)	ANHYDRITE w/ SILTSTONE; light bluish gray (5B 7/1) w/ moderate brown (5YR 5/2); coalesced nodular anhydrite w/ minor silty remnant (8“) grades upward to discrete nodular anhydrite (5/10X1“) w/ more including silty remnant; sharp and wavy upper contact.
4146.60(1263.88)	2.78(0.85)	ANHYDRITE; light bluish gray (5B 7/1) w/ grayish olive; bedded massive anhydrite (8“) is overlain by more mosaic shaped anhydrite (22.5“) w/ wavy lamination in local, pseudomorphic felted displacive anhydrite (1“) and back to massive anhydrite (2.5“); sharp and wavy upper contact.
4143.82(1263.04)	0.82(0.25)	SILTSTONE w/ ANHYDRITE; pale brown (5YR 5/2) w/ moderate brown (5YR ¾); deformed wavy laminated siltstone w/ pseudomorphic felted anhydrite (1“) grades upward to massive siltstone w/ rosette structured pseudomorphic displacive anhydrite (9.5“); gradational upper contact.
4143.00(1262.79)	0.77(0.23)	ANHYDRITE w/ SILTSTONE; pale brown (5YR 5/2) w/ moderate brown (5YR ¾); coalesced nodular anhydrite w/ minor moderate brown silty remnant (3.5“) grades upward to mosaic anhydrite (5“) w/ siltstone; sharp and planar upper contact.
4142.23(1262.55)	0.23(0.07)	ANHYDRITE; light bluish gray (5B 7/1) w/ moderate brown (5YR ¾); massive anhydrite (2.5“); missing upper contact
4142.00(1262.48)	0.08(0.02)	LOST INTERVAL.
4141.92(1262.46)	0.32(0.10)	ANHYDRITE; light bluish gray (5B 7/1); massive anhydrite; wavy and sharp upper contact
4141.60(1262.36)	1.33(0.41)	SILT- to SANDSTONE w/ ANHYDRITE; silt- to very fine-grained; light olive gray (5Y 5/2) w/ light bluish gray (10Y 4/2); thick-bed ripple to wavy laminated and deformed wavy laminated sandstone w/ displacive pseudomorphic felted anhydrite (14“) is overlain by massive sandstone w/ nodular anhydrite (3“); missing upper contact.
4140.27(1261.95)	0.39(0.12)	SANDSTONE; fine-grained sandstone; light olive gray (5Y 5/2) w/ grayish olive (10Y 4/2); massive sandstone w/ rip-up mud clasts and scour surface at 4,140.27 ft; missing upper contact.
4139.88(1261.84)	0.25(0.08)	LOST INTERVAL.
4139.63(1261.76)	0.13(0.04)	SILT- to SANDSTONE; silt- to very fine-grained; light olive gray (5Y 5/2) w/ grayish olive (10Y 4/2); thin massive sandstone; wavy and sharp upper contact
4139.50(1261.72)	3.33(1.01)	SILT- to SANDSTONE; silty to very fine-grained; light olive gray (5Y 5/2) w/ grayish olive (10Y 4/2); deformed ripple cross laminated very fine sandstone w/ burrow (6.5“) grades upward to algal wavy laminated sandstone

		w/ organic-rich laminae (11“), convolute laminated silty to very fine grained sandstone w/ load cast (2“); the above this, massive and faintly wavy laminated sandstone w/ small anhydrite (6“), and deformed wavy lamination w/ load cast by syn- and postdepositional loading (5.5“). The size of nodule at 4,137 ft is less than 1/20“; gradational upper contact.
4136.17(1260.70)	1.22(0.37)	SILT- to MUDSTONE; light bluish gray (5Y 6/4) w/ olive gray (5Y 5/2); deformed wavy laminated sandstone w/ many kinds of slumping and load structures such as micro-faults, rip-up mud clasts and deformed laminae; missing upper contact.
4134.95(1260.33)	0.09(0.03)	LOST INTERVAL.
4134.86(1260.30)	0.25(0.08)	SILT- to MUDSTONE; dusky yellow (5Y 6/4) w/pale olive (10Y 6/2); deformed wavy laminae by loading; gradational upper contact.
4134.61(1260.23)	0.91(0.28)	SILT- to SANDSTONE w/ MUD; silt- to very fine-grained sandstone; dusky yellow (5Y 6/4) w/ pale olive (10Y 6/2); convolute folded laminated sandstone by syndeformational activity w/ mud flake; sharp and wavy upper contact.
4133.70(1259.95)	0.25(0.07)	SANDSTONE; very fine- to fine-grained; pale olive (10Y 6/2); massive sandstone; sharp and wavy upper contact
4133.45(1259.88)	1.81(0.55)	SILT- to SANDSTONE w/ MUD; silt- to very fine-grained sandstone; dusky yellow (5Y 6/4); massive sandstone grades upward to discontinuous faint planar horizontal laminated sandstone w/ some burrow; missing upper contact.
4131.64(1259.32)	0.20(0.06)	SANDSTONE; fine-grained sandstone; dusky yellow (5Y 6/4); massive sandstone w/ burrow; missing upper contact.
4131.44(1259.26)	0.08(0.02)	LOST INTERVAL.
4131.36(1259.24)	1.79(0.55)	SAND- to SILTSTONE w/ MUD; silt- to very fine- grained sandstone; dusky yellow (5Y 6/4) w/ light bluish gray (5B 7/1); massive sandstone w/ rip-up mud clasts and burrow (5.5“) grades upward to the alternation of ripple laminated sandstone (4 to 6“) and faintly discontinuous planar horizontal laminae (4”) w/ reworked nodular anhydrite (2/10X2/10“ in diameter) (4“).; missing upper contact.
4129.57(1258.69)	0.65(0.20)	SANDSTONE; dusky yellow (5Y 6/4); faintly planar horizontal laminated sandstone w/ nodular anhydrite (3/10X3/10“ in diameter); missing upper contact.
4128.92(1258.49)	0.81(0.25)	SILT- to SANDSTONE; silt- to very fine-grained sandstone; yellowish gray (5Y 7/2) w/ pale olive (10Y 6/2); ripple cross laminae (3“) grades upward to very thin planar horizontal laminae (0.5“), very thin ripple cross laminae (1“), very thin planar cross laminae (1.5“) and very thin planar horizontal laminae (3“); missing upper contact.
4128.21(1258.28)	0.09(0.03)	LOST INTERVAL.
4128.13(1258.25)	1.43(0.44)	SILT- to SANDSTONE; silt- to very fine-grained sandstone; dusky yellow (5Y 6/4) w/ light bluish gray (5B 7/1); wavy and ripple cross laminated sandstone (8“) grades upward to massive sandstone w/ nodular anhydrite (2/10X2/10” to 8/10X8/10“ in diameter) and deformed wavy laminated sandstone (6“); sharp and planar upper contact
4126.70(1257.81)	0.20(0.06)	DOLOMUDSTONE; dolomudstone; olive gray (5Y 3/2); very thin organic rich horizontal planar laminae; gradational upper contact
4126.50(1257.75)	1.77(0.54)	DOLOMUDSTONE w/ ANHYDRITE; dolomudstone; yellowish gray (5Y 7/2) w/ light bluish gray (5B 7/1); cryptalgal laminated dolomite w/ enterolithic and nodular anhydrite (5.5“) grades upward to brecciated dolomite intraclasts w/ horse tail stylolite (5.5“), massive dolomite (1“) and wavy laminated dolomite (4“).; missing upper contact
4124.73(1257.22)	0.08(0.02)	LOST INTERVAL.
4124.65(1257.19)	0.08(0.02)	DOLOMUDSTONE; dolomudstone; grayish olive (10Y 4/2); remnant wavy laminated dolomite grades upward to organic rich wavy laminated dolomite w/ stylolite; sharp and planar upper contact
4124.57(1257.17)	0.34(0.10)	DOLOMUDSTONE w/ ANHYDRITE; dolomudstone; yellowish gray (5Y 7/2) w/ light bluish gray (5B 7/1); birds eye structured dolomite (2“) grades upward to wavy laminated dolomite w/ nodular anhydrite (2.5“); sharp and wavy upper contact
4124.23(1257.07)	0.08(0.02)	DOLOMUDSTONE; dolomudstone; grayish olive (10Y 4/2); massive dolomite; gradational upper contact
4124.15(1257.04)	2.39(0.73)	DOLOMUDSTONE TO DOLOWACKESTONE w/ ANHYDRITE; dolomudstone to peloidal dolowackestone; yellowish gray (5Y 7/2) w/ light bluish gray (5B 7/1); massive dolomite w/ nodular anhydrite, organic wavy laminae, and stylolite (7“) grades upward to ripple cross and wavy laminated

		dolomite w/ anhydrite w/ sheet crack and bird's eye structure (8.5") and then faint wavy dolomitic laminae w/elongated ellipsoidal to oval-shaped fenestral fabric anhydrite (1X3/10" to less than 1/20"); gradational upper contact
4121.76(1256.31)	1.68(0.52)	DOLOWACKESTONE w/ ANHYDRITE; peloidal dolowackestone; yellowish gray (5Y 7/2) w/ light bluish gray (5B 7/1); remnant wavy laminated dolomite w/ fenestral fabric very tiny anhydrite (4.5") grades upward to relatively massive and faintly wavy laminated dolomite w/ coalesced nodular anhydrite and stylolite. The sizes of nodule range from 3/10X5/10" to 1X1" in diameter; gradational upper contact
4120.08(1255.80)	0.60(0.18)	DOLOMUDSTONE; dolomudstone; yellowish gray (5Y 7/2); remnant discontinuous wavy laminated dolomite w/ small anhydrite (2.5") grades upward to more deformed wavy laminated dolomite (5.5"); gradational upper contact
4119.48(1255.62)	0.56(0.17)	DOLOMUDSTONE w/ ANHYDRITE; dolomudstone; yellowish gray (5Y 7/2) w/ light bluish gray (5B 7/1); massive dolomite w/ coalesced nodular anhydrite, vertical fractures and organic rich laminae (5") grades upward to planar cross laminated w/ coalesced nodular anhydrite. The sizes of nodule range from less than 1/20 to 2X2" in diameter and 2" in thick; missing upper contact
4118.92(1255.45)	0.08(0.02)	LOST INTERVAL.
4118.84(1255.42)	0.84(0.26)	DOLOMUDSTONE w/ ANHYDRITE; dolomudstone; yellowish gray (5Y 7/2) w/ light bluish gray (5B 5/1); wavy laminated dolomite w/ stylolite and coalesced nodular anhydrite. The sizes of nodule range from less than 1/20" to 7/10"X1.5"; sharp and planar upper contact.
4118.00(1255.16)	0.30(0.09)	ANHYDRITE; light bluish gray (5B 5/1); massive anhydrite; gradational upper contact.
4117.70(1255.07)	0.66(0.20)	ANHYDRITE w/ SILTSTONE; light bluish gray (5B 5/1) w/ grayish brown (5YR 5/2); enterolithic anhydrite w/ minor siltstone remnant in fracture (5") grades upward to mosaic anhydrite w/ wavy laminated siltstone (3"); gradational upper contact.
4117.04(1254.87)	0.65(0.20)	ANHYDRITE; light bluish gray (5B 7/1); massive anhydrite; gradational upper contact.
4116.39(1254.68)	0.29(0.09)	ANHYDRITE w/ SILTSTONE; light bluish gray (5B 7/1) w/ grayish brown (5YR 5/2); mosaic anhydrite w/ minor grayish brown silt remnant; gradational upper contact
4116.10(1254.59)	0.58(0.18)	ANHYDRITE; light bluish gray (5B 7/1); massive anhydrite grades upward to discontinuous remnant wavy laminated anhydrite; gradational upper contact
4115.52(1254.41)	1.10(0.34)	ANHYDRITE w/ SILTSTONE; light bluish gray (5B 7/1) w/ grayish brown (5YR 5/2); massive anhydrite w/ minor silt remnant grades upward to mosaic anhydrite w/ silt remnant; gradational upper contact
4114.42(1254.08)	0.12(0.04)	SILTSTONE; pale brown (5YR 5/2); massive siltstone; gradational upper contact
4114.30(1254.04)	1.17(0.36)	ANHYDRITE; light bluish gray (5B 7/1); massive anhydrite; sharp and wavy upper contact
4113.13(1253.68)	0.17(0.05)	SILT- to MUDSTONE; pale brown (5YR 5/2); deformed wavy laminated siltstone w/ scour surface at 4,113.13 ft; missing upper contact
4112.96(1253.63)	0.08(0.02)	LOST INTERVAL.
4112.88(1253.61)	0.88(0.27)	SILT- to SANDSTONE w/ ANHYDRITE; silt- to very fine-grained sandstone; pale brown (5YR 5/2) w/ light bluish gray (5B 7/1); continuous ripple cross laminated silt- to sandstone w/ minor pseudomorphic felted displacive anhydrite in local (5.5") grades upward to discontinuous deformed wavy and ripple laminated sandstone w/ pseudomorphic displacive anhydrite (6"); sharp and wavy upper contact
4112.00(1253.34)	2.00(0.61)	SANDSTONE w/ ANHYDRITE; pale olive (10Y 6/2) w/ medium bluish gray (5B 5/1); deformed ripple cross laminated sandstone w/ displacive pseudomorphic felted anhydrite in local (9") grades upward to non-deformed ripple laminated sandstone (2") and relatively massive sandstone w/ coalesced nodular anhydrite in local (10.5"); Top of core interval at upper contact
4110.00(1252.73)		

Core Description
R.M. Means #9-25 (API #: 420033334900)
Core Depth Interval: 4266.0–4312.3 ft
Means Field, Andrews County, Texas

DEPTH (ft/m)	THICKNESS (ft/m)	DESCRIPTION
4312.30(1314.39)	0.65(0.20)	DOLOMUDSTONE w/ ANHYDRITE; yellowish gray (5Y 7/2) w/ medium bluish gray (5B 5/1); slightly planar horizontal laminated dolomite grades upward to deformed planar cross laminated dolomite w/ elongated displacive anhydrite in local; gradational and irregular upper contact
4311.65(1314.19)	0.58(0.18)	ANHYDRITE w/ MUDSTONE and DOLOMITE; grayish red (10R3/4) w/ yellowish gray (5Y 7/2); mosaic anhydrite w/ void filled dolomite (6“) grades upward to slightly very thin planar cross laminated Anhydrite w/ dolomite and mudstone (2.5“); wavy and sharp upper contact.
4311.07(1314.01)	0.63(0.19)	ANHYDRITE w/ MUDSTONE; pinkish gray (5YR 6/1); massive, more mosaic anhydrite (7“); missing upper contact.
4310.44(1313.82)	0.08(0.02)	LOST INTERVAL.
4310.36(1313.80)	0.53(0.16)	ANHYDRITE w/ MUDSTONE and DOLOMITE; grayish red (5R 4/2); massive and mosaic anhydrite (2.5“) grades upward to planar cross laminated anhydrite w/ remnant algal lamination (3“); gradational upper contact.
4309.83(1313.64)	1.71(0.52)	ANHYDRITE w/ DOLOMITE; medium bluish gray (5B 5/1) w/ yellowish gray (5Y 7/2); massive anhydrite (20“) w/ dolomitic remnant in void at the middle part of bed; sharp and planar upper contact.
4308.12(1313.11)	0.21(0.06)	MUDSTONE w/ ANHYDRITE; grayish red (5R 4/2) w/ medium bluish gray (5B 5/1); ripple laminated mudstone (1“) grades upward to massive mudstone w/ displacive anhydrite and small sparse distributed nodular anhydrite (3“); gradational upper contact
4307.91(1313.05)	0.18(0.05)	ANHYDRITE w/ DOLOMITE; medium bluish gray (5B 5/1) w/ yellowish gray (5Y 7/2); massive anhydrite w/ minor wavy dolomitic laminae; gradational upper contact.
4307.73(1313.00)	0.39(0.12)	ANHYDRITE w/ MUDSTONE; moderate brown (5R 6/2) w/ medium bluish gray (5B 5/1); elongated coalesced nodular anhydrite (1X1.75“) w/massive muddy remnant in void (3.5“) grades upward to nodular anhydrite w/ deformed wavy and ripple muddy laminae (1.5“); upper gradational upper contact.
4307.34(1312.88)	0.73(0.22)	ANHYDRITE w/ DOLOMITE; medium bluish gray (5B 5/1) w/ medium gray (N5); massive anhydrite w/ irregular deformed dolomitic laminae; sharp and planar upper contact.
4306.61(1312.65)	0.11(0.03)	MUDSTONE; moderate brown (5YR 4/4); massive mudstone; sharp and wavy upper contact.
4306.50(1312.62)	2.37(0.72)	Interbedded ANHYDRITE w/ MUDSTONE and DOLOMITE; medium bluish gray (5B 5/1) w/ moderate brown (5R 6/2); massive anhydrite w/ deformed wavy dolomitic and muddy laminae (2.5 to 7“) interbedded w/ deformed wavy laminated mudstone (2“). The mud beds become thicker and the anhydrite bed become more mosaics with upward direction. The mud bed is thinner and w/ more planar laminae with upward direction.; sharp and wavy upper contact.
4304.03(1311.87)	1.50(0.46)	ANHYDRITE w/ SILTSTONE; medium bluish gray (5B 5/1) w/ moderate brown (5R 6/2) and olive gray (5Y 6/2); mosaic anhydrite w/ minor moderate brown and olive gray deformed wavy laminated siltstone grades upward to nodular anhydrite w/ minor muddy remnant and deformed dolomitic laminae. Each bed thickness is thicker than that of the bottom. The size of nodule range from 0.5X1“ to 0.7X1“; sharp and wavy upper contact.
4302.90(1311.52)	1.10(0.34)	SILTSTONE w/ ANHYDRITE; moderate brown (5YR 4/4) w/ medium bluish gray (5B 5/1); planar cross-laminated siltstone w/ rip-up mud clasts and scour surface (5“) grades upward to deformed wavy and ripple cross-laminated siltstone w/ thin bedded massive and small nodular anhydrite (8.5“).; sharp and wavy upper contact.
4301.80(1311.19)	0.29(0.09)	ANHYDRITE w/ SILTSTONE; medium bluish gray (5YR 4/4) w/ moderate brown (10R 2/2); massive bedded anhydrite (1.5“) grades upward to nodular anhydrite w/ minor deformed wavy mud laminae (2“); sharp and wavy upper contact.
4301.51(1311.10)	0.01(0.03)	SANDSTONE; very fine-grained; moderate brown (5YR 3/4); massive sandstone; sharp and wavy upper contact.
4301.50(1311.09)	0.40(0.12)	ANHYDRITE; light bluish gray (5B 7/1); mosaic and massive anhydrite; sharp and wavy upper contact.
4301.10(1310.98)	0.10(0.30)	SANDSTONE w/ ANHYDRITE; light olive gray (5Y 5/2) w/ medium bluish

		gray (5B 5/1); very fine-grained sandstone; ripple cross-laminated sandstone w/ small nodular anhydrite; sharp and wavy upper contact.
4301.00(1310.94)	1.20(0.37)	ANHYDRITE w/ SILTSTONE; pale red (5R 6/2) w/ dark reddish brown (10R3/4); pseudomorphic felted nodular anhydrite w/ deformed wavy and ripple cross silty laminae and desiccation crack (5“) grades upward to thicker enterolithic structure anhydrite w/ little silty remnant (3“); the above this, thick coalesced nodular anhydrite w/ slightly deformed wavy muddy laminae (4“) and mosaic anhydrite w/ minor silty remnant (2.5“).; gradational upper contact.
4299.80(1310.58)	1.28(0.39)	ANHYDRITE w/ DOLOMITE; light bluish gray (5B 7/1) w/ pale olive (10Y ¾) and dark reddish brown (10R 6/2); mosaic anhydrite w/ minor pale olive dolomitic laminae remnant (7.5“) grades upward to massive anhydrite (7“); missing upper contact.
4298.52(1310.19)	0.02(0.06)	LOST INTERVAL.
4298.50(1310.18)	1.28(0.39)	ANHYDRITE; light bluish gray (5B 7/1); massive anhydrite; sharp and wavy upper contact.
4297.32(1309.82)	1.79(0.55)	ANHYDRITE w/ SILTSTONE; medium bluish gray (5B 5/1) w/ moderate brown (5YR3/4); mosaic anhydrite w/ minor silty remnant.; missing upper contact.
4295.53(1309.28)	0.10(0.30)	LOST INTERVAL.
4295.43(1309.25)	0.10(0.30)	SILTSTONE w/ ANHYDRITE; light olive gray (5Y 5/2) w/ grayish brown (5YR 3/2); deformed slight wavy and horizontal, parallel silty laminae w/ small anhydrite; sharp and wavy upper contact.
4295.33(1309.22)	0.27(0.08)	ANHYDRITE w/ SILTSTONE; pale brown (5YR 5/2) w/ medium bluish gray (5B 5/1); mosaic anhydrite w/ minor silty remnant; sharp and wavy upper contact. **TOP OF GRAYBURG FORMATION**
4295.06(1309.13)	0.56(0.17)	SANDSTONE w/ ANHYDRITE; very fine-grained; pale brown (5YR 5/2) w/ dark yellowish brown (10YR 4/2); slight deformed wavy laminae (4.5“) grade upward to deformed wavy laminae (2“) w/ nodular anhydrite. The size of nodule is 5/10X5/10“; gradational upper contact.
4294.50(1308.96)	1.34(0.41)	SILTSTONE w/ ANHYDRITE; moderate brown (5YR 5/2) w/ pale red (5R 6/2); thin-bed coalesced nodular anhydrite w/ minor silty remnant (1“) grades upward to deformed silty wavy laminae w/ pseudomorphic felted anhydrite (14.5“); gradational upper contact
4293.16(1308.56)	1.83(0.56)	ANHYDRITE w/ SILTY MUDSTONE; pale red w/ moderate brown; mosaic anhydrite w/ minor silty laminae remnant; gradational upper contact.
4291.33(1308.00)	1.42(0.43)	ANHYDRITE w/ DOLOMITE; pale red (5R 6/2) w/ yellowish gray (5Y 7/2); mosaic anhydrite w/ dolomitic laminae remnant; missing upper contact.
4289.91(1307.56)	0.04(0.01)	LOST INTERVAL.
4289.87(1307.55)	0.37(0.11)	ANHYDRITE w/ MUDSTONE; light bluish gray (5YR 6/1) w/ grayish brown (5YR 3/2); mosaic anhydrite w/ minor grayish brown muddy laminae remnant; sharp and wavy upper contact.
4289.50(1307.44)	0.55(0.17)	MUDSTONE; dusky brown (5YR 2/2) w/ grayish brown (5YR 3/2); very thin horizontal, planar laminae (4.5“) grades upward to massive mudstone (1.5”). The desiccation is found at 4,289.5 ft; sharp and wavy upper contact.
4288.95(1307.27)	0.12(0.04)	DOLOMUDSTONE; light gray (N7); wavy laminated dolomite w/ scour surface at 4,188.95 ft; gradational upper contact.
4288.83(1307.24)	1.58(0.48)	ANHYDRITE w/ DOLOMITE; light bluish brown (5B 7/1) w/ yellowish gray (10Y 8/2); mosaic anhydrite w/ dolomitic algal laminae and dolomitic remnant in void (7.5“) grades upward to mosaic anhydrite w/ minor dolomitic remnant (10.5“); gradational upper contact.
4287.25(1306.75)	0.33(0.10)	ANHYDRITE; light bluish gray (5B 7/1); massive anhydrite; missing upper contact.
4286.92(1306.65)	0.06(0.02)	LOST INTERVAL.
4286.84(1306.63)	0.40(0.12)	ANHYDRITE; light bluish gray (5B 7/1); massive anhydrite; gradational upper contact
4286.44(1306.51)	0.28(0.09)	ANHYDRITE w/ DOLOMITE; light bluish gray (5B 7/1) w/ yellowish gray (5Y 7/2), mosaic anhydrite w/ dolomitic algal laminae and dolomitic remnant in void; gradational upper contact.
4286.16(1306.42)	1.35(0.41)	ANHYDRITE; light bluish gray (5B 7/1); massive anhydrite; sharp and irregular upper contact.
4284.81(1306.01)	0.51(0.16)	ANHYDRITE w/ SILTSTONE; pale brown (5YR 5/2) w/ moderate brown (5YR 4/4); mosaic anhydrite w /minor moderate brown silty remnant. The subaerial exposure surface is found at 4,284.81 ft.; missing upper contact
4284.30(1305.85)	0.29(0.09)	LOST INTERVAL.
4284.11(1305.80)	1.63(0.50)	ANHYDRITE w/ SILTSTONE; medium bluish gray (5B 5/1) w/ moderate

		brown (5YR3/4); mosaic anhydrite w/ minor silty remnant (12“) grades upward to pseudomorphic felted anhydrite and some enterolithic anhydrite w/ minor planar parallel muddy laminae (6“); sharp and wavy upper contact.
4282.48(1305.30)	1.08(0.33)	SILTSTONE w/ ANHYDRITE; moderate brown (5YR3/4) w/ medium bluish gray (5B 5/1); deformed wavy and ripple laminated siltstone w/ enterolithic structure anhydrite and pseudomorphic felted anhydrite. The sizes of enterolithic anhydrite are 1.2 to 0.7 X 2.5“; missing upper contact.
4281.40(1304.97)	0.15(0.05)	LOST INTERVAL.
4281.25(1304.93)	1.29(0.39)	SANDSTONE w/ ANHYDRITE; very fine-grained; moderate brown (5YR 4/4) w/ medium bluish brown (5B 5/1); very thin cross laminated sandstone w/ displacive nodular anhydrite (7“) grades upward to coalesced nodular anhydrite (2.5“) and then deformed wavy laminated sandstone w/ collapsed breccia anhydrite (7.5“). The sizes of anhydrite nodule range from less than 2/10 to 2/10X 5/10“. The shapes of nodules are various and elongated ellipsoid; sharp and wavy upper contact.
4279.96(1304.53)	0.96(0.29)	SANDSTONE; very fine-grained; dusky yellow (5YR 4/4) w/ pale olive (5YR 4/3); deformed wavy and ripple laminae (9.5“) grades upward to massive sandstone (2.5“); sharp and planar upper contact.
4279.00(1304.24)	0.55(0.17)	ANHYDRITE; medium bluish gray (5B 5/1); mosaic anhydrite; sharp and wavy upper contact
4278.45(1304.07)	3.00(0.91)	ANHYDRITE w/ SILTSTONE; medium bluish gray (5B 5/1) w/ pale brown (5YR 5/2); the alternation of thick-bed massive anhydrite w/ minor silty remnant (7“) grades upward to mosaic anhydrite w/ minor silty remnant in void and fracture (3 to 9“); missing upper contact.
4275.45(1303.16)	0.05(0.02)	LOST INTERVAL.
4275.40(1303.14)	0.30(0.09)	ANHYDRITE w/ SILTSTONE; medium bluish gray (5B 5/1) w/ pale olive (10Y 6/2); mosaic anhydrite w/ minor silty laminae remnant; gradational upper contact.
4275.10(1303.05)	1.16(0.35)	SANDSTONE w/ ANHYDRITE; very fine-grained; medium bluish gray (5B 5/1) w/ pale olive (10Y 6/2); deformed wavy laminated sandstone w/ displacive pseudomorphic anhydrite and collapsed breccia anhydrite; gradational upper contact.
4273.94(1302.70)	0.24(0.07)	SANDSTONE w/ MUD LAMINAE; very fine-grained; yellowish gray (5Y 7/2); massive sandstone w/ mud collapse breccia and mud laminae remnant; sharp and wavy upper contact.
4273.70(1302.62)	1.20(0.37)	SANDSTONE; fine-grained; yellowish gray (5Y 7/2) w/ medium bluish gray (5Y 5/2); massive and discontinuous horizontal planar- and wavy-laminated sandstone w/ scour surface at 4,273.7 ft; gradational upper contact
4272.50(1302.26)	0.50(0.15)	SANDSTONE w/ MUD LAMINAE and ANHYDRITE; fine-grained; yellowish gray (5Y 7/2) w/ medium bluish gray (5B 5/1); massive sandstone w/ displacive nodular anhydrite (2“) grades upward to wavy and ripple cross laminated sandstone w/ remnant muddy laminae (4“); missing upper contact
4272.00(1302.11)	0.28(0.09)	LOST INTERVAL.
4271.72(1302.02)	0.18(0.05)	SANDSTONE; very fine- to fine-grained; light olive gray (5Y 5/2) w/ pale olive (10Y 6/2); planar cross laminated sandstone; missing upper contact
4271.54(1301.97)	0.27(0.08)	LOST INTERVAL.
4271.27(1301.88)	1.57(0.48)	SANDSTONE; very fine- to fine-grained; light olive gray (5Y 5/2) w/ pale olive (10Y 6/2); ripple cross laminated sandstone (16“) grades upward to planar cross laminated sandstone (2.5“).; gradational upper contact
4269.70(1301.40)	0.70(0.21)	SILT- to SANDSTONE; silt- to very fine-grained; yellowish gray (5Y 7/2) w/ light olive gray (5Y 5/2); very thin planar cross laminated sandstone (7“) grades upward to wavy laminated sandstone (2.5“); missing upper contact
4269.00(1301.19)	0.14(0.04)	LOST INTERVAL.
4268.86(1301.15)	0.23(0.07)	SILTSTONE; siltstone; yellowish gray (5Y 7/2); very thin planar horizontal and wavy laminated sandstone w/ mud clasts; missing (?) and sharp upper contact
4268.63(1301.08)	0.78(0.24)	MUDSTONE w/ ANHYDRITE; dark greenish gray (5GY 4/1); planar horizontal and wavy ripple cross laminated mudstone w/ burrow and pseudomorphic anhydrite; missing (?) and sharp upper contact
4267.85(1300.84)	1.41(0.43)	DOLOMUDSTONE w/ ANHYDRITE; Peloidal Dolomudstone; yellowish gray (5Y 8/1) w/ light bluish gray (5B 7/1); wavy and planar horizontal laminated dolomite w/ anhydrite in birds eye structured (8“) grades upward to planar horizontal laminated dolomite (4“), massive dolomite w/ anhydrite in fenestral pores and fractures (4“), and ripple cross laminated dolomite (2“); sharp and planar upper contact
4266.44(1300.41)	0.24(0.07)	ANHYDRITE w/ SILTSTONE; moderate brown (5YR3/4) w/ light bluish

4266.20(1300.34) 4266.00(1300.28)	0.08(0.02)	gray (5B 7/1); pseudomorphic anhydrite w/ deformed wavy laminated siltstone; sharp and planar upper contact. ANHYDRITE; brownish gray (5YR 4/1) or light bluish gray (5B 7/1); massive bedded and mosaic anhydrite; Top of core interval at upper contact

Well Name:RMM 9-25

Depth difference between core and well log: +4 feet in core depth

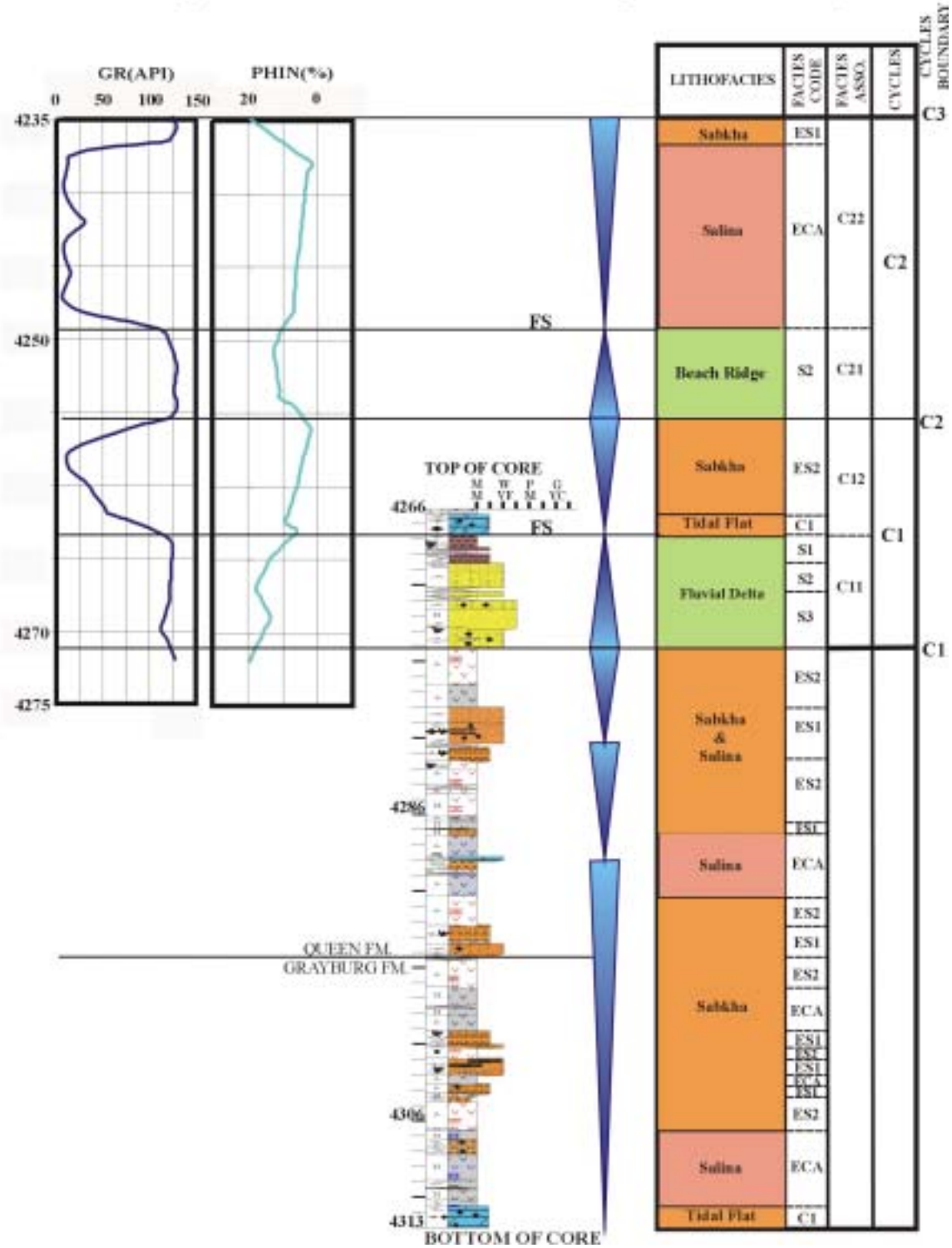

Core Description
R.M. Means #95-15 (API #: 420033338000)
Core Depth Interval: 4096.0–4153.25 ft
Means Field, Andrews County, Texas

DEPTH (ft/m)	THICKNESS (ft/m)	DESCRIPTION
4153.25(1265.91)	1.15(0.35)	SILT- to SANDSTONE w/ ANHYDRITE; moderate brown (5YR 4/4) w/ medium bluish gray (5B 5/1); siltstone and very fine-grained sandstone; deformed wavy laminated sandstone and massive sandstone w/ enterolithic structure anhydrite; The thickness of enterolithic structure range from 0.5 to 1.5“; sharp and wavy upper contact
4152.10(1265.56)	0.50(0.15)	ANHYDRITE; light brownish gray (5YR 6/1); mosaic anhydrite; missing upper contact.
4151.60(1265.41)	0.10(0.03)	LOST INTERVAL.
4151.50(1265.38)	2.03(0.62)	ANHYDRITE w/ DOLOMITE; light bluish gray (5B 7/1) w/ yellowish gray (5Y 5/2); the alternation of massive anhydrite (10 to 12“) and mosaic anhydrite (6“); wavy and sharp upper contact.
4149.47(1264.76)	0.79(0.24)	ANHYDRITE w/ SILT to MUDSTONE; pale brown (5YR 5/2) w/ olive gray (5Y 3/2); mosaic and coalesced nodular anhydrite w/ minor silty and muddy remnant; missing upper contact.
4148.72(1264.53)	0.07(0.02)	LOST INTERVAL.
4148.65(1264.51)	1.55(0.48)	ANHYDRITE w/ MUDSTONE and DOLOMITE; medium bluish gray (5B 5/1) w/ light olive gray (5Y 5/2); mosaic anhydrite w/ minor olive gray muddy remnant (8“) grades upward to mosaic anhydrite w/ dissolved dolomitic remnant in void (5“). It changes into the association with thin silty and muddy laminae remnant (6“); sharp and wavy upper contact.
4147.10(1264.04)	0.97(0.30)	MUDSTONE w/ ANHYDRITE; grayish brown (5YR 3/2) w/ moderate brown (5YR3/4); deformed wavy silty laminae w/ various shaped nodular anhydrite grades upward to relatively massive and deformed muddy or silty wavy laminae w/ coalesced nodular anhydrite. The mudstone changes into silty mudstone to the top of bed. The size of anhydrite nodules ranges from 3/10X 3/10” to 0.7X1.2“ in diameter. The nodules tend to increase their size upward. Some dissolved anhydrite horizons are found at 4,147.1 ft and 4,146.66 ft; missing upper contact.
4146.13(1263.74)	0.07(0.02)	LOST INTERVAL.
4146.08(1263.73)	1.38(0.42)	SILT- to MUDSTONE w/ GYPSUM and ANHYDRITE; moderate brown (5YR 4/4) w/ grayish blue (5PB 5/2); massive and some deformed wavy muddy laminae w/ oval shaped nodular anhydrite (9“) grades upward to massive mudstone w/ pseudomorphic felt gypsum or anhydrite crystal (8“). The size of nodules range from 1/10X1/10” to 1X1.5“ in diameter; gradational upper contact
4144.70(1263.30)	1.50(0.46)	ANHYDRITE w/ MUDSTONE; pale red purple (5RP 6/2) w/ moderate brown (5YR 4/4); mosaics and massive anhydrite w/moderate brown minor muddy remnant, the chicken-wire structured anhydrite is found at between 4,144 ft and 4,144.7 ft.; gradational upper contact.
4143.20(1262.85)	1.80(0.55)	ANHYDRITE w/ DOLOMITE; medium bluish gray (5B 5/1) w/ pale brown (5YR 5/2); mosaic anhydrite and some chicken-wire structure anhydrite around 4,142 ft w/ minor pale brown dolomitic remnant in void; sharp and planar upper contact. **TOP OF GRAYBURG FORMATION**.
4141.40(1262.30)	0.77(0.23)	MUDSTONE; olive gray (5Y 3/2); wavy laminae (1.5”) grades upward to very thin horizontal planar laminae (5”); missing upper contact.
4140.63(1262.06)	0.10(0.03)	DOLOMUDSTONE; dolomudstone; yellowish gray (5Y 3/2) w/ pale brown (5GY 5/2), massive dolomite; missing upper contact.
4140.53(1262.03)	0.27(0.08)	ANHYDRITE w/ DOLOMITE; medium bluish gray (5B 5/1) w/ yellowish gray (5Y 7/2); mosaic anhydrite w/ minor wavy dolomitic laminae in void; missing upper contact.
4140.26(1261.95)	0.10(0.03)	LOST INTERVAL.
4140.16(1261.92)	2.36(0.72)	ANHYDRITE w/ DOLOMITE; medium bluish gray (5B 5/1) w/ moderate brown (5YR 4/4); the alternation of mosaic and massive anhydrite w/ minor void filled dolomitic remnant; sharp and wavy upper contact.
4137.80(1261.20)	0.80(0.24)	ANHYDRITE w/ MUDSTONE; pale brown (5YR 5/2) w/ moderate brown (5YR 4/4); mosaic anhydrite w/ thin minor muddy and desiccation cracks at 4,137.23 ft and 4,137.80 ft; sharp and irregular upper contact.
4137.00(1260.96)	0.80(0.24)	ANHYDRITE w/ DOLOMITE; medium bluish gray 95B 5/2); massive bedded w/ minor dolomitic remnant in void; missing upper contact.
4136.20(1260.71)	2.00(0.61)	ANHYDRITE w/ SILT- to MUDSTONE; pale brown (5YR 5/2) w/ moderate brown (5YR 4/4); the alternation of massive and mosaic anhydrite

		w/ irregular, thin muddy and silty laminae on the top of enterolithic anhydrite. Some vertical fracture and enterolithic anhydrite structures are found between 4,134.36 ft and 4,134.86 ft.; sharp and wavy upper contact.
4134.20(1260.10)	2.00(0.61)	MUDSTONE w/ GYPSUM or ANHYDRITE; moderate brown (5YR 5/2) w/ medium bluish gray (5YR 4/4); The deformed wavy muddy laminae interbedded w/ minor the coalesced nodular anhydrite (6.5") and pseudomorphic felted anhydrite and gypsum crystals (4.5"). The interbed grades upward to the alternation of relatively massive and very thin horizontal, planar laminated mudstone w/ more bedded anhydrite (8") and pseudomorphic felted anhydrite (5.5"). The size of nodules range from 1/20X1/10 to 2/10X1.2" in diameter and their shape are generally elongated oval between bed.; gradational upper contact.
4132.20(1259.49)	0.15(0.05)	SILT- to SANDSTONE; siltstone and very fine-grained; pale brown (5YR 5/2) w/ moderate brown (5YR 4/4); very thin horizontal planar laminated siltstone and sandstone; sharp and wavy upper contact.
4132.05(1259.45)	0.25(0.08)	SILT- to SANDSTONE; siltstone and very fine-grained; pale yellowish green (5YR 4/4) w/ dusky yellowish green (5B 5/1); deformed wavy laminated w/ nodular anhydrite; The sizes of nodules range from 2/10X 2/10 to 2/10X7/10" in diameter; sharp and wavy upper contact.
4131.80(1259.37)	1.10(0.34)	SILT- to SANDSTONE; siltstone and very fine-grained; light olive gray (5Y 5/2) w/ medium bluish gray (5B 5/1); massive, chaotic and trough cross laminated sandstone w/ angular mud rip-up clasts (6") grades upward to deformed wavy laminated sandstone w/ slumping structure and micro-faults (6"). The scour surface is found at 4,132.8 ft. The sizes of clasts range from 1/10 to 7/10" in diameter; sharp and wavy upper contact.
4130.70(1259.04)	1.30(0.40)	SILT- to SANDSTONE; siltstone and very fine-grained; light olive gray (5Y 5/2) w/ medium bluish gray (5B 5/1); planar and trough cross laminated sandstone w/ mud rip-up clasts (4") grades upward to deformed wavy laminated sandstone (11.5"). The sizes of mud clasts range from 1/0 to 3/10" in diameter; the above this, deformed wavy laminated sandstone (3"); missing upper contact.
4129.40(1258.64)	0.20(0.06)	LOST INTERVAL.
4129.20(1258.58)	0.30(0.09)	SANDSTONE; very fine-grained; moderate brown (5YR 4/4) w/ medium bluish gray (5B 5/1); massive and mottled sandstone w/ nodular anhydrite; The sizes of nodules is 3/10 X 5/10" in diameter; gradational upper contact.
4128.90(1258.49)	0.80(0.24)	ANHYDRITE w/ DOLOMITE; medium bluish gray (5B 5/1) w/ pale olive (10Y 6/2); mosaic anhydrite w/ minor dolomitic remnant laminae; gradational upper contact.
4128.10(1258.24)	2.80(0.85)	ANHYDRITE w/ MUDSTONE; pale brown (5YR 5/2) w/ moderate brown (5YR 4/4); massive anhydrite w/ very thin muddy laminae and mud remnant in void (13") grades upward to massive anhydrite w/ very well laminated dolomite (18"); gradational upper contact.
4125.30(1257.39)	1.30(0.40)	ANHYDRITE w/ DOLOMITE; medium bluish gray (5B 5/1) w/ pale olive (5YR 5/2); mosaic anhydrite w/ minor dolomitic remnant; missing upper contact.
4124.00(1256.99)	0.54(0.16)	LOST INTERVAL.
4122.46(1256.53)	0.86(0.26)	SANDSTONE; fine-grained; dusky yellow (5Y 6/4); faintly discontinuous horizontal planar laminated sandstone; sharp and wavy upper contact.
4121.60(1256.26)	1.60(0.49)	SANDSTONE w/ ANHYDRITE; fine-grained; light olive gray (5Y 5/2) w/ medium bluish gray (5B 5/1), massive sandstone w/ nodular anhydrite; The sizes of nodules range from 1/10X1/10 to 5/10X8/10" in diameter; missing upper contact.
4120.00(1255.78)	1.00(0.30)	LOST INTERVAL.
4119.00(1255.47)	0.60(0.18)	SANDSTONE w/ ANHYDRITE; fine-grained; light olive gray (5Y 5/2) w/ medium bluish gray (5B 5/1); faintly discontinuous horizontal planar laminated sandstone; sharp and wavy upper contact.
4118.40(1255.29)	1.20(0.37)	DOLOMUDSTONE w/ SILTY MUDSTONE; dolomudstone; yellowish gray (5Y 7/2) w/ light olive gray; massive mudstone w/ many desiccation cracks and some burrow; sharp and planar upper contact.
4117.20(1254.92)	0.79(0.24)	DOLOMUDSTONE w/ ANHYDRITE; dolomudstone; yellowish gray (5Y 7/2) w/ medium bluish gray (5B 5/1); faintly discontinuous horizontal planar laminated dolomite w/ some organic laminae and coalesced nodular anhydrite; The sizes of anhydrite nodules range from 7/10X 1 to 1.2 X 2" in diameter; missing upper contact.
4116.41(1254.68)	0.31(0.09)	LOST INTERVAL.
4116.10(1254.59)	0.70(0.21)	DOLOMUDSTONE w/ ANHYDRITE; dolomudstone; yellowish gray (5Y

		7/2) w/ medium bluish gray (5B 5/1); planar and algal wavy laminated dolomite w/ nodular anhydrite and displacive anhydrite in void; sharp and wavy upper contact.
4115.40(1254.37)	2.20(0.67)	ANHYDRITE w/ MUDSTONE; pale brown (5YR 5/2) w/ grayish brown (5YR 3/2); mosaic anhydrite w/ minor grayish brown muddy remnant; missing upper contact.
4113.20(1253.70)	0.13(0.04)	LOST INTERVAL.
4113.07(1253.66)	2.21(0.67)	ANHYDRITE w/ SILT- to MUDSTONE; medium bluish gray (5B 5/1) w/ dusky yellow green (5GY 5/2); Interbedded the mosaic with massive bedded anhydrite w/ minor muddy and silty laminae remnant in dissolved horizon of 4,111 ft; sharp and wavy upper contact
4110.86(1252.99)	1.08(0.33)	MUDSTONE; silty mudstone; grayish brown (5YR 3/2); massive and faintly parallel muddy laminae; sharp and irregular upper contact
4110.70(1252.94)	0.30(0.09)	ANHYDRITE w/ MUDSTONE; medium bluish gray (5B 5/1) w/ pale brown (5YR 5/2); massive anhydrite w/ minor muddy remnant; missing upper contact.
4110.40(1252.85)	0.03(0.01)	LOST INTERVAL.
4110.37(1252.84)	1.67(0.51)	ANHYDRITE w/ MUDSTONE; medium bluish gray (5B 5/1) w/ dusky yellow green (5GY 5/2); mosaic and massive bedded anhydrite w/ minor muddy remnant; sharp and wavy upper contact.
4108.70(1252.33)	0.55(0.17)	SANDSTONE; very fine-grained; medium bluish gray (5B 5/1) w/ grayish brown (5YR 3/2); slightly planar, low angle cross laminated sandstone (5") grades upward to sabkhatized massive sandstone (3").; sharp and wavy upper contact.
4108.10(1252.15)	0.39(0.12)	SILT- to SANDSTONE; siltstone to very fine grained; medium bluish gray (5B 5/1) w/ yellowish gray (10Y 6/2); wavy laminated sandstone (2") grades upward to massive and planar horizontal laminated sandstone w/ desiccation cracks (3"); sharp and planar upper contact.
4107.71(1252.03)	0.14(0.04)	DOLOMUDSTONE w/ ANHYDRITE; dolomudstone; yellowish gray (5Y 7/2) w/ light bluish gray (5B 7/1); wavy algal laminated dolomite w/ minor bedded massive anhydrite; missing upper contact.
4107.57(1251.99)	0.07(0.02)	LOST INTERVAL.
4107.50(1251.97)	0.10(0.03)	DOLOMUDSTONE; dolomudstone; yellowish gray (5Y 7/2) w/ light bluish gray (5B 7/1); wavy algal laminated dolomite; missing upper contact
4107.40(1251.94)	3.70(1.13)	ANHYDRITE w/ MUDSTONE; pale brown (5YR 5/2) w/ moderate brown (5YR 4/4); Interbedded enterolithic structure and nodular anhydrite w/ massive and extensive deformed wavy muddy laminae remnant (8 to 23.5") grades upward to pseudomorphic felted anhydrite w/ massive and extensive deformed wavy laminated mudstone (14"). The size of nodules range from 1/20 to 2X 1/10" in diameter. Their size decrease upward to the top of bed. The anhydrite rosette structures and rip-up clasts are found frequently; sharp and wavy upper contact
4103.70(1250.81)	0.24(0.07)	MUDSTONE w/ ANHYDRITE; grayish olive (10Y 4/2) w/ medium blush gray (5B 5/1); wavy algal laminated mudstone w/ nodular anhydrite between beds. The sizes of nodules are less than 1/20" in diameters; sharp and wavy upper contact.
4103.46(1250.73)	1.06(0.32)	SANDSTONE w/ ANHYDRITE, very fine- to fine- grained; medium bluish gray (5B 5/1) w/ grayish red (5Y 7/2); massive sandstone w/ thin bedded massive anhydrite and desiccation cracks grades upward to very thin algal wavy laminated sandstone w/ dissolved nodular anhydrite and many desiccation cracks. Some weathered horizon of anhydrite is found between 4,102.4 ft and 4,103 ft. The size of nodules is 2/10 X 2/10" in diameter; sharp and wavy upper contact.
4102.40(1250.41)	0.10(0.03)	MUDSTONE; light olive gray (5Y 5/2); very thin planar, horizontal laminated mudstone; sharp and planar upper contact.
4102.30(1250.38)	0.50(0.15)	ANHYDRITE w/ DOLOMITE; medium bluish gray (5Y 5/2) w/ yellowish gray (5Y 7/2); massive anhydrite w/ minor deformed dolomitic laminae due to the growth of gypsum and anhydrite and some pseudomorphic felted anhydrite; missing upper contact.
4101.80(1250.23)	0.10(0.03)	LOST INTERVAL.
4101.70(1250.20)	2.90(0.88)	ANHYDRITE w/ DOLOMITE; medium bluish gray (5B 5/1) w/ yellowish gray (5Y 7/2); massive anhydrite w/ minor planar, horizontal dolomitic laminae due to the growth of gypsum (20") grades upward to massive anhydrite w/ minor deformed dolomitic wavy laminae (15"); missing upper contact
4098.90(1249.34)	0.10(0.03)	LOST INTERVAL.

4098.80(1249.31) 4096.70(1248.67) 4096.60(1248.64) 4096.00(1248.46)	2.10(0.64) 0.10(0.03) 0.60(0.18)	ANHYDRITE w/ DOLOMITE; medium bluish gray (5B 5/1) w/ yellowish gray (5Y 7/2); massive anhydrite w/ minor deformed wavy dolomitic laminae (10”) grades upward to massive anhydrite w/ minor planar, horizontal dolomitic laminae (3”) and deformed dolomitic wavy laminae (13.5”). The desiccation crack is found at 4,096.7”; sharp and irregular upper contact SANDSTONE; silty sandstone; light olive gray (5B 5/1) w/ dusky yellowish gray (5Y 7/2); ripple cross-laminated sandstone; sharp and planar upper contact. ANHYDRITE w/ DOLOMITE; medium bluish gray (5B 5/1) w/ yellowish gray (5Y 7/2); the alternation of massive anhydrite w/ deformed wavy dolomitic laminae (1 to 11.5”) grades upward to massive anhydrite w/ horizontal, planar dolomitic laminae (3”). Some desiccation crack are found at 4,096.7 ft.; Top of core interval at upper contact

Well Name:RMM9 5-15

Depth difference between core and well log: -9 feet in core depth

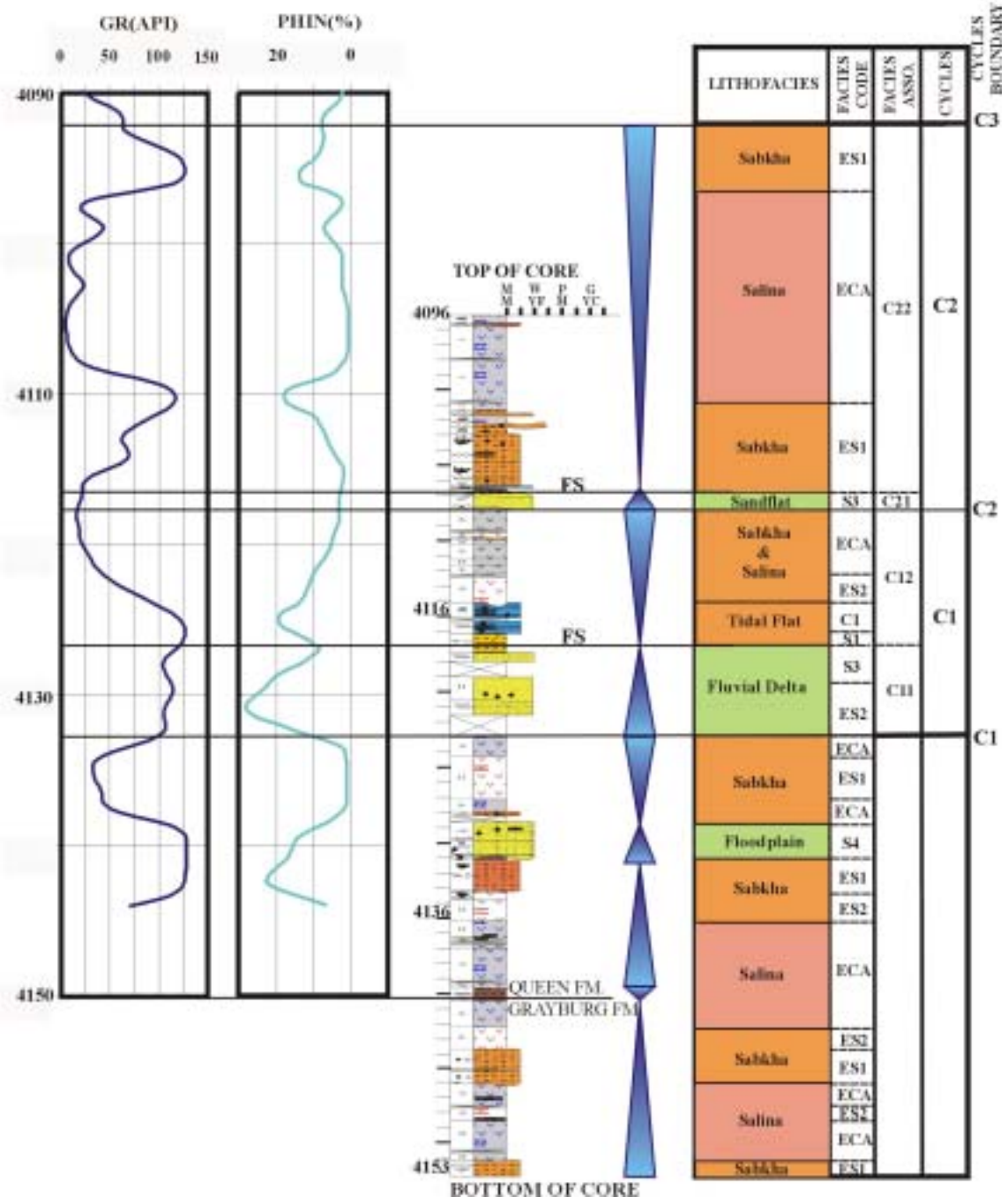

Core Description
R.M. Means #7-51(API #: 420033338400)
Core Depth Interval: 4118.58–4174.88 ft
Means Field, Andrews County, Texas

DEPTH (ft/m)	THICKNESS (ft/m)	DESCRIPTION
4174.88(1272.50)	1.22(0.37)	ANHYDRITE w/ MUDSTONE; medium bluish brown (5B 5/1) w/ moderate brown (5YR 3/4); mosaic anhydrite w/ minor moderate brown void filled muddy laminae remnant; missing or gradational upper contact
4173.66(1272.13)	1.21(0.37)	ANHYDRITE w/ DOLOMITE; medium bluish gray (5B 5/1) w/ yellowish gray (5Y 7/2); mosaic anhydrite w/ collapsed voids filled dolomite. The collapsed dolomitic breccia are between mosaic anhydrite; sharp and planar upper contact.
4172.45(1271.76)	1.20(0.37)	MUDSTONE w/ ANHYDRITE; pale yellowish brown (10YR 6/2) w/ medium bluish gray (5B 5/1); planar, horizontal laminated mudstone interbed with ripple cross laminated mudstone w/ very small nodular anhydrite and coalesced nodular anhydrite. The size of nodules ranges from less than 1/20 to 0.5X1.2” in diameter; sharp and wavy upper contact.
4171.25(1271.40)	6.66(2.03)	ANHYDRITE w/ DOLOMITE; medium bluish gray (5B 5/1) w/ yellowish gray (10YR 6/2); mosaic anhydrite w/minor wavy and planar dolomitic laminae remnant (23”) grades upward to more massive and bedded anhydrite (25”); the above this, mosaic anhydrite w/ minor yellowish gray wavy dolomitic laminae remnant and collapsed dolomitic breccia (17.5”) grades upward to mosaic anhydrite w/ voids filled grayish brown muddy laminae (6.5”); missing upper contact.
4164.59(1269.37)	0.24(0.07)	LOST INTERVAL.
4164.25(1269.26)	2.80(0.85)	ANHYDRITE w/ SILT- to MUDSTONE; light brownish gray (5YR 6/1) w/ dark reddish brown (10R 3/4); mosaic and nodular anhydrite w/ minor muddy laminae remnant (5”) grades up to massive and thin laminated mudstone w/ tiny and coalesced anhydrite nodules (5”); the above this, mosaic and nodular anhydrite w/ minor muddy laminae remnant (9”), massive and thin laminated mudstone w/ tiny and coalesced anhydrite nodules (5”) and enterolithic anhydrite w/ siltstone remnant (8”). The size of anhydrite nodules range from 1/10X1/10 to 2/10X2/10” in diameter; missing upper contact.
4161.45(1268.41)	0.10(0.03)	LOST INTERVAL.
4161.35(1268.38)	1.05(0.32)	ANHYDRITE w/ SILTSTONE;, light bluish gray (5B 7/1) w/ moderate brown (5YR 4/4); massive and mosaic anhydrite (2 to 5”) interbedded with very thin horizontal, planar or slightly wavy laminated mud- to siltstone (0.3 to 2”); sharp and planar upper contact.
4160.30(1268.06)	0.75(0.23)	MUDSTONE w/ ANHYDRITE; pale red (10R 6/2) w/ dusky red (10R 2/2), the deformed wavy laminated mudstone w/ nodular anhydrite grades upward to the massive mudstone w/ displacive pseudomorphic anhydrite. The size of nodules ranges from 2/10X2/10 to 9/10X1.2” in diameter. The desiccation crack is found at 4,160.3 ft.; gradational upper contact.
4159.55(1267.83)	0.65(0.20)	ANHYDRITE w/ MUDSTONE; very light gray (N8) w/ grayish brown (5YR 5/2); mosaic and massive bedded anhydrite w/ thin slight wavy laminated and void filled grayish olive mudstone. The scour surface is located at the bottom of bed (4,159.55 ft); missing upper contact. **TOP OF GRAYBURG FORMATION**
4158.90(1267.63)	0.20(0.06)	LOST INTERVAL.
4158.70(1267.57)	0.91(0.28)	ANHYDRITE w/ SILTSTONE; light bluish gray (5B 7/1) w/ pale olive (10Y 6/2), mosaic anhydrite w/ very thinly wavy silty laminae (6”) grades upward to the massive anhydrite w/ silty laminae (4.5”). The silty laminae are deformed slightly.; sharp and wavy upper contact.
4157.79(1267.29)	1.91(0.58)	SANDSTONE w/ ANHYDRITE and MUD CLASTS; silt to very fine-grained; pale olive (10Y 6/2) w/ light bluish gray (5B 7/1); wavy and ripple laminated sandstone w/ rip-up mud clasts and nodular anhydrite (13”) grades upward to planar cross laminated sandstone w/ nodular anhydrite and mud clasts (4”). It is overlain by deformed laminated sandstone w/ burrows and load structures (5”).; sharp and wavy upper contact.
4155.88(1266.71)	1.51(0.46)	SANDSTONE w/ ANHYDRITE; very fine-grained; light olive gray (5Y 5/2) w/ medium bluish gray (5B 5/1); deformed wavy laminated sandstone w/ mud collapsed breccia (6.5”) grades upward to massive and mottled sandstone w/ mud clasts and nodular anhydrite in burrow; sharp and missing upper contact.
4154.37(1266.25)	1.24(0.38)	SANDSTONE w/ ANHYDRITE; fine-grained; grayish olive (10Y 4/2) w/ dusky brown (5YR 3/2); deformed wavy laminated sandstone due to intensive

		bioturbation w/ mud laminae content and nodular anhydrite The sizes of nodular anhydrite is 1/10X 6/10” in diameter.; sharp and wavy upper contact.
4153.13(1265.87)	3.13(0.95)	ANHYDRITE w/ SILTSTONE, light bluish gray (5B 7/1) w/ grayish yellow green (5GY 7/2), mosaic anhydrite w/ silty laminae remnant (10.5”) grades upward to the massive and bedded anhydrite w/ very thin planar cross silty laminae (16.5”) and very thin organic and algal laminae (3”); missing upper contact.
4150.00(1264.92)	0.84(0.26)	LOST INTERVAL.
4149.16(1264.66)	0.53(0.16)	SANDSTONE w/ MUD CLASTS; fine-grained; dusky yellow (5Y 6/4) w/ light olive gray (5Y 5/2); deformed wavy laminated and mottled sandstone w/ micro-fault, load structure and mud clasts; missing upper contact.
4148.63(1264.50)	0.18(0.05)	SANDSTONE; very fine-grained; yellowish gray (5Y 7/2); faintly discontinuous planar laminated sandstone; missing upper contact.
4148.46(1264.45)	0.25(0.08)	LOST INTERVAL.
4148.21(1264.37)	0.45(0.14)	SANDSTONE w/ ANHYDRITE; fine-grained; yellowish gray (5Y 7/2) w/ light olive gray (5Y 5/2); massive and mottled sandstone w/ disseminated very tiny anhydrite crystals and burrow; missing upper contact.
4147.75(1264.23)	0.25(0.08)	LOST INTERVAL.
4147.50(1264.16)	0.50(0.15)	SANDSTONE w/ ANHYDRITE; fine-grained; yellowish gray (5Y 7/2) w/ light olive gray (5Y 5/2); massive and mottled sandstone w/ disseminated very tiny anhydrite crystals and burrow; missing upper contact.
4147.00(1264.01)	0.24(0.07)	LOST INTERVAL.
4146.76(1263.93)	0.46(0.14)	SANDSTONE w/ ANHYDRITE; fine-grained; yellowish gray (5Y 7/2) w/ light olive gray (5Y 5/2); massive and mottled sandstone w/ disseminated very tiny anhydrite crystals and burrow; missing upper contact.
4146.30(1263.79)	1.39(0.42)	SANDSTONE; very fine-grained; yellowish gray (5Y 7/2) w/ light olive gray (5Y 5/2); massive and faintly ripple cross-laminated sandstone w/ small anhydrite nodule; sharp and wavy upper contact.
4144.91(1263.37)	2.20(0.67)	DOLOMUDSTONE w/ ANHYDRITE; dolomudstone to argillaceous mudstone; yellowish gray (5Y 7/2) w/ light olive gray (5Y 5/2); massive, algal wavy and deformed wavy laminated dolomite w/ dispersed displacive nodular anhydrite (4 to 6”) interbedded with planar horizontal and deformed wavy laminated dolomudstone w/ small mud clasts (0.5 to5”). The thickness of dolomudstone decrease upward to the top of bed; gradational upper contact
4142.71(1262.70)	3.76(1.15)	DOLOMUDSTONE TO WACKSTONE w/ ANHYDRITE; dolomudstone to peloidal dolowackestone; yellowish gray (5Y 7/2) w/ light bluish gray (5B 7/1); massive dolomite (2”) grades upward to muddy and organic laminated dolomite w/ many stylolites and nodular anhydrite (11”) and relatively massive dolomite w/ nodular anhydrite (5”). The sizes of anhydrite nodule range from 1/20X1/20 to 3/10 X 3/10” in diameter; the above this, massive, continuous and discontinuous peloidal dolomite w/ displacive anhydrite in peloidal moldic pores (8”), ripple cross laminated dolomite w/ chicken-wire structure anhydrite (4”) and very thin slightly wavy and planar laminated dolomite (7”); sharp and planar upper contact.
4138.95(1261.55)	4.23(1.29)	ANHYDRITE w/ MUDSTONE; medium bluish gray (5B 5/1) w/ pale red (5YR 4/4); the massive anhydrite w/ displacive pseudomorphic anhydrite including 3” thick planar cross laminated mudstone (16”) grades upward to the mosaic and enterolithic anhydrite w/ minor blackish red mudstone remnant (36”); sharp and planar upper contact.
4134.72(1260.26)	1.88(0.57)	SILT- to SANDSTONE; silt to very fine-grained; pale red (5R 6/2); the relatively massive but locally developed discontinuous wavy and ripple laminae; missing upper contact.
4133.84(1259.99)	0.68(0.21)	LOST INTERVAL.
4133.16(1259.79)	0.26(0.08)	SILT- to SANDSTONE; silt to very fine grained; pale red (5R 6/2); the relatively massive but locally developed discontinuous wavy and ripple laminae; sharp and planar upper contact.
4132.90(1259.71)	3.74(1.14)	ANHYDRITE w/ SILT to MUDSTONE; medium light gray (N7) w/ grayish brown (5YR 3/2); mosaic and massive bedded anhydrite w/minor mudstone remnant; sharp and wavy upper contact
4129.16(1258.57)	0.76(0.23)	SILTSTONE w/ ANHYDRITE; siltstone; moderate brown (5YR 3/4) w/ grayish brown (5YR 3/2); deformed wavy laminated siltstone w/anhydrite, gradational upper contact
4128.40(1258.34)	2.70(0.82)	SILT- to SANDSTONE w/ ANHYDRITE, silt to very fine-grained, light olive gray (5Y 5/2) w/ grayish olive (10Y 4/2); deformed wavy and ripple laminated siltstone w/ tiny nodular anhydrite; the above this, massive, deformed wavy and ripple laminated sandstone w/ displacive and nodular

		anhydrite and algal wavy laminae; gradational upper contact.
4125.70(1257.51)	2.27(0.69)	SANDSTONE w/ MUDSTONE; silt to very fine grained; yellowish gray (5Y 7/2) w/ light olive gray (5Y 5/2); algal wavy laminated sandstone (7") grades upward to planar horizontal laminated sandstone (2"), ripple cross laminated sandstone (3") and algal wavy laminated sandstone (13.5"); gradational upper contact.
4123.43(1256.82)	0.17(0.05)	MUD- to SANDSTONE; light olive gray (5Y 5/2) w/ olive gray (5Y 3/2); very thin horizontal planar laminae; sharp and wavy (truncation surface) upper contact.
4123.26(1256.77)	1.68(0.51)	SANDSTONE w/ MUDSTONE; very fine-grained; yellowish gray (5Y 7/2) w/ light olive gray (5Y 5/2); ripple and algal laminated sandstone (17.5") grades upward to slightly planar horizontal laminated sandstone (2").; gradational upper contact.
4121.58(1256.26)	0.68(0.21)	SANDSTONE w/ ANHYDRITE; very fine-grained; medium bluish gray (5Y 7/2) w/ yellowish gray (5Y 5/2); planar horizontal and wavy algal laminated sandstone w/ dispersed small anhydrite crystals; sharp and erratic upper contact.
4120.90(1256.05)	2.32(7.07)	ANHYDRITE w/ DOLOMITE; medium bluish gray (5B 5/1) w/ yellowish gray (5Y 7/2); massive bedded anhydrite w/ minor deformed wavy dolomitic laminae; Top of the Core at upper contact.
4118.58(1255.34)		

Well Name:RMM 7-51

Depth difference between core and well log: -3 feet in core depth

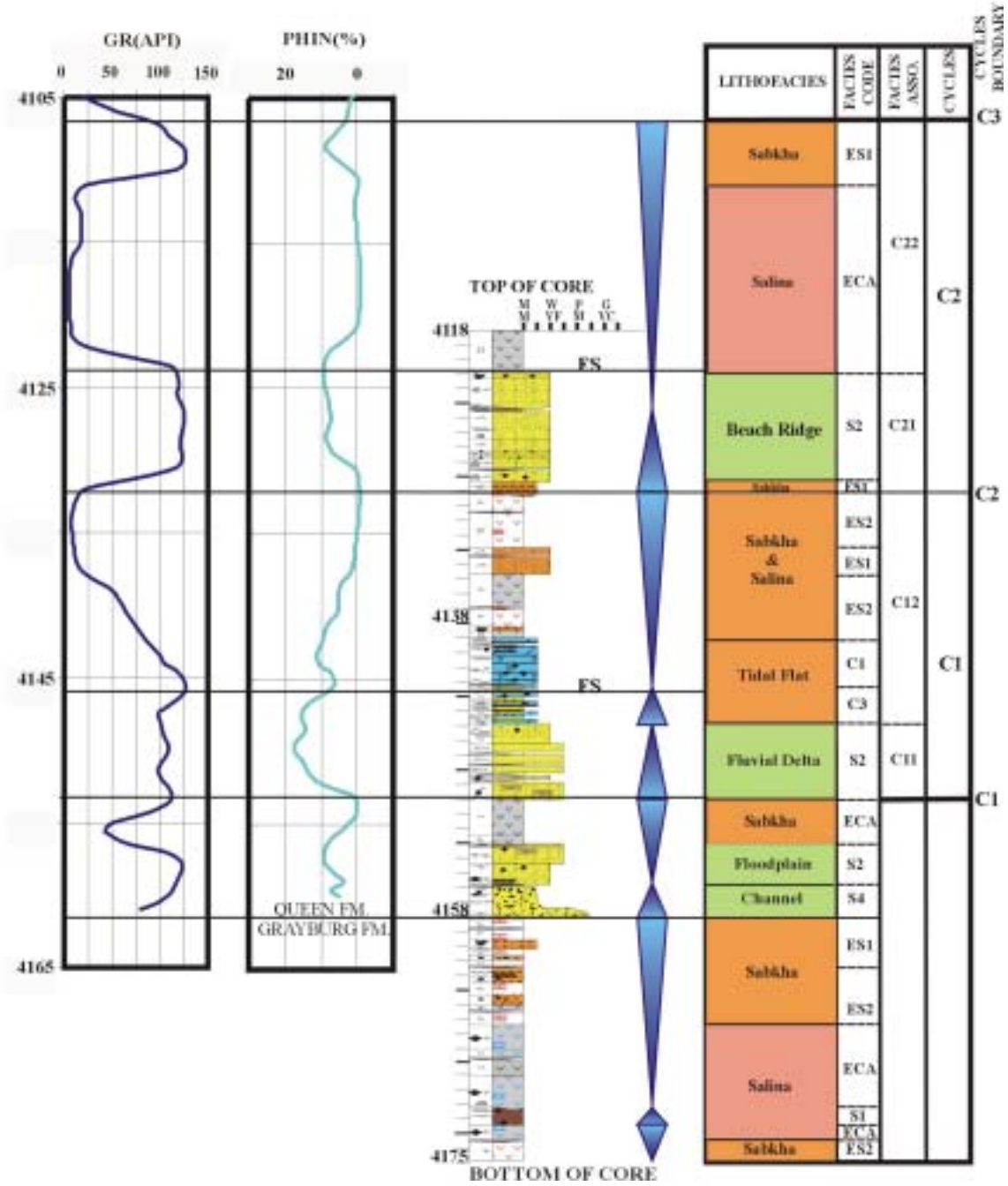

Core Description
R.M. Means #4-25 (API #: 420033338800)
Core Depth Interval: 4568.00–4594.50 ft
Means Field, Andrews County, Texas

DEPTH (ft/m)	THICKNESS (ft/m)	DESCRIPTION
4594.50(1400.40)	2.10(0.64)	SANDSTONE w/ MUD CLASTS; fine-grained; pale olive (10Y 6/2) w/ moderate brown (5YR 3/4); massive and mottled sandstone w/ burrow and mud clasts (10”) grades upward to faintly discontinuous planar horizontal laminated sandstone w/ mud clasts (6”) and massive and mottled sandstone w/ mud clasts (5”); missing upper contact
4592.40(1399.76)	0.40(0.12)	LOST INTERVAL.
4592.00(1399.64)	0.30(0.09)	MUDSTONE w/ DOLOMITIC CLASTS; yellowish gray (5Y 7/2) w/ light olive gray (5Y 5/2); massive mudstone w/ mud and dolomitic clasts; sharp and wavy upper contact.
4591.70(1399.55)	0.30(0.09)	DOLOMUDSTONE; yellowish gray (5Y 7/2); massive dolomite; missing upper contact.
4591.40(1399.46)	0.50(0.15)	LOST INTERVAL.
4590.90(1399.30)	0.38(0.12)	DOLOMUDSTONE; dolomudstone; yellowish gray (5Y 7/2); massive dolomite w/ anhydrite in birds eyes structure; sharp and irregular upper contact.
4590.52(1399.19)	0.27(0.08)	ANHYDRITE; light bluish gray (5B 7/1) w/ pale reddish brown (10R 5/4); mosaic anhydrite w/ minor silty remnant; sharp and irregular upper contact.
4590.25(1399.11)	0.25(0.08)	MUDSTONE; olive gray (5Y 3/2); chaotic deformed wavy laminated mudstone; sharp and planar upper contact.
4590.00(1399.03)	1.34(0.41)	DOLOMUDSTONE TO DOLOWACKESTONE w/ ANHYDRITE; dolomudstone to peloidal dolowackestone; yellowish gray (5Y 7/2) w/ light brown (5YR 6/4); faintly cryptalgal laminated dolomite w/ small anhydrite in peloidal moldic pores (7”) grades upward to wavy laminated dolomite w/ some nodular anhydrite (9”); missing upper contact
4588.66(1398.62)	3.16(0.96)	LOST INTERVAL.
4585.50(1397.66)	0.24(0.07)	ANHYDRITE; light bluish gray (5B 5/1); mosaic and massive anhydrite; missing upper contact.
4585.26(1397.59)	0.96(0.29)	SANDSTONE; very fine-grained; light olive gray (5Y 5/2) w/ olive gray (5Y 3/2); faintly ripple cross laminated sandstone (5”) grades upward to faintly cryptalgal wavy and discontinuous wavy laminated sandstone (8”); missing upper contact.
4584.30(1397.29)	1.70(0.52)	LOST INTERVAL.
4582.60(1396.78)	2.60(0.80)	SANDSTONE; fine-grained; dusky yellow (5Y 6/4) w/ light bluish gray (5B 5/1); faintly ripple cross laminated sandstone w/ tiny anhydrite crystals of which sizes is less than 1/20” (16.5”) grades upward to stacked ripple cross laminated sandstone (11”); missing upper contact.
4580.30(1396.08)	0.30(0.09)	LOST INTERVAL.
4580.00(1395.98)	1.40(0.43)	SANDSTONE; very fine- to fine-grained; dusky yellow (5Y 6/4) w/ light olive gray (5Y 5/2); faintly slight discontinuous ripple cross laminated sandstone (12”) is overlain by faintly discontinuous planar horizontal laminated sandstone (5”); missing upper contact.
4578.60(1395.56)	5.30(1.62)	LOST INTERVAL.
4573.30(1393.94)	1.55(0.47)	ANHYDRITE w/ DOLOMITE; light bluish gray (5B 7/1) w/ yellowish gray (5Y 7/2); massive anhydrite w/ minor crenulated wavy dolomitic laminae; missing upper contact.
4571.75(1393.47)	0.75(0.23)	LOST INTERVAL.
4571.00(1393.24)	2.10(0.64)	ANHYDRITE; light bluish gray (5B 7/1) w/ yellowish gray (5Y 7/2); massive anhydrite w/ crenulated wavy dolomitic laminae remnant; missing upper contact
4568.90(1392.60)	0.40(0.12)	ANHYDRITE; light bluish gray (5B 7/1) w/ yellowish gray (5Y 7/2); massive anhydrite w/ crenulated wavy dolomitic laminae remnant; sharp and wavy upper contact
4568.50(1392.48)	0.04(0.01)	DOLOMUDSTONE; moderate yellow brown (10YR 4/2); cryptalgal wavy laminated dolomite; Top of core interval at upper contact
4568.46(1392.47)		

Well Name:RMM4-25

Depth difference between core and well log:+2 feet in core depth

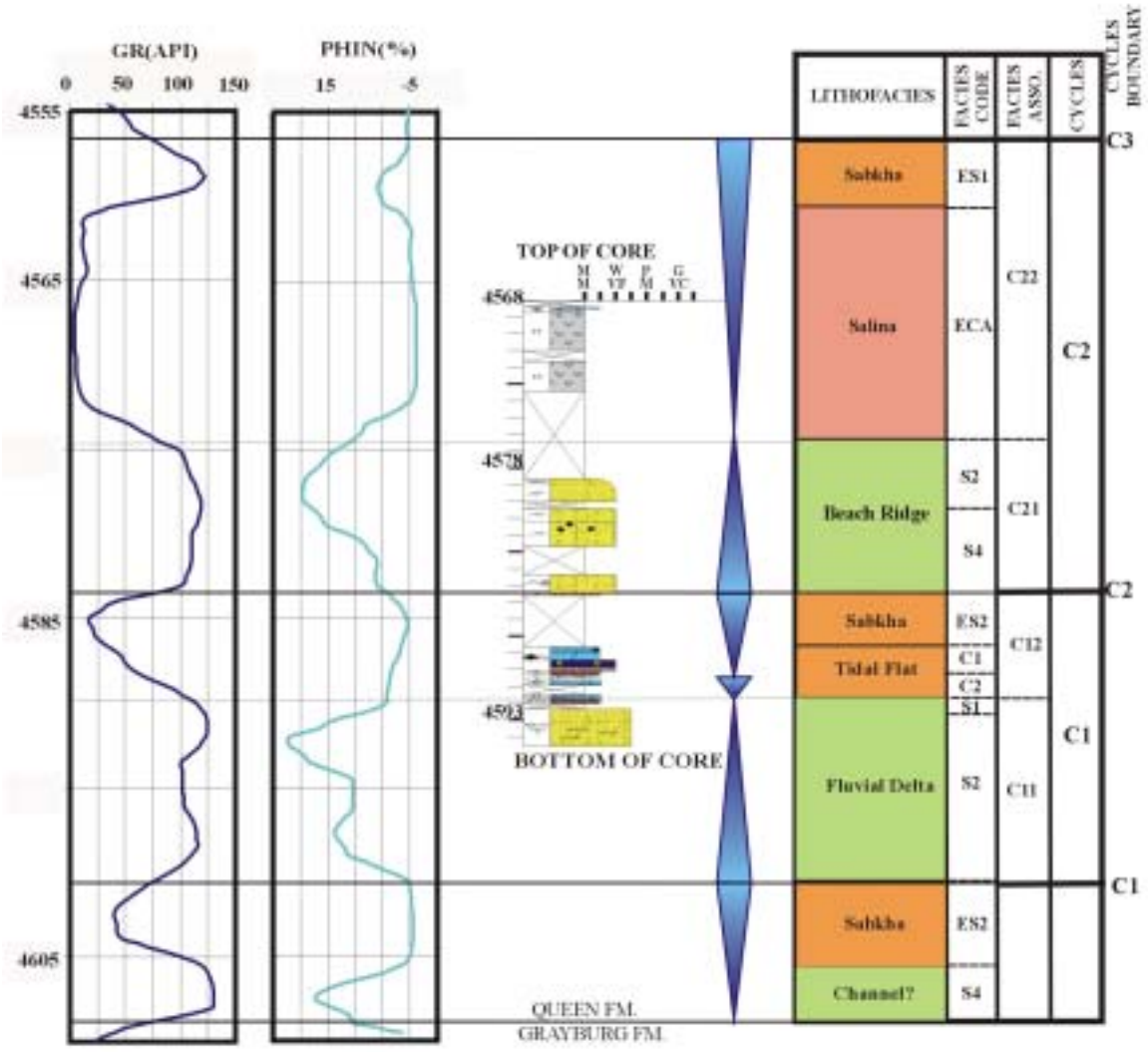

Core Description
MSAU #59-60 (API #: 420033447700)
Core Depth Interval: 4009.3–4054.9 ft
Means Field, Andrews County, Texas

DEPTH (ft/m)	THICKNESS (ft/m)	DESCRIPTION
4054.90(1235.93)	0.90(0.27)	ANHYDRITE w/ DOLOMITE; medium bluish brown (5B 5/1) w/ olive gray (5Y 3/2); bedded mosaic anhydrite w/ minor olive gray dolomitic remnant; missing upper contact
4054.00(1235.66)	0.17(0.05)	LOST INTERVAL.
4053.83(1235.61)	0.48(0.15)	ANHYDRITE w/ MUDSTONE; light bluish gray (5B 5/1) w/ olive gray (5Y 3/2); interbedded thin massive anhydrite (1”) with massive mudstone (2” to 4”); missing upper contact.
4053.35(1235.46)	0.19(0.06)	DOLOMUDSTONE w/ ANHYDRITE; dolomudstone; yellowish gray (5Y 7/2) w/ light bluish gray (5B 7/1); wavy laminated dolomite w/ displacive nodular anhydrite and bedded massive anhydrite; missing upper contact.
4053.16(1235.40)	0.40(0.12)	MUDSTONE; olive gray (5Y 4/1); massive mudstone; missing upper contact
4052.76(1235.28)	0.16(0.05)	DOLOMUDSTONE; dolomudstone; yellowish gray (5Y 7/2) w/ light olive gray (5Y 6/1); wavy, cryptalgal-laminated dolomudstone; missing upper contact.
4052.60(1235.23)	1.60(0.49)	ANHYDRITE; bluish white (5B 9/1) w/ light olive gray (5Y 7/2); massive anhydrite (10.5”) grades upward to mosaic anhydrite (9”); missing upper contact.
4051.00(1234.74)	1.00(0.30)	ANHYDRITE w/ MUDSTONE; light bluish gray (5B 7/1) w/ grayish olive (10Y 4/2); mosaic and coalesced nodular anhydrite w/ minor grayish olive mudstone remnant; sharp and wavy upper contact.
4050.00(1234.44)	0.08(0.24)	MUDSTONE w/ ANHYDRITE; light bluish gray (5B 7/1) w/ grayish olive (10Y 4/2); massive mudstone w/ minor nodular anhydrite; sharp and wavy upper contact.
4049.92(1234.42)	0.46(0.14)	ANHYDRITE; light bluish gray (5B 7/1) w/ grayish olive (10Y 4/2); mosaic and coalesced nodular anhydrite w/ small muddy remnant; missing or gradational upper contact
4049.46(1234.28)	0.30(0.09)	ANHYDRITE w/ SILTSTONE; grayish brown (5YR 3/2) w/ light bluish gray (5B 7/1); pseudomorphic felted flatten anhydrite w/ increasing silty and muddy remnant. The size of anhydrite crystal is less than 1/10”; missing or gradational upper contact.
4049.16(1234.18)	0.16(0.05)	ANHYDRITE; light bluish gray (5B 7/1); massive anhydrite; missing or gradational upper contact.
4049.00(1234.14)	0.70(0.21)	ANHYDRITE w/ SILT- to MUDSTONE; grayish brown (5YR 3/2) w/ pale brown (5YR 3/2); the coalesced nodular anhydrite w/ minor silty and muddy remnant. The size of nodules ranges from 2/10X2/10 to 1X1” in diameter; missing upper contact.
4048.30(1233.92)	1.60(0.49)	SILT- to MUDSTONE w/ ANHYDRITE; dusky brown (5YR 2/2) w/ light bluish gray (5B 7/1); thin grading planar laminated siltstone w/ coalesced nodular anhydrite (4”) grades upward to siltstone w/ pseudomorphic felted anhydrite crystal (4”). The size of nodules and crystals range from less than 1/10 to 5/10X5/10”.; gradational upper contact. **TOP OF GRAYBURG FORMATION.**
4046.70(1233.43)	0.90(0.27)	ANHYDRITE; light bluish gray (5B 7/1) w / dusky brown (5YR 2/2); mosaic anhydrite w/ minor dusky brown muddy remnant; gradational upper contact.
4045.80(1233.16)	0.50(0.15)	SILT- to MUDSTONE w/ ANHYDRITE; dusky brown (5YR 2/2) w/ light bluish gray (5B 7/1); massive siltstone w/ nodular and enterolithic structure anhydrite (3”) grades upward to deformed planar cross and ripple laminated mud and siltstone w/ pseudomorphic felted anhydrite (6”); missing upper contact.
4045.30(1233.01)	0.40(0.12)	LOST INTERVAL.
4044.90(1232.89)	0.50(0.15)	SANDSTONE w/ ANHYDRITE and MUD CLASTS; very fine-grained; pale olive (10Y 6/2) w/ grayish olive (10Y 4/2); massive and discontinuous ripple cross-laminated sandstone w/ mud clasts; sharp and wavy upper contact.
4044.40(1232.73)	0.60(0.18)	ANHYDRITE w/ MUD- to SILTSTONE; medium bluish gray (5B 5/1) w/ light olive gray (5Y 5/2); nodular and mosaic anhydrite w/ minor muddy and silty laminae remnant; missing upper contact.
4043.80(1232.55)	1.10(0.34)	SILT- to MUDSTONE w/ ANHYDRITE; silt to very fine-grained; olive gray (5Y 3/2) w/ medium bluish gray (5B 5/1); wavy laminated and massive sandstone w/ mud brecciated clasts and slumping structure (4.5”) grades upward to deformed wavy and ripple laminated sandstone (2”), and discontinuous ripple cross laminated sandstone; missing upper contact.

4042.70(1232.21)	0.87(0.27)	SILTSTONE w/ ANHYDRITE; olive gray (5Y 3/2) w/ medium bluish gray (5B 5/1); faintly discontinuous ripple laminated siltstone w/ nodular anhydrite and mud rip-up clasts; The sizes of anhydrite nodules is 2/10X2/10” in diameter; sharp and inclined upper contact.
4041.83(1231.94)	0.73(0.22)	SANDSTONE w/ ANHYDRITE; very fine-grained; grayish olive (10Y 4/2) w/ olive gray (5Y 3/2); deformed ripple cross laminated sandstone w/ burrow, slumping structure and nodular anhydrite at the top of bed; wavy and sharp upper contact.
4041.10(1231.72)	0.30(0.09)	SILTSTONE w/ SANDSTONE; grayish olive (10Y 4/) w/ olive gray (5Y 3/2); discontinuous ripple cross-laminated sandstone w/ siltstone bed; gradational upper contact.
4040.80(1231.64)	0.90(0.27)	ANHYDRITE w/ SILTSTONE; bluish white (5B 9/1); massive and mosaic anhydrite w/ minor silty remnant; missing upper contact.
4039.90(1231.36)	0.44(0.13)	ANHYDRITE; bluish white (5B 9/1) w/ pale olive (10Y 6/2); massive anhydrite; gradational upper contact.
4039.46(1231.23)	2.26(0.69)	ANHYDRITE w/ SILTSTONE; bluish white (5B 9/1) w/ pale olive (10Y 6/2); nodular anhydrite w/ minor silty cryptalgal laminae (18.5”) grades upward to massive anhydrite w/ minor wavy silty laminae remnant (7.5”); gradational upper contact.
4037.20(1230.54)	0.32(0.10)	ANHYDRITE; bluish white (5B 9/1); massive and mosaic anhydrite w/ minor silty laminae remnants; missing upper contact.
4036.92(1230.45)	0.50(0.15)	SANDSTONE w/ ANHYDRITE; fine-grained; yellowish gray (10Y 6/2) w/ light bluish gray (5B 7/1); massive and faintly deformed wavy laminated sandstone w/ pseudomorphic felted and nodular anhydrite. The sizes of anhydrite nodule range from 1X1 to 5/10X 5/10” in diameter; gradational upper contact.
4036.42(1230.30)	0.42(0.13)	SANDSTONE; fine-grained; yellowish gray (5Y 7/2); faintly discontinuous wavy and ripple laminated sandstone; missing upper contact
4036.00(1230.17)	2.70(0.82)	LOST INTERVAL.
4033.30(1229.35)	1.30(0.40)	SANDSTONE; fine-grained; yellowish gray (5Y 7/2); massive and mottled sandstone w/ some burrow; missing upper contact.
4032.00(1228.95)	0.04(0.01)	LOST INTERVAL.
4031.96(1228.94)	0.86(0.26)	SANDSTONE; fine-grained; light olive gray (5Y 5/2); massive and mottled sandstone w/ some burrow; missing upper contact.
4031.10(1228.68)	1.24(0.38)	SANDSTONE; very fine-grained; light olive gray (5Y 5/2) w/ pale olive (10Y 6/2); massive and pyrite bearing thin wavy laminated sandstone; missing upper contact.
4029.87(1228.30)	0.04(0.01)	DOLOMUDSTONE; dolomudstone; light bluish gray (5B 7/1) w/ olive gray (5Y 5/2); massive dolomudstone; missing upper contact.
4029.83(1228.29)	1.00(0.30)	SANDSTONE; very fine-grained; olive gray (5Y 3/2); massive and pyrite bearing thin wavy laminated sandstone w/ some burrow grades upward to continuous planar horizontal laminated sandstone w/ little deformed laminae due to fluidized flow; missing or sharp upper contact
4028.83(1227.99)	0.25(0.08)	SILTSTONE; olive gray (5Y 4/1); very thin-stacked ripple cross-laminated siltstone; missing upper contact.
4028.58(1227.91)	1.42(0.44)	DOLOMUDSTONE; dolomudstone; light olive gray (5Y 6/1); interbedded mosaic and remnant wavy laminated anhydrite; the above this, relatively massive and dark pyrite bearing very thin wavy laminated mudstone and peat; sharp and wavy laminae, sharp and wavy upper contact.
4027.16(1227.48)	2.49(0.76)	DOLOWACKESTONE w/ ANHYDRITE; peloidal dolowackestone; yellowish gray (5Y 7/2) w/ light bluish gray (5B 7/1); relatively massive dolomite w/ anhydrite in fenestral and peloidal moldic pores, vertical fracture and stylolites. The fenestral pores horizon is usually brecciated bed by stylolite; gradational upper contact.
4024.67(1226.72)	0.43(0.13)	DOLOMUDSTONE w/ ANHYDRITE; dolomudstone; yellowish gray w/ bluish gray; massive and some wavy laminated dolomite w/ nodular anhydrite. The sizes of nodule range from less than 1/10” to 7/10” X 1” in diameter; gradational contact.
4024.24(1226.59)	1.04(0.32)	DOLOMUDSTONE TO DOLOWACKESTONE w/ ANHYDRITE; peloidal dolomudstone to dolowackestone; yellowish gray (5Y 7/2); massive dolomite w/ anhydrite in peloidal moldic pores and desiccation crack at 4,023.9 ft (4”) grades upward to wavy and ripple cross laminated dolomite w/ anhydrite in peloidal moldic pores (7”); gradational upper contact
4023.20(1226.27)	0.34(0.10)	LOST INTERVAL.
4022.96(1226.20)	2.26(0.69)	DOLOMUDSTONE; dolomudstone; yellowish gray (5Y 7/2); massive dolomite and cryptalgal wavy laminated dolomite w/ many stylolites,

		enterolithic structure and coalesced nodular anhydrite; missing at upper contact
4022.72(1226.13)	0.41(0.12)	LOST INTERVAL.
4022.31(1226.00)	1.51(0.46)	ANHYDRITE w/ DOLOMITE; light bluish gray (5Y 7/2); mosaic anhydrite w/ minor light olive gray silty remnant (3.5”) change into mosaic anhydrite w/ minor dolomitic remnant (4”) and finally grades upward to massive anhydrite w/ thin wavy dolomitic laminae (5”); missing upper contact.
4020.80(1225.54)	4.97(1.51)	ANHYDRITE; light bluish gray (5B 7/1) w/ grayish olive (5Y 5/2); the alternation of thick massive anhydrite (about 15 to 30”) and the relatively thin mosaic anhydrite (8”). Some enterolithic anhydrite structure are found at the 4017.2 ft; wavy and sharp upper contact.
4015.83(1224.02)	1.33(0.41)	SILTSTONE w/ ANHYDRITE; olive gray (5Y 3/2) w/light bluish gray (5B 7/1); deformed wavy laminated siltstone w/ slumping structure and nodular anhydrite (9”) grades upward to deformed muddy laminated and massive siltstone w/ nodular and pseudomorphic anhydrite (5.5”). The scour surface is found at 4,015.8 ft. The sizes of nodule is 2.5/10 X 5/10” in diameter; missing upper contact.
4014.50(1223.62)	0.07(0.02)	LOST INTERVAL.
4014.43(1223.60)	1.20(0.37)	SANDSTONE; very fine-grained; light olive gray (5Y 3/2) w/ olive gray (5B 7/1); massive and mottled sandstone w/ ball and pillow structure, load cast and burrow (10”) grades upward to deformed wavy and ripple laminated sandstone w/ burrow (7”); wavy and sharp upper contact
4013.23(1223.23)	0.09(0.03)	SANDSTONE w/ ANHYDRITE; very fine-grained; yellowish gray (5Y 7/2) w/ bluish white (5B 9/1); massive sandstone w/ pseudomorphic felted anhydrite and mud clasts; wavy and sharp upper contact.
4013.14(1223.21)	0.14(0.04)	SANDSTONE; very fine-grained; light olive gray (5Y 3/2) w/ olive gray (5B 7/1); ripple cross laminated sandstone grades upward to wavy mud laminated drape w/ displacive anhydrite.; wavy and sharp upper contact
4013.00(1223.16)	1.20(0.37)	SANDSTONE w/ ANHYDRITE; very fine-grained; yellowish gray (5Y 7/2) w/ light olive gray (5Y 5/2); mottled and massive sandstone w. burrow (5”) grades upward to deformed wavy and ripple laminated sandstone w/ small nodular anhydrite (5.5”) and finally deformed wavy laminated sandstone w/ dewatering structure and burrows (3”); wavy and sharp upper contact.
4011.80(1222.80)	1.12(0.34)	SANDSTONE; very fine-grained; yellowish gray (5Y 7/2) w/ olive gray (5Y 3/2); very thin wavy and planar laminated sandstone (10”) grades upward to cryptalgal wavy laminated and massive sandstone (6”); gradational upper contact.
4010.66(1222.45)	0.91(0.28)	SILTSTONE; yellowish gray (5Y 7/2) w/ olive gray (5Y 3/2); very thin planar horizontal laminated siltstone (5”) grades upward to massive and faintly discontinuous wavy massive siltstone (6.5”); missing or planar upper contact.
4009.75(1222.17)	0.70(0.21)	ANHYDRITE w/ DOLOMITE; light bluish gray (5B 7/1) w/ yellowish gray (5Y 7/2); massive anhydrite w/ minor wavy dolomitic laminae remnant; Top of core interval at upper contact
4009.05(1221.96)		

Well Name:MSAU 59-60

Depth difference between core and well log: +1 feet in core depth

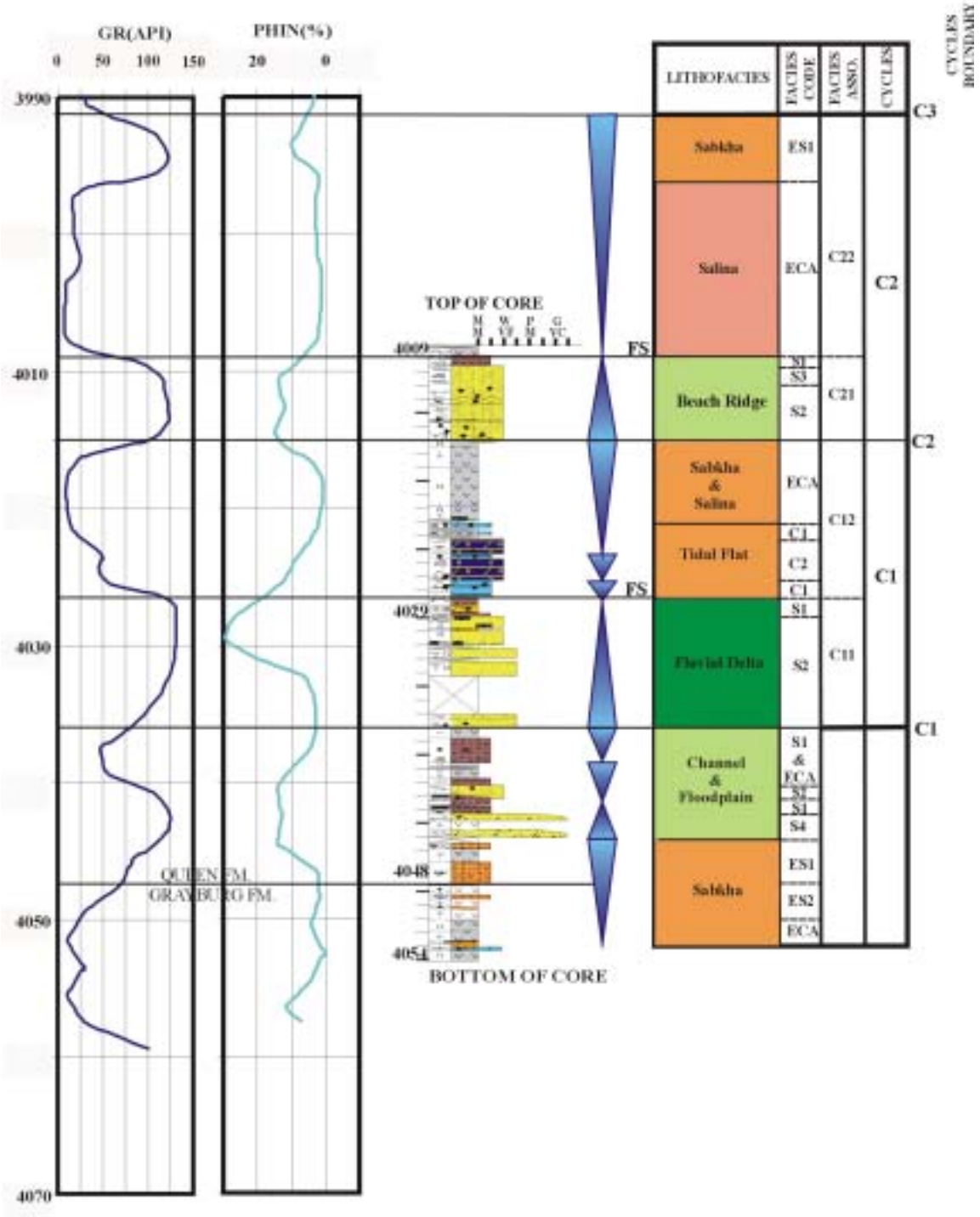

VITA

NAME: Changsu Ryu

BIRTH PLACE: Seoul, Korea

CITIZENSHIP: Republic of Korea

EDUCATION: Texas A&M University
College Station, Texas
Ph.D., Geology, 2002

Korea University
Seoul, Korea
M.S., Geology, 1989

Korea University
Seoul, Korea
B.S., Geology, 1987

PROFESSIONAL EXPERIENCE: SK E&P Company (2002-)

Korea National Oil Corp.(1992-1997)

LG-EDS Company (1991-1992)

PERMANENT ADDRESS: 511-9 Wonsung-dong
Cheon-An, Chungnam
Korea 330-070